Functional Composite Inorganic Nanoparticles/Polyelectrolyte Microcapsules: Synthesis and Properties

A Thesis Submitted to the University of London for

the Degree of Doctor of Philosophy

By

Hui Gao

Supervisor: Professor Gleb B. Sukhorukov

School of Engineering and Materials Science

Queen Mary University of London

July 2016

Declaration

I certify that the present work is prepared solely by me during the course of my studies at Queen Mary, University of London. It has not been submitted for a degree at this or any other University. Any words and/or figures from the work of other people are fully acknowledged according to standard referencing.

This thesis fully combines with the regulations set by the University of London and the Queen Mary, University of London.

Hui GAO

July 2016

Abstract

Functionalization of drug carriers using engineered inorganic nanoparticles (NPs) is currently an important topic. Polyelectrolyte microcapsules, as one of potential drug delivery systems, can be facilely functionalized with various modifiers including inorganic NPs. In recent years, gold NPs, Fe_3O_4 and ZnO were incorporated into polyelectrolyte multilayers, forming polyelectrolyte/inorganic NPs composite capsules. Despite the fact that the physiochemical properties of these composite capsules were investigation by several scientific groups in the world, application of this special inorganic/organic composite capsules in drug delivery provides enormous amount of work to be done, such as encapsulation of small molecules. Except loading of cargos with different molecule weight, microcapsules used for drug delivery should also meet other constraints, which contains the controlled release of them via external triggering or irradiation that are harmless to living body.

The main aim of this work is to design and synthesis of composite microcapsules with potential to seal small molecules and unique external triggering responsive properties. Different from incorporating pre-fabricated inorganic NPs into polyelectrolyte multilayers, NPs were synthesized and incorporated in one step in this study. Such method provides possibility to concrete soft polymer and rigid inorganic NPs into one integrity. Three different NPs, *i.e.* silica, TiO_2 and fluorescent carbon dots (CDs) were chosen to functionalize polyelectrolyte layer-by-layer (LbL) microcapsules. The properties and applications of the formed composite capsules were studied in detail.

The feasibility of incorporating *in situ* formed NPs into soft polyelectrolyte multilayers was demonstrated in this thesis. For silica coating, the formed polyelectrolyte/silica composite

shells showed a reduced permeability, strengthened mechanics and enhanced ultrasound sensitivity. They were able to seal small molecules inside the cavities and to prevent acid molecules going through the shells. As an example model, Rh-B molecules were *in situ* encapsulated inside and released by ultrasound treatment. The biocompatibility of silica coated capsules was proved by MTT assays. In addition, capsules composed of biodegradable polyelectrolytes and *in situ* coated silica NPs were investigated and the results demonstrated that they can be degraded in B50 cells. For TiO_2 coating, the formed TiO_2 NPs on the surface of the composite capsules showed a fiber-like morphology, and behaved as a UV absorber and an ultrasound enhancer, enabling the capsules to be dual-responsive to ultrasound and UV light. For CDs incorporation, they were introduced into polyelectrolyte multi-layered microcapsules by hydrothermal carbonization of dextran. The formed composite capsules were endowed with strong fluorescent signal and became detectable. The feasibilities to *in situ* encapsulate Rh-B inside the polyelectrolyte/CDs capsules and to break them *via* ultrasound treatment (20 kHz, 50 W) and NIR laser irradiation (840 nm) were demonstrated.

Table of Contents

Acknowledgements

First of all, I would like to thank my supervisor, Prof. Gleb Sukhorukov, who offered me an opportunity to work in his group and always provided his constant encouragement and helpful guidance. I would also like to thank my second supervisor, prof. Dongsheng Wen, and my MSc supervisor, prof. Baorang Li, for also being responsible for me to have this opportunity to study at QMUL.

I'm thankful to colleagues and friends, who helped me with performing experiments, particularly, Dr. Zofia Luklinska, Dr. Nadezda V. Tarakina, Dr. Russell Bailey, Dr. Kyrstelle Mafina and Dr Alice Williams for the sample mearsurement, Jierong Liang for TiO_2 coating and Olga Goriacheva and Ahamed Thaaqib Nazar for some part of work on silica coating. I also appreciate constant help of Dr. Chris Mole for his help with general lab equipment use and lab management.

It was a great honour for me to work with our collaborators, prof. Maria-Magdalena Titirici and Dr. Andrei Sapelkin, for the part of project of carbon dots.

There are also people, all the members of Gleb's group, who contribute a nice working environment for free communication, learning together, sharing skill and knowledge about experiments. I am also grateful to my parents, Zhongliang Hu and other friends who gave me a lot of help and time in listening to me, and without them, I would not be where I am today.

List of Figures

List of Tables

List of Symbols and Abbreviations

NPs – nanoparticles

CDs – carbon dots

LbL – layer-by-layer (method)

PAH – poly(allylamine hydrochloride)

PSS – polystyrene sulfonate

DNA – deoxyribonucleic acid

PECs – polyelectrolyte complexes

PEMs – polyelectrolyte multilayers

HA – hyaluronic acid

PLL – poly(lysine)

RF – radio frequency

AZO – azobenzene

PVS – poly(vinyl sulfate)

p(HPMA-DMAE) – poly(hydroxypropylmethacrylamide dimethylaminoethyl)

PGA – poly(glutamic acid)

PEG – poly(ethylene glycol)

PAZO – poly[1-[4-(3-carboxy-4-hydroxyphenylazo)-benzenesulfonamid o]-1,2-ethanediyl, sodium salt]

FAS – fluoroalkyl silane

SPR – surface plasmon resonance

CNTs – carbon nanotubes

DMEM – Dulbecco's minimum essential media

FBS – fetal bovine serum

DMSO – Dimethyl sulfoxide

FTIR – Fourier Transform Infrared Spectroscopy

AFM – atomic-force microscopy

PAA – poly(acrylic acid)

PEO-b-PCL – poly(ethylene oxide)-block-poly (β-caprolactone)

GE – gelatin

TA – tannic acid

PAN – polyacrylonitrile

C-T – charge-transfer

pH – a measure of acidity/basicity of aqueous solution

PDADMAC – poly(diallyldimethylammonium chloride)

MF – melamine formaldehyde

PS – polystyrene (PS)

THF – tetrahydrofuran

PLA – polylactic acid

PLGA – polylactic-co-glycolic acid

HF – hydrofluoric acid

EDTA – ethylene diamine tetraacetic acid

NaOCl – sodium hypochlorite

PARG – poly-L-arginine

DXES – dextran sulfate sodium salt

VERO-1 cells – African green monkey kidney cells

UV – ultraviolet

IR – near-infrared

BP – benzophenone

FITC – fluorescein isothiocyanate

CLSM–confocal laser scanning microscopy

PBS – potassium buffer saline

pKa – acid dissociation constant

SEM -scanning electron microscopy

SFM – scanning force microscopy

TEM – transmission electron microscopy

TRITC – tetramethylrhodamine isothiocyanate

1. Introduction

1.1 Background

Organic/inorganic composite materials consisting of both organic compounds and inorganic compounds with potential of providing new promising functions have received extensive attentions in recent years. Because such organic/inorganic composites are expected to combine both the flexibility of organic materials and the hardness of inorganic materials.[2] Polymer-inorganic composite microcapsules, as one type of organic/inorganic composite materials have been widely investigated due to their wide range of potential applications in pharmaceutical fabrication processes, controlled drug delivery, agriculture chemicals, and food and cosmetics industries.[3]

Polymeric capsules with shells made of polyelectrolyte multilayers have already been intensively studied in the past few decades. A versatile approach to produce such capsules with proper control over their stability, size, shell thickness, encapsulation and release properties is the layer-by-layer (LbL) assembly technique.[4] The first idea of LbL method was suggested by Iler,[5] where it was used to prepare films by depositing alternating layers of oppositely charged inorganic nanoparticles (NPs). Such approach was expended by Decher and Hong in 1991 on the preparation of LbL coating composed of oppositely charged polyelectrolytes.[6]

In 1998, the LbL approach was applied to spherical templates by the international group of researchers from Max Plank Institute of Colloids and Interfaces, and hollow polyelectrolyte microcapsules were obtained.[7] Later more than sixty research groups have extensively worked under the synthesis of polyelectrolyte microcapsules and investigated their physicochemical properties. As the polyelectrolyte capsules exhibit controllable permeability and surface

functionality, this enables many applications in drug delivery systems.[8] The most remarkable results were obtained in the direction of the influence of wall thickness, temperature,[9] pH change[10] and ionic strength[11] on the permeability of polyelectrolyte multilayer shells. Although a substantial number of *in vivo* experiments with polyelectrolyte microcapsules were successfully demonstrated but there are still several problems that have not yet been fully resolved: (1) controlled release of the encapsulated drugs *via* external triggering or irradiation; (2) *in situ* encapsulation of small molecular drugs; (3) chemical addressing of the capsules; (4) physical addressing of capsules, realizing by magnetic field gradient, optical tweezers, acoustic fields. Regarding to these problems, remote control of the shell permeability and the *in situ* encapsulation of small molecules inside polyelectrolyte microcapsules remains the most important issues.

Compared with polymeric capsules, inorganic capsules used for drug delivery possess good mechanical strength, however, the permeability of these inorganic capsules is not controllable, which strongly limits their application.[8] Hence, what is needed is a polymeric/inorganic composite capsule, in which the inorganic building blocks yields mechanical strength to withstand, for example, drying and osmotic pressure, and the polymer fraction enables control on the shell permeability. Moreover, the embedded inorganic particles may also contribute specific optical,[12] magnetic[13] and sonication properties[14]. Hence, incorporating functional inorganic NPs into polyelectrolyte shells is one facile way to solve the above-mentioned weakness for both pure organic capsules and inorganic capsules, for example, the ability to encapsulate small molecules and to tune shell permeability.[15]

Up to date, there is a great number of publications devoted to composite polyelectrolyte microcapsules with inorganic phase into the shell and/or capsules cavity. Despite a variety of

inorganic NPs that can be employed for capsule preparation one may consider two general approaches to build-up a composite shell: (1) Adsorption of the particles from the previously prepared sol or suspension; (2) *In situ* growing of the particles directly into the capsules shell. In fact, current design and synthesis of polymeric/organic composite capsules were mainly focused on assembling prefabricated inorganic NPs into soft polyelectrolyte shells using the first method.[16] One important attribution of LbL approach is the availability to assembly any chargeable inorganic NPs and polyelectrolytes on templates to facilely form organic/inorganic composite capsules. To date, various kinds of inorganic NPs were assembled into polymeric shells *via* LbL approach, forming polymer/inorganic NP composite capsule. One of the most attractive features of such hybrid capsules is that the incorporated inorganic NPs allow them to be sensitive to a remote exposure, which including ZnO for ultrasound-triggered release,[14] Fe_3O_4 for magnetically navigated drug delivery,[17] and gold for visible and near-infrared (NIR) light responsive capsule systems.[18] This method can produce capsules with relatively good control over the stimuli responsive properties of the formed capsules, but poses considerable challenges in encapsulating small molecules as well as that in controlling the distribution of NPs in shells. If the inorganic NPs can grow directly within or on the surfaces of polyelectrolyte shells and finally concrete together with polymers into an integrity, it would provide possibilities to decrease the shell permeability. Because NPs would first *in situ* nucleate and grow in pores of polymer shells (the positions with lower energy) and 'crosslink' with soft multilayers, yielding dense composite shells with a reduced porosity. The second method of *in situ* growing NPs was rarely explored in the past few decades. Ion-exchange reactions proposed by Shchukin *et al*.[8,19] were used to synthesize YF_3, magnetite Fe_3O_4, and hydroxyapatite $Ca_{10}(PO_4)_6(OH)_2$ composite microcapsules. Metal NPs such as Ag were synthesized and assembled into polyelectrolyte capsules via ion reduction method. However, the procedure of

these *in situ* formation of inorganic NPs seems quite complicate and is difficult to control the reaction, and the properties of the formed composite capsules were not well investigated.

1.2 Motivation and Aims

According to all the mentioned above, it can be clearly seen, that assembly pre-fabricated inorganic NPs has been intensively investigated but the ability of loading small molecules by the formed composite capsules was not proved, and that incorporation of *in situ* formed inorganic NPs is lack of study and leaves lots of works to explore. Notably, to fully address the issues of sealing small molecules and physically controlled release, functionalization of polyelectrolyte capsules *via in situ* formed inorganic NPs need to be further explored.

In terms of external triggered release, the chemical responsiveness such as pH, temperature and ion strength can be usually achieved in pure polyelectrolyte capsule systems but has limited use in biological and medical systems. For example, changing pH and temperature in human body to realize tuning shell permeability of capsules are associated with large side effects. In contrast, physical responsiveness is focusing on application of various fields for microcapsules activation, such as external magnetic gradient field,[20] laser,[21] and acoustic fields[22] which are more promising techniques. Fortunately, a large amount of publications proved that the physical responsive effect on the permeability of polyelectrolyte capsules can be achieved by introducing inorganic NPs into polymeric shells. It has shown that the shell permeability of capsules embedding with pre-fabricated inorganic NPs (*i.e.*, Fe_3O_4, Au, ZnO) responsive to ultrasound and capsule rupture was observed.[14,23,24] Similarly, it is expected that incorporating of *in situ* formed NPs will increase the ultrasound responsive effect on the permeability of the obtained composite capsules.[14] If the *in situ* formed NPs are intrinsically sensitive to other kinds of stimuli, such as ultra-violet (UV), NIR light, magnetic, *etc.*, the formed hybrid

polyelectrolyte/inorganic NP capsules are expected to be at least dual-responsive. There are many kinds of polymer/inorganic NPs composite capsules with possible responsive abilities, but to the best of our knowledge, using inorganic NPs to effectively densify capsule shells to push forward to entrap small molecules inside their cavities are still lacking. In fact, for encapsulation of small molecules, the process of the *in situ* formation NPs and their distribution is of great importance. Additionally, for biomedicine usage, the issue of biocompatibility must be considered. The employed drug carriers should be not toxic to cells. Here, silica, TiO_2 and carbon dots (CDs) were chosen as examples of modifying agents in this thesis, due to their excellent biocompatibility, good water solubility, facile synthesis process and low cost.[25,26,27] Apart from the mentioned common merits, silica NPs is famous for its biodegradability and is also popularly used as drug carriers;[25] TiO_2 is a good UV absorber;[28] and CDs have outstanding fluorescent properties and have already employed for cell imaging study.[27]

SiO_2 NPs are among the most abundant and widely used synthetic materials applied in drug delivery systems, as they are generally accepted as to be biocompatible and nontoxic to cells.[29] As reported before, amorphous silica can be degraded in biological systems, and their degradation by-product is the nontoxic silicic acid that is naturally found in numerous tissues.[30] In addition, silica NPs can be facilely synthesized by the sol-gel method based on Stöber process.[31] Hollow mesostructured silica nano/microparticles were successfully prepared *via* Stöber process and templating approach. This idea is to deposit silica on the surface of template and further remove the template to obtain hollow-structured mesoporous silica spheres. Similarly, employing polyelectrolyte capsules as templates, silica can also be deposited and incorporated into their shells. Therefore, **Chapter 4** offers a sol-gel method to nucleate and grow silica in polyelectrolyte multilayers. Such method provides opportunities to reduce shell permeability, increase mechanics and enhance ultrasound sensitivity of the capsules. Whether

the shells with *in situ* formed silica are thick and compact enough to entrap small molecules or prevent small molecules diffusing inside are check in this chapter. Besides, the ultrasound effects on polyelectrolyte/silica composite capsules are investigated. As amorphous silica are proved to be degradable in biological systems,[29,30] hopefully, biodegradable polyelectrolyte capsules with silica can also be degraded in cells. Such hypothesis is examined in this chapter.

Design capsules with multi-responsiveness is of high scientific and technical importance, since single stimulus-responsive capsules are not sufficient for many practical applications.[32,33] In practical, microcapsules possess multi-responsive properties simultaneously is more promise due to that multifunctional materials can overcome challenges that cannot be solved by their individual components. As mentioned that the introduce of inorganic NPs into polyelectrolyte multilayer endows a potential of ultrasound sensitivity, and that if the used NPs are intrinsically sensitive to other stimuli such as UV light or NIR laser, such secondary stimuli sensitivity could be inherited by the formed composite capsules, obtaining double-stimuli responsive composite capsules. Beside its excellent biocompatibility, TiO_2 is a type of good UV absorbers, which have been widely used for photocatalytic application.[28,34] However, only a few reports are about polymer/TiO_2 capsules but they were not synthesized by *in situ* process and not proved to be bifunctional capsules. **Chapter 5** proposes a novel strategy of incorporating TiO_2 *in situ* into an LbL capsules to prepare multifunctional composite microcapsules that possess both ultrasound and UV responsive functionalities. A study on dual stimuli induced release of TRITC-dextran from the composite capsules will be performed.

Beside the intrinsic high permeability, LbL polyelectrolyte capsules have poor optical traceability.[10,27] This problem is usually addressed by incorporating fluorophores: tagging with fluorescent dyes and semiconducting quantum dots (QDs), but a number of intrinsic

problems of these systems such as photobleaching, toxicity, stability in biological environments can not be avoided. To address these challenges, integrating CDs into polyelectrolyte shells is a promising approach, which could provide new opportunities for yielding multifunctional and traceable capsules. To date, CDs have been widely explored and investigated, however, there is no report on *in situ* incorporating them in polyelectrolyte multilayers. **Chapter 6** therefore employs for the first time a method, *one-step* assembly-and-synthesis of fluorescent CDs in polyelectrolyte multilayers *via* a facile hydrothermal treatment. This method is inspired by recent numerous reports of conversion of a variety of aromatic hydrocarbons to light emitting carbon dots (CDs) under relatively mild conditions of hydrothermal carbonisation (HTC).[35] Due to the observation of the absorbance of dextran in polyelectrolyte shells,[36] dextran is used as the carbon source. Hopefully, the dextran could be converted into fluorescent CDs and embedded in polyelectrolyte multilayers, forming fluorescent polyelectrolyte/CDs composite capsules and 2D films. Furthermore, these composite multilayers are expected to be responsive to ultrasound treatment and NIR laser irradiation.

In general, the aim of this thesis is to explore the one-step synthesis and assembly procedures for functionalization of polyelectrolyte microcapsules with three types of inorganic NPs, *i.e.*, silica, TiO_2 and carbon dots (CDs). The ultimate purpose of this thesis is to design and synthesize functional composite capsules with features such as a small molecule encapsulation, a responsiveness to ultrasound, UV and NIR laser, as well as fluorescent properties. The most challenging task is to explore a proper method to introduce inorganic NPs under careful control. Generally, silica and TiO_2 are introduced in the pre-fabricated polyelectrolyte microcapsules by sol-gel method. Small molecules, rhodamine B (Rh-B) are used as typical example for *in situ* small molecule encapsulation and ultrasound-induced release studies. CDs are introduced

by hydrothermal carbonization (HTC) method. Basic mechanisms for synthesis and assembly each type of NPs and their influences on morphologies and physiochemical properties of the capsules are investigated. The most essential attribution of this work is to provide a strategy to functionalize polymer capsules with one-step method and demonstrate the possible promising features of composite capsules, which have a great guiding significance for the research fields such as surface science, composite materials, biomedicine and photochemistry areas.

2 Literature Review

This review mainly focuses on the modification and functionalization of polyelectrolyte microcapsules, with particular emphasis on development of inorganic nanoparticles (NPs) functionalized polyelectrolyte microcapsules in recent years. With rigid inorganic NPs embedded in the soft polyelectrolyte multilayers, the obtained microcapsules definitely show differences in shell thickness, porosity and permeability, mechanical strength, and potential sensitivity to external triggers. Generally, three areas will be covered: (1) polyelectrolyte microcapsule preparation process, (2) inorganic NPs incorporation and functionalization, and (3) stimuli-responsive microcapsules. The different preparation strategies using NPs to modify polyelectrolyte microcapsules are highlighted, simultaneously, their potential application are discussed.

2.1 Polyelectrolytes

Polyelectrolytes refer to one kind of charged polymeric molecules, composed of ionized or ionisable monomers and counter-ions, the monomers of which will dissociate in aqueous solutions and consequently generate the corresponding charged polymers and free ions.[37] The resulting polyelectrolyte solutions are electrically conductive. If the dissociated monomers are positively charged in the solution, this polyelectrolyte is called as a polycation, whereas is referred to as polyanion. Typical examples for polyelectrolytes include the synthetic ones like poly(allylamine hydrochloride) (PAH), polystyrene sulfonate (PSS), *etc.*, and the biological molecules like polypeptides and deoxyribonucleic acid (DNA).[38,39]

Polyelectrolytes can be classified into “strong” and “weak” types, depending on their dissociation degree in polar solutions for reasonably pH values. Strong polyelectrolytes can

completely dissociated in solution so that they are fully charged over a normal pH range. On the contrary, weak ones are only partially dissociated in solutions and their ionization degree corresponds to the pH value of the solution. If the weak polyelectrolyte (*HA*) is dissolved in water, the polyelectrolyte ion pair should dissociate as below:

$$HA \longleftrightarrow H^{+}+A^{-} \tag{1.1}$$

Considering the weak polyelectrolyte *HA* is not fully dissociated in water, so the charge of weak polyelectrolytes is defined by dissociation constant (*Ka*) of ionic group, severely depending on pH.

$$Ka=[H^{+}][A^{-}]/[HA] \tag{1.2}$$

Where the brackets denote the concentration of each species. When logarithm is taken, a form of the Henderson-Hasselbalch equation is obtained as below:

$$pKa=pH-lg\ [A^{-}]/[HA] \tag{1.3}$$

If the charge density along the polymer chain is taken into account, empirical parameter n arises. Thusly, the acid dissociation constant *pKa* is described as a modified Henderson-Hasselbalch equation, showing as below:

$$pKa= pH-n\cdot lg\ [\alpha]/1-[\ \alpha] \tag{1.4}$$

Where the parameter *pKa* is acid dissociation constant, n refers to the extension of the polymer chains, which depends on their charge, α is degree of protonation or occupancy. Equation 1.4 indicates that the dissociation is improved for a polyanion when pH > *pKa*, because the negatively charged neighboring ions attract the proton, which promotes the separation of proton from the acid group more easily. Similarly, the repressed dissociation when pH < *pKa* due to the increased amount of positively charged neighbouring ions is understandable. Whereas for a polycation, the pH-dependent dissociation behaviour is exactly the opposite situation.

Actually, polyelectrolytes play an important role in various fields ranging from materials science and colloids to biophysics. These polymers are widely used as coatings, biomedical implants, rheology modifiers, adsorbents, colloidal stabilizing agents, and suspending agents for pharmaceutical delivery systems.[40] In the past few decades, polyelectrolytes were assembled into 2D films or 3D capsules, which can be facially modified by inorganic materials, showing a great potential in drug delivery.[41,42,43] The above mentioned pH-dependent behaviour of weak polyelectrolytes is practically important, which can help researchers carry out the synthesis of polyelectrolyte multilayers and realize their potential applications. For instance, one can adjust the pH to get a fully charged polyelectrolyte solution; the permeability and stability of the capsules including weak polyelectrolytes can be adjusted by the environment pH values.

In addition, linear charge density (charge per single monomer unit) determines the size of polyion in aqueous solutions. The presence of salts in solutions affects its size and properties, since salts can screen the charges of polyion molecules from each other, and therefore decrease repulsion force and result in the unwrapping of the molecules. A considerable concentration of salt (~1 M) can lead to the disappearance of coulomb repulsion, and the molecule size becomes equal to that of uncharged one. If the salt concentration higher than this point, polyelectrolyte will be separated into a new phase, usually liquid. In terms of long polymers, Gaussian model is the simplest and often used model to describe the average conformation of a flexible neutral polymer in dilute solution. This model considers a phantom chain, made up of orientationally uncorrelated (freely-jointed) links, where the length of any link vector r has a probability distribution.[44]

$$G(r)= (3/2\pi b^2)^{3/2} \cdot \exp(-3r^2/2b^2) \quad (1.5)$$

$$< r^2 > = b^2 \quad (1.6)$$

In the above equations, *b* is the expectation for the link length. The scaling of the end-to-end distance is

$$< R_e^2 > \sim \alpha^2 N \tag{1.7}$$

Where α is the single monomer size, and *N* is the number of monomers. It shall be mentioned that R_e of uncharged polymers is much smaller than the length of the extended polymer, and this model only describes uncharged polymers. For charged polyelectrolytes, it is more complicated and Flory theory is commonly used for their description.[37] The end-to-end distance h_0 can be displayed as below:[45]

$$< h_0^2 >= 2L(P_0 + P_e) = 2LP_T \tag{1.8}$$

Where *L*= contour length of the chain; P_0 = steric length (corresponding to persistence length of an equal length uncharged polymer); P_e corresponds to electrostatic contribution; P_T = total persistence length. Persistence length is an average projection of the end-to-end vector on the tangent to the chain contour at a chain end in the limit of infinite chain length, which is characteristic to a hypothetical linear macromolecule consisting of an infinite thin chain of continuous curvature with random directions at any point of the chain. It can be referred as Porod-Kratky chain. Its steric and electrostatic contributions are described by the so-called Odjik-Skolnick-Fixmann approach, which is particularly useful for representing stiff chains:[46]

$$P_0 = \gamma kT,\ P_e = \frac{l_B}{4}\left(\frac{k^{-1}}{A}\right)^2,\ l_B = \frac{q^2}{4\pi\epsilon\epsilon_0\, kT}$$

$$k^{-1} = \left(\frac{\epsilon\epsilon_0\, kT}{2N_0\, e^2 I}\right)^{1/2},\ \mathrm{I} = \frac{1}{2}\sum Z_i^2 C_i \tag{1.9}$$

Where: γ = elasticity of the polymer chain; *k* = Boltzmann constant; *T* = temperature;

l_B = Bjerrum length (the separation at which the electrostatic interaction between two elementary charges is comparable in magnitude to the thermal energy scale *kT*); k^{-1} = Debye length (the scale over which mobile charge carriers screen out electric fields); *A* = distance between elementary charges in the chain; *q* = elementary charge; ε = dielectric permeability of

the medium (water); N_A = Avogadro's number; I = ionic strength of the solution; Z_i = charge valency of i^{th} ion; C_i = concentration of i^{th} ion.

From the above relations, the main conclusion is obtained that it is more favourable to make a coiled conformation of polyelectrolyte with addition of salt makes, and to lead to elongated one at relatively low ionic strength.[44]

2.2 Polyelectrolyte Complexes

Polyelectrolyte complexes (PECs) are formed by mixing oppositely charged polyelectrolytes solutions together without any chemical covalent cross-linker. Their formation is mainly driven by the coulombic interactions (attraction between oppositely charged polyions) or the increase in entropy as releasing the counter-ions.[47] Other interactions such as covalent bonding,[48] hydrogen bonding,[49,50] base pair interactions,[49,51] *etc.* may play as an additional part. Depending on the reaction factors, the mixed solution may finally show a relatively dilute phase and a concentrated complex coacervate phase, or it may display a more-or-less compact precipitate or gel. Also, the complexes can remain in solution if their concentration is low. It is known from loads of previous reports that the properties of PECs are influenced not only by chemical composition of the polyelectrolytes (their molecular weight, stereo-chemical fitting, charge densities, *etc.*), but also by secondary experimental conditions like the concentrations of the polyelectrolytes prior to mixing, their mixing ratio, ionic strength of the solution, mixing order, duration of the interaction, additive salts and pH of the reaction medium, *etc.*[52,53] For example, the addition of salt (*e.g.*, NaCl) or conductive polyelectrolyte in the PECs system has a profound impact on their formation and stability, because these additives will affect the attractions between the opposite-charged polyelectrolytes.[54] This kind of influence is quite complicated for the PECs systems consist of weak polyelectrolytes with significant different

molecular weights, and many corresponding studies have been reported by a few groups such as Andrey V. Dobrynin.[40]

The potential applications of PECs locate various fields, including medicine, tissue engineering, catalysts, biosensor and drug delivery systems.[52,55] Compared with the chemically cross-linked complexes, PECs is generally more biocompatible. Because chemical cross-linkers may induce toxicity if un-reacted residuals are not further purified carefully.[47] Therefore, PECs consisted of polysaccharides and proteins has been extensively investigated and widely used recently for biomedical applications.[47,56,57]

2.3 LbL Self-assembly Polyelectrolyte Multilayers

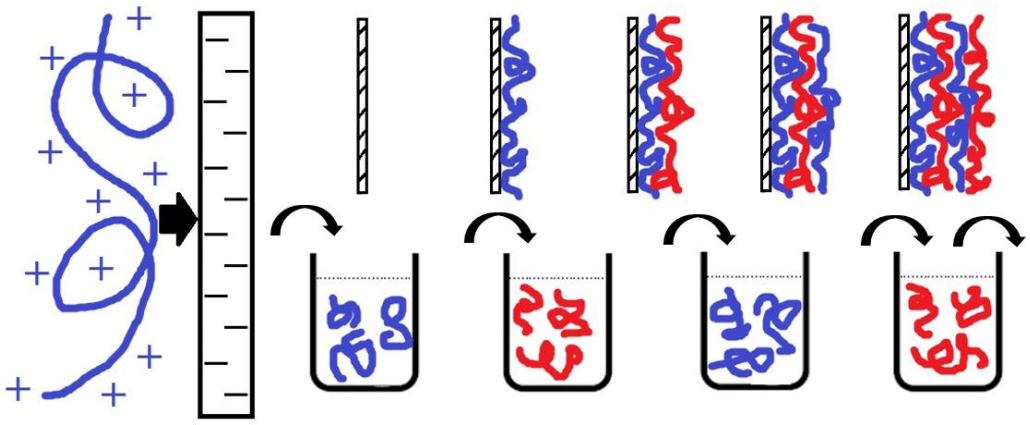

Figure 2.1 The procedure of LbL self-assembly of multilayers on planar substrates.

Polyelectrolyte multilayers can be easily prepared by the method of layer-by-layer (LbL) self-assembly.[58,59] The planar substrates with a charged surface such as glass, silica or mica can be employed. When place a charged substrate in an oppositely charged polyelectrolyte solution, the free polyelectrolytes will adsorb onto its surface due to the electrostatic attraction effect.[60] If the incubation time and the amount of polyelectrolytes in solution are enough (usually 15

minutes), the absorbed polyelectrolytes will fully cover the solid surface. Thusly the polyelectrolyte-coated substrate will carry the charge of the 1st polyelectrolyte, providing an electro-absorbable surface for the 2nd polyelectrolyte. Finally, alternating deposition of the oppositely charged polyelectrolyte on a solid surface with a specific layer number will form polyelectrolyte multilayers (PEMs) (as shown in **Figure 2.1**). It worth mentioning that after a typical adsorption time of 15-20 minutes for each polyelectrolyte layer, the substrate is washed in DI-water to remove excess polymer. The general procedure for multilayer fabrication is the so called Layer-by-Layer assembly.

LbL assembly is a promising tool to produce nanostructured multilayer materials with nanometer precision and requires, driven by electrostatic interaction between the components,[61] or other interactions including hydrogen bonding, polar interactions, or van der Waals forces.[62] Since reported in 1990s firstly, PEMs has earned lots of attentions from researchers and progressed rapidly in their development. In the past 25 years, this technique has become very popular, especially for their potential application in drug delivery and biosensors.[61,63] One can facilely control the properties of the resulting LbL films if polyelectrolytes are employed as the building blocks. For example, the composition, thickness, surface roughness, and morphology of the films can be adjusted by modifying the assembly conditions. When using natural macromolecules such as polysaccharides and proteins which are biocompatible, it is possible to obtain biocompatible and biodegradable coatings, which can be applied for biomedicine areas. In terms of their characterization, techniques including small angle X-ray reflectivity, optical absorption, atomic-force microscopy (AFM), *etc.* can be employed for the property measurement. Recently, novel techniques were also used to investigate these PEMs. Assisted by these investigations, researchers could characterize their

chemical components, structure (thickness, pore size and pore distribution), surface roughness, hydration properties, elasticity and mechanical properties.[64,65]

2.3.1 Driving Forces

Driven forces for the formation of LBL multilayers mainly include electrostatic interactions, hydrogen bonding, hydrophobic interactions and van der Waals forces.[60]

2.3.1.1 Electrostatic Interaction

As described above, oppositely charged building blocks can be assembled into multilayers driven by the electrostatic interactions, which is the most deeply studied driving force for LbL self-assembly, as proved by the overwhelming majority of publications until now. This method is suitable to fabricate homogeneous multilayer films composed of different materials, which usually carried out in aqueous solutions. A variety of substrates can be employed for the preparation of LbL films and their thickness can be tuned by layer numbers.[60] In terms of mechanism of film formation, it was suggested in early publications that the electrostatic interaction between oppositely charged molecules was the main driven force for assembly of the multilayer films. It was further supported by the finding that a minimum molecule charge density is needed for a stable layer growth.[66] Based on this theory, the adsorption should stop when the coated substrate reach a net neutral surface charge. However, later research work demonstrated that some polymers with unexpectedly low charge density were also successfully deposited into films, which indicated that the initially proposed concept of a minimum value of charge density was oversimplified.[66,67]

Later, it was proved other driving interactions may also play as a key role in the fabrication and growth of LbL multilayer films.[67]

2.3.1.2 Hydrogen Bonding

Besides the electrostatic interaction, hydrogen bonding is another investigated driving force to build up LbL films. It allows to introduce various uncharged building blocks into multilayer films if they can serve as hydrogen bonding donors and acceptors. For example, poly(acrylic acid) (PAA) can act as an H-bond donor while poly(ethylene oxide)-block-poly (β-caprolactone) (PEO-b-PCL) micelles act as an H-bond acceptor, these two polymers be constructed into a film driven by hydrogen bonding under acidic conditions.[68]

Interestingly, hydrogen-bonded LbL films can also be prepared by one component which can simultaneously act as both hydrogen bonding donors and acceptor. A typical example is dendrimers that with various carboxyl groups.[69] It should point out that, LbL multilayers assembled driven by hydrogen bonding force are less stable than the films obtained driven by the electrostatic interaction. In general, hydrogen-bonded LbL multilayers are responsive to environment parameters like temperature, pH, ionic strength, *etc*..[70] Therefore, some pH-, temperature- and/or ion- responsive drug delivery systems can be explored based on their sensitivity properties. Interested readers are suggested to refer the review mainly about hydrogen bonding LbL materais by Kharlampieva, Kozlovskaya and Sukhishvili.[55]

2.3.1.3 Hydrophobic Interactions

More and more research work demonstrated that when considering LbL multilayer formation, hydrophobic interactions must be taken into account. Generally, hydrophobic interaction means the interaction formed between hydrophobic groups in an aqueous environment, which is induced by the fact that the hydrophobic groups cluster prefer to reduce their exposure to water molecules under enthalpy effect and entropy effect. Kotov[71] confirmed the contributions of hydrophobic interactions for forming polyelectrolyte multilayers, indicating that it was one

of the decisive factors for the film formation. For instance, it can promote the assembly process and increase the growth rate of film thickness of weak polyelectrolytes. Recently, novel gelatin (GE)/tannic acid (TA) membranes were prepared by LbL self-assembly process on polyacrylonitrile (PAN) ultrafiltration membranes driven by hydrophobic interaction and then reinforced by hydrogen bond force.[72] The schematic presentation of hydrophobic interactions is shown in **Figure 2.2**.

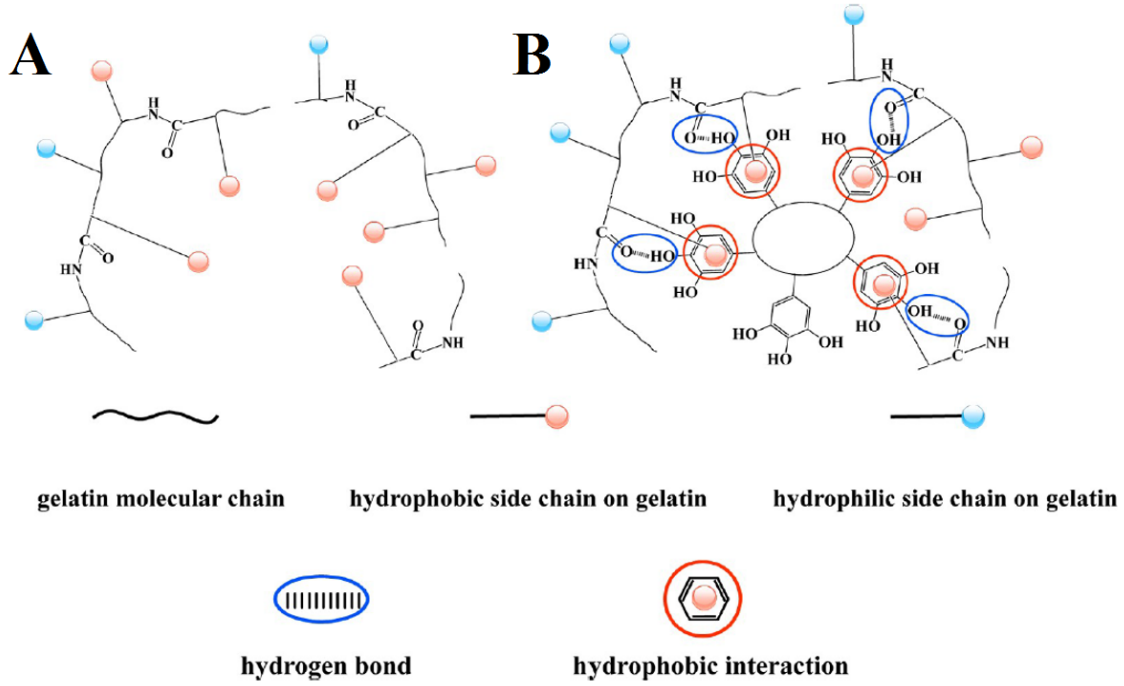

Figure 2.2 Schematic presentation of the hydrophobic pocket of gelatin (A) with and (B) without tannic acid.[72]

2.3.1.4 Charge-Transfer Interaction

Driven by charge-transfer (C-T) interaction, LbL assembled multilayer films can also be fabricated by an alternate deposition of two types of non-ionic molecules: one with electron-accepting and the other one with electron-donating functional groups in the side chains (**Figure 2.3**). This kind of LbL films was first reported by Shimazaki and co-workers.[73] Poly[2-(9-carbazolyl)ethyl methacrylate] (electron-donating) and poly[2-[(3,5-dinitrobenzoyl)oxy]ethyl

methacrylate] (electron-accepting) were successfully adsorbed onto the gold surface and the quartz substrates alternatively from the solutions in methylene chloride (organic solvent).[73] It should be mentioned most of the C-T complexes show low association constants which limit their potential for construction of well-ordered and stable multilayer assemblies.[70]

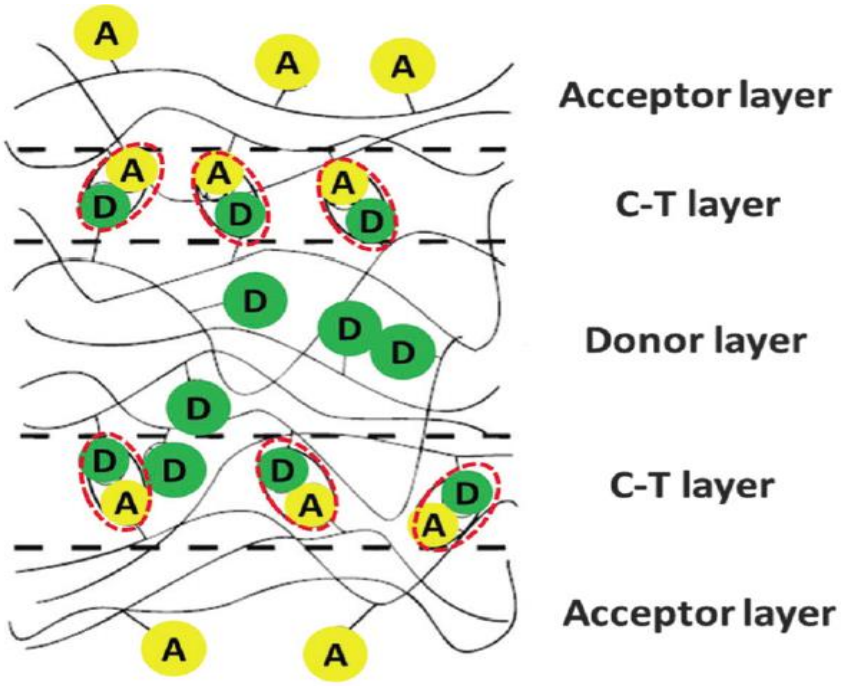

Figure 2.3 Side-view illustration of the LbL assembled multilayer thin film prepared by charge-transfer interaction. D and A denote a carbazolyl group and a 3,5-dinitrobenzoyl group, respectively. The interaction of D and A is highlighted with a red circle.[70,73]

2.3.1.5 Covalent Bonding Interaction

Covalent bonding is another driving force to assemble LbL films. Different from the weak interactions like electrostatic interaction, hydrogen bonding, *etc.*, covalent bonding can significantly increase the stability and strength of the formed multilayer films. Moreover, it provide opportunities to integrate various functional groups in the assembled multilayers *via* reaction with the excess reactive groups within the multilayers. Hence, it also enables researchers to design and fabricate various tailored multifunctional assemblies.[53] Indeed, the

work on covalent bonding based LbL assembly was firstly presented in 2001 by Crooks and co-workers,[74] in which maleic anhydride and dendrimers were used to assemble multilayer films on different substrates such as glass, silicon and gold coated silicon wafers. Later, a more efficient covalent LbL assembly were stimulated along with the concept of click chemistry that was introduced by Caruso and co-workers.[75,76] Their work demonstrated that covalently linked LbL multilayers was obtained based on the copper(I)-catalyzed click reaction between azide and alkyne to form an stable 1,2,3-triazole linkage. More reported works can be referred to a recent review by João Borges and João F. Mano.[53] It should be stressed that despite the above outstanding properties, covalent bonding interaction still has some shortcomings, for example, it is limited to molecules with complementary functional groups, and some side products might be difficult to move out form the multilayers.

Other molecule interactions driven the LbL assembly of multilayers include host-guest interaction, biospecific interaction, coordination chemistry interaction, Van der Waals force, etc. Readers are suggested to refer to the review article by João Borges and João F. Mano, which summarized all the molecule interactions that attribute to the formation of LbL multilayers in detail.[53]

2.3.2 Influence Factors for LbL Assembly

The structures and behaviours of LbL multilayer films are greatly influenced by various parameters, including the environment pH, temperature, ionic strength, solvent, electrolyte type, and properties of polyelectrolytes such as their charge density, molecular weight, concentration, and architecture.[70]

2.3.2.1 pH

The solution pH plays great influence on the growth and stability of LbL multilayer films, as demonstrated by the vast number of publications. As mentioned above, strong polyelectrolytes with substantial charges are fully charged and thusly independent of pH; however, weak polyelectrolytes with carboxylic acid or amine functional groups are highly sensitive to the solution pH. Bieker, *et al.*[77] and Shiratori, *et al.*[78,79] deeply investigated the impact of solution pH on LbL multilayers comprising weak polyelectrolytes such as PAH and PAA. It was found that a small change in the solution pH would cause a pronounced transformation in the film thickness, level of interpenetration depths and surface wettability. Hence, the PAH/PAA film thickness can be adjusted by modifying the solution pH. Besides, it was also possible to control the number of nonionized carboxylic acid groups that contained within the multilayers or on their surfaces. Similarly, multilayers prepared by depositing PAH and PSS was also studied.[80,53] The influence of pH on other polyelectrolyte systems were investigated in the past two decades and reviewed by lots of researchers in detail.[77-79]

2.3.2.2 Temperature

Temperature has a great effect on the properties (thickness, stability, permeability, *etc.*) of LbL multilayers.[81,82] Multilayer films obtained under high temperature showed a significant difference with those fabricated under ambient conditions.[83] In general, the formed films became thicker, lower permeability and more stable. In addition, the effect of temperature on the LbL multilayers is similar for both 2D and 3D structures.[84]

2.3.2.3 Ionic Strength

Ionic strength have also been widely explored to study its influence on the stability, permeability, internal structure and growth of multilayers.[53] It was reported by Dubas and Schlenoff [85,86] that the thickness of polyelectrolyte multilayer films comprising Poly(diallyldimethylammonium chloride) (PDADMAC)/PAA or PDADMAC/PSS was depended on the salt concentration. There was an optimum salt concentration of 0.3 M for these multilayer systems. Below 0.3 M, the film thickness increased when increasing salt concentration, but decreased above 0.3 M and even disassembled when then salt concentration higher than 0.6 M. The film dissociation was attributed to the competition of polyelectrolyte pairs induced by external salt ions. Other researchers also investigated the influence of salt type and salt concentration on the morphology, permeability, stability, thickness, swell properties and mechanics of multilayer films.[87,88] For instance, the impact of salt concentration and salt type (NaCl, NaF, and NaBr) on the structure and water content of PSS/PDADMAC multilayers was studied by Klitzing and co-workers through neutral reflectivity.[54] The results indicated that increasing salt concentration and ion size would increase the multilayer thickness and water content.

2.3.2.4 Solvent

The structure of polyelectrolytes can be influenced by the solvent, and thusly the growth of LbL multilayer films is also affected by the solvent conditions. Evgeni Poptoshev and co-workers investigated the effect of solvent quality on the growth of PAH/PSS multilayer films by varying the ethanol amount in the aqueous polyelectrolyte solutions.[89] Their study demonstrated that an increase of film thickness and mass loading can be achieved by increasing the ethanol amount, due to the reduced solvating effect of aqueous solutions containing electrolyte ions. Therefore, solvent for preparation of polyelectrolyte solutions is important for LbL assembly of multilayers.

Other influence factors such as molecule weight of the employed polymers, concentration, charge density, *etc.* could also affect the final structures of the formed LbL multilayers. For detailed information, readers are suggested to refer to a recent review by Fang-Xing Xiao and co-worker.[70]

2.4 Polyelectrolyte Multilayer Capsules

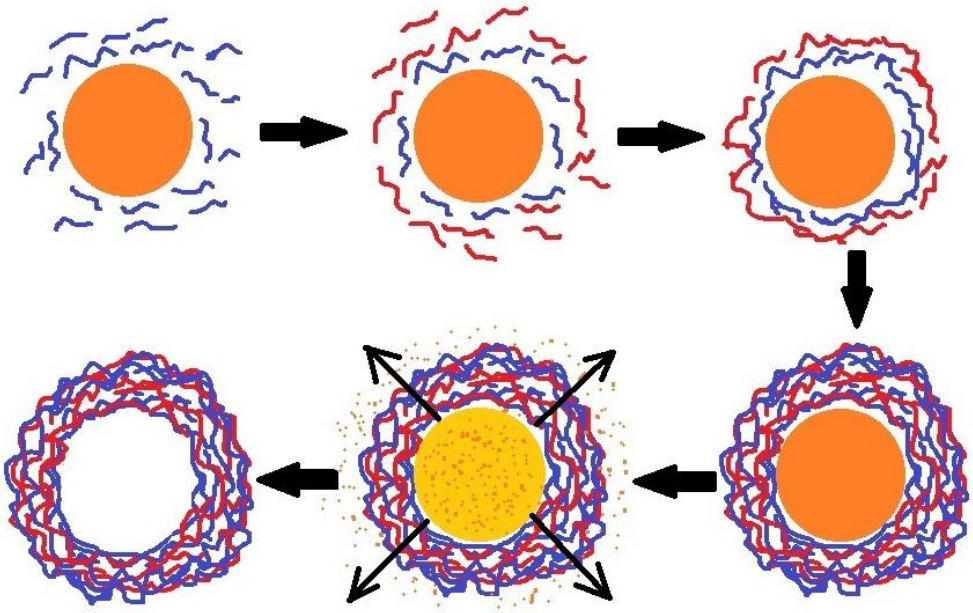

Figure 2.4 The procedure of LbL self-assembly of multilayers on 3D particles.

LbL assembly is a promising tool for the construction of drug carriers not only in the form of multilayer films (for example on implants) but also in the form of micro-or nanocapsules.[61] When the LbL assembly is applied onto removable 3D substrates such as colloidal particles, the formation of polyelectrolyte shelled particles is facially achieved by the alternating addition of polycations and polyanions to the particle dispersion. For each polymer deposition cycle, the excess free polyelectrolytes are removed by following wash steps using either centrifugation or micro-filtration setups. After certain coating layers, hollow capsules could be

obtained by removing the cores.[90,91] In total, three steps are involved in the polyelectrolyte capsule preparation procedure: (1) colloidal templates employment; (2) stepwise deposition of polyelectrolyte; (3) template removement, as shown in **Figure 2.4**.

2.4.1 Templates

The preparation procedure of microcapsules is a multistep process. Their properties depend strongly on lots of factors, including the choice of employed polyelectrolytes, adsorption conditions such as ionic strength, temperature, pH value of the solvent, number of layers, *etc.*, as well as an extremely important step which determines success of the capsule preparation, *i.e.*, the proper choice of the used templates.[92] Generally, templates play as supports for depositing polyelectrolyte multilayer and they are eliminated by certain methods at the end[92-94]. In order to obtain intact capsules consisting only of the employed material used for coating, the dissolution process should result in 100% elimination of the templates without affecting the polyelectrolyte multilayers. Indeed, to remove the core completely seems to be a complicated and difficult task. Until now, different kinds of cores have been employed to template hollow capsules. Briefly, they can be classified into three groups: (1) organic cores made of water-insoluble oligomers; (2) core dissoluble into small molecules and ions; (3) core subjected to strong oxidation.

2.4.1.1 Organic Cores

The wildly studied organic colloidal templates used for depositing polymeric capsules are melamine formaldehyde (MF) particles, polystyrene (PS) cores which are soluble in tetrahydrofuran (THF), and bio-friendly polylactic acid/polylactic-co-glycolic acid (PLA/PLGA) which are soluble in acetone/N-methyl-2-pyrrolidinone mixture.[92,95,96] Their

chemical structure are shown in **Figure 2.5**. MF particles are stable at pH value above 5 and dissolvable at low pH and in some organic solvents, therefore LbL assembly process can be carried out at neutral pH while MF cores can be dissolved by incubation them with 0.1M HCl solution.[97] In spite of an excellent monodisperisty of MF particles, the disadvantages of using MF cores is that the formed oligomers upon dissolution are too large to diffuse out from the capsules. These oligomers will get entangled with capsule shells and stick to the shells, which results in the difficulty of getting rid of the MF core material completely even after several washing cycles.[92, 98] It was reported by Gao *et al.* that the residues of MF in hollow polyelectrolyte capsules was shown to reach 30% of the whole capsule weight.[99] Another problem is that bulk deposition of these oligomers onto capsule shells will lead to a high osmotic pressure inside, which resulting in swelling behaviours of capsules and even rupture of polyelectrolyte shells.[94] In some cases the capsule keeps intact during the dissolution process only if the assembled polyelectrolyte layer number of capsules is less than 10.[97, 99,100] With increase of multilayer numbers more, this osmotic pressure effect increases remarkably, which will lead to possible breakage and high permeability of the polyelectrolyte capsules.[101] PS particles and bio-friendly PLA/PLGA have the similar problems for template LbL capsules, *i.e.*, the by-product of large oligomers upon dissolving process can't be totally removed.

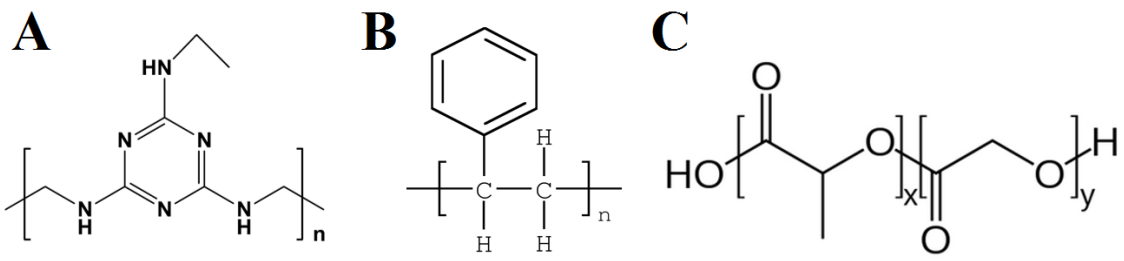

Figure 2.5 Chemical structure of (A) MF, (B) PS and (C) PLA/PLGA.

2.4.1.2 Inorganic Cores

Different form the above-mentioned organic templates, various inorganic cores can be more promising because only small ions or molecules are produced upon core dissolution, which minimizes osmotic stress and LbL shell disruption.[102] At present, SiO_2 particles and different kinds of carbonate particles ($CaCO_3$, $CdCO_3$ and $MnCO_3$)[102-105] have been widely used for assembly of polyelectrolyte multilayer capsules. A typical morphology of porous $CaCO_3$ templates is given in **Figure 2.6**.

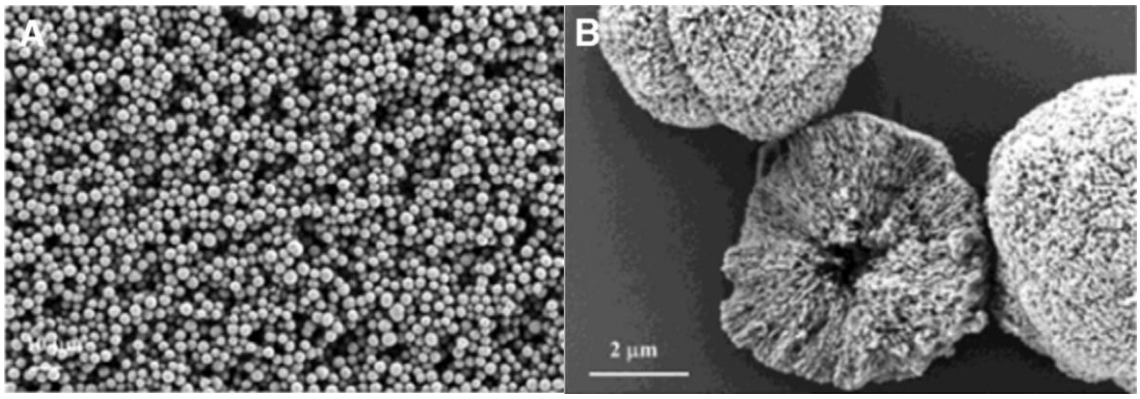

Figure 2.6 SEM images of porous $CaCO_3$ cores.[103]

Most of the commercial available SiO_2 particles are mono-disperse solid ones with a size range from nano- to micro-meter (Micro-particle GmbH, Germany). Indeed, mesoporous silica spheres were also employed as sacrificial templates for polyelectrolyte multilayer formation.[106] These kind of silica templates can be quickly decomposed by suspending them in 1M hydrofluoric acid (HF) and leave intact polyelectrolyte capsules.[104,107] Comparing with the capsules template on MF and PS particles, the capsules obtained by assembly on SiO_2 possess a quite intact structure, can be comprised of a high number of layers and have permeability lower than that of the MF-templated capsules.[102,107] However, a notable drawback of SiO_2 templates is that quite dangerous HF acid is used for core dissolution.

Carbonate particles which could be facially removed with treatment by acid solution were developed as templates for LbL capsules. Generally, calcium carbonate ($CaCO_3$),[108] cadmium carbonate ($CdCO_3$),[102] and manganese carbonate ($MnCO_3$)[105] are used and showed quite good performance in loads of reports. These particles can be easily prepared in lab with different sizes. For example, cubic $CdCO_3$ particles by prepared by adding 2 M cadmium nitrate into 4 M urea solution in a Pyrex round-bottom flask with a Teflon-lined screw cap, and the obtained mixture was aged at 80 °C for 16 h.[102] These $CdCO_3$ were coated with polyelectrolyte multilayers and dissolved by shaking the coated particles dispersion for four hours in 0.8M HCl solution yielding LbL shaped hollow capsules. Spherical $CaCO_3$ can be produced by mixing same volume 0.33M $CaCl_2$ with 0.33M $NaCO_3$ solution at room temperature and can be further used as templates [16]. After a desired deposition cycles, core dissolution can be achieved by incubation in mild weak acid, ethylene diamine tetraacetic acid (EDTA). It is worth mentioning that due to the intrinsic porous structure of $CaCO_3$, capsule using them as a template can be easily loaded with sensitive molecules such as enzymes or mRNA that are relatively large and have therapeutic applications.[109-112]

2.4.1.3 Cores Subjected to Strong Oxidation.

A typical example of the templates subjected to strong oxidation is biological cells, which possess a wide variety of sizes and shapes, and thusly using them as templates would empower the produced capsules with a wide range of morphologies.[92,113] Assembly of polyelectrolyte multilayers can be carried out using fixed erythrocyte cells[92,114] and red blood cells[113] as templates. Hollow capsules are obtained by removing the cell templates, which can be accomplished by an oxidation process with sodium hypochlorite (NaOCl) solution. Actually, biological cells represent a monodisperse and naturally very cheap source of templates that can be used for capsules production. But for scientific study such as analysis of capsule permeablity,

their use is limited by the range of possible employed polyelectrolytes and the difficulty to define the shell chemical modification. In addition, a problem caused by the treatment with NaOCl solution to remove cells templates is that chemical composition of the capsules might be changed drastically.[92] Oxidation of polyelectrolytes and appearance of covalent bonds lead to cross-linking of the polymer chains.

2.4.1.4 Other Templates

Apart from the above three kinds of templates, a large variety of other materials can be used as the capsule templates. Microbubbles,[115] hydrogel with different shapes,[116] oil emulsions,[117] gold particles,[118] *etc.* have also been used as sacrificial templates to fabricate hollow capsules. If the cargo materials could be produced with proper morphology and surface properties, they could be used as templates directly for LbL polyelectrolyte multilayer assembly. In this way, no addition step to remove cores is needed. Specially, this strategy may facilitate the possible encapsulation of various biological payloads like gene, virus, drugs, *etc.*

2.4.2 Polymeric Capsule Formation

As various materials such as charged polyelectrolytes,[91,119] inorganic NPs,[14,18,120] and natural proteins[121,122] can be used as building blocks, the stepwise self-assembly deposition procedure offers versatility of the produced capsules with different composition and functionality.[123] Pure polymers and polymeric/inorganic composite materials can be introduced into the capsule shells, with specific functionalities.[123,115] In most cases, pure polymers (polyelectrolytes) were used to fabricate capsules for application in drug delivery, tissue engineering and biosensors.[61,91,124] Here, we focus on the preparation of pure polymeric capsules. Using the above-mentioned different types of templates, hollow polymeric capsules can be facilely produced by LbL approach with different morphologies and sizes. A the typical example is the

capsule composing of PAH and PSS templated on MF resin microparticles[125,126] and $CaCO_3$ cores[127], as shown in **Figure 2.7**. Usually, the mean thickness of capsules composing of PAH and PSS is 1~2 nm per single polyelectrolyte layer [16,125]. The polymeric capsules are spherical when suspended in aqueous solution. But after drying, creases and folds can be found due to the water evaporation, as demonstrated by the CLSM and SEM results showing in **Figure 2.7**.

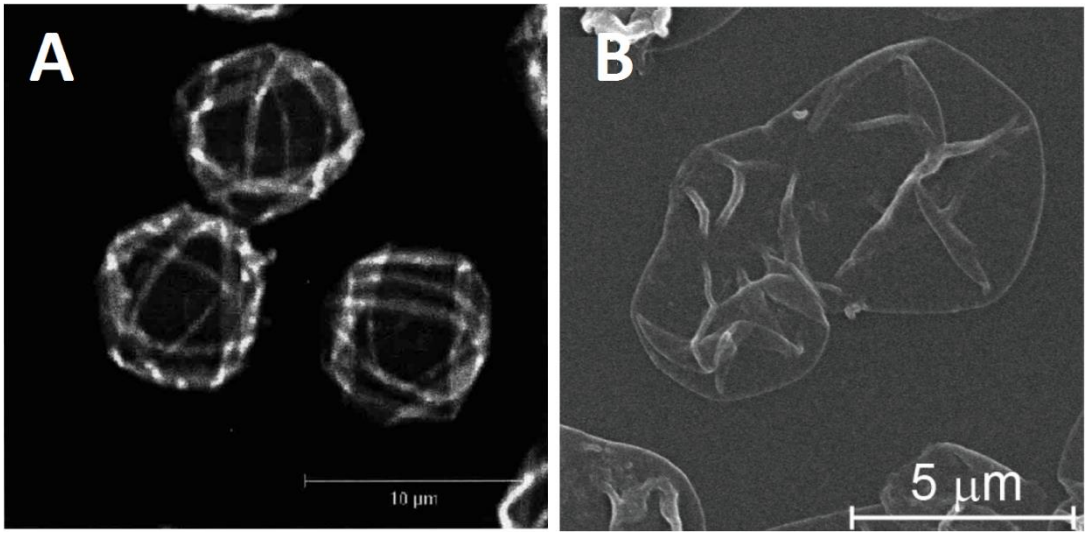

Figure 2.7 (A) CLSM image of $(PSS/PAH)_4$ capsules prepared on MF [125] and (B) SEM image of dry $(PSS/PAH)_4$ capsules prepared on $CaCO_3$ cores.[127]

Other types of polymeric capsules have also been fabricated and investigated in the past few years. The selection of the building components for LbL capsule shells plays an important role in their potential application. For example, microcapsules composed of diazo-resin showed a UV sensitive activity which can be used for triggered drug release.[107] Capsules produced by natural materials such as poly-L-arginine (PARG, Mw >70 kDa) and dextran sulfate (DEXS, Mw ≈ 10 kDa) were proved to be intracellularly degraded by African green monkey kidney cells (VERO-1 cells).[128] Indeed, this kind of biocompatible and biodegradable capsules are very promising to be employed for next-generation drug carrier systems. As the self-assembly is a typical method in which the building blocks arrange themselves into ordered structures or

pattern driven by a secondary force, one can choose different shell materials to synthesize various polymeric capsules depending on their specific application.[129,130]

2.4.3 Encapsulation Cargo Substances in Polyelectrolyte Capsules

Capsules, as one kind of potential drug carriers, cargos encapsulation is one of the most important properties for them. It can be briefly distinguished into two approaches: pre-loading and post-loading, depending on whether the encapsulation takes place before or after LbL assembly.[131] ‘‘Preloading’’ means that the payload materials are encapsulated during the preparation of capsules, for example, co-precipitation drugs within $CaCO_3$ cores.[124] “Postloading” means that capsules are fabricated first, and then loaded with the cargos of interest by altering the permeability of capsule shell.[132] In this case, external stimuli such as salt concentration, pH, temperature, light, magnetic fields can be used to adjust the permeability of polyelectrolyte multilayers.

2.4.3.1 Encapsulation by Preloading

Either by means of co-precipitation or by physical adsorption/pore diffusion during synthesis of the microcapsules, species of interest can be successfully preloaded into templates. Co-precipitation technique refers to that templates are created by a direct precipitation method. Molecules are added during the co-precipitation process, and, therefore, they are homogeneously distributed and entrapped into the template, as demonstrated in **Figure 2.8**. Subsequently, the obtained template is assembled with polyelectrolyte multilayers and then removed to producing capsules.[131] Most frequently, such a method has been applied for carbonate templates.[133,134] Encapsulation of big molecules *via* co-precipitation method is very

convenient, because such molecules cannot travel through the polymeric shell. Proteins, enzymes, dextran and NPs are easily to be loaded into porous $CaCO_3$ particles.

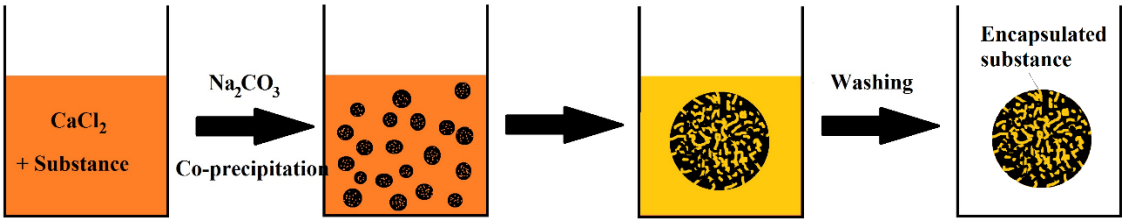

Figure 2.8 Pre-encapsulation in $CaCO_3$ templates by co-precipitation method.

Porous particles such as SiO_2 and $CaCO_3$ can be employed to load molecules by adsorption method, which is attractive due to ease of fabrication. In this method, molecules are added to pre-fabricated templates, and then adsorption takes place probably driven by electrostatic interactions, hydrogen bonding, *etc.*, **Figure 2.9**. The biggest disadvantages of this approach are the difficulty in loading small molecules (Mw ≤ 1000 Da) and the limited loading capacity. For example, due to the porous structure of $CaCO_3$, rhodamine B (Rh-B) molecules could not be loaded within $CaCO_3$ for a long time. In the case of loading capacity for macromolecules, the limitation arises from the surface area, not the pore volume, where adsorption takes place. Hence it can be regulated by the porosity of templates. As for the non-porous particles, adsorption of cargos is made directly onto their surface. Compared with porous template, the absence of pores makes them with the loading even less pronounced.

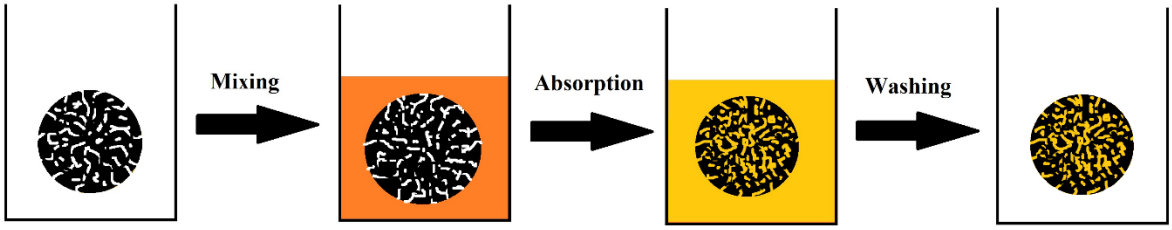

Figure 2.9 Schematic of encapsulation *via* absorption by porous templates prior to coating with polyelectrolytes.

In addition, insoluble substances, crystals, nanoparticles or their aggregates can be encapsulated by direct assembly polyelectrolytes on their surfaces, *i.e.*, using the substances themselves as the templates,[135] thus making it the method of the last group. It is based on different solubilities of molecules in various solvents.[136]

2.4.3.2 Postloading

"Postloading" of cargos is usually based on shell permeability change after that the LbL process is completed and the template is dissolved. Such a technique is only applicable for the substances that can penetrate freely through capsule shells. It is commonly know that the LbL capsule shell is selective permeable to low-molecular-weight compounds such as ions and small molecules like water, but impermeable to macromolecular components (Mw > 5 kDa).[92,137] Hence, it's impossible to encapsulate macroscopic objects (such as nanoparticles and their aggregates) in its initial condition via this process. However, by switching the shell wall permeability through variation of the environmental conditions, *i.e.* ionic strength, pH and temperature, the macromolecules of interest can be possibly loaded.[137] The encapsulation can also be accomplished by solvent exchange, *i.e.* re-dispersing the capsules in different solvent.[138-140]

(1) Shrinkage/Expansion by pH and Light

As shown in **Figure 2.10**, pH and light can also be used to encapsulate cargos inside capsules. Adjusting environment pH to realize encapsulation can be applied for capsules composed of at least one weak polyelectrolyte, which are only stable within a limited range of pH values.[139-142] They works by means of electrostatic interaction. When the pH is set beyond this range for one of the polyelectrolytes, microcapsules swell with an increased permeability. For example,

PAH/PSS capsules swell when increase pH to 11. Because its charge density decreases as well as the electrostatic attraction between the layers. In the meantime, the charges of the second polyion's become relatively higher and cannot be overcompensated by the first polyion, which leads to repulsion between the layers and consequently makes the capsule shells swell and more penetrable.[143] Hence, micro-molecules can go inside their cavities. It worth mentioning that if left them for a long time at an inappropriate pH, the capsules can be totally disassembled and destroyed. On the contrary, if we reduce the pH value, their pores close and entrap the molecules into their cavities. In addition, the shell permeability of capsules can also be changed by re-suspending capsules in polar organic solvent. Because the solvent dielectric constant change will consequently change the electrostatic interactions between polyions. This approach was proved to make the PAH/PSS film penetrable for urease by switching the solvent to ethanol and making it impenetrable again by switching the solvent back to water.[144]

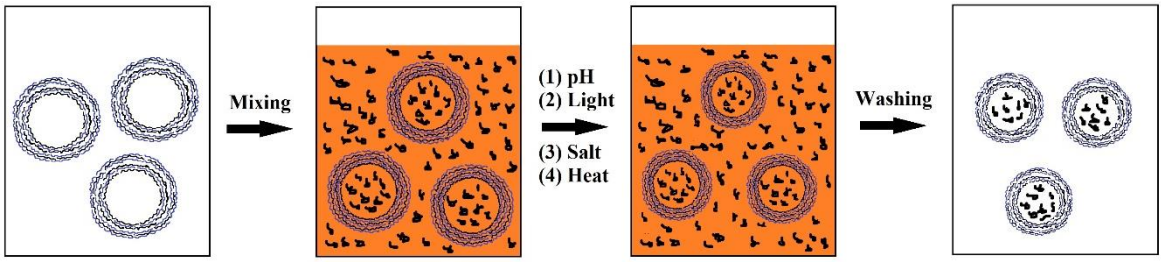

Figure 2.10 Cargos encapsulation: shrinkage of capsules by (1) pH; (2) light; (3) salt; (4) temperature.

Light induced encapsulation requires that the capsules should contain special molecules which are sensitive to light. A typical example is employing azobenzene molecules, which undergo transitions from cis- to trans-configuration upon exposure to light to close the pores in a cooperative way, and thusly entrapping molecules inside the capsules.[104,107,145-147] Another light induced encapsulation and release arising from the photo-acid generation was also in

recent years.[148] It should note that the methods of encapsulation induced by pH and light have a significant disadvantage: the obtained microcapsules are mechanically weak.[131]

(2) Irreversible Shrinkage by Salt and Temperature

Ionic strength of the solution [149] have a great influence on the morphology of polyelectrolytes, while temperature [150] and its thermo-chemistry [151] induces a similar effect. In particular, ionic strength of the solution can be facilely changed by addition of salt. The solution with a low ionic strength makes the capsule shell more penetrable by weakening the polyions interactions, but the capsules are still maintaining the structural integrity.[152] So the molecules which normally cannot penetrate through the shells are allowed to go inside the capsule cavities. On the contrary, if the capsules are dispended in a solution with high ionic strength, their shell will restructure and the capsules tend the shrink to close the pores. Because the hydrophobic part of the polymer main chain gains a significant force, and they prefer to reduce the capsules' exposure to water.[138] For example, the PAH/PSS capsules can be triggered "open" and "close" alternatively by crossing the 0.5-2$\cdot 10^{-2}$ M salt concentration barrier.[152] The main drawback of this approach is that the treated capsules become fragile and can even totally dissolve when the excess salt is added.

Heat treatment affects the behaviour of polyelectrolyte capsules, and they can shrink or swell upon increasing temperature, depending on their construction.[153,154] Capsules with even number of layers, shrink under heat treatment if they are dispersed in proper solution, resulting in an increase in shell thickness and a decrease in shell permeability.[153] So the substance can be sealed inside their cavities *via* raising temperature.[9,153,155] In contrast, capsules with an odd number of layers swell during heating to a few folds of their initial size and follow by their complete rupture.[153] It was demonstrated, that the balance of electrostatic force of charges and

hydrophobic force of main chain determines the response to temperature of capsules. The whole charge of capsule with even-layered shell is close to neutral, so the electrostatic repulsion between the similarly charged layers can be neglected. Heating them in aqueous solution leads to structure rearrangement driven by the hydrophobic forces, and the capsules tend to decrease the surface area of the shell that exposed to the solvent. On the contrary, if the number of the layers is uneven, the process the effects from electrostatic forces greatly surpass that from hydrophobic forces, and as a consequence, raising temperature will result in swelling of polyelectrolyte multilayers, which can even lead to a complete deconstruction of the shells.[153]

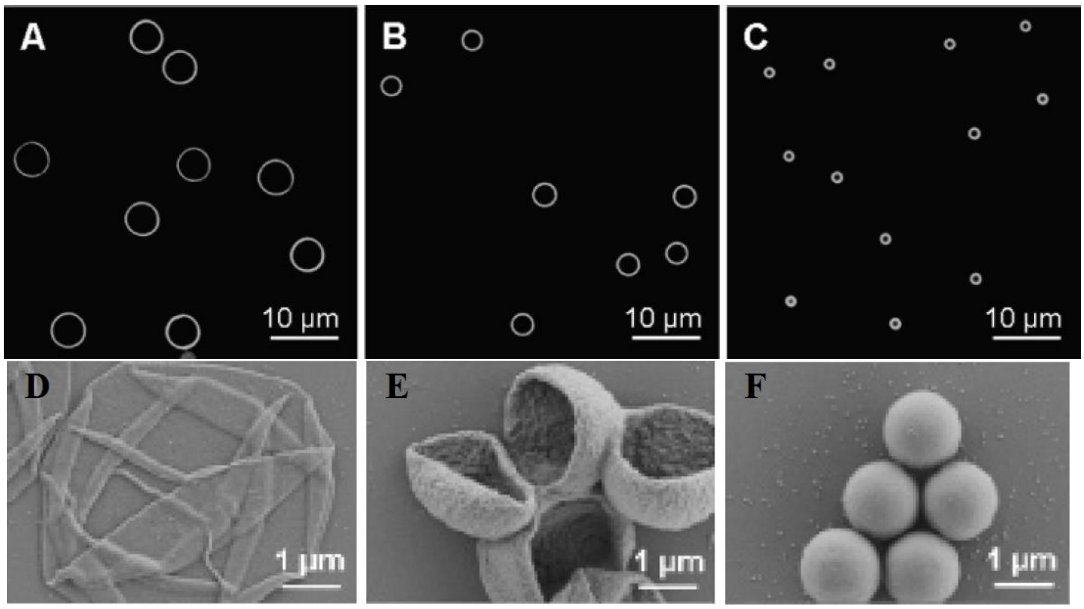

Figure 2.11 CLSM images of $(PDADMAC/PSS)_4$ capsules made on 4.55 µm silica cores before (A) and after incubation for 20 min at 50 °C (B) and 70 °C (C). SEM images (D-F) of $(PDADMAC/PSS)_4$ showing different sizes after heat treatment.[153]

The hollow polyelectrolyte multilayer capsules consisting of poly(diallyldimethylammonium chloride) (PDADMAC) and poly(styrene sulfonate) (PSS) with a different number of layers was investigated as a typical sample. After heating, $(PDADMAC/PSS)_4$ capsules (even layer number) showed a significant shrinkage, as demonstrated by the confocal laser scanning microscopy images (CLSM) and SEM images in **Figure 2.11**. The soft polyelectrolyte

multilayers shrink and squeeze out the H_2O inside their pores, showing results of decrease in size, increase in shell thickness and enhancement in shell density. On the contrary, capsules with an odd number of multilayers, $(PDADMAC/PSS)_4$/PDADMAC, swelled to nearly 5-fold of their initial size, **Figure 2.12**. The SEM images in **Figure 2.13** demonstrated that heating $(PDADMAC/PSS)_4$/PDADMAC capsules at 55 ^oC for 20 minutes induced the complete rapture of the capsules.[153]

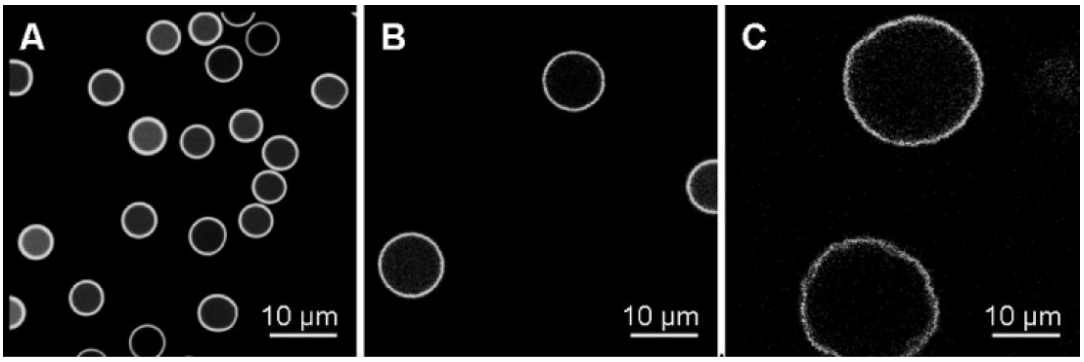

Figure 2.12 CLSM and SEM images of $(PDADMAC/PSS)_4$PDADMAC capsules made on 4.55 µm silica cores before (A) and after incubation for 20 min at 45 ^oC (B) and 55 ^oC (C).[153]

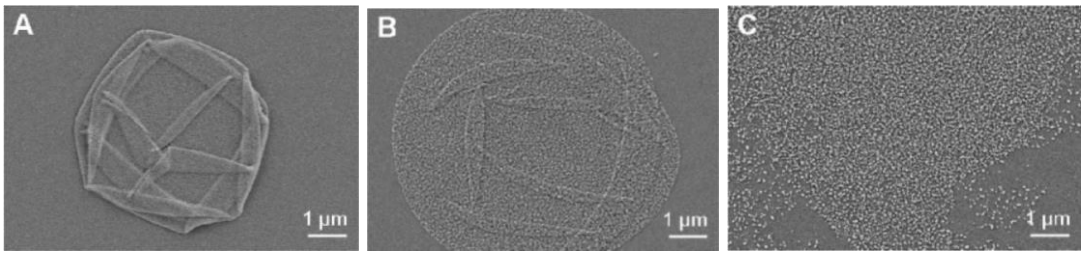

Figure 2.13 SEM images of $(PDADMAC/PSS)_4$PDADMAC made on 4.55 µm silica cores before (A) and after incubation for 20 min at 40 °C (B) and 55 °C (C).[153]

Based on the above description, there is no doubt that the heating can be used to encapsulate the substances into the shells with even number of layers, as illustrated in **Figure 2.13**. This method are extremely attractive because they also allow production of mechanically strong capsules, showing a free-standing structure.[153,154] It should be noted that the temperature and

duration time must be carefully controlled, because the polyelectrolyte capsules can shrink into solid spheres (without cavities).[153]

2.4.4 Modulated Release from Polyelectrolyte Capsules

Apart from loading cargos, another main task for drug delivery systems is controlled release of the payload at the target area. For polymeric microcapsules, the release methods are related to changing the shell permeability or rupturing the shells. This can be realized *via* the above-mentioned methods (such as pH, ionic strength) applied for cargo encapsulation, or can be achieved by some other external triggers, such as ultrasonic treatment, laser or ultraviolet (UV) irradiation. The modulated release for polymeric capsules could be classified into three categories: physical, chemical and biological.

2.4.4.1 Physical

Physical triggers, including near-infrared (IR) laser, magnetic field and ultrasound, have been used to disrupt the multilayer shell by direct mechanical deformation. But for every specific trigger, the polymer shells should contain the active components that could response to the trigger. Usually, to enhance effects of these physical triggers on the shell permeability, inorganic NPs need to be introduced into the soft polymer shells, to form the composite shells, which will be discussed on the part of composite capsules. Here, we focused on physical stimuli triggered release from pure polymeric capsules.

Ultrasound was already applied for the pure polymeric capsule without metal NPs was reported before. It proved that ultrasound with high power and low frequency (*e.g.*, 120 W, 20 kHz [24]; 500 W, 20 kHz[23]) has shown the ability to split the polyelectrolyte shells into piece, which is

based on the shear forces generated from acoustic cavitation in liquids under ultrasonic vibrations.

Light is another physical stimuli, which could be used for the LBL capsule systems. Indeed, light stimuli responsive capsules that are capable to affect their micro-/nano- structures come in the form of remote control triggered by external light (*e.g.*, sun light) without requirement of direct contact or interactions. They are of great importance for the applications in the fields of surface sciences and environmental applications, where sometimes lights would be the only available stimuli to drive the systems. If the employed polyelectrolytes maintain UV-responsive groups, such as benzophenone (BP), azobenzene (AZO), diazonium and o-Nitrobenzyl groups, the formed capsules would have a strong responsiveness to the UV irradiation. For example, diazonium group can be decomposed rapidly and readily when exposed to UV irradiation around 380 nm, which makes the diazonium groups ideally as UV light triggered crosslinkable sites based on photolysis.[147] Similarly, polyelectrolytes with groups responsive to visible light are promising to build visible light sensitive capsules. For example, porphyrin has a strong adsorption regions at 400-500 nm.[156] Phtalocyanines display strong adsorption around 670 nm, and their adsorption in red region could be used for biomedical applications.[156]

2.4.4.2 Chemical

The above-mentioned methods (such as pH, ionic strength) applied for cargo encapsulation could also be used for cargo release. For the capsules with pH-sensitive weak polyelectrolytes, their stability is strongly associated to the environmental pH conditions. Because the charges or ionization degrees along the polyelectrolytes could be changed by varying the pH value of the solution. A typical examples is PAH, which is a weak polyelectrolyte with an apparent

dissociation constant pKa = 8.7.[157] Kentaro Yoshida and co-workers investigated the pH triggered release of insulin from PAH/PSS, PAH/poly(vinyl sulfate) (PVS), and PAH/DEXS microcapsules, revealing that the encapsulated insulin released rapidly from (PAH/PVS)5 and $(PAH/DEXS)_5$ microcapsules at pH 7.4 and 9.0, while the release was slower from $(PAH/PSS)_5$ microcapsules.[127]

Ionic strength is another parameter that can influence the capsules' morphology[158] and shell permeability. Because ions can screen the charges along the polyelectrolyte molecular chains or form some possible defects within multilayers. For example, an increase of the ionic strength decreases the free energy of polyelectrolyte interactions, which proportionally influences the permeability.[159] Actually, the effects of ion strength on the capsule shell permeability could be facilely determined by study the release behaviour upon varying the ion strength in solution.[159]

2.4.4.3 Biomedical

Biomedical responsive capsules involve employing bio-degradable polymers as the building blocks of the capsule shells and using biological stimuli to reduce shell integrity. Several bio-degradable polymers, such as DNA[160], polypeptides[161] and polysaccharides[162], are promising candidates to build up such capsules. Their biodegradation in cells are mainly originated from enzymatic reactions or hydrolysis. For example, PARG is enzymatically degradable and carbonate ester of poly(hydroxypropylmethacrylamide dimethylaminoethyl) (p(HPMA-DMAE)) is hydrolytically degradable in cells, so capsules composed of these polyelectrolytes are expected to be degraded inside cells. In addition, capsules composed of hyaluronic acid and poly(lysine) (HA/PLL) were used for targeted intracellular drug delivery.[163] Another example of the bio-degradable microcapsules is composed of PARG/DXES, which were found to be internalized into VERO-1 cells within a few hours, then

degraded due to a possible enzymatically degradation and enabled the encapsulated cargos released outside, as shown in **Figure 2.14**.[128] Since the shell materials can be degraded and eliminated by cells after the drugs released at the targeted areas, the side effects caused by the external materials should be possibly reduced, which is good for biological systems.

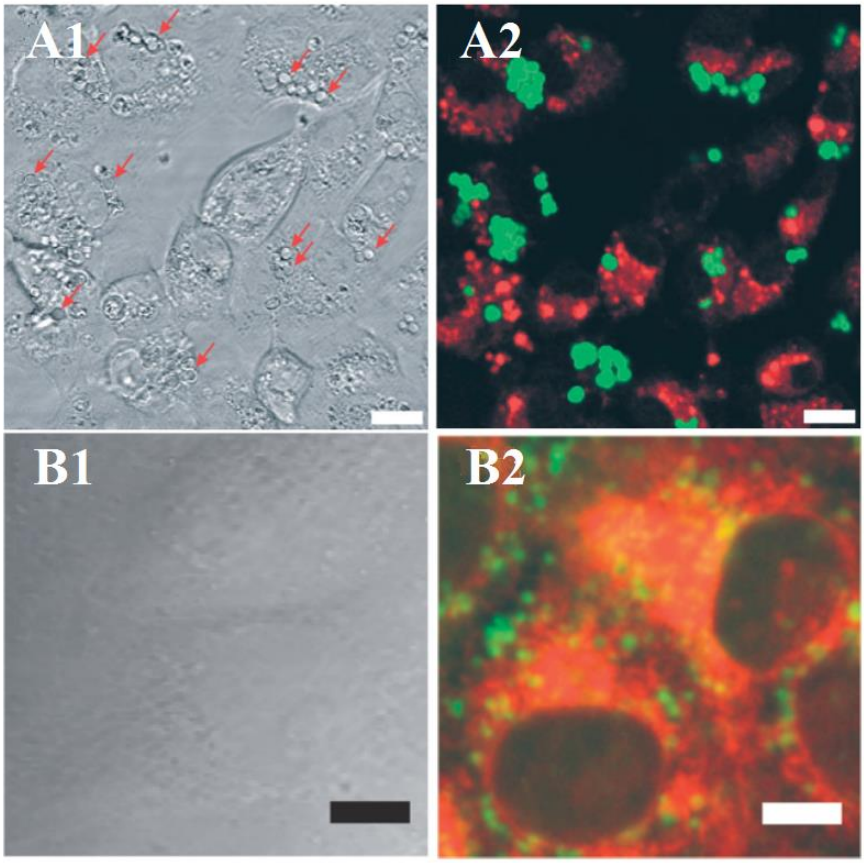

Figure 2.14 Transmission (A1, B1) and confocal (A2, B2) image of DEXS/PARG capsules filled with FITC-dextran taken up by VERO-1 cells after 20 h (A1, A2) and 60h (B1, B2) incubation. The red arrows in the transmission image indicate the presence of intact capsules. In the confocal image LysoTracker Red, which stains the lysosomes in the cytosol red, was used. The green structures are the DEXS/PARG capsules filled with FITC-dextran present in the cells. Scale bars represent 10 µm.[128]

2.5 Polyelectrolyte-Based Nanocomposite Films

Inorganic/organic nanocomposite films comprising functional inorganic NPs and polymers, as one novel and unique class of nanomaterials, are widely studied in recent years, since they synergistically combine and enhance the best properties of inorganic and organic materials.[164] They show quite wide range of potential application fields including biosensors, biomaterials, drug delivery systems, catalysts, *etc.* In practical, there are lots of such composite films fabricated based on LbL process, which benefit from one of the main advantages of LbL process: any charged substances can be assembled on a substrate. Hence, NPs, dyes, proteins, viruses, nanowires, nanotubes, *etc.* can be easily incorporated into polyelectrolyte multilayer film in a controlled order. The soft polymers perform like a glue to stick these incorporated particles together, smooth the interface, and uniform the surface charge. The scheme of the interaction behaviours between two oppositely charged polyelectrolytes and inorganic NPs is shown in **Figure 2.15,** where silica colloids are chosen as an example. If the charged polyelectrolytes and inorganic NPs are deposited stepwise on a substrate, the nanocomposite films are prepared, as indicated in **Figure 2.16**.

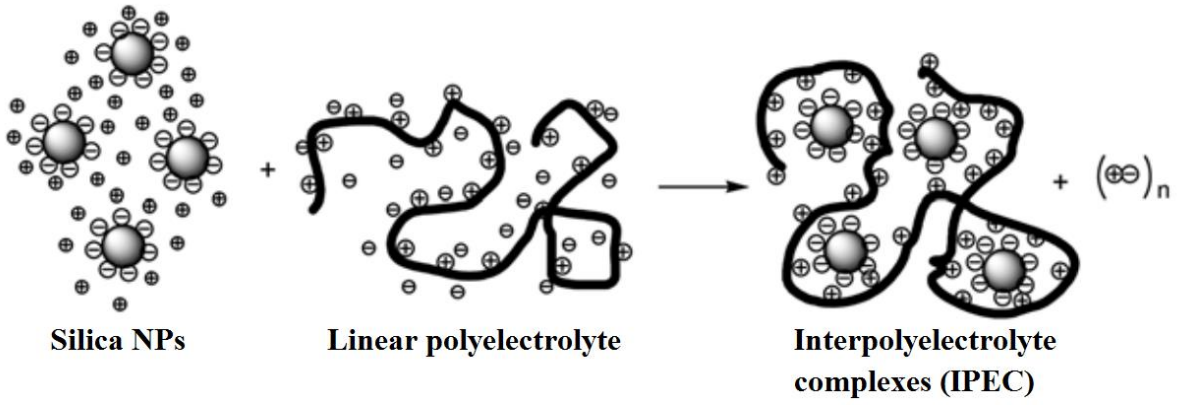

Figure 2.15 Scheme of interpolyelectrolyte complexes formation between silica sols and linear polyelectrolytes.[164]

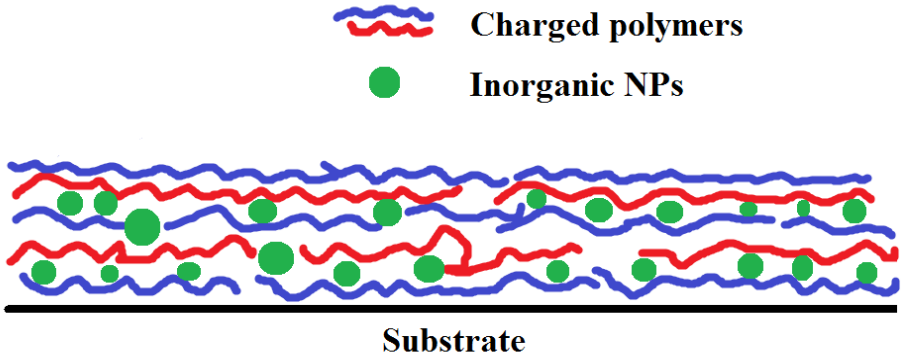

Figure 2.16 Schematic of nanocomposite structure depositing on a substrate.

Mainly depending on the properties of the introduced inorganic NPs, different kinds of properties and functions are endowed with the formed composite films. To date, many unique mechanical, optical, magnetic and catalytic properties were studied by different research groups in last two decades.[64,164,165] Various pre-fabricated NPs such as silica,[164] TiO_2,[166] gold[167], carbon nanotubes[168] and semiconductor NPs[169] were applied as they normally have noticeable surface charges due to the corresponding synthesis method. Besides, the other approach to incorporate inorganic materials in to LbL polyelectrolyte films is to grow NPs directly on the films. For example, Iffat F. Patel and the co-workers facilely incorporated $CaCO_3$ into polyelectrolyte films.[64] By dipping the formed films into the calcium chloride and sodium carbonate solutions alternately, the fabrication-and-assembly of $CaCO_3$ into polymeric films forming polyelectrolyte/$CaCO_3$ composite films was achieved.

2.6 Polyelectrolyte-Based Nanocomposite Capsules

For complex tasks such as drug targeting, tracing, detection and triggered release, several different components need to be assembled in one entity to yield multifunctional carriers.[123] Similar to the above-discussed composite films, polyelectrolyte capsules can also be facilely well-modified by embedding various inorganic NPs with size about 1-100nm such as Ag, TiO_2

NPs, carbon nanotubes, gold NPs, *etc.* within and on top of their wall,[93] and the obtained composite capsules can be endowed with novel properties, such as unique optical, magnetic, catalytic and mechanical features. For example, polyelectrolyte capsules embedding with fluorescent semiconductor NPs can be easily detected by detecting the fluorescence signal with noninvasive optical techniques.[170] To date, different kinds of inorganic NPs with specific functionalities were employed as modifying agents to tune the physical, chemical, optical and mechanical properties of polyelectrolyte capsules. The synthesis and properties studies were investigated by different research groups in last two decades.[171-175]

2.6.1 Methods for Functionalization Capsules with Inorganic NPs

Generally, considering the LbL procedure for the polyelectrolyte capsule fabrication, there are two time points for introduction of the inorganic NPs. One is during the LbL assembly process, and another one is after the LbL deposition procedure. Hence, there are two approaches to build-up composite shells: (1) Adsorption of the NPs from the previously prepared sol or suspension; (2) *In situ* synthesis of the NPs directly into the capsules shell.

2.6.1.1 Adsorption of NPs from the Previously Prepared Sol or Suspension

The approach that widely studied for preparation of composite organic/inorganic multilayer capsules is related to adsorption of the prefabricated inorganic NPs from solution. As indicated in **Figure 2.17**, the method is based on the principle of the LbL assembly, *i.e.*, different types of charged components can be assembly into one entity by employing electrostatic forces between them, so the charged NPs can be assembled onto the oppositely charged polymeric layer.[93,176]

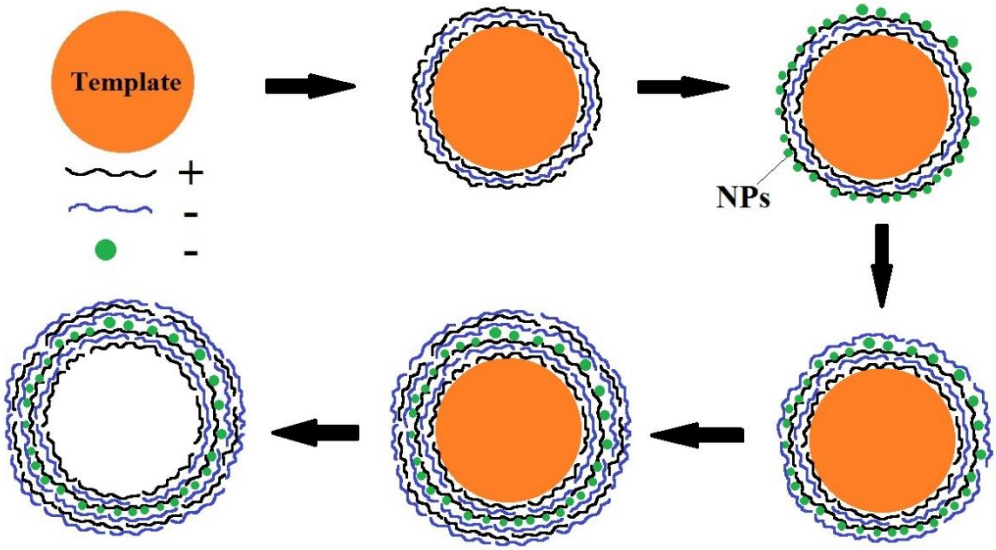

Figure 2.17 Schematic of nanocomposite structure assembled with charged NPs.

Particularly, gold NPs with different morphologies (nanospheres, nanorods, or nanobelts) can be introduced by this method. Due to the synthesis method, gold NPs normally negatively charged, with a zeta-potential about -35 mV.[177] Hence, they can be easily absorbed onto polycation layer. It is worth mentioning that the deposition time, to allow NPs adherence, tends to be longer than that for the polyelectrolytes,[167] as a result of the low concentration of the NPs enlaved by the synthesis method. In a more or less similar way, negatively charged magnetic NPs, *i.e.* Fe_3O_4, were incorporated into the capsule shells.[3,13] For this kind of method, all the NPs have to be synthesized first, then followed by an LbL assembly step. This method could produce capsules with relatively good control over capsule size, stability and stimuli responsive properties. But the formed composite capsules are lack of an appreciable integrity and stability due to the week interactions between NPs and soft polyelectrolytes. Another vital issue remaining unsolved by this method is that the inherent high permeability of LbL polyelectrolyte multilayers cannot be reduced by this kind of modification.[16,93,178] In order to solve these challenges, one-step 'synthesis and assembly' method, that can better control the morphology, distributions and densification of NPs within in the polyelectrolyte matrixes,

should open novel avenues to fabricate functional composite polyelectrolyte/NPs capsules with specific features.[16]

2.6.1.2 *In Situ* Synthesis of the NPs Directly into the Capsules Shell

The second way is to synthesis and incorporate NPs into the pre-fabricated polyelectrolytes multilayer in one step, *i.e.*, *in situ* synthesis method. In this method, polymeric capsules are employed as a substrate to grow inorganic NPs and finally obtain composite organic/inorganic microcapsules. This enables to control the shell permeability and increase the chemical stability of the capsules. S. Anandhakumar and the co-workers reported that silver NPs could be *in situ* formed and incorporated into PAH/DEXS capsules.[179] $AgNO_3$ was used as precursor for the formation of silver NPs and reduction was performed at 50 ^oC in the presence of poly(ethylene glycol) (PEG). The formed composite capsules showed thicker shell with a uniform NPs distribution. Other methods for *in situ* synthesis of inorganic NPs into the capsules shell include chemical condensation and ion-exchange reactions. Fe_3O_4 NPs were synthesized by chemical condensation of Fe^{3+} and Fe^{2+} ions in the suspension of PAH/PSS or polylysine/dextran sulfate capsules.[179] Shchukin *et al*. employed ion exchange reaction method to *in situ* growing inorganic particles into polyelectrolyte microcapsules.[8] In general, the template core was covered with insoluble PAH/citrate complex where citrate ion was substituted to desired anion that acted as precipitating agent to grow the insoluble inorganic phase exclusively inside the shell by simple exposing of the capsules to solution of corresponding cation. As a result, YF_3, magnetite Fe_3O_4, and hydroxyapatite $Ca_{10}(PO4)_6(OH)_2$ composite microcapsules were shown as examples of this approach.

Compared with the two step incorporation approach, such *in situ* synthesis and assembly method shows advantages in control the NPs distribution and saving time. Notably, this kind of method has lots of attractive advantages, however, such approach has not been intensively studied. More research works are needed to promote the development and application of the *in situ* synthesis and assembly method to incorporate inorganic NPs into polymer matrixes to obtain unique and novel functional materials.

2.6.2 Different Types of Inorganic NPs

2.6.2.1 Metal NPs

Embedding noble metal NPs within ultrathin films is important in materials research because of their unique electronic, catalytic, and optical properties.[172] Plasmonic gold NPs have been demonstrated unique size-dependent optical and photothermal properties due to their collective oscillation of free electrons in the conduction bands.[180,181] Gold NPs with different shape like nano-rods, nano-shells and nanopheres have been verified a tunable photothermal response to NIR light, radio frequency (RF) radiation and laser.[181,182] For the capsules with incorporation of gold NPs, upon irradiation, the major part of the absorbed light energy by each nanoparticle is transformed into heat. The use of silver NPs was also reported.[179,183,184] S. Anandhakumar, *et al.* successfully synthesized and assembled silver NPs within poly(allylamine hydrochloride) (PAH) / dextran sulfate (DS) capsule shells. The formed composited capsules with porous structure, rougher surfaces and thicker shells, as shown in **Figure 2.18**, proved to be more permeable to big molecules, *i.e.* FITC-dextran of 70 kDa.[179]

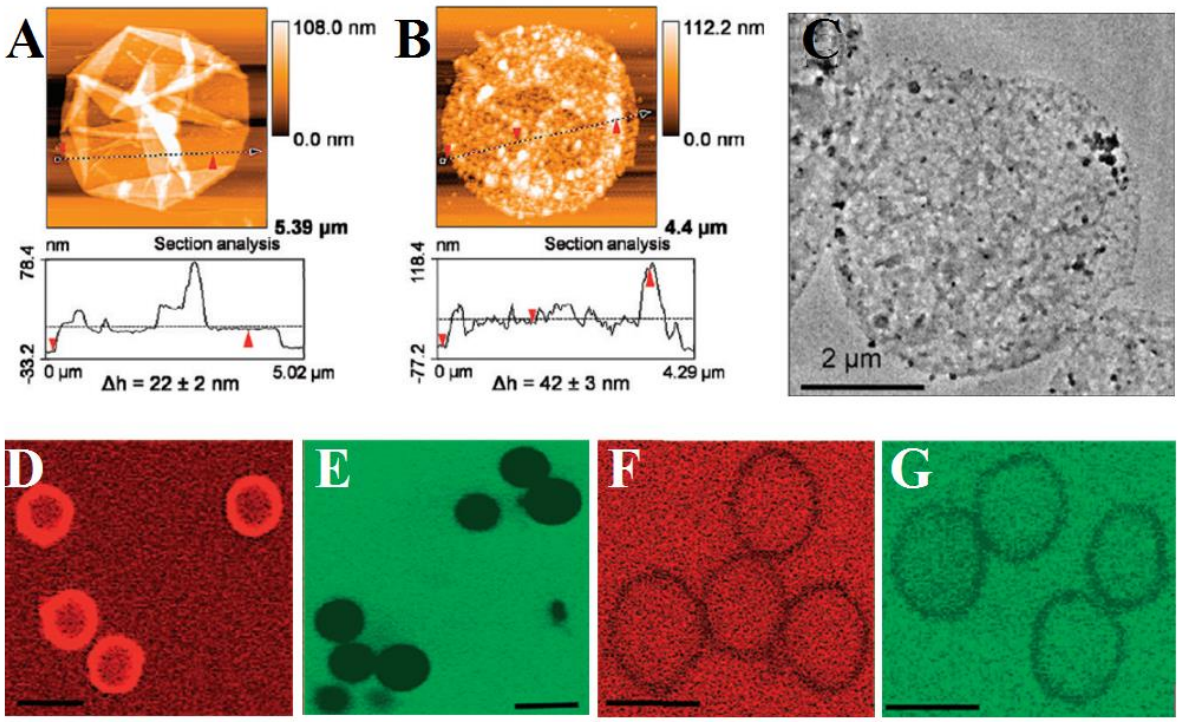

Figure 2.18 Deposition of silver NPs in the PAH/DEXS capsule shell at 25 mM $AgNO_3$ concentration. AFM images of hollow capsules without (A) and with (B) incorporated silver NP and corresponding TEM image (C) of silver NP incorporated capsules. CLSM images of capsules without (D, E) and with (F, G) silver NPs incorporated capsules treated with rhodamine (D, F) and FITC-dextran of 70 kDa (E, G). Scale bar = 5 µm.[179]

One of the attractive application for these metal NPs based on their collective effect to amplify the heating effect upon light irradiation, resulting in an increase in temperature in the surrounding areas.[185] The collective effect is due to under the plasmon resonance phenomenon. For example, when the the energy of incident photons is close to the plasmon frequency of an Au NP, the heating effect will become especially strong.[185] Therefore, by embedding the metal NPs into the walls of polyelectrolyte capsules, the integrity/ permeability of the walls can be selectively perturbed.[18,186] Additionally, in recent years, platinum(IV) that was pre-conjugated to PLL was assembled with poly(glutamic acid) (PGA) through a LbL approach, obtaining one

kind of biodegradable PGA/PLL-Pt(IV) multilayer capsules.[38] Such composite capsules showed great potential in anti-cancer application.

2.6.2.2 Oxide NPs

Besides the above-mentioned metal NPs, various oxide NPs are also developed as modifying agents to functionalize polyelectrolyte capsules. One typical example is iron oxide, of which the unique magnetic properties make them attractive candidates as one of advanced biomedical materials. In practical applicaion, they can serve as contrast agents in MRI, as miniaturized heaters capable of killing malignant cells and as colloidal carriers for drug delivery targeted at cancer diagnosis and therapy.[13,187,188] The negatively charged citrate-stabilized Fe_3O_4 NPs were facilely assembled into PAH/PSS capsules, and the obtained magnetic-responsive composite capsules were demonstrated with a potential in targeted delivery in cells.[13] Other inorganic particles such as SiO_2, $MnFe_2O_4$, Gd_2O_3, and TiO_2, which have undergone *in vitro* and *in vivo* investigations as targeted theranostics, were proved to be useful functionalization materials for polyelectrolyte capsules.[189]

SiO_2 NPs are among the most abundant and widely used synthetic materials applied in drug delivery systems, as it is water dispersible and generally accepted as biocompatible and nontoxic to cells.[30,30,190,108,191] It is already proved by the researchers, in recent year, amorphous silica can be dissolved and degraded in biological systems[190] and the biodegradation by-product of silica is the nontoxic silicic acid that is naturally found in numerous tissues.[30,108,191] These silicic acid can act as a source of Si and is useful for the formation of connective tissue such as bones.[191] Furthermore, the excess silicic acid in human body can be efficiently excreted from the body through the urine.[192] And the hydrophilic surface of the SiO_2 NPs is favourable for cellular uptake. Therefore, silica is a promising additive to modify polyelectrolyte microcapsules. Usually, SiO_2 NPs are pre-fabricated and introduced by the Pickering emulsion polymerization method. For example, by this method,

polyacrylamide/silica (PAM/SiO_2) composite capsules consisted of a particle monolayer and inner polymer layer were synthesized.[193] The robust SiO_2 can effectively strengthen the capsules' mechanical strength and increase their shell thickness. One of the major disadvantages of such method is the challenge to control the size of the formed composite capsules.

TiO_2 NPs have been widely used in various areas such as photocatalysis, solar cells and cosmetics industries, due to its excellent biocompatibility, good chemical stability, and great UV-responsive performance.[194-196] In terms of drug delivery systems, it is expected that the drug carriers embedding with TiO_2 NPs would possess UV sensitivity and could be used for UV-induced release.[123,197] Until now, there are only a few reports that were associated with TiO_2-polymer capsules.[198] In 2003, polyamide microcapsules were coated with TiO_2 by liquid phase deposition (LPD), yielding hybrid polymer/TiO_2 capsules with enhanced mechanical strength.[199] J. Marques, *et al.* synthesized one polymeric microcapsule bonded with TiO_2 NPs, which was proved to be able to release the encapsulated volatile compounds from them upon UV irradiation.[200] Such reservoirs were expected to find applications, for example, in the controlled release of insecticides, repellents, or fragrances, amongst other substances.

2.6.2.3 Fluorescent Semiconductor NPs

Practical applications often require the drug carriers with the ability to be visualized in biological media or in tissue, in order to realize the tracing, detection and monitoring of therapeutic efficacy simultaneously.[201-203] For this purpose, polyelectrolyte capsules were usually labelled with fluorescent agents which endow them optical properties for easy tracing by detecting their fluorescence signal. The most widely used fluorescent agents for labelling polyelectrolyte capsules are organic dyes, which are particularly advantageous in biological

research because of their low toxicity and high sensitivity.[204,205] But their intrinsic photoquenching feature limits their applications for long-term tracing.[206] To solve this challenge, semiconducting quantum dots (QDs) is developed as another attractive fluorescent imaging agent, which is not only due to their better stability and intensive fluorescence compared with traditional organic dyes, but also because of their excellent resistance to photobleaching allowing them suitable for long-term measurements.[206] They have emerged as versatile tools for biological imaging. By incorporation with the luminescent colloidal CdTe and CdSe QDs, the obtaind polyelectrolyte/QDs composite capsules were proved to be endowed with an excellent fluorescent property.[170,207-209] However, semiconducting QDs have certain problems associated with the inherent heavy metal toxicity, high cost and bad biocompatibility.[187]

2.6.2.3 Carbon Related NPs

Recently explored fluorescent carbon dots (CDs) with tunable emission show excellent superiority in biochemical applications over semiconductor QDs and conventional organic dyes due to their excellent biocompatibility, low photobleaching, chemical stability, and facile production with low cost.[210] Indeed there have been many successful reports on the synthesis of CDs [35,211,212] and applied them as bio-imaging agents and sensors, but to our best knowledge, only one publication about assembly them into polyelectrolyte capsules was report in 2013 and no further work related to this topic was continued.[213] In fact, Xiaoling Yang and the co-workers first reported carbon dots-embedded polyelectrolyte microcapsules, and proved their fluorescent property.[213] Utilizing the method of pre-loading the pre-fabricated CDs inside meso-porous silica templates followed by LbL polyelectrolyte coating and the method of assembly the pre-fabricated CDs after PAH layer on the sacrificial templates, these CDs-embedded capsules were obtained. The used CDs were approximately 3-4 nm in size and -38.3

mV in zeta-potential value. Obviously, the attached CDs in polymeric layers were driven by electrostatic absorption force. However, morphology and hollow structure of the formed polyelectrolyte/CDs capsules can't be found in the fluorescent images and they were all collapsed under dry state, as indicated by SEM images. Additionally, permeability of such weak fluorescent capsules was not investigated in the report. Hence, to achieve one ultra-strong fluorescent capsules with excellent biocompatibility, developing one technique to incorporate the CDs within polyelectrolyte capsule shells is needed in the near future.

Different from CDs, there are few reports about incorporation of carbon particles with bigger size into polyelectrolyte capsules. For example, carbon nanotubes, one kind of cylindrical graphene sheets, which can be used for hyperthermic ablation of cancer cells due to their strong optical absorption in NIR region as well as for drug delivery to cancer cells owing to their high surface areas, were used as NIR absorber to modify polymeric capsules.[214,12] Haruyuki Saito and Noritaka Kato assembled single-walled carbon nanotubes (SWCNTs) into polyelectrolyte capsules based on a combination of the layer-by-layer and template-assisted methods. They proved that the anti-cancer drug was post-loaded into the capsules and released by NIR laser irradiation.[12] Another carbon related NPs, graphene oxide (GO) sheets, were introduce into PAH/PSS capsules *via* LbL assembly on erythrocyte cell templates and the properties of the formed hybrid graphene oxide/polyelectrolyte were studied but their superiority in biomedicine area was not well proved.

2.6.2.4 Other NPs

In addition, to date, functional composite capsule with other kinds of oxides, including $LiNbO_3$,[215,216] $CaCO_3$,[217] YF_3,[218] *etc.* were reported as well. Usually, incorporating rigid

inorganic NPs into soft polymeric multilayer should improve the mechanical strength, for example, the effects of YF3 precipitation on the mechanical properties of polyelectrolyte multilayer capsules were studied and reported by Frédéric Dubreuil, *et al.* in 2004. Except of the NPs that are already reported, there are still lots of inorganic NPs with attractive properties but have not been employed as modifiers to functionalize polyelectrolyte capsules, such as carbon nanowires, dielectric NPs, *etc.*

2.6.3 Encapsulation Cargo Substances in Composite Capsules

Generally, two ways can be used to encapsulate cargo substances inside the cavities of composite capsules: pre-loading and post-loading. For the preloading method, it is similar with that of pure polyelectrolyte capsules. Species of interest can be preloaded either by means of co-precipitation or by physical adsorption/pore diffusion into templates. But post-loading presents big differences especially for the capsules with *in situ* incorporated inorganic NPs. Because their sensitivities to pH, light and ion strength change, the regulation of such conditions that can be used to reduce shell permeability of pure polyelectrolyte capsules may not be effective and useful for composite capsules. Small molecules like DOX should be able to diffuse inside their cavities or attach in the composite shells, but most of the DOX diffuses outside during the washing procedure and only left a small amount in the capsules. Hence, problems matter in the post-loading method for composite capsules. In order to seal the substance inside, the permeability of capsules must be reduced. For *in situ* incorporating NPs in polymer capsules, one possible way is to *in situ* encapsulate small molecules during the NPs synthesis and assembly process. But such method have not been reported previously.

2.6.4 Stimuli Induced Release from the Composite Capsules

Apart from loading cargos, another main task for drug delivery systems is controlled release the payload at the targeted area. Different from pure polyelectrolyte capsules, the methods to change the shell permeability or rupturing the shells of composite capsules are mainly physical method. Generally, this can be achieved by external physical triggers, such as ultrasonic treatment, magnetic fields, laser and UV irradiation.

2.6.4.1 Magnetic Fields

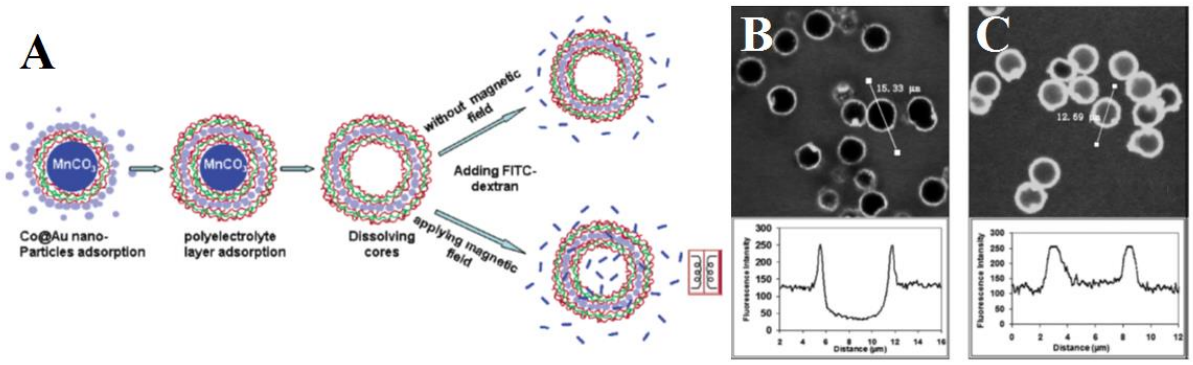

Figure 2.19. Scheme of the assembly and permeability test for microcapsules embedded with Co@Au NPs under an oscillating magnetic field. CLSM image of the formed magnetic capsules $[(PSS/PAH)_4(PSS/Co@Au)_1(PSS/PAH)_6]$ mixed with FITC-dextran (B) without applying an alternating magnetic field for 1 hour and (C) after applying an alternating magnetic field for 30 mins. The corresponding optical density profiles are also shown.[220]

One of the main functions of magnetic field applied in drug delivery systems is targeting the capsules embedding with magnetic NPs (*e.g.*, Fe_3O_4). If the magnetic field is also used for triggered release of these magnetic capsules, it is expected that the therapeutic performance of capsules is improved.[219] It was demonstrated by Lu and the co-workers that the permeability of capsules were adjusted by magnetic field, due to their influence on the NPs aggregates.[220] Ferromagnetic gold-coated cobalt (Co@Au) NPs were incorporated into PAH/PSS multilayers

together, forming the $(PSS/PAH)_4(PSS/Co@Au)_1(PSS/PAH)_6$ capsules, **Figure 2.19**, and then the formed capsules were treated by alternating magnetic fields (100-300 Hz, 1200 Oe). The data showed an increased permeability and a consequent release of the encapsulated cargos.[220]

The release from the magnetic capsules is usually not caused by the shell rapture, but attributed to the phase transition of the lipid membrane, rotation and motion of the embedded magnetic NPs, or by heat effects of magnetic NPs under magnetic field.[17,219] The site-specific release of encapsulated doxorubicin from liposomes under a static magnetic field was found, as a result of liposome melting induced by a local temperature increase.[221] Although these previous works probed that magnetic activation is a good choice to trigger magnetic capsules, a problem for biological applications is that, in order to permeabilize the drug containers, long exposure time and strong magnetic intensity are needed, and the resulted increase in temperature not good for the tissues and the body.

2.6.4.2 Mechanical Deformation

Mechanical property is an important issue for microcapsules. Capsules have to provide enough robustness to avoid membrane rupture before they release the protect cargos. In addition, for artificial microcapsules, shell rupture induced by external triggers can serve as a pathway for fast and efficient release. The mechanics enhancement of soft polyelectrolyte capsules can be achieved by incorporating rigid inorganic NPs, such as gold, silver, Fe_3O_4, carbon nanotubes, *etc.*, and the formed composite capsule can be ruptured by mechanical force and let the payload release outside.[214,219,222] Upon mechanical deformation, release of fluorescently labeled dextran molecules from capsules was detected and studied by Paulo A. L. Fernandes and the co-workers.[222]

2.6.4.3 Microwave Triggering

The term “microwaves” implies electromagnetic irradiation with a frequencies between 300 MHz and 300 GHz. Up to now, it already finds a biomedical application in a microwave therapy.[223] For changing permeability of capsules by microwaves, there are two ways: one based on the thermal effect of microwave radiation; the other based on possible oscillation effects on charged species of polyelectrolytes or proteins.[224,225]

Up to date, there have not been made of many efforts to rupture capsules shells by microwave radiation. It was shown that ferrite and carbon nanostructures effectively absorb microwaves and convert the electromagnetic energy to heat due to magnetic and dielectric losses.[224] Similarly, composite capsules containing this kind of NPs will be heated in a rapid and homogeneous.[226] Gorin *et al.* demonstrated the destruction of PAH/PSS microcapsules with Ag NPs in the shell under 2.45 GHz, 13.5 W/cm^2 microwave radiation.[227] The damage of the capsules shells was attributed to microwave heating of the Ag NPs. More recently, Gulyaev *et al.* exposed PAH/PSS microcapsules with three layers of magnetite NPs to microwave pulse that resulted in significant rupture of the shell.[228] Moreover, the microwave adsorption properties of inorganic NPs can be varied depending on their aspect ratio[229] that seems to be promising for design of microcapsules with tunable microwave adsorption.

2.6.4.4 Ultrasound-Triggered Release

Ultrasound, which is already employed as diagnostics and therapeutic method for many diseases, is promising due to its long penetration depth and low invasive nature.[14] Indeed, the response to ultrasound treatment of the capsules is varied by their shell composition. For pure polyelectrolyte capsules, ultrasound with high power and low frequency, for example, 120 W,

20 kHz[24] and 500 W, 20 kHz[23], can be applied to break the capsule shells. Such results are caused by the shear forces generated from acoustic cavitation in liquids under ultrasonic vibrations. If the polyelectrolyte capsules are functionalized by inorganic NPs (*i.e.*, Ag,[24] ZnO,[14] Fe_3O_4,[230] Au[231]), the shell permeability of the formed composite capsules is more sensitive to ultrasound.[16,23] Because the robust inorganic NPs enhance and accelerate the acoustic cavitation effect. The strengthened effect was attributed to the low elasticity and high brittleness of the nanoparticle/polyelectrolyte shell as well as the resulted higher density gradient, which led to reflection and superposition of the acoustic waves.[23]

Effect of ultrasound on microcapsules was studied in the literature. For example, rupturing of composite microcapsules with ZnO NPs was shown to be dependent on shell construction, ultrasonication time and power of the ultrasound, as show in **Figure 2.20**.[14] The CLSM images indicated that with the presence of ZnO NPs in the shell, the sensitivity to ultrasonic treatment of such microcapsules drastically increased, showing that pure polyelectrolyte microcapsule were only slightly deformed while the capsules with ZnO NPs were broken into fragments within a few seconds. Interestingly, the size of the pieces decreased when increased the ultrasound treatment time and increased the amount of ZnO NPs in the shells.

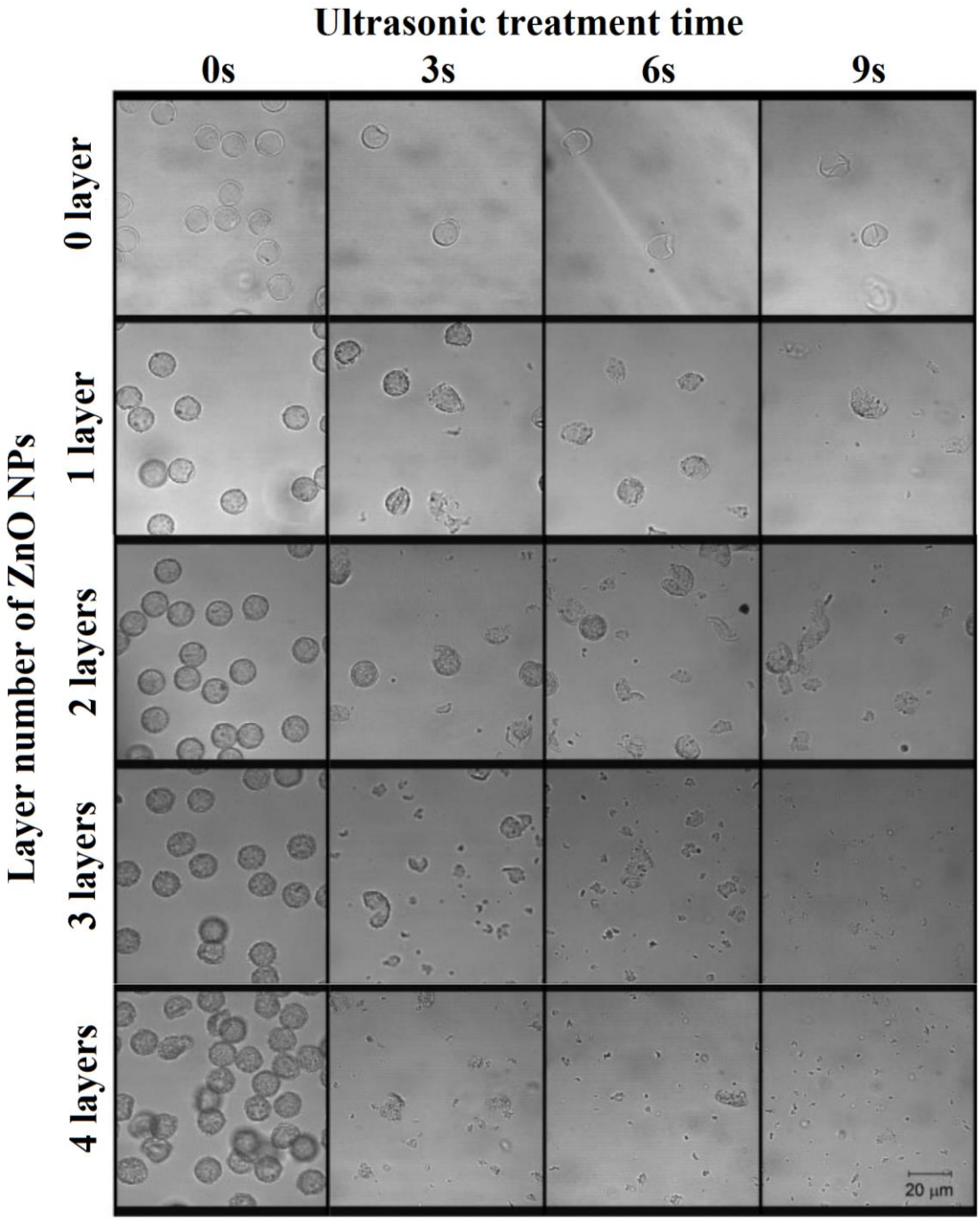

Figure 2.20 CLSM investigation of microcapsule response to ultrasound with respect to the sonication time and capsules shell composition.[14]

It is worth mentioning that the low frequency ultrasound at high power is not suitable for practical biomedical applications, because the strong wave intensity might cause permanent damage to tissue or body. In order to minimize the side effects, ultrasound of low power and

high frequency (~1 MHz) is employed in recent years in medicine. In practice, it is already used for diagnosis, and also for treatment of diseased or injured organs or bodily structures which is quite distinct from diagnostic ultrasound applications.[232] Compared with low-frequency ultrasound, the focusing ability of high-frequency ultrasound is better. Thus, several high frequency ultrasonic transducers can be focused in one small region to create a relatively high power intensity, and avoid bring damage to the tissue by controlling the energy level. In addition, as ultrasonic oscillations of matter are mechanical in nature, in order to maximize effect, the microcapsules size should be relevant to wavelength of oscillations, which, for water dispersion, would be about 7 cm for 20 kHz and 1.4 mm for 1 MHz. Hence it might be expected, that higher frequencies would be more effective as the wavelength is closer to the size of the object being irradiated. Furthermore, some change in effect would be expected to occur when introducing rigid NPs inside soft polymeric shells, because the rigid particles increase the movements of the shells, stimulating cargo release from the containers. Moreover, the presence of NPs will also favour the formation of bubble nuclei decreasing the cavitation threshold.[233] V. F. Korolovych, *et al.* investigated the impact of high-frequency (1.2 MHz) ultrasound with a power density of 0.33 $W \cdot cm^{-2}$ on microcapsule nanocomposite shells with embedded ZnO NPs *via* modelling simulations and direct visualization. The results revealed that the nanocomposite microcapsules were destroyed more effectively by the action of high-frequency (1.2 MHz) ultrasound in comparison to the low frequency (20 kHz) one with the same power density.[234] The corresponding simulations was given in **Figure 2.21**.

The simulations in **Figure 2.21** demonstrated that an increase of ultrasound power and its frequency leads to an increase of the equivalent stress on the shell surface, and that increasing the microcapsule shell thickness reduces the amplitude of deformations emerging on the surface.[234] In summary, rigid NPs enhanced the response of capsules to ultrasound, and with

high frequencies we get the possibility of more effective (in effect/power terms) focused irradiation.

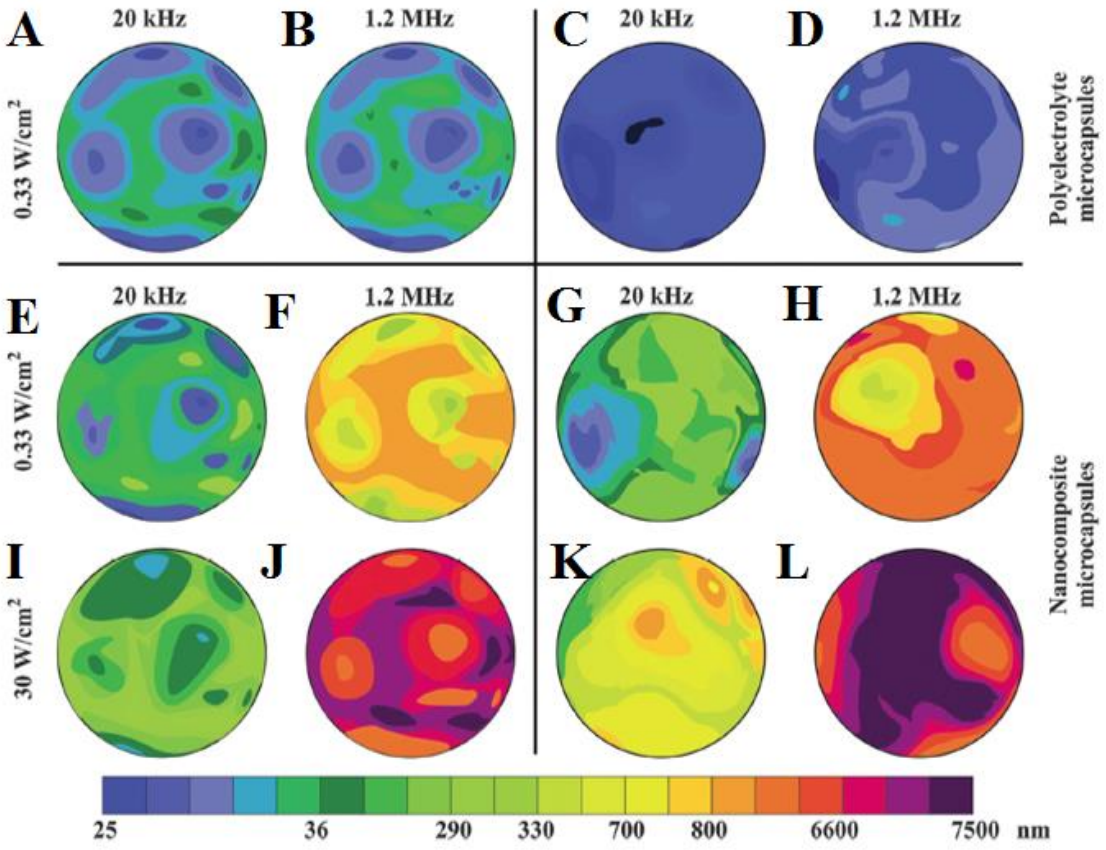

Figure 2.21 The deformation distribution in the polyelectrolyte microcapsule shells with a thickness of 17 nm (A, B) and 32 nm (C, D) under the influence of low (20 kHz) and high frequency (1.2 MHz) ultrasound at a power density of 0.33 $W \cdot cm^{-2}$. The deformation distribution for the nanocomposite microcapsule shells with a thickness of 256 nm (E-H) and 97 nm (I-L) under the ultrasound influence with given parameters.[234]

2.6.4.5 UV Irradiation

UV sensitive vesicle is one of the optimized options for applications in agriculture, environment and cosmetics areas, due to the abundant existence of UV light in sunlight. Capsules with ultraviolet (UV) light sensitivity are desirable for controlled releases, and the

fabrication of such capsules can be generally categorized into two approaches. The first approach is using polyelectrolytes with either photo-responsive or photo-cleavable groups as the layer material. Examples included LbL microcapsules containing azobenzene using poly[1-[4-(3-carboxy-4-hydroxyphenylazo)-benzenesulfonamid o]-1,2-ethanediyl, sodium salt] (PAZO) and PDADMAC as the assembling materials, and the UV responsiveness was achieved by UV induced isomerization of PAZO.[14,15] However, such an approach is constrained by the building materials and polyelectrolytes where special groups have to be used. The second approach is to assemble inorganic NPs that can absorb UV light. Due to its excellent biocompatibility, great UV-responsive performance, and good ability of immobilizing biomolecules onto their surfaces, TiO_2 NPs have been widely used.[194, 235,26] However only a few reports involved TiO_2-polymer capsules based on pre-fabricated NPs.[2, 19, 20] Most of these research demonstrated that it was possbile to introduce TiO_2 NPs into polymer shells, but they have not proved those composite with the potentials of loading cargos. Recently, fluoroalkyl silane (FAS)-loaded polystyrene capsules with size from 150 nm to 890 nm were synthesized *via* Pickering emulsion polymerization using SiO_2 and TiO_2 NPs as the Pickering agents, wherein the nanoparticles were modified with a Triton X-100-tethered silane coupling agent. The formed capsules were demonstrated with UV responsiveness, showing a UV-induced release of the encapsulated FAS.

2.6.4.6 Laser Irradiation

In the past decades, the use of NIR light is particularly attractive in biomedical applications due to the weak absorption in this range by most tissues. Hence, the development of NIR laser responsive drug carriers gained more and more attentions from the researchers. In particular, laser-induced permeability change can be divided

into two groups: (1) by heating, happened upon irradiation absorption by some agents (nanoparticles), or (2) by photochemical reactions.

The first mechanism is based on heat generation when the radiation is adsorbed by the active agents. The increased temperature can change the shells' permeability properties. However, usually pure polyelectrolytes are not sensitive to laser irradiation. In order to endow capsules with laser responsiveness, modifying agents have to be incorporated into the capsules shells. To date, researcher assembled the negatively or positively charged substances such as silver and gold NPs with proper size into LbL capsules. The schematic of the process is given in **Figure 2.22**. These embedded NPs can be heated by the laser irradiation, which leads to the structure change of the shells and finally results in the release of payload. It is worth mentioning that the release can be achieved without a complete rupture the whole shells, but just by reversible permeability change.

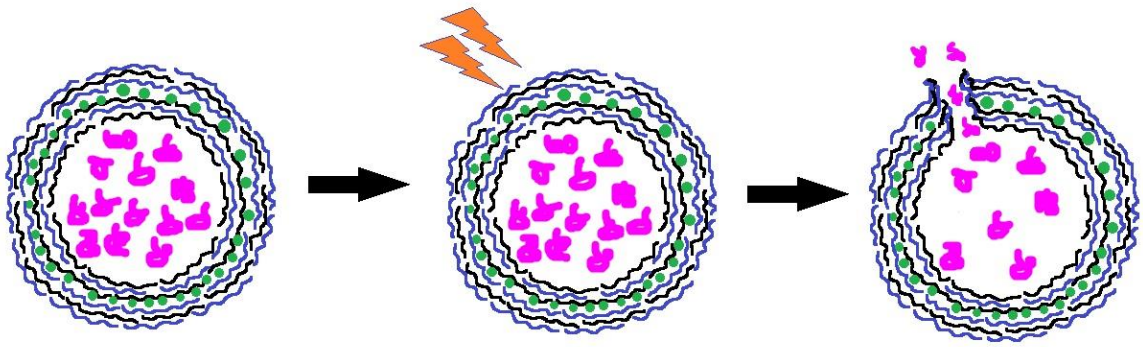

Figure 2.22 Laser-induced release by heat generation of NPs.

With a good biocompatibility, silver NPs were firstly proposed and employed as light-absorbing agents to modify the polyelectrolyte capsules.[179] S. Anandhakumar and co-workers prepared the PAH/dextran sulfate capsules *via* LbL technique and incorporated with Ag NPs by *in situ* synthesis and assembly process. For formed composite capsules

displayed a strong response upon laser irradiation, showing a complete destruction after only 10 seconds of laser irradiation, **Figure 2.23**.[179]

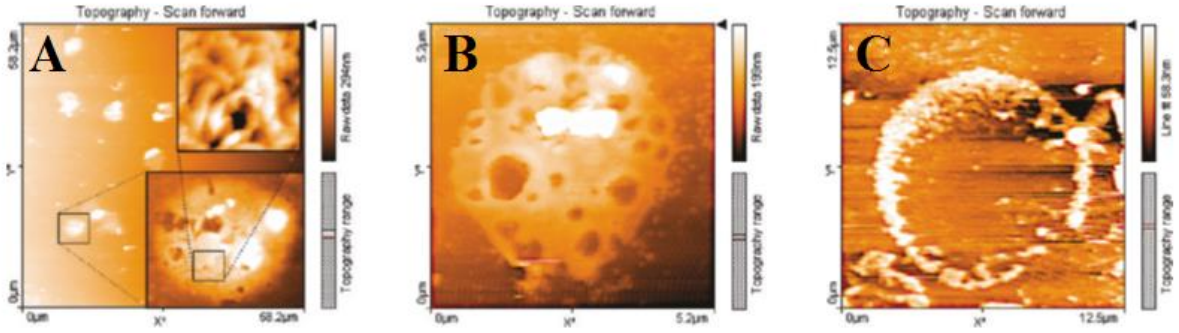

Figure 2.23. AFM investigations to show rupturing of silver NPs deposited capsules under laser exposure. Ruptured capsules after (A) 5, (B) 8, and (C) 10 s of laser exposure. Insets show the zoomed cross-section areas of the image marked in rectangular boxes.[179]

In a similar way, gold NPs with a good biocompatibility can also absorb NIR light and induce heating effect, which means that NIR laser irradiation can be used to modify the permeability of the capsule with incorporation of gold NPs.[18,236-238] The gold NPs with carboxyl groups on their surface were incorporated into polyelectrolyte multilayers *via* a combination with PAH.[236] The report proved the formation of the PAH/Au composite particles and finally resulting in the disruption of the composite membrane.[236] Very recently, the capsules can be broken by NIR laser irradiation, because the gold NPs can absorb IR-light causing in a local heating of the network of Yingjie Wu and the co-authors demonstrated that a membrane fusion of polyelectrolyte multilayer based microcapsules bearing surface-attached gold NPs can be achieved by laser irradiation the composite capsules in aqueous media. The whole fusion process of two connected capsules was observed by SEM and optical microscopy, as shown in **Figure 2.24**.[238]

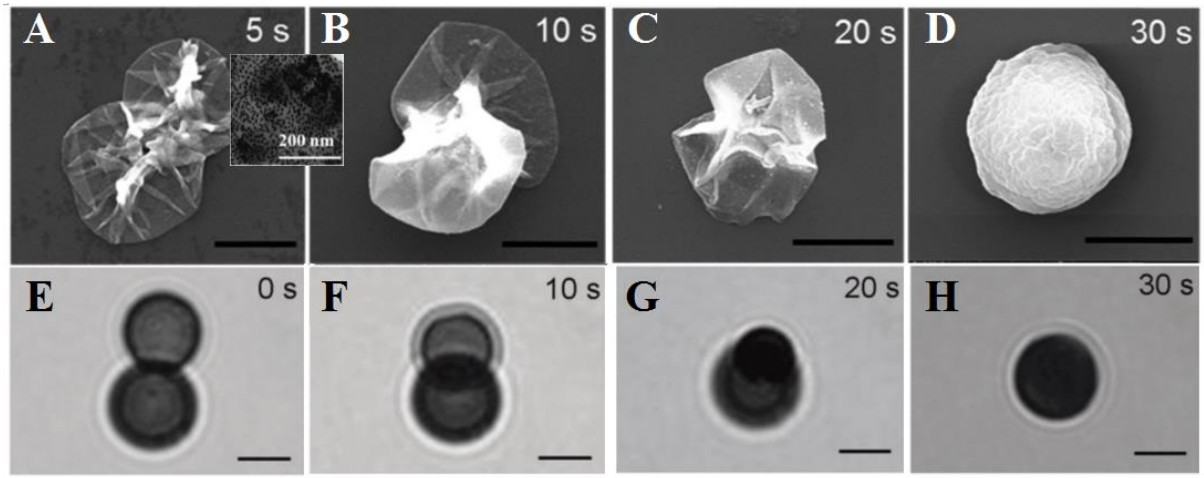

Figure 2.24 Representative SEM (A-D) and optical microscopy images (E-H) of the fusion of two $(PDADMAC/PSS)_5$/Au microcapsules with a gold NP surface coverage of 30%. Scale bar = 5 μm.[238]

Gold and silver NPs are known to produce heat upon light absorption due to surface plasmon resonance (SPR).[238,239] The electrons oscillation in the electromagnetic field of the irradiation caused the adsorption by the NPs with a narrow peak at specific position. The previous reports demonstrated that the position of the adsorption peak can be adjusted by the NPs properties, such as varying their size, as shown in **Figure 2.25**.[1] In terms of Ag and Au NPs, usually their plasmon resonance peak positions are around 420 and 520 nm, respectively. As mentioned above, however, biomedical applications require the response to the light in the IR region, where the tissues are more transparent, than for visible or UV light.[240] Instead of controlling the size of the NPs, to solve this problem, aggregations of small metal NPs were proposed to use, because the plasmons of the NPs situated nearby are coupled, and consequently showing a shift of the adsorption peak to the red range.[1]

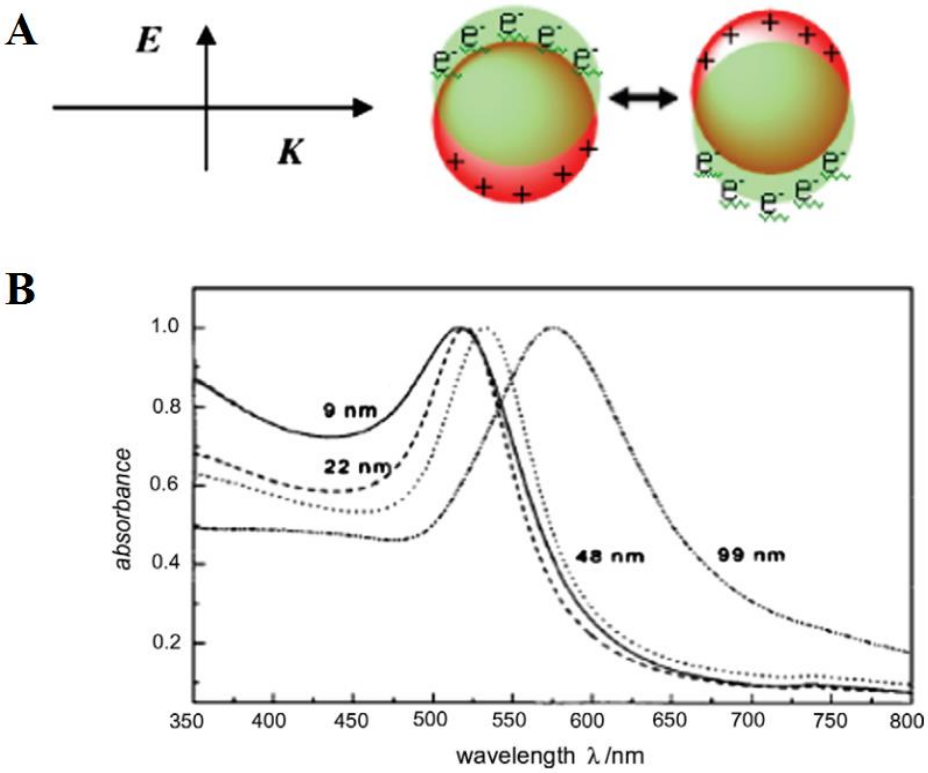

Figure 2.25 (A) Schematic illustration of surface plasmon resonance in plasmonic NPs.[1] (B) Extinction spectra of gold NPs in different sizes. The electric field of incident light induces coherent collective oscillation of conduction band electrons with respective to the positively charged metallic core. This dipolar oscillation is resonant with the incoming light at a specific frequency that depends on particle size and shape. For gold NPs, the SPR wavelength is around 520 nm depending on the size of the NPs.[241]

At the very beginning, the studies of employing NPs to modify the microcapsules involved a great amount of NPs and pulsed laser source with higher energy density, resulting in destruction of the containers. Then in later research, a more mild 840 nm pulsed laser was used for the IR irradiation, and it was focused onto an individual microcapsule.[15] Since high concentration of the metal NPs and high irradiation energy density might induce more side effects on the tissues and the body, Skirtach and the co-workers made efforts to solve this challenge, by

incorporating relatively low amounts of pre-aggregated gold and employing constant laser with average intensity much lower instead of using the single pulse intensity of pulsed lasers.[21,242]

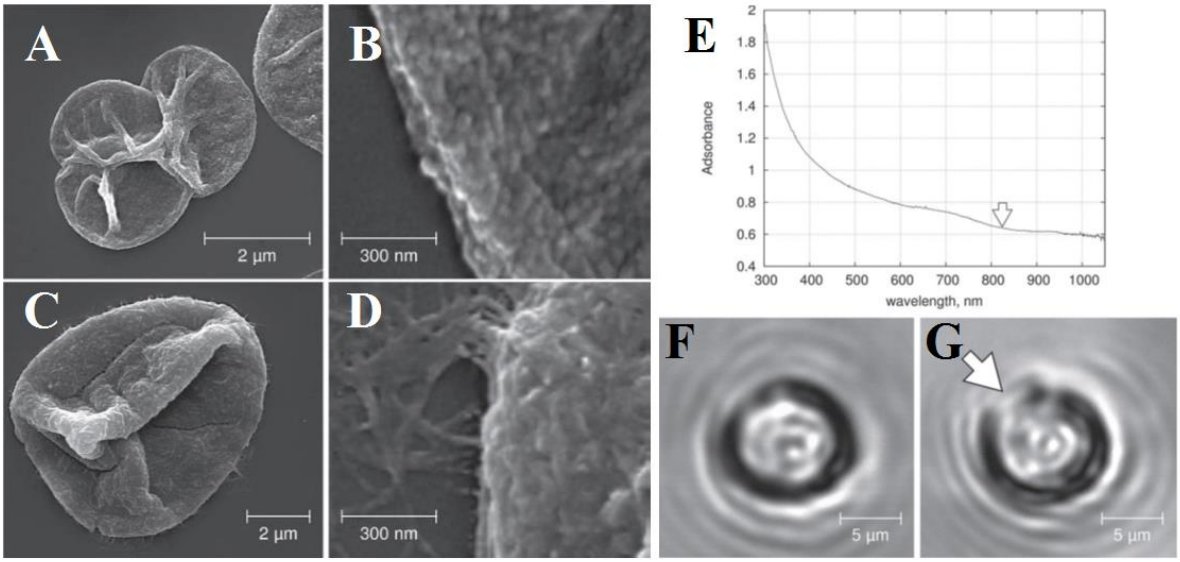

Figure 2.26 SEM images of microcapsules: (A, B) with glutaraldehyde treatment and without carbon nanotubes; (C, D) with glutaraldehyde treatment and carbon nanotubes in the microcapsule shells; (E) Absorption spectrum of carbon nanotubes in water; Optical microscopy images of microcapsules before (F), and after (G) near-IR laser (830 nm) activation. The scale bars in b and c correspond to 5 µm. The arrow in E indicates the laser wavelength, while the arrow in G shows the laser spot used for remote opening.[214]

Besides plasmonic materials, CNTs and graphenes also possess strong absorption in a wide range of wavelength. To date, a few reports are about the application of photothermal activities of CNTs and graphenes to therapies using NIR light.[12,214,243,244] Those works proved that CNTs and graphenes are good NIR-absorbing agents for the NIR-responsive capsules. For example, CNTs were facilely assembled onto surfaces of the polyelectrolyte shells, showing thicker folds and filber-like particles on the surfaces after CNTs incorporation, **Figure 2.26 A-D**. The formed composite capsules were successfully broken by NIR laser irradiation, as showing in **Figure 2.26 E-G**. The advantages of CNTs and graphenes include that they are

cheap in cost compared with gold and silver NPs, and that their property of light absorption does not depend on the size or shape of the capsules,[214] whereas the gold nanostructures show a significant dependence of the absorption spectra on its shape and size.[245]

2.6.5 General Current Challenges of Composite Capsules

It can be clearly seen, that by the time LbL is highly developed technique, especially when it comes to control of chemical and physical properties of microcapsules. Benefiting from its great advantages of the feasibility to assembly various charged polymers and to incorporate different kinds of charged inorganic NPs or other objects into the shells, a huge amount of functional composite capsules were prepared and investigated in the past few decades. Different species can be encapsulated inside the cavities of capsules and be released by external stimuli under control. However, challenges still exist in this area, for example, design and synthesis of capsules with the abilities: (1) loading small molecules; (2) multifunctional properties; (3) fluorescent, good photo-stability and chemical durability; (4) good biocompatibility.

As mentioned, incorporation of pre-fabricated inorganic NPs can't bring significant change in shell permeability, and *in situ* growth and assembly of NPs in polyelectrolyte multilayers indicates the possibility but lacks of research on this issue. Hence, in this thesis, we utilize the *in situ* growth and assembly method to incorporate inorganic NPs and to investigate the best reaction conditions for each kind of NPs we choose. Hopefully, with well control on the reaction conditions, the formed composite capsules will be fully and uniformly covered by *in situ* formed NPs, and the NPs and soft polymers will be stick firmly together resulting in a compact and densified composite shells with lower permeability. In total, three different inorganic NPs are chosen as examples. Silica will be first chosen as modifier due to its good

biocompatibility, biodegradability and easy synthesis procedure based on sol-gel method. The morphology, structure, shell permeability, cell viability and degradation property of formed polyelectrolyte/silica composite capsules will be investigated. To realize multi-functionalities, a good UV absorber, TiO_2 will be used as an example to fabricate multi-functional composite capsule by *in situ* incorporating method. The use of CDs to functionalize polyelectrolyte capsules was very insufficient, even though CDs possess lots of superior advantages over organic dyes and semiconductor QDs. One method to *in situ* synthesis and assembly of CDs needs to be developed, which will have a great significance for the future research work in carbon related functionalization of polyelectrolyte capsules.

3. Materials, Methods and Instrumentation

3.1 Materials

3.1.1 Chemicals

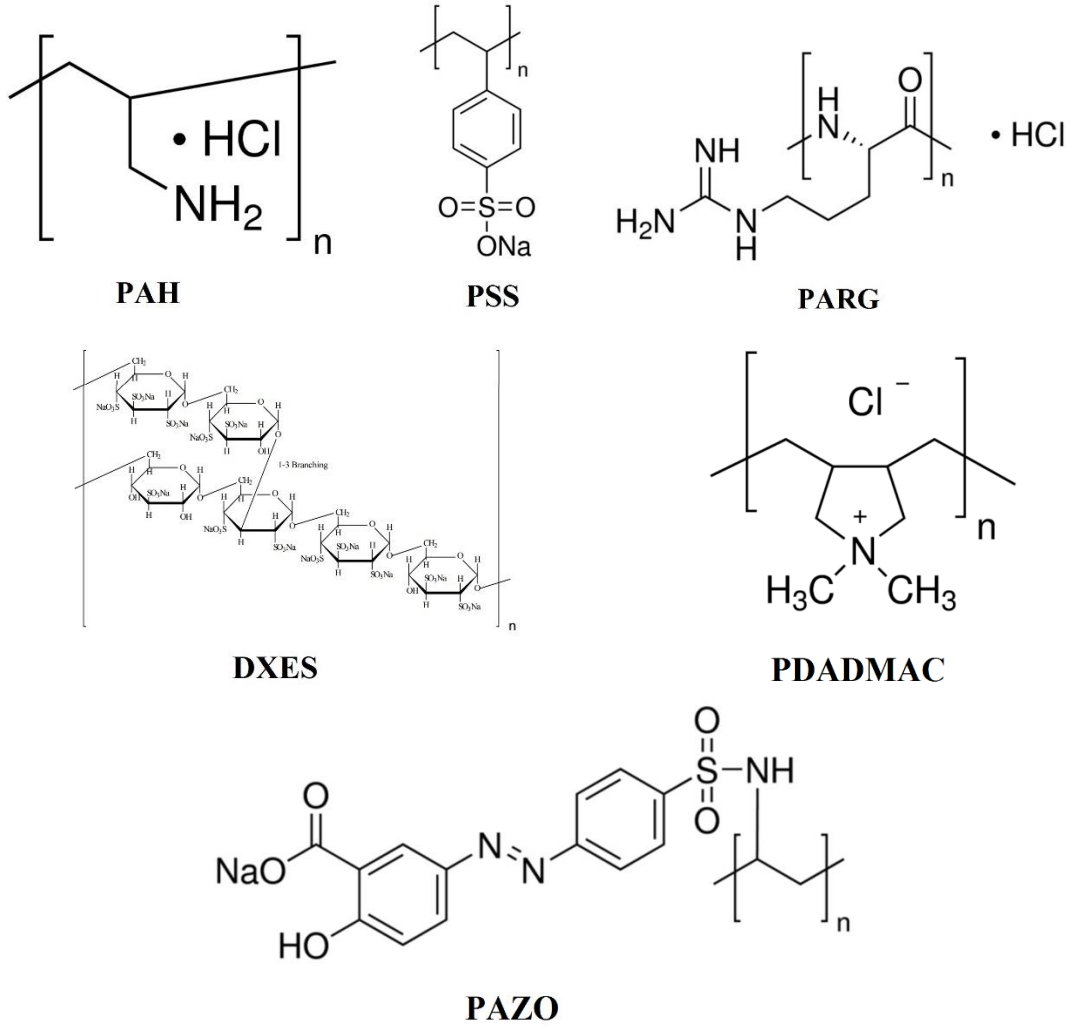

Figure 3.1 Structural formulas of polyelectrolytes used for capsule preparation.

Poly(allylamine hydrochloride) (PAH, 70 kDa), poly(styrenesulfonate sodium salt) (PSS, 70 kDa), poly-L-arginine hydrochloride (PARG, 15-700 kDa), dextran sulfate sodium salt (DEXS, 10 kDa), poly(diallyldimethylammonium chloride) (PDADMAC, 200-50 kDa, 20 wt% in H_2O), poly[1-[4-(3-carboxy-4-hydroxyphenylazo)benzenesulfonamido]-1,2-ethanediyl, sodium salt] (PAZO, ~100 kDa), dextran, ethylenediaminetetraacetic acid (EDTA), sodium

carbonate (Na_2CO_3), $CaCl_2$, tetraethyl orthosilicate (TEOS, Si-$(OC_2H_5)_4$), titanium butoxide (TIBO), were purchased from Sigma-Aldrich. The structures of the polyelectrolytes are given in **Figure 3.1**. Silicon dioxide microparticles (SiO_2, 4.99 ± 0.22 μm) were purchased from microparticles GmbH (Germany). Other chemical agents including ammonium fluoride (NH_4F), ammonium hydroxide (NH_4OH, 28% NH_3 in H_2O), Hydrofluoric acid (HF, 48 wt. % in H_2O), and hydrogen peroxide (H_2O_2, 30%) were purchased from Sigma-Aldrich. All the chemicals were used as received without further purification. All solutions were prepared with water from three stage Millipore Milli-Q 185 water purification system (Millipore, USA) with a resistivity higher than 18.2 Ω·cm.

Rhodamine B (Rh-B, Mw = 479), Tetramethylrhodamine isothiocyanate-Dextran (TRITC-Dextan, 500 kDa), were purchased from Sigma-Aldrich. Their molecular structures are shown in **Figure 3.2**.

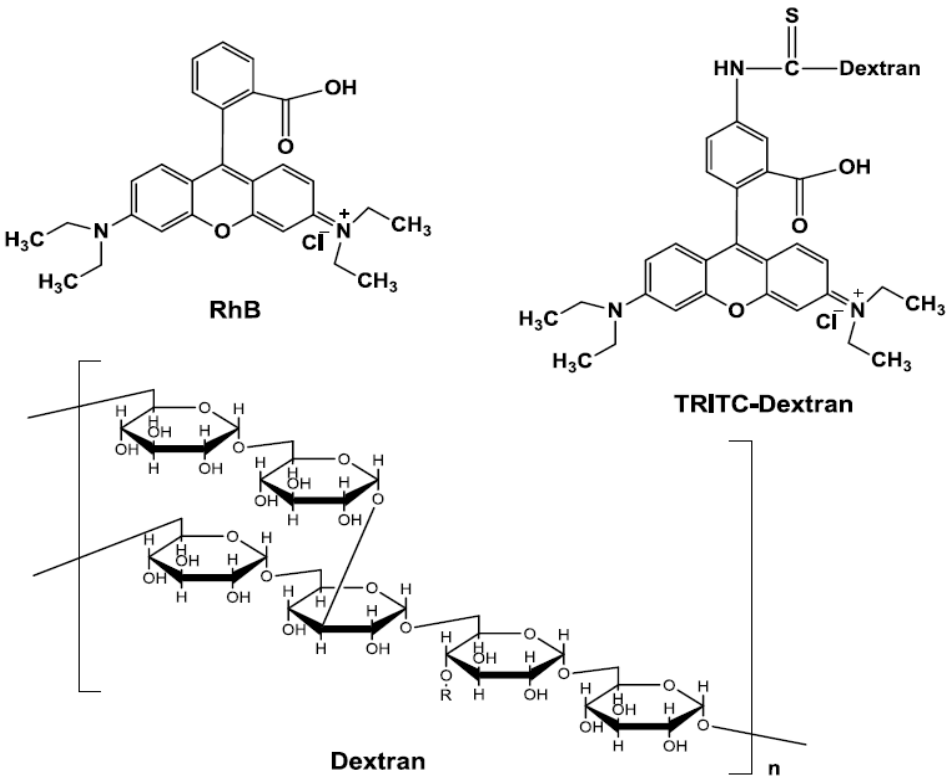

Figure 3.2 Structural formulas of fluorescent polymer and monomers.

Materials used for cell culture and cell viability studies including Dulbecco's modified eagles media (DMEM), fetal bovine serum (FBS), penicillin, streptomycin, trypsin, thiazolyl blue tetrazolium bromide (MTT) and methyl sulfoxide (DMSO) were also supplied by Sigma.

3.1.2 Consumables

For cells incubation, 35 mm µ-dishes were purchased from Ibidi, Germany. ULA flasks for cells incubation (25 cm^2, 75 cm^2) and pipettes (Corning) were purchased from Appleton Woods. Disposable 4.5 mL and 1.5mL cuvettes for UV-Vis-NIR spectroscopy and fluorimetry were also purchased from Roth (8128, 4.5 mL Acryl; Y196.1, 4.5 mL PMMA; Y197.1, 1.5 mL PMMA).

Cuvettes for zeta-potential and zeta-size measurements were purchased from Malvern.

3.2 Methods

3.2.1 Microcapsules preparation technique

For each experiment in this thesis, microcapsules were prepared following the same protocol, fitting it to meet exact needs. Usually, four bilayers of oppositely charged polymers were deposited on the employed template ($CaCO_3$ and SiO_2), and finally the template was dissolved. To form the polyelectrolyte layers, 2 mg/mL solutions of different polyelectrolytes were used. PAH and PSS were dissolved in 0.5M NaCl, while PDADMAC, PAZO, PARG and DEXS were dissolved in 0.15 M NaCl water solution. Depositing of each layer was performed under shaking for 15 minutes. After that, triple wash/centrifugation steps were carried out.

3.2.1.1 $CaCO_3$ templated microcapsules

$CaCO_3$ cores were prepared by adding equal volume of 0.33 M $CaCl_2$ into 0.33 M Na_2CO_3 solution under magnetic stirring. If any species with big molecular weight need to be encapsulated, they were co-precipitated, *i.e.* were mixed with $CaCl_2$ before addition of Na_2CO_3. After 30 second stirring, the solution was left for 5 seconds. After that, the precipitation was washed and collected (centrifugation at 5000 r/min for 30 seconds).

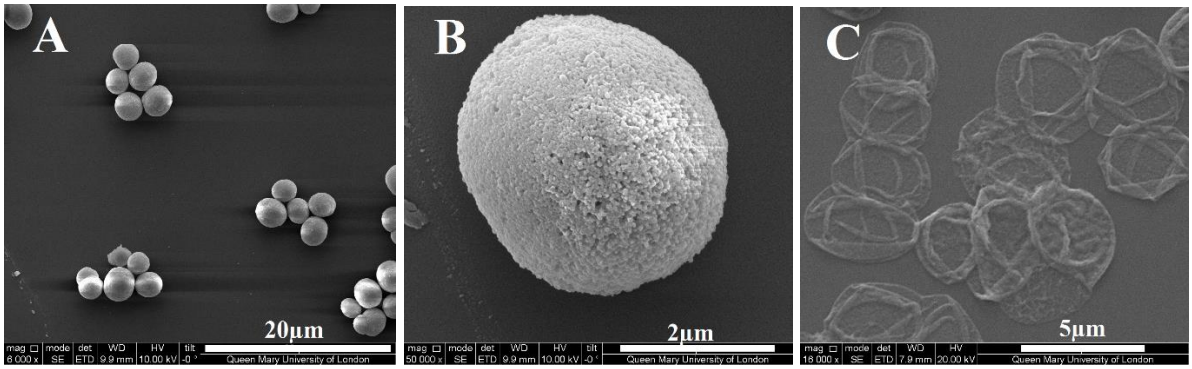

Figure 3.3 SEM images of $CaCO_3$ templates (A, B) and $(PAH/PSS)_4$ microcapsules (C) prepared using these particles. Images obtained by the author and are presented just to show general appearance of $CaCO_3$ particles and the microcapsules prepared on them.

Polyelectrolyte shells were deposited on top of washed $CaCO_3$ templates following LbL assembly procedure, by alternate deposition of oppositely charged polyelectrolytes. Specific constitution of shells was chosen according to experimental requirements. For PAH/PSS capsules, the freshly synthesised $CaCO_3$ cores were first coated with a PAH layer by incubation in 1.5 mL of PAH solution (2 mg/mL, 0.5 M NaCl) for 15 min, followed by three centrifugation (2000 rpm for 1 min)/wash cycles. Subsequently, they were incubated in 1.5 mL of PSS solution (2 mg/mL) for 15 min, followed by three centrifugation (2000 rpm for 1 min)/wash cycles. The PAH and PSS adsorption steps were repeated until the desired number of layers was built on $CaCO_3$ templates. $(PARG/DXES)_4$ multilayers were obtained following the same procedure.

After desired number of layers is deposited, the $CaCO_3$ cores were dissolved in 0.2 M EDTA solution, obtaining hollow $(PAH/PSS)_4$ and $(PARG/DXES)_4$ capsules. First, particles were re-dispersed in 1 mL of EDTA solution (in 2 mL tube). After shaking for 7 minutes, another 1 mL of EDTA was added and shaking for 7 minutes. After that, the samples were centrifuged and re-disperse in EDTA solution until no gas generation was observed (usually 3 times). Finally, samples was washed 3 times with DI-water.

3.2.1.2 SiO_2 templated microcapsules

SiO_2 particles (4.99 ± 0.22 µm, Microparticles GmbH) were pre-treated with a solution of 25% NH_4OH : 30% H_2O_2 : H_2O (1 : 1 : 5) for 15 min at 75 ^oC to ensure better attachment of the first layer onto the surfaces of SiO_2 particles, and then washed 3 times with DI-water.

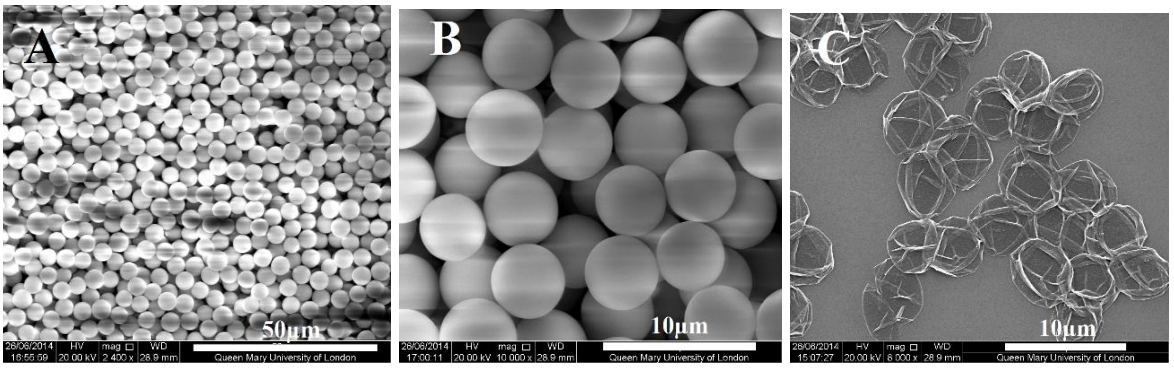

Figure 3.4 SEM images of SiO_2 templates (A, B) and $(PDADMAC/PAZO)_4$ microcapsules (C) prepared using these particles. Images obtained by the author and are presented just to show general appearance of SiO_2 particles and the microcapsules prepared on them.

Polymeric layers were deposited following the same LbL procedure, starting with positively charged PDADMAC as the first layer. After 15 minutes with shaking, they were washed and then covered with the second layer with PAZO. After deposition with 4 bilayers, the SiO_2

templates were removed by treatment with a 0.2 M NH_4F/ HF buffer solution at pH=4.5. Finally, $(PDADMAC/PAZO)_4$ capsules were obtained after several wash steps.

3.2.2 Multilayer Film Preparation

Glass substrates were carefully cleaned with DI-water. LbL deposition was carried out using the dipping system. The slides were alternately immersed in oppositely charged polyelectrolyte solutions for 15 min each, followed by 3 times wash with water. Specific constitution of polyelectrolyte multilayers was obtained according to experimental requirements.

3.2.3 One-step Synthesis and Assembly of Inorganic NPs into Polyelectrolyte Shells

3.2.3.1 SiO_2

For silica coating, two precursor solutions were prepared: NH_4OH-H_2O (1:5 in volume) and TEOS-ethanol (1:2 in volume). The polyelectrolyte capsules prefabricated by LbL assembly were dispersed in 6 mL of ethanol. In order to determine the best reaction conditions for silica growth and incorporation, $(PSS/PAH)_4$ capsules were used as an example, and the parameters like temperature, amount of the precursor solutions and their adding order were varied and studied in detail. The silica coating for other polyelectrolyte capsules like $(PAH/PSS)_4$, $(PDADMAC/PAZO)_4$, $(PARG/DEXS)_4$ was prepared according to the determined best conditions.

3.2.3.2 TiO_2

In order to guarantee the as-prepared composite particles with good morphology and properties, the reaction conditions were carefully controlled and studied. TIBO was diluted by mixing with ethanol, forming a precursor solution with TIBO : ethanol = 1 : 15 (in volume). Another precursor solution was obtained by diluting DI-H_2O with ethanol, forming H_2O: ethanol = 1:10

(in volume). $(PAH/PSS)_4$ capsules were firstly washed with ethanol to remove H_2O. Then different volume of solution TIBO-ethanol was added to the $(PAH/PSS)_4$ capsules system. After that, different amount of H_2O-ethanol solution was dropwise added inside. They were sealed and left for reaction. Finally, the precipitate was washed and collected for further characterization.

3.2.3.3 CDs

Recently, numerous reports of conversion of a variety of precursors such as glucose, chitosan, chitin, banana juice and protein into luminescent CDs under relatively mild conditions of hydrothermal carbonisation (HTC). [35,210,246] Inspired by this, introduce CDs into polyelectrolyte multilayers is expected to fabricate fluorescent composite capsules or films. As dextran is found to be efficiently absorbed by amino-terminated polyelectrolytes, it was used as the carbon source to produce fluorescent NPs. Generally, two procedures were employed: (1) Polyelectrolyte capsules or multilayer films were incubated in dextran/H_2O solution and then heated at 160 ^oC for 20 h; (2) dextran source were introduced into polyelectrolyte multilayers first and then heated in pure H_2O at 160 ^oC for 20 h. Finally, they were washed and collected for measurements.[246]

3.2.4 Cargo Encapsulation

The encapsulation of Rh-B was realized during the synthesis, assembly and condense process of NPs. In terms of silica coating, 400 μg Rh-B were firstly mixed with 6 mL ethanol and a certain amount of polyelectrolyte capsules. After 1 hour stirring at a steady speed of 500 rpm, the deposition of silica was carried out in the same procedure as described above. In the case of CDs incorporation, Rh-B and dextran were mixed together with capsules, then heated at 160 ^oC for 20 h. Finally, composite capsules loading with Rh-B were obtained. To fabricate dextran

encapsulated microcapsules, TRITC-dextran was co-precipitated with $CaCO_3$ microparticles by mixing 0.33 M $CaCl_2$, 0.33 M Na_2CO_3 water solutions and 2 mg/mL TRITC-dextran water solution while vigorously stirring in a 1 : 1 : 1 proportion. The obtained $CaCO_3$ with TRITC-dextran inside were use as temples to assembly polyelectrolytes. Polyelectrolytes with TRITC-dextran entrapped were obtained by dissolving the core by EDTA.

3.2.5 Capsules Treatments

3.2.5.1 Ultrasound Treatment

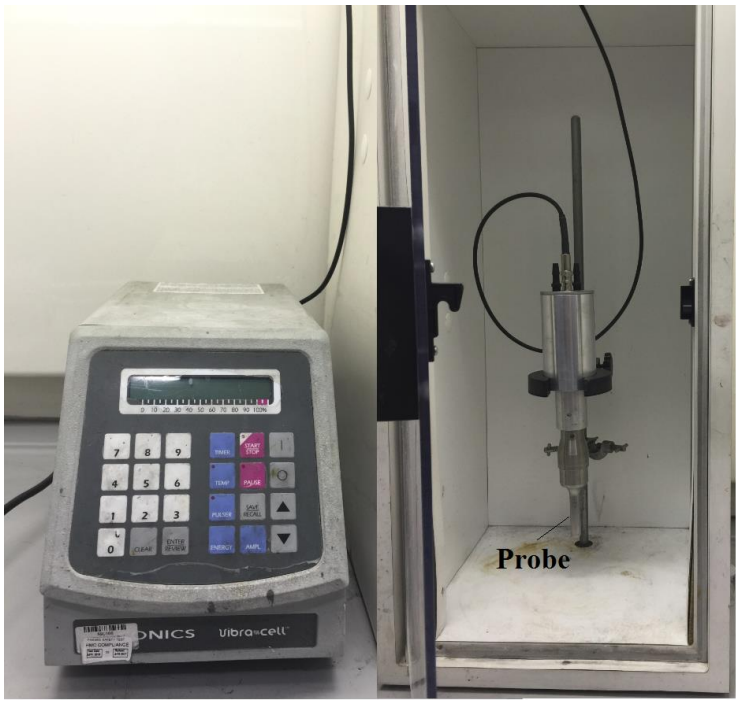

Figure 3.5 Ultrasonic equipment photographs.

To investigate the ultrasound stimulated cargo release, such as Rh-B, the obtained Rh-B containing capsule suspensions were split into two portions for further study: one was for the release study without any treatment and the other for ultrasound triggered release. Then the suspensions were diluted into 20 mL, respectively. At specific time intervals, 1 mL of the

capsule samples from these two portions with or without ultrasound treatment was taken out for measurement. The capsule cargo mixture was centrifuged, the supernatant was carefully collected, diluted and then used for Rh-B quantification. The fluorescence intensity of each sample (in supernatant) was determined and normalized with the standard fluorescent solutions with known concentrations. All the samples were kept at the same dilution factors during the experiments and the release amount was determined by the supernatant fluorescence intensity. Ultrasonic treatment was performed by an ultrasonic processor GEX 750 (Sonics & Materials, Inc., USA) operating at 20 kHz and 50 W, as shown in **Figure 3.5**. The probe of the ultrasonicator inserts into a capsule suspension in a plastic tube. An ice bath was applied to ensure that the temperature change of the capsule suspensions was less than 5 ºC.

3.2.5.2 UV Irradiation

Capsules with TiO_2 NPs were treated with UV irradiation. Briefly, microcapsules containing TiO_2 NPs, $(PAH/PSS)_4$-TiO_2, were irradiated with a UV lamp (OmniCure® 2000, Lumen Dynamics Group Inc.) with the effective working wavelength ranging from 320 nm to 500 nm. The irradiation intensity was detected by using ILT1400 radiometer (International Light Technologies Inc.). The capsules were dispersed in pure water in a cuvette and stirred with a magnetic stirrer, and exposed to UV directly. To reduce temperature increases, an ice bath was applied to ensure that the temperature change of the capsule suspension is less than 5 ℃.

3.2.5.3 Laser Irradiation Setup

A homemade optical setup was used for the laser irradiation on samples, and the setup schematic is shown in **Figure 3.6**. Two modes was used for the equipment setup: conventional and inverted. When irradiating sample chambers, conventional mode was used, and a simple optical microscope was employed to provide necessary rigidity for the components and also

simplify XY and Z moving stages. In fact, using microscope eased the justification of the system. As for the inverted mode, the setup was assembled solely of Thorlabs supplied parts, including XYZ moving stage. As shown in **Figure 3.6**, the laser beam travels through the lens, focuses and targets the sample. There is a small part of the beam that would be reflected back and go into the CCD camera, and the optical image of the sample viewed through the same lens can be obtained. Hence, when justified and focused on a sample, one can see the optical image of the sample together with a small dot of the laser beam. It should be pointed out that in this system the laser is focused slightly above the plane, where the image is visualized.

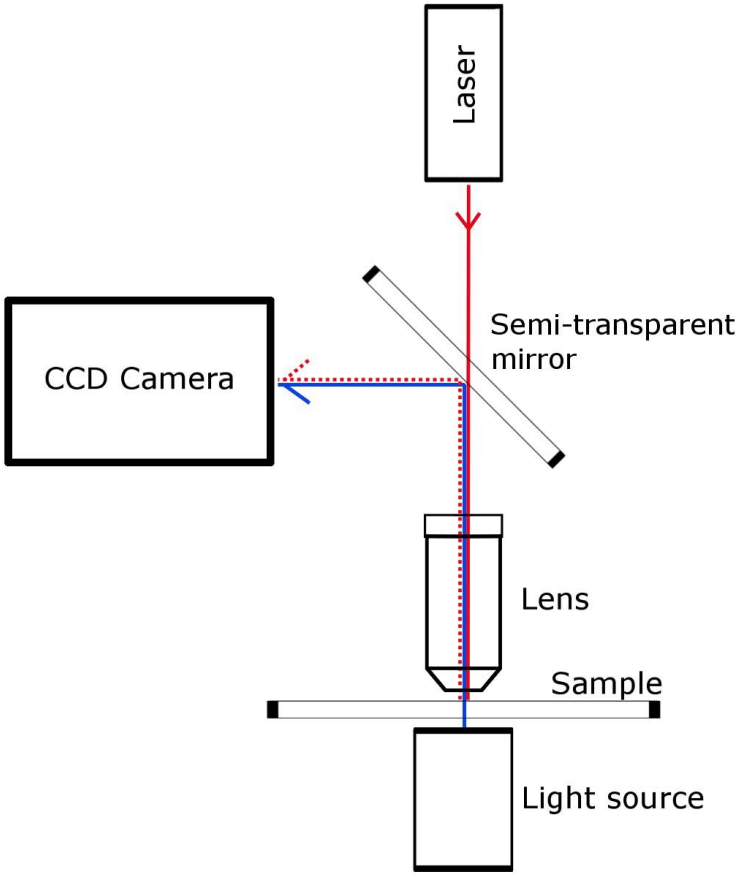

Figure 3.6 Laser irradiation setup schematic.[44]

The main idea of this homemade setup is to realize the irradiation of the sample at one specific point with the focused laser beam and visualization the image of irradiation site simultaneously.

When operating in inverted mode, the light on the sample was provided with 150 W halogen lamp, and collimated light of microscope lamp was used when in conventional mode. For imaging, a highly sensitive b/w 720p analog camera was connected to the computer *via* digitizing interface. A laser diode with mean wavelength of 840 nm and the power of up to 100 mW was applied for the laser irradiation on samples in the experiments. Precautions must be taken to avoid any harm due to power of 100 mW IR laser, because this invisible laser is strong enough to damage retina.

3.2.6 Cells

Research involving cell culturing, treatment and characterisation was performed during the project. Cell culture work needs special precautions and sterile appliances. Culture manipulations were performed in laminar flow fume hood. All the equipment and packaging of consumables (pipette tips, boxes, *etc.*) used was sprayed with 70% ethanol solution prior to be placed to the fume hood.

B50 rat neuronal cells were obtained from European Collection of Animal Cell Cultures (ECACC, Porton Down, UK). These cells are an ethylnitros urea induced tumor cell line with neuronal morphology. They were cultured in the Dulbecco's minimum essential media (DMEM, Sigma) supplemented with 10% fetal bovine serum (10% FBS, Sigma) and penicillin-streptomyosin (1%, Sigma) containing 5% CO_2 /95% air at 37 °C.

3.2.6.1 Cell Viability Assays

For cell viability studies, B50 cells were plated at 20000 cells per well on 96 well plates. The next day and microcapsules were added at different ratios of capsules per cell to triplicate wells.

Similarly, CDs with different concentration dispersed in the cell culture medium were added to the wells. The experiment was terminated later when total incubation times reached 24, 48 and 72 h for respective wells. Then 100 µl MTT solution (5 mg/mL in cell culture medium) was added to each well, plates were briefly shaken and then incubated for 3 hours before Dimethyl sulfoxide (DMSO) was added. Finally cell viability after co-culturing with capsules for 24-72 h was assessed (compared with the control) and read by a BMG Fluostar Galaxy plate reader and Multiscan Ascent Plate Reader.

3.2.6.2 Cellular Uptake and Biodegradability Study

Cellular uptake and biodegradable behaviours of capsules were visualized by a Leica SP5 and Leica TS confocal microscopes equipped with 63x oil immersion objectives. It should be pointed out that the cells were cultured in 35 mm µ-Dish (Ibidi GmbH), allowing to observe and irradiate them with high magnification lens (up to 100x), and also very useful for life support of the cells, isolating them inside friendly environment during experiments.

3.3 Instruments

3.3.1 Electron Microscopy

3.3.1.1 Scanning Electron Microscopes

By using a focused electronic beam to scan the surface of specimens and collecting emitted secondary electrons from the sample which are excited by primary focused electrons, the scanning electron microscopes (SEM) allows imaging surfaces of the samples, and thusly investigating the roughness, quality and the“visual” appearance of the samples. Conventionally, SEM relies on electron interactions at the surface, therefore in order to avoid accumulation of the electrostatic charges at the sample

surfaces, specimens should be conductive. Nonconductive specimens can be coated with an ultrathin gold or carbon layer (nanometers thick) either by low-vacuum sputter coating or by high-vacuum evaporation.

In this thesis, the morphologies of all samples were observed by SEM (FEI Inspect-F) using an accelerating voltage of 20 kV. Images of the employed SEM instrument used in this work and its schematic diagram is presented in **Figure 3.7**. The diluted microcapsule suspension was dropped on a glass slide, air dried, and coated with gold before observation.

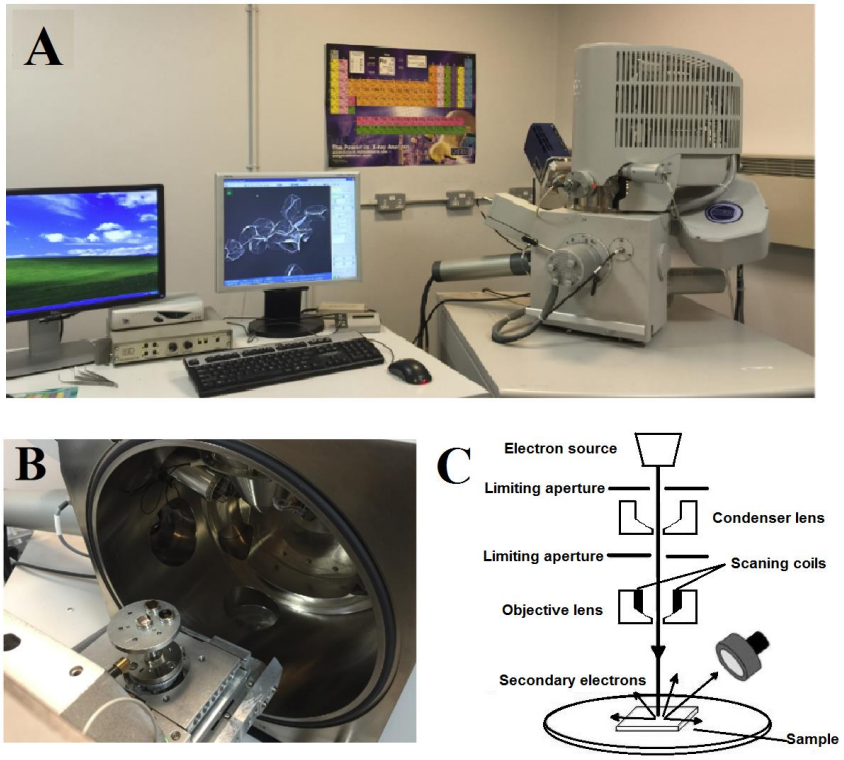

Figure 3.7 FEI Inspect F scanning electron microscope: (A) microscope general view photograph; (B) vacuum chamber with specimens fitted; (C) Schematic diagram.

3.3.1.2 Transmission Electron Microscopy

Different from SEM, in transmission electron microscope (TEM), the detector is placed underneath the sample to collect the electrons that pass through the specimen. Briefly, the electron beam is accelerated by an anode, with a high acceleration voltage (hundreds of kV), focused by electrostatic and electromagnetic lenses, and then strike on specimen. The detected electrons provide the information of the sample structures. Image contrast comes from the differences in material densities of the specimen. It is very useful to measure the structure of the samples, for example, capsule shell thickness could be easily characterized by TEM.

In our work, the structure of capsules as well as the distribution of inorganic NPs and shell thickness were studied using a JEOL 2010 transmission electron microscope with LaB_6 filament, operated at 200 kV. The equipment and its schematic diagram is shown in **Figure 3.8**. To prepare the TEM specimen, the diluted microcapsule suspension was dropped on a copper grid with holey carbon film and left to dry for 5 minutes.

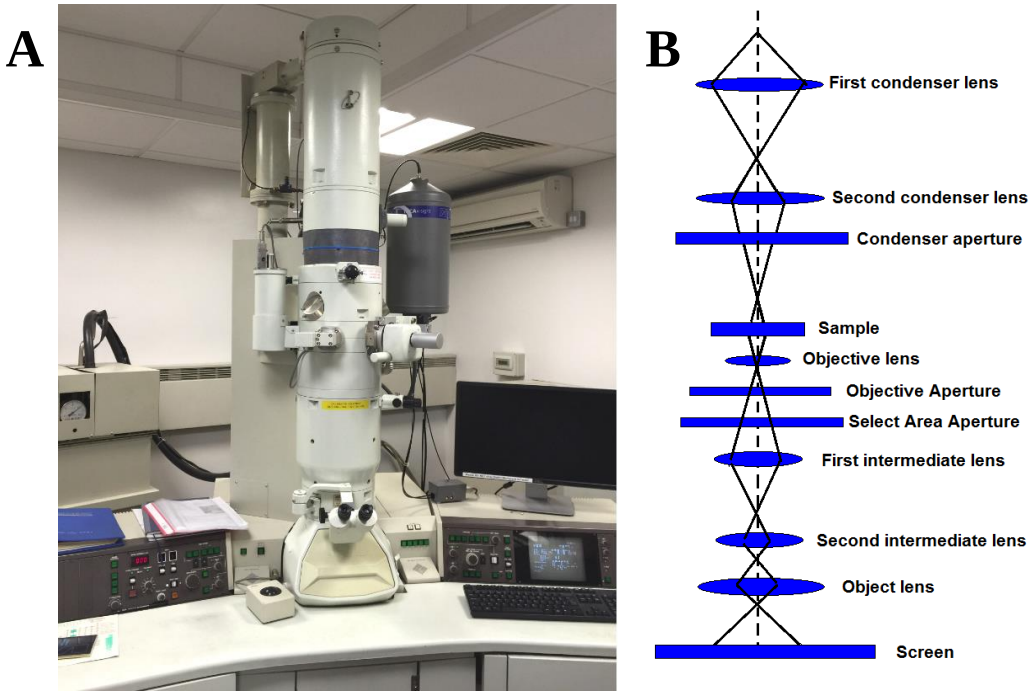

Figure 3.8 (A) Photo and (B) Schematic diagram of the TEM instrument.

3.3.2 Confocal Laser Scanning Microscopy

In this thesis, Confocal laser scanning microscopy (CLSM) images were taken with Leica TS laser scanning confocal microscope, using 63x f/1.4 oil-immersion lens. The image of the CLSM equipment can be seen in **Figure 3.9 A.** CLSM is a non-destructive technique, usually used for biomedical research. CLSM allows capturing high resolution images and 3D reconstruction. Compared with the traditional optical microscopy and fluorescent microscopy, CLSM only visualizes the objects in focus, as only a small fraction of the out-of-focus emission finds its way to the camera. Such feature is achieved by employing 2 pinholes (**Figure 3.9 B**) and using fluorescent dyes to make the specimen detective under laser irradiation.

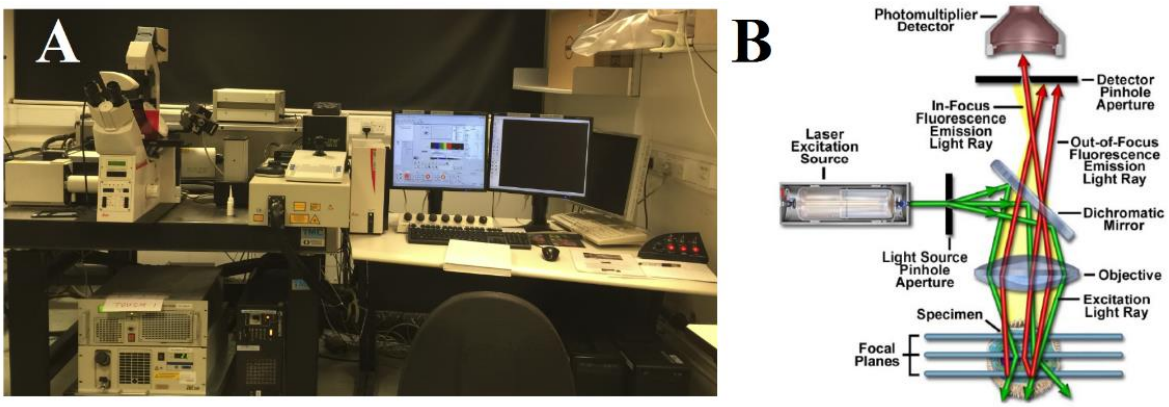

Figure 3.9 (A) Photo of the equipment of confocal laser scanning microscopy; (B) schematics of the CLSM.[247]

3.3.3 UV-Visible Spectrophotometer

Ultraviolet-Visible (UV-Vis) spectrophotometer can detect the light absorption or reflection behaviours of the sample. This technique can also be used for quantification purposes by measure the absorption or reflection intensity of the substances, including measuring film thickness, detecting DNA, proteins and fluorescent dyes concentration.

In this study, an UV-Visible spectrophotometer (LAMBDA950, Perkin-Elmer) was employed to investigate the UV absorption of the composite capsule suspension. Light path of the equipment is shown in **Figure 3.10.** Measurements were made by using quartz spectrophotometer cuvettes (Sigma, S10C).

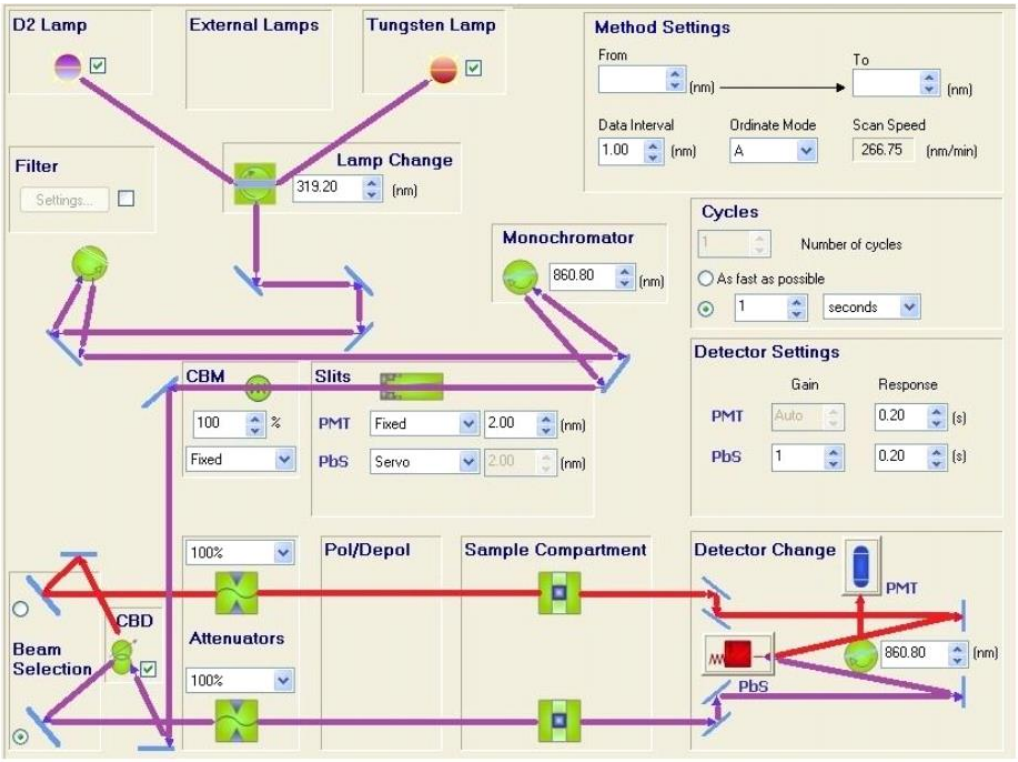

Figure 3.10 Light path of the UV-Vis spectrometer.[247]

3.3.4 Fourier Transform Infrared Spectroscopy

Fourier Transform Infrared Spectroscopy (FTIR) is a technique that can be used to obtain infrared spectrum of absorption or emission of organic or inorganic samples (solid, gas or liquid). Such infrared spectrum can be applied to identify the chemical composition according to the peak information of chemical bonds. Generally, the infrared spectra of pure compounds/chemicals with known components are used as standards or “fingerprint” to interpret chemical components of the samples. Therefore,

the chemical bonds in a sample can be determined when comparing the obtained infrared spectrum with the infrared spectra of known compounds.

In this work, FTIR spectra of freeze dried microcapsule samples were obtained using an infrared spectroscopy (FTIR spectrometer 100, Perkin Elmer). All data were collected at a spectral resolution of 4 cm^{-1} ranging from 4000 cm^{-1} to 400 cm^{-1}. The equipment image and the corresponding light path illustration are shown in **Figure 3.11.**

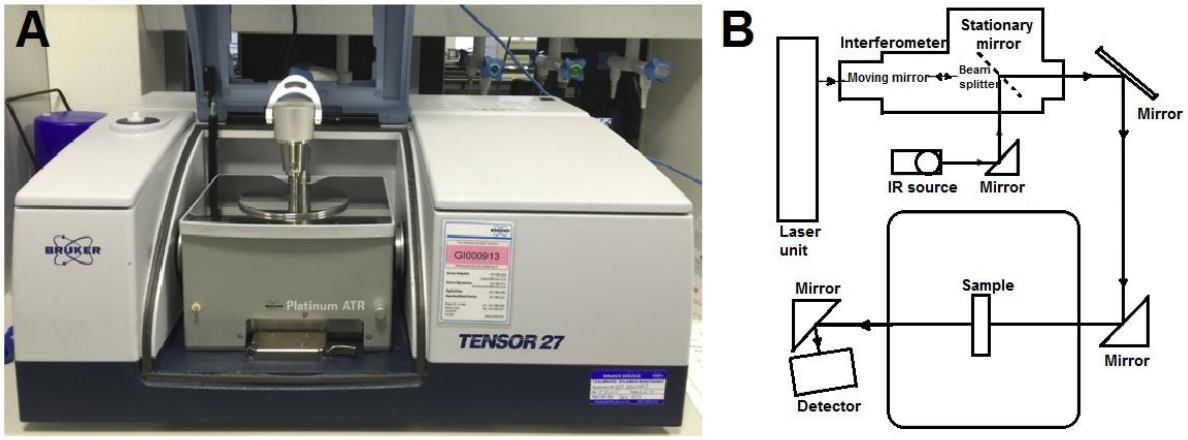

Figure 3.11 (A) Photograph and (B) schematic illustration of FTIR equipment.

3.3.5 Zeta-Potential

Zeta potential is the potential difference between the dispersion liquid medium and the stationary layer of fluid attached to the solid particle surface. Several mechanisms might induce the zeta potential. For example, they may arise from the dissociation of ionogenic groups on the particle surface and the differential adsorption of ions from disperse solution into the surface region. Actually, the net surface charge of the particle will affect the ion distribution in its nearby region, and it will increase the concentration of counter ions close to the surface. Thus, an electrical double layer will form at the interface between the solid particle and the disperse liquid, with an inner region that ions

bound to the surface and an outer region where the ion distribution is determined by the balance of electrostatic forces and random thermal motion. The potential in the region depends on the distance value from the surface. As shown in **Figure 3.12**, at sufficient distance, it decreases to the bulk solution value. **Figure 3.12** also indicated that the zeta potential is the value at the surface of shear.

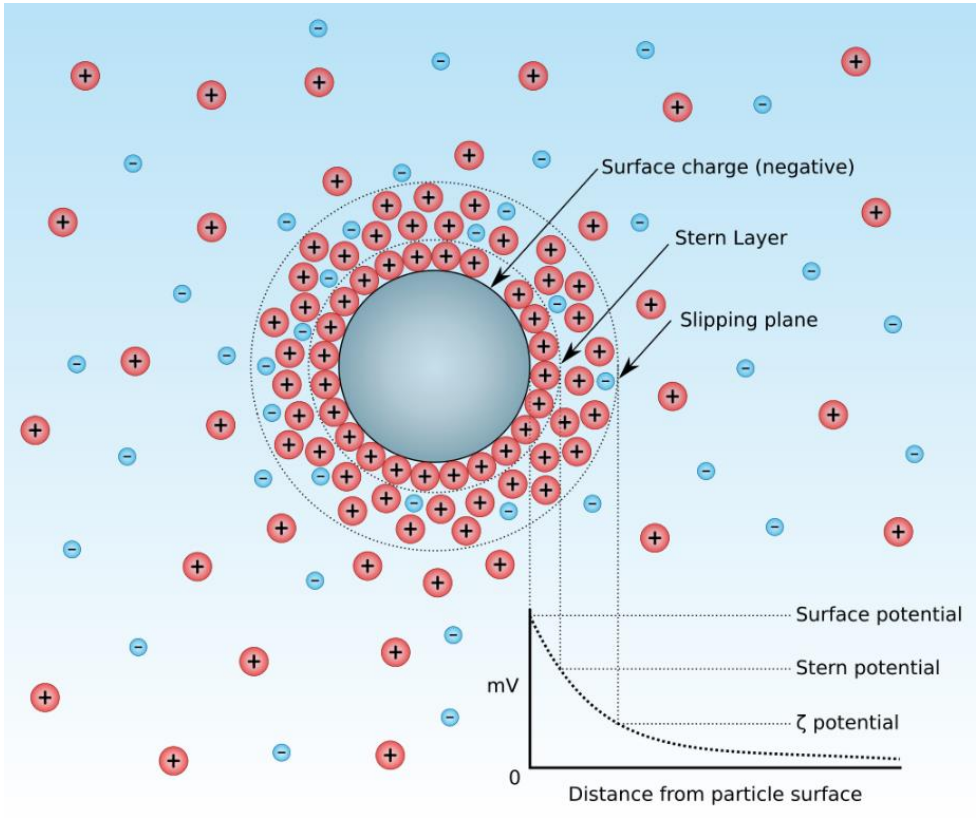

Figure 3.12 Potential distribution near the particle surface.[248]

Under an electric field, the particle and its most closely associated ions move as a unit, and the potential at the surface of shear between this unit and its surrounding medium is known as the zeta potential. Hence, zeta potential is a function of the surface charge of the particle. It can be experimentally measured and applied to analyse stability of particle dispersions. Because the magnitude of the zeta potential reveals the degree of electrostatic repulsion between the adjacent and same charged particles in a dispersion.

In this study, zeta potential of CDs and capsules with different compositions were measured.

3.3.6 Fluorescence Spectrometry

Fluorescence spectrometry is a fast, simple and inexpensive technique to analyse the fluorescence property of a sample dispersed in liquid. Different from the UV-Vis Spectrophotometer, it measures emission spectra of electronic transitions from excited state to ground state. If the analyte is known, fluorescence spectrometry can be used to determine the concentration of the analyte.

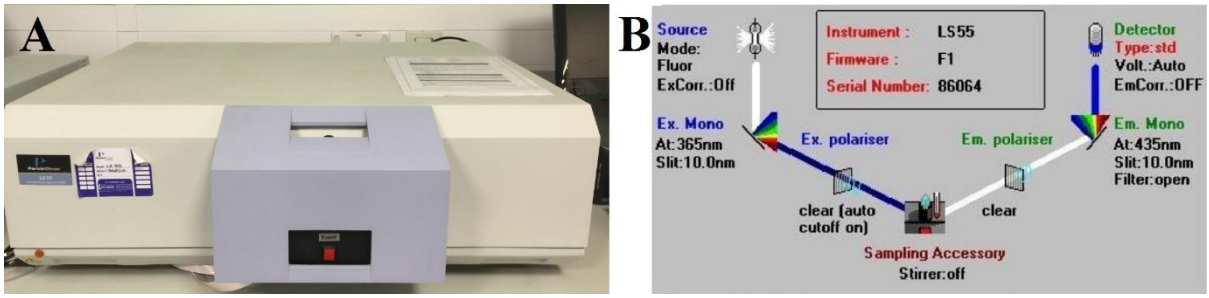

Figure 3.13 Equipment photo (A) and the light path (B) of fluorescence spectrometer.

In this thesis, FLs55 (PerkinElmer, UK) was used to record fluorescence spectra of the samples, and the the light path of fluorescence spectrometry is given in **Figure 3.13**. For all the measurements, the emission mode was chosen. Under this mode, the excitation light with wavelength form 300-500 nm (generated by high energy pulsed Xenon source) hits the Ex. Mono (monochromator), and generates a desired light with single wavelength. This monochromatic light passes the slit and irradiates on the sample. The irradiated samples generate some excited molecules, which emit in the form of light. The emission light partly passes through the Em. Mono (another monochromator) and is detected by the detector.

3.3.7 Multiskan Ascent

Cell viability was assessed *via* a standard MTT assay and the fluorescent intensity was examined by a Multiskan Ascent plate reader. The equipment is shown in **Figure 3.14**.

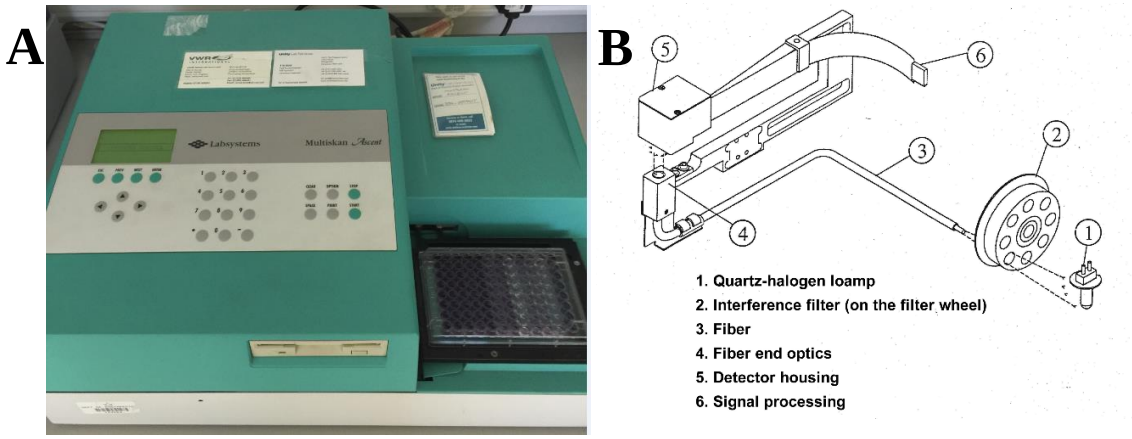

Figure 3.14 (A) Equipment photo and (B) scheme of the optical system of the Multiskan Ascent plate reader.[249]

4. Polyelectrolyte/SiO_2 Composite Shells

4.1 Background

Stimulated by the feature of natural materials composing of organic and inorganic building blocks, interest in design artificial organic-inorganic composite materials has been improved by both scientific research and technological applications. Particularly, polymer-inorganic composite microcapsules have a wide range of applications in pharmaceutical fabrication, controlled drug delivery, agriculture chemicals, and food and cosmetics industries.[250] A versatile approach to produce structured capsules with proper control over their stability, size, shell thickness, encapsulation and release properties is the LbL assembly technique.[251,252] Inorganic NPs can also be used as building blocks to functionalize polymeric LbL microcapsules. The introduction of inorganic NPs could not only increase the shell's mechanical strength, it would also empower the capsules with new capabilities such as responsiveness to various stimuli in surrounding environments.[253,254] Typical examples include the capsules with Fe_3O_4 NPs for magnetic targeting [237] and gold NPs for visible and NIR light responsive.[18] In addition, it has shown that the shell permeability of capsules embedding with inorganic NPs (*i.e.*, Fe_3O_4 or Au) was very responsive to ultrasound and capsule rupture was observed under high irradiation power (*i.e.*, 100W) for 1-2 minutes.[23,24]

However, the LbL capsules with incorporation of inorganic NPs still have considerable challenges in achieving the encapsulation of low-molecular-weight molecules (including drugs). Because polyelectrolyte-shelled capsules are porous in structure, small molecules can go through freely. Usually, increasing shell thickness is a possibility to reduce the permeability, but many layers are required to have a salient change.[255] For example, it was demonatrated that sealing small molecule (Mw $\leq$ 1000 Da) was still a challenge even increasing the

polyelectrolyte layer number to 18.[256] In addition, an increased shell thickness of pure polyelectrolyte capsules would increase the difficulty of cargo release. For the capsule embedding with rigid inorganic NPs, their shell thickness is indeed increased, but the incorporated NPs do not change the porous structure of the polyelectrolyte multilayers and on the contrary, they even increased the porosity of the formed shells. Hence, cargos with molecular weight under 1000 Da can't be sealed inside the cavities of this kind of composite capsules. In practical, most drugs being developed and marketed by the pharmaceutical industry are small molecules under 1000 Da.[257,258] Small molecules, although in routine use as chemotherapeutic agents for cancer treatment, have characteristics that limit their therapeutic efficacy, including a lack of water solubility, suboptimal biodistribution, and nonspecific targeting as well as low intracellular absorption.[259] An effective method to circumvent these limitations is to encapsulate the small drugs in proper carriers which are able to protect and delivery the drugs to the target areas and release them to realize their particular functions.[257,260] Hence, using capsules for the loading and delivery of small molecules for application in anticancer therapy is of significant importance.[260-262]

In order to load small molecules, the shell of capsules must be densified and compacted by the incorporated NPs, *i.e.*, forming a dense, compact and thicker shell, such capsules are expected to be able to keep small molecules inside. An idea stimulated by this is that growing and depositing the NPs directly on polymeric shells. The formed NPs are expected to block pores within polyelectrolyte multilayers and to concrete together with the soft polymer into an integration. It is expected that during the reaction, the NPs would nucleate and grow in pores of polymer shells and 'crosslink' with polyelectrolyte multilayers, yielding dense composite shells with a reduced permeability. Silica NPs were chosen as this kind of modifier, as they can be facilely synthesized at relatively low temperature and they are water dispersible and biocompatible.[263,25] Polyelectrolyte/silica composite capsules were made by *in situ* nucleation

and growth of silica NPs inside or on the polyelectrolyte shell surfaces based on the hydrolysis of tetraethyl orthosilicate (TEOS). It is hypothesized that the hydrolysis of TEOS would consume water in polymer shells and form robust SiO_2 during the precipitation process, yielding dense shells with a reduced permeability and adjustable mechanical characteristics. In terms of controlled release, with the rigid silica NPs in the shells, ultrasound can be used as a trigger to break the formed composite capsules.

Another important issue for drug carriers is their toxicity to cells. Silica NPs were proved as biocompatible materials. In fact, silica can be dissolved and degraded in biological systems [264] and the biodegradation by-product of silica is the nontoxic silicic acid that is naturally found in numerous tissues.[30,108,191] These silicic acid can act as a source of Si and is useful for the formation of connective tissue such as bones.[191] Furthermore, the excess silicic acid in human body can be efficiently excreted from the body through the urine.[192] It's also worth mentioning the hydrophilic surface of the SiO_2 NPs is favourable for cellular uptake. Therefore, the incorporated silica NPs in capsule walls should not increase toxicity effect to cells. Microcapsules composed of biocompatible and biodegradable PARG/DEXS polymer and *in situ* formed silica NPs are expected to combine the merits of biodegradability and small molecule encapsulation together, which are promising for the encapsulation and delivery of small drugs into cells.

In this chapter, polyelectrolyte capsules with different composition, non-degradable PAH/PSS capsules and biodegradable PARG/DEXS capsules, were modified by *in situ* formed silica NPs. Their morphology, structure, shell permeability and biocompatibility were studied. In addition, with a reduced permeability, such composite shells can also be applied for the $CaCO_3$ core protection. Therefore, $CaCO_3$ cores wrapped by PAH/PSS/silica shells with acid treatment were studied in detail.

4.2 Aim and Objectives

The aim here is to fabricate novel polyelectrolyte/silica hybrid shells, in which the silica NPs were *in situ* formed within the soft polymeric multilayers. Such composite shells were used as potential microcontainers for small molecules. In addition, they can also be used as protective shell for the core particles. For the composite capsule system, the incorporated robust silica NPs increase the ultrasound sensitivity. In this chapter, shell with different composition were fabricated and studied.

Therefore the main objectives of this chapter are:

1) To fabricate polyelectrolyte capsules $(PSS/PAH)_4$, $(PAH/PSS)_4$, and $(PARG/DEXS)_4$ and to functionalize them with silica NPs *via in situ* nucleation and growth of silica NPs inside or on the polyelectrolyte shell surfaces based on the hydrolysis of TEOS .

2) To investigate the reaction parameters corresponding to *in situ* formation and assembly SiO_2 in $(PSS/PAH)_4$ capsules.

3) To prepare PAH/PSS/silica and PARG/DEXS/silica capsules using the best reaction condition, and to study their permeability change, ultrasound responsiveness and cell degradation properties.

4) To coat $CaCO_3$ microparticles by PAH/PSS and densify them by silica coating, and then study their behaviour under acid treatment.

4.3 Fabrication of Polyelectrolyte/Silica Composite Capsules

According to the Stöber process, two steps are involved in silica growth process: one is the hydrolysis of TEOS and the other is the condensation of SiO_2 onto the seed surface.[15,34,35] The reactions can be simply described as :

$$Si(OC_2H_5)_4 + 4H_2O \xrightarrow{NH_3/Alcohol} Si(OH)_4 + 4C_2H_5OH \quad (4.1)$$

$$Si(OH)_4 \xrightarrow{NH_3/Alcohol} SiO_2 + 2H_2O \quad (4.2)$$

$(PSS/PAH)_4$ capsules were prepared first for growth and deposition of silica NPs. Hydrolysis reactions of TEOS into silica were given as the above equations. Due to the exist of the $(PSS/PAH)_4$ capsules which played as substrates, the nucleation and growth of silica directly onto $(PSS/PAH)_4$ multilayers *via* a heterogeneous process is strategically feasible.[15,36] **Figure 4.1** illustrated a schematic process of silica incorporated into polyelectrolyte multilayers. After introducing TEOS, NH_4OH and H_2O into the mixture of polyelectrolyte capsules (*e.g.*, PAH/PSS) and ethanol, silica would firstly nucleate and deposit inside or on the surface of polyelectrolyte multilayers under appropriate growth environment; Secondly, as SiO_2 particles grow larger, they interact with each other and finally cover the whole shell.

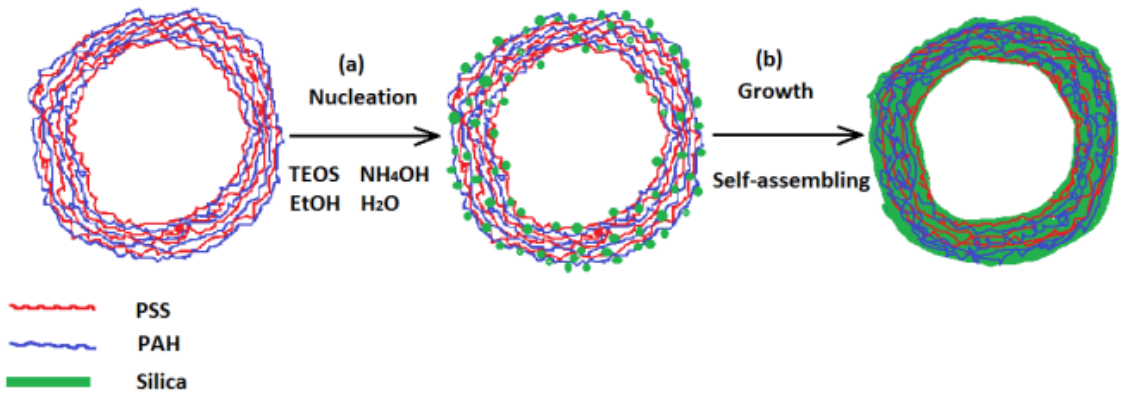

Figure 4.1 Schematic illustration of $(PSS/PAH)_4$ microcapsule incorporated and strengthened by *in situ* formed silica NPs. (a) silica nucleation and deposition; (b) growth and ripeness process.

4.3.1 Fabrication of PSS/PAH/silica Capsules

4.3.1.1 Experimental Details

The 2mL $(PSS/PAH)_4$ capsule suspension was washed three time with ethanol and then was re-dispersed in 6 mL ethanol. Keeping this solution magnetically stirred, certain amounts of NH_4OH-H_2O (1 : 5 in volume) solution and TEOS-ethanol (1 : 2 in volume) solution were introduced into the capsule suspension. The nucleation and growth of the silica nanoparticles were first accelerated at a relatively high temperature (T= 50-60 ^oC) for different duration times (10-120 minutes). A further growth of silica was allowed to ripen the composite shells at room temperature (25 ^oC) for 20 hours under continuous stirring. Finally the precipitation was washed with ethanol and DI-H_2O.

4.3.1.2 Influence of Reaction Conditions on Morphology

Table 4.1 Detailed reaction conditions of different silica coated samples.

		Amount of solution and adding order	Reaction temperature and time
Sample (S_1)	**1**	0 0	0
Sample (S_2)	**2**	0.1 mL TEOS/ethanol, then 2.5 mL NH_4OH/H_2O	25^{o}C-20 h
Sample (S_3)	**3**	0.1 mL TEOS/ethanol, then 2.5 mL NH_4OH/H_2O	60 ^{o}C-10 min; 25 ^{o}C-20 h
Sample (S_4)	**4**	2.5 mL NH_4OH/H_2O, then 0.1 mL TEOS/ethanol	60 ^{o}C-10 min; 25 ^{o}C-20 h
Sample (S_5)	**5**	2.5 mL NH_4OH/H_2O, then 0.1 mL TEOS/ethanol	60 ^{o}C-30 min; 25 ^{o}C-20 h
Sample (S_6)	**6**	2.5 mL NH_4OH/H_2O, then 0.1 mL TEOS/ethanol	50 ^{o}C-30 min; 25 ^{o}C-20 h
Sample (S_7)	**7**	2.5 mL NH_4OH/H_2O, then 0.1 mL TEOS/ethanol	50 ^{o}C-120 min; 25 ^{o}C-20 h
Sample (S_8)	**8**	2.5 mL NH_4OH/H_2O, then 0.5 mL TEOS/ethanol	60 ^{o}C-10 min; 25 ^{o}C-20 h

In principle, the nucleation and growth rate of inorganic NPs were strongly dependent on the reaction environment such as temperature, reaction time, pH, surfactants, concentration of

solutions, *etc*..[16] For silica coating on $(PSS/PAH)_4$ capsules, reaction parameters will determine the final morphology and properties of the formed composite capsules. Hence, in order to better control the capsule morphologies, the influence of some key parameters were investigated, as shown in **Table 4.1**, and SEM images of the resulting microcapsules are presented in **Figure 4.2**.

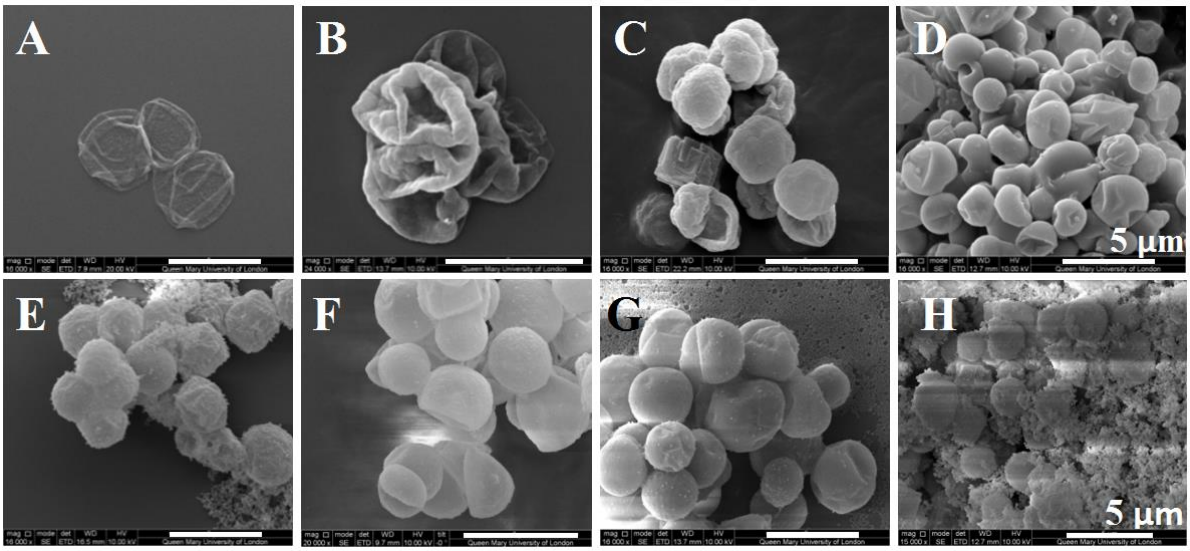

Figure 4.2 SEM images of composite samples produced by various reaction conditions: (A) sample 1; (B) sample 2; (C) sample 3; (D) sample 4; (E) sample 5; (F) sample 6; (G) sample 7; (H) sample 8.

By fixing the volume ratio of the ammonia to TEOS solution at 25:1, the effects of temperature, solution adding order and holding time on the morphology of the composite microcapsules were studied. Without heat treatment, 0.1 mL TEOS/ethanol solution was firstly introduced into polyelectrolyte capsule suspension, and then 2.5 mL ammonia solution was added dropwise, keeping stirring the mixture at room temperature (25 ^oC) for 20 h to obtain Sample 2 (S_2). SEM images indicated that the composite capsules (S_2, **Figure 4.2 B**) shrunk but were not as flat as those without treating with TEOS (S_1, **Figure 4.2 A**). A rough surface with many wrinkles and thicker folds were observed, but no spherical shape. S_C was obtained by only

changing the reaction temperature to 60 ^{o}C for 10 minutes, and the capsules became more robust and most had spherical shape, indicating that the reaction temperature has a great influence on the capsule mechanics. Higher temperature could increase the mobility of reactive components, which therefore facilitates a higher rate of reactivity (hydrolysis, nucleation and growth). It is believed that high temperature accelerated the TEOS hydrolysis rate and promoted the condensation of silica (nucleation), resulting in more silica NPs formed and embedded in the layers. Meanwhile, heat treatment would also affect the morphology of polyelectrolyte capsules due to the (PSS/PAH) shell's sensitivity (shrinkage) to heat.[42] Different to Leporatti *et al.*,[42] who observed that $(PSS/PAH)_5$ microcapsules collapsed in dry state despite of annealing at 70 ^{o}C for 2 h, here we showed that only slight shrinkage of polyeloectrolyte/SiO_2 capsules was observed after heating at 60 ^{o}C for 10-30 minutes.

Comparing S_3, changing the adding order of silicon source and ammonia produced composite capsules (S_4) with a smooth surface, indicating that silica NPs distributed more uniformly on the shell. If ammonia/H_2O solution was firstly added, **Figure 4.2** D, the whole system was like an aqueous phase. The subsequently dropped TEOS under fast magnetic stirring was dispersed as droplets in the aqueous phase with abundant ammonia catalyst and H_2O. In this case, TEOS was hydrolyzed very fast according to the hydrolysis reaction equations (1) [265,266] and the partially hydrolysed species were expected to be located on the capsule surfaces. The synthesis would produce the smallest particles due to the initial nucleation of a larger number of particles.[44] Moreover, the presence of ammonia would render the new formed silica particles with a negative surface charge so that those silica particles would be attached to the positive charged polyelectrolyte capsule shells.[263] However, on the contrary, if TEOS was added first, **Figure 4.2** C, much rougher shell surface was observed, which may be ascribed to a few

reasons: (1) TEOS would firstly react with the drops of the newly joined ammonia/H_2O solution and the hydrolysed dispersible Si was hardly dispersed uniformly initially due to insufficient amount of H_2O; (2) The initial nucleation number of particles was much less than that of S_4; and (3) The formed negatively charged silica would attach on capsule surfaces during the stirring process and might be slightly aggregated, all these resulting in rough surfaces.

The effects of duration time were also studied. By prolonging the reaction time at 60 ^oC to 30 minutes, a more robust structure was obtained as more spherical shaped capsules with lesser folders were appeared in sample 5. Their surface became much rougher and a small amount of excessive free silica NPs was found in **Figure 4.2 E**. The size of the NPs became larger due to a rapid growth of silica under relatively high temperature (60 ^oC) for a longer period.[44] In order to lower the growth rate of silica particles to avoid this problem, sample 6 (S_6) was prepared by reducing the reaction temperature to 50 ^oC but keeping the same duration (*i.e.*, 30 minutes). **Figure 4.2 F** shows that all capsules possessed smooth surfaces with strengthened free-stranding structure without any breakage. NPs embedded in their shells distributed homogeneously, and no excess free NPs existed. However, if the duration time at 50 ^oC was increased to 120 minutes, the composite capsules were still in smooth spherical shape, **Figure 4.2 G**, but a large number of excessive silica NPs were produced, which is consistent with some early observation.[45] Clearly both temperature and duration time played important roles in controlling the quality of silica coating.

Compared with S_4, *i.e.*, only decreasing the volume ratio of the ammonia to TEOS solution (5:1), **Figure 4.2 H** showed that large excessive of silica NPs were produced

and distributed everywhere. This is, because additional TEOS accelerated the undesired homogeneous nucleation process that produced free silica NPs.[36,46] It was difficult to separate these extra silica NPs from the composite microcapsules. All these results show that the reaction conditions should be controlled carefully to fabricate polyelectrolyte/silica composite capsules with good qualities. S_6 sample was so far the most promising sample and was chosen for further studies. Zeta potential of S_6 was monitored during the preparation process, as shown in **Figure 4.3**. In our practical work, the capsules terminated with positively charged PAH should become negatively charged after silica coating, which was demonstrated by the Zeta potential data.

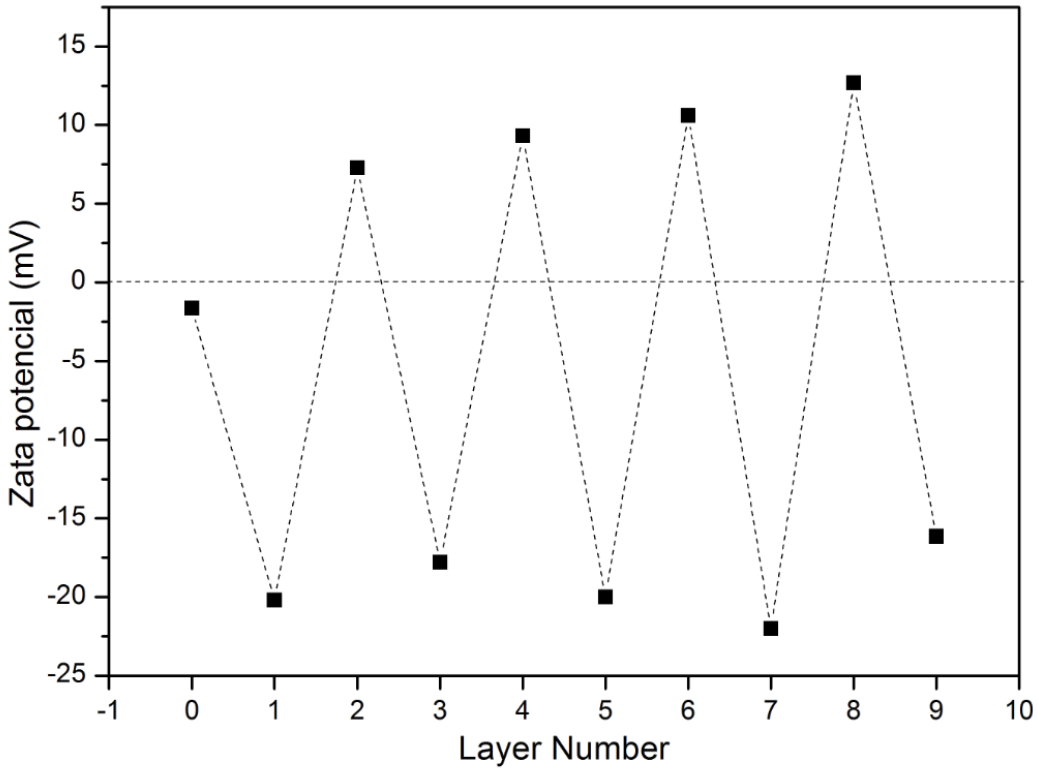

Figure 4.3 Zeta potencial vs. layer number for the LBL self-assembly of PSS, PAH and silica coating. The layer numbers 1, 3, 5 and 7 correspond to PSS assembly and 2, 4, 6 and 8 correspond to PAH assembly. Layer number 9 corresponds to silica coating. Layer number 0 corresponds to $CaCO_3$ cores.

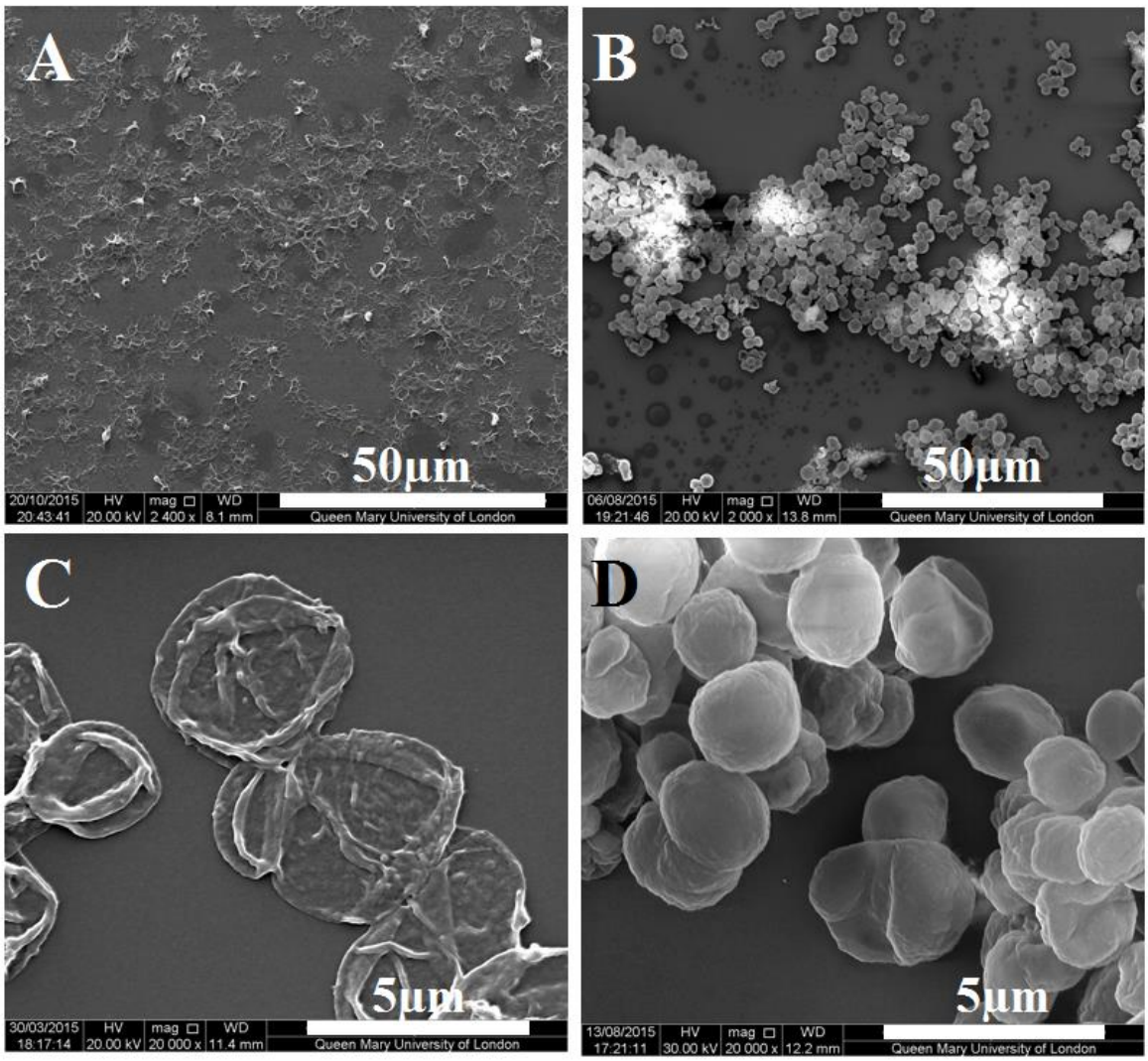

Figure 4.4 SEM images with different magnification of $(PAH/PSS)_4$ capsules before (A, C) and after (B, D) silica coating.

Interestingly, capsules terminated by negatively charged PSS, *i.e.*, $(PAH/PSS)_4$, were also coated with silica NPs under the same condition for preparation sample S_6. SEM images of the $(PAH/PSS)_4$ before and after silica coating were shown in **Figure 4.4**. The obtained PAH/PSS/silica composite capsules presented a similar morphology with PSS/PAH/silica capsules (S_6), which indicated that the surface charge of the employed polyelectrolyte capsules was not a key influence factor to determine the final

morphology of the composite capsules. These capsules introduced to the reaction systems were mainly served as external substrates providing positions with low energy where silica preferred to nucleate. Further study on the element composition, morphology and structure of PSS/PAH/silica capsules (S_6) was carried out and displayed as below.

4.3.1.3 Element Analysis

In order to further study whether silica were successfully incorporated, EDX and FTIR were used to analyse the composition of as-prepared hybrid microcapsules. EDX spectrum (**Figure 4.5 A**) of the composite capsules demonstrated that a large number of C, O, and Si atoms were contained, proving that the capsule wall was built up by the polymer layer and silica. Small amount of Na might come from the original solution, which was not washed out completely. Other small peaks were attributed to Au coating. Meanwhile, $CaCO_3$ was all removed by EDTA because no calcium element was found from the spectrum. The FTIR transmittance spectrums of PAH, PSS and composite capsules are shown in Figure 3b. The characteristic bands at 1064, 956 and 798 cm^{-1} were correspond to the stretching, stretching and bending frequencies respectively. The position and the shape of the main Si-O vibrational band at 1064 cm^{-1} proved a stoichiometric silicon dioxide structure. Small peak at 956 cm^{-1} belonged to Si-OH stretching and that at 798 cm^{-1} attributed to Si-O bending. Moreover peaks in the spectral range at 511 cm^{-1}, 1537 cm^{-1}, 1644 cm^{-1}, 1824 cm^{-1} and 3646 cm^{-1} were attributed to vibrations of carbon atoms coming from polyelectrolyte part of the composite capsules. Both showed clearly that SiO_2 NPs were successfully incorporated into PSS/PAH shells.

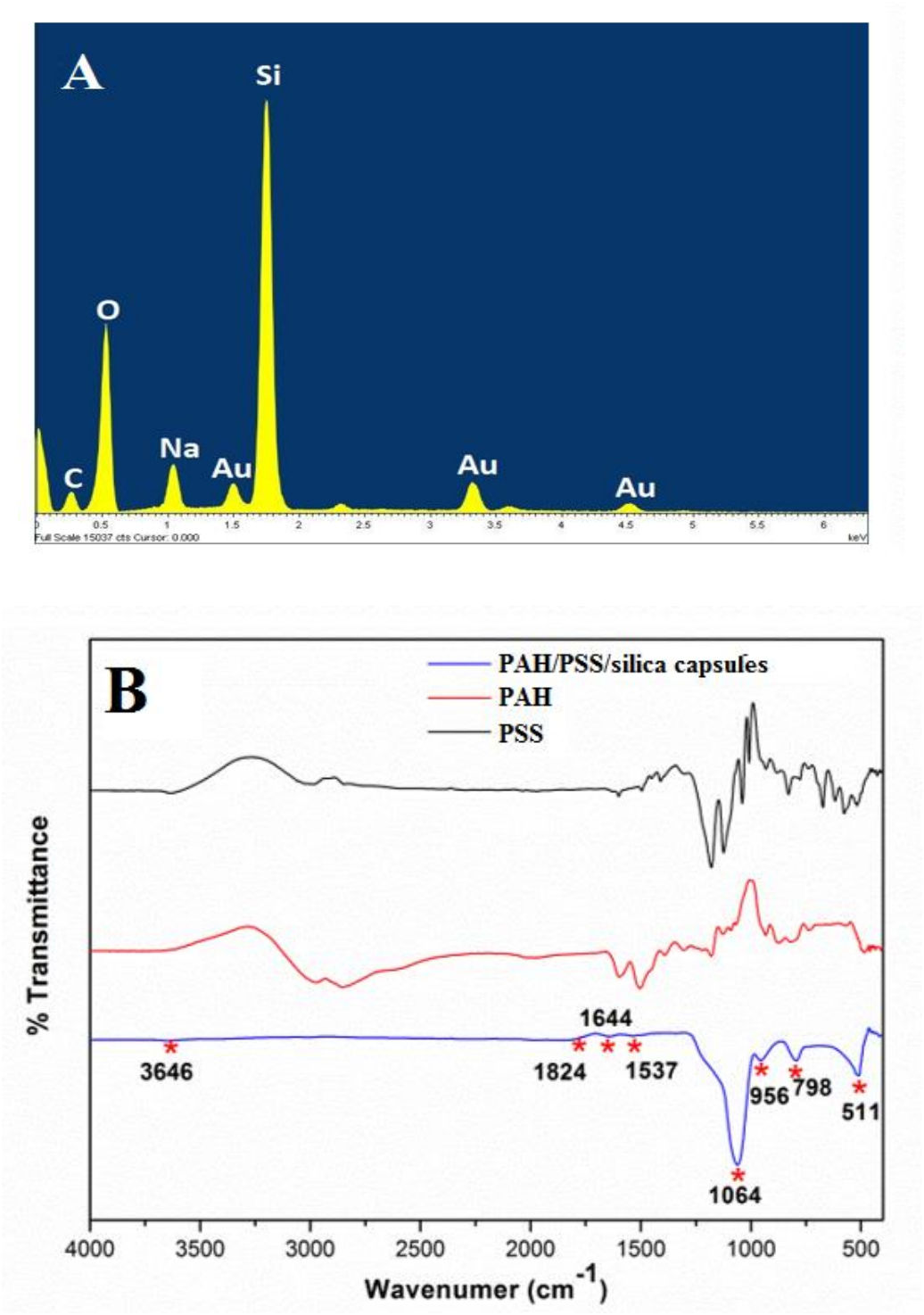

Figure 4.5 (A) EDX and (B) FTIR spectrums of capsules after silica incorporation (sample S_6).

4.3.1.4 Morphology and Structure Analysis

To further investigate the influence of silica incorporation on capsule morphology and their structure, sample S_6 was measured by SEM and transmission electron microscopy (TEM), as given in **Figure 4.6** and **Figure 4.7** respectively.

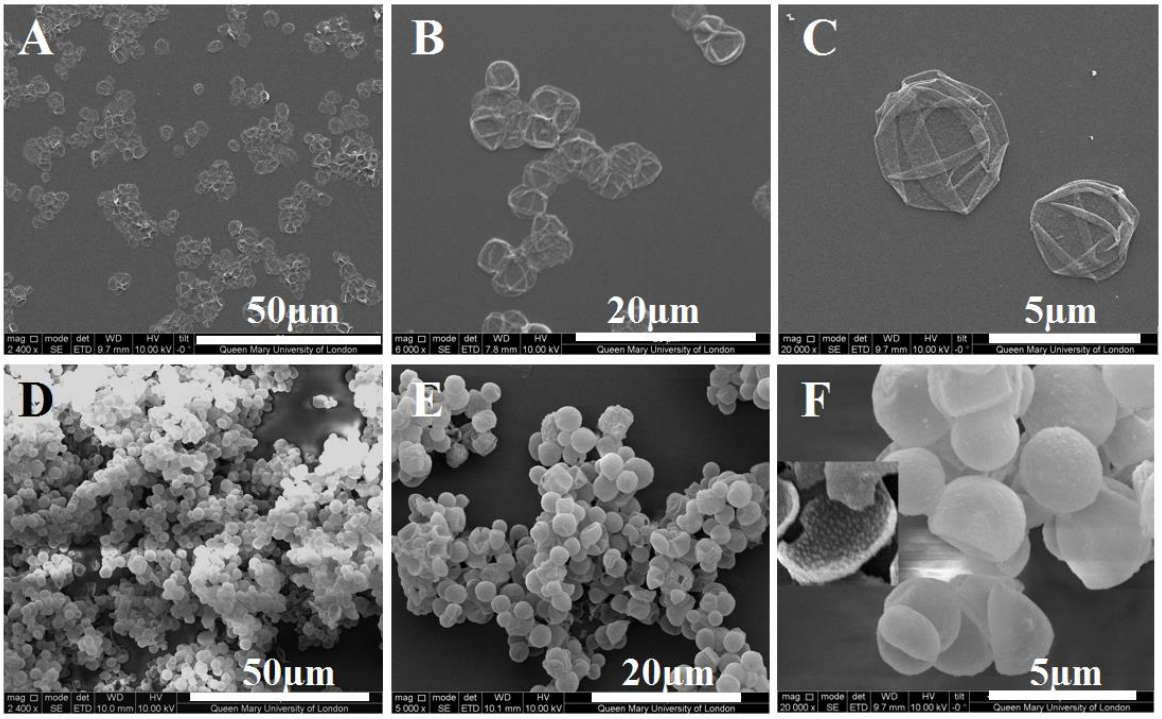

Figure 4.6 SEM images of $(PSS/PAH)_4$ microcapsules before (A-C) and after (D-E) silica coating (sample S_6).

Figure 4.6 showed that the incorporation of silica NPs in the PSS/PAH shells led to significant morphology changes in comparison with nanoparticle-free capsules. Without silica incorporation, all the $(PSS/PAH)_4$ microcapsules were collapsed and flat (**Figure 4.6 A-C**), but on the contrary, the composite microcapsules were structurally reinforced into robust free standing capsules, having three dimensional appearance (**Figure 4 D-F**). The external surface consisted of homogeneously distributed SiO_2 NPs embedded in the polyelectrolyte shell, as shown in the image with high magnification in **Figure 4.6 F**, indicating that the as-made multilayers were sufficiently incorporated by the *in situ* formed SiO_2 NPs. This was also verified by TEM images (**Figure 4.7**). The inset

was the SEM image of composite capsules broken by an external force, showing a rough interior surface of the composite shell, which revealed that silica NPs were not only deposited on the exterior surface of the polymeric shell but also being embedded within it and on their interior surfaces. Analysis of SEM of samples before and after silica coating indicated the diameter of dried capsules decreased from ~4.05 μm to ~3.2 μm. The shell thickness increased a lot, from less than 20 nm to ~300 nm. Apart from the slight shrinkage of polyelectrolyte layers caused by heat treatment, it is thought that the *in situ* formation of SiO_2 particles would cross-link and compress the capsule, resulting in a decrease in capsule size yet with an increase in the shell thickness and shell mechanics.[16]

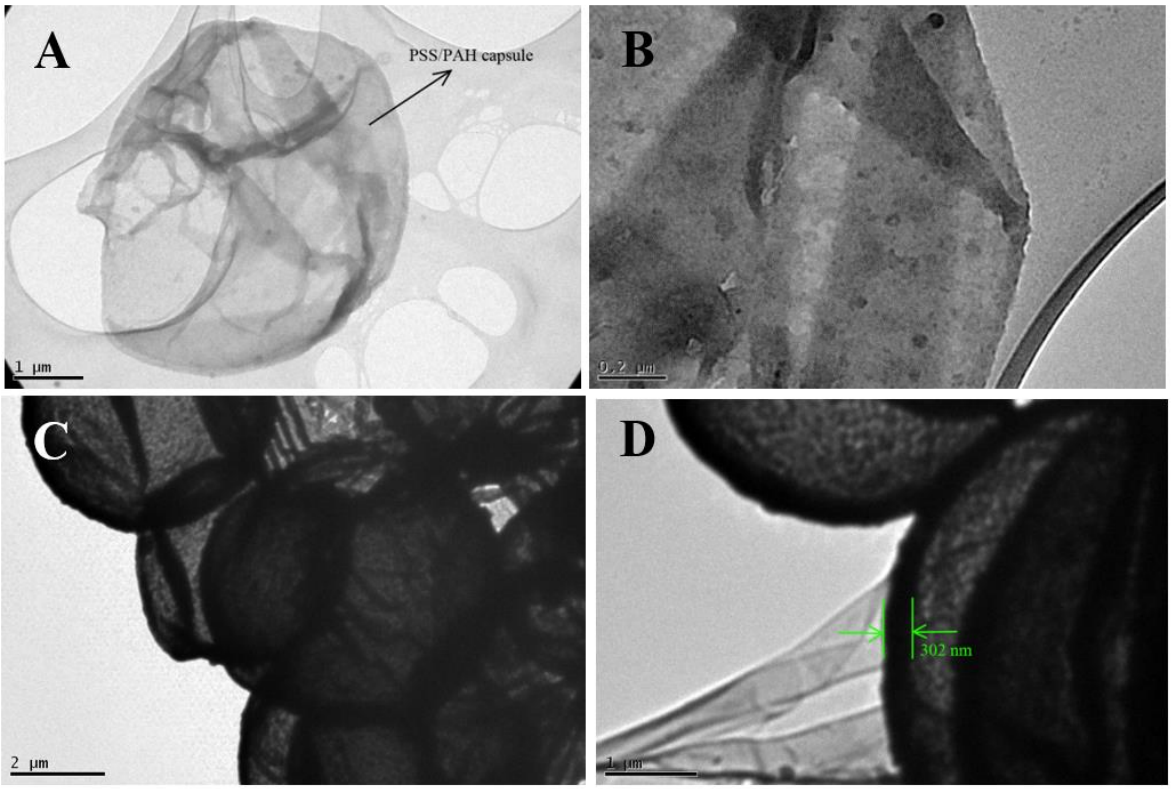

Figure 4.7 TEM images of capsules without (A, B) and with (C, D) silica coating (sample S_6).

Some previous studies reported a problem of limited thickness of the capsule shell even after coating several silica layers.[15,49] However, as shown in **Figure 4.7**, the shell thickness

increased drastically from a few nanometers to a few hundred nanometers (*i.e.* ~ 300 nm). The above analysis of SEM images also qualitatively confirmed this. For samples without silica coating, the capsule had relatively smooth surface and in collapsed form, as shown in **Figure 4.7 A** and **B**, while small dark dots can be found on the surface of composite microcapsules, given in **Figure 4.7 C** and **D**. Clearly the composite shell became more compact and its permeability should be effectively lowered down due to (1) the decrease in capsule size, (2) the increase in shell thickness and (3) a possible increase in the shell density. In particular, benefiting from a better mechanical property of inorganic materials, the incorporation with *in situ* formed silica NPs would lead to a reinforcement of composite shell mechanics.

4.3.2 Silica Coating for Different Polyelectrolyte Capsules

As the reaction condition used for preparation of sample S_6 is the best one, the silica coating for all the following polyelectrolyte capsules were fabricated under this condition. According to the same reaction procedure, other kinds of polyelectrolyte capsules, including $(PARG/DEXS)_4$, $(PDADMAC/PAZO)_4$ and $(PAH/PSS)_4$-Fe_3O_4, were also modified by *in situ* synthesis and assembly of silica NPs.

4.3.2.1 Fabrication of PARG/DEXS/Silica Composite Capsules

Biodegradable $(PARG/DEXS)_4$ capsules were functionalized by silica NPs under the same reaction condition of the above discussed sample S_6. SEM images in **Figure 4.8** illustrates that collapsed flat PARG/DEXS capsules were strengthened to free standing composite capsules, consistent well with the previous results of the PAH/PSS capsule systems. Specifically, contrast to the rather thin pancake structure of pure PARG/DEXS capsules (**Figure 4.8 A** and **B**), the composite capsules showed a robust structure in the absence of huge amount of silica NPs (**Figure 4.8** C and D), indicating the incorporation with *in situ* formed SiO_2 NPs in

PARG/DEXS multilayers increased their mechanical strength significantly. Besides, by the well-controlled hydrolysis of TEOS the PARG/DEXS multilayers were fully covered by silica NPs and no excess free silica particles exist along with the composite capsules. Similar with PAH/PSS systems, SiO_2 NPs can be clearly found on the surface of the composite capsules, as demonstrated by the SEM and TEM images, achieving a slightly rough shell surface (**Figure 4.8 D** and **F**). Nevertheless, they were compactly concrete together with the soft polyelectrolyte multilayers with a uniform distribution. Furthermore, TEM data in **Figure 4.8 E** and **F** also verified their hollow structures and the increased shell thickness reaching to around 128 nm that make capsules strong enough to support themselves upon drying. The inset diffraction pattern revealed these silica NPs are amorphous in nature, as no diffraction spots or rings were obtained.[267] It shall be noted that the shell thickness of PARG/DEXS/silica was less than that of PSS/PAH/silica capsules, which might be due to a small amount of shrinkage of PARG/DEXS multilayers during the reaction and deposition process.

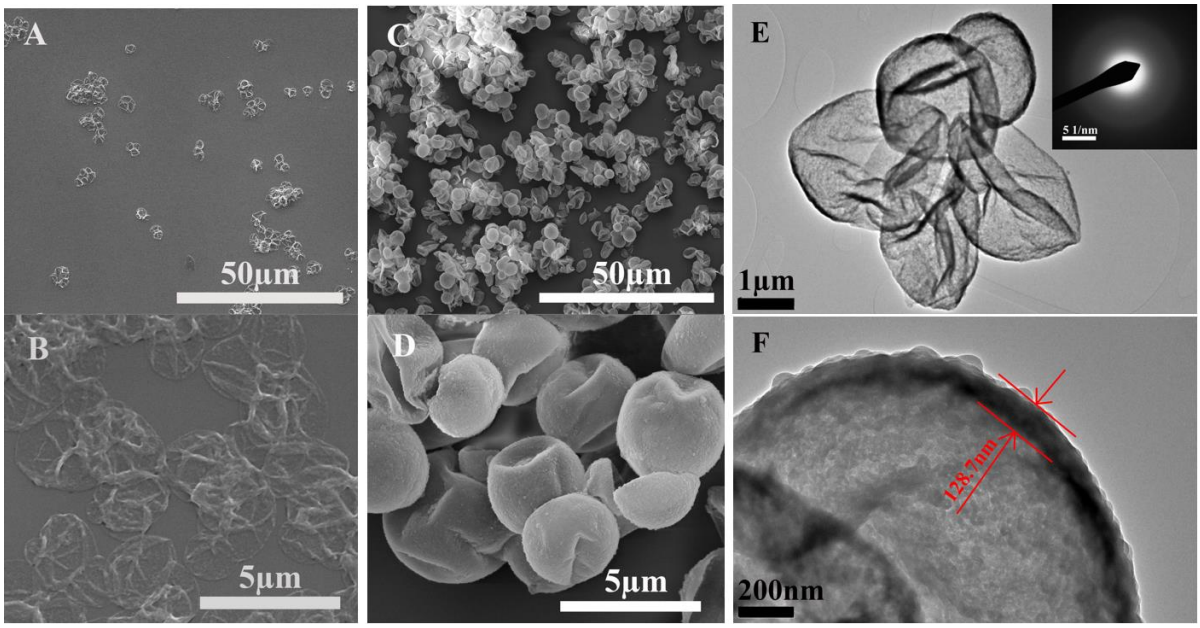

Figure 4.8 SEM and TEM images of $(PARG/DEXS)_4$ capsules before (A, B) and after silica coating (C-F).

4.3.2.2 Fabrication of PDADMAC/PAZO/Silica Composite Capsules

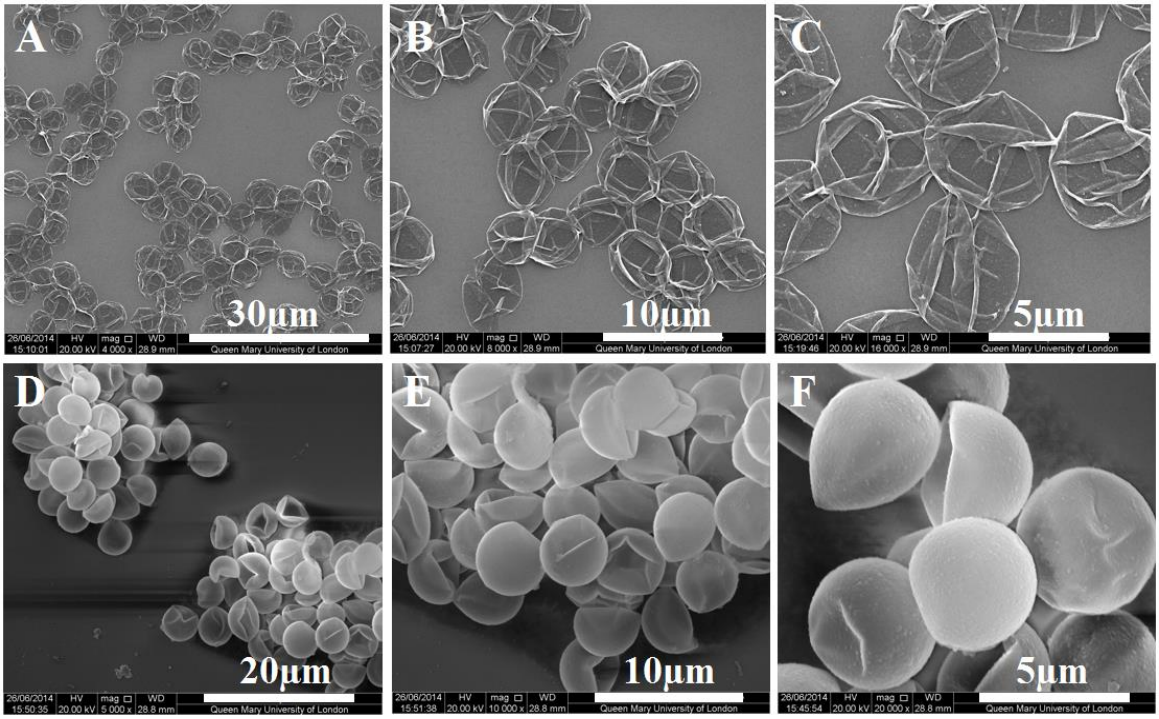

Figure 4.9 SEM images of $(PDADMAC/PAZO)_4$ capsules before (A, B) and after (C-F) silica coating.

$(PDADMAC/PAZO)_4$ were also modified by *in situ* synthesis and assembly of silica NPs. The samples were characterized by SEM, as shown in **Figure 4.9**. The SEM images revealed that silica NPs were successfully fabricated and incorporated into PDADMAC/PAZO capsules. The formed composite PDADMAC/PAZO/silica capsules showed ball-like shapes with relatively rough surfaces and decreased size. NPs can be found on their surfaces but no free silica NPs existed along with the capsules.

As it was proved by our group previously that $(PDADMAC/PAZO)_4$ microcapsules exposed to UV light showed a gradual swelling and further disassembling process.[104] Here, to investigate the influence of silica coating on their UV sensitivity, we exposed $(PDADMAC/PAZO)_4$ microcapsules without and with silica coating to UV irradiation (55 mW

cm^{-2}) for 2 h, and characterized with SEM. During all the irradiation processes, an ice bath was used to prevent the increase of temperature to keep the whole capsule suspension in a thermo-stable environment. It is clearly seen from **Figure 4.10** that, after 2 h of irradiation, the collapse $(PDADMAC/PAZO)_4$ capsules were all ruptured into pieces along with some needle-like formations, such results were in good accordance to the results obtained by Q. Yi and the co-workers.[104] However, different from pure PDADMAC/PAZO capsules, we found that the $(PDADMAC/PAZO)_4$ microcapsules functionalized with silica NPs did not present similar breakage, showing no change in their morphology and structure, **Figure 4.10**.

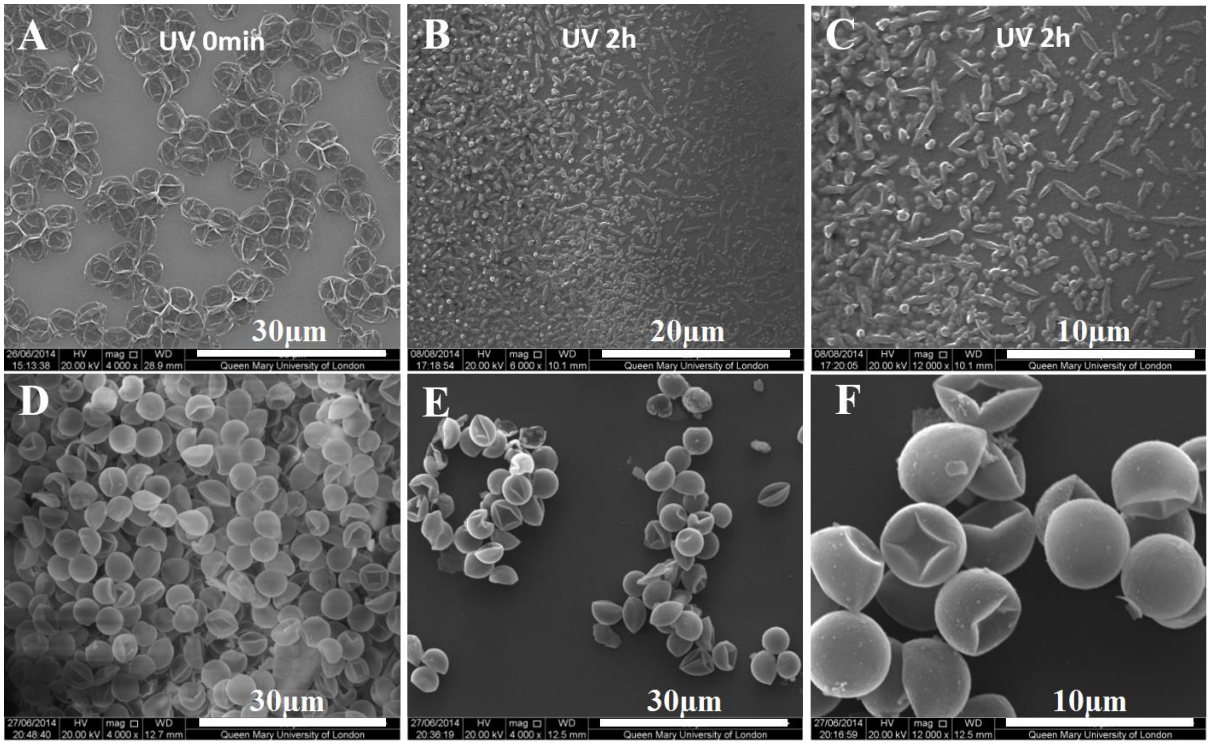

Figure 4.10 SEM images of $(PDADMAC/PAZO)_4$ capsules without (A-C) and with (D-F) silica coating before and after UV irradiation for 2 h.

Such phenomenon could be explained in detail. Except the most well-known phenomenon that azobenzene molecular conformation change in-plane, azobenzene molecules also change their dipole moment if irradiated by UV light. Azobenzenee moieties are conducted to form plane-

to-plane or end-to-end aggregates, also known as H- or J-aggregates respectively, depending on the mutual orientation of the interacted dipole moments between the counterpart molecules.[107] Most importantly, it was found that, for PDADMAC/PAZO capsule system, the J-aggregate formations of azobenzene were favoured when the capsules were exposed to UV light. [107] The J aggregate assemblies destroyed the integrity of capsule shells and thusly destroy the capsules if they were exposed to UV light for enough time. For silica coated PDADMAC/PAZO capsules, it seems that the incorporated rigid inorganic NPs played as rigid supports to prevent the capsules collapsing or rupturing. This offered a new way to protect UV-responsive materials, *i.e.*, silica building blocks in UV-sensitive matrixes formed as rigid integrate supports.

4.3.2.3 Fabrication of PAH/PSS/Fe_3O_4/Silica Composite Capsules

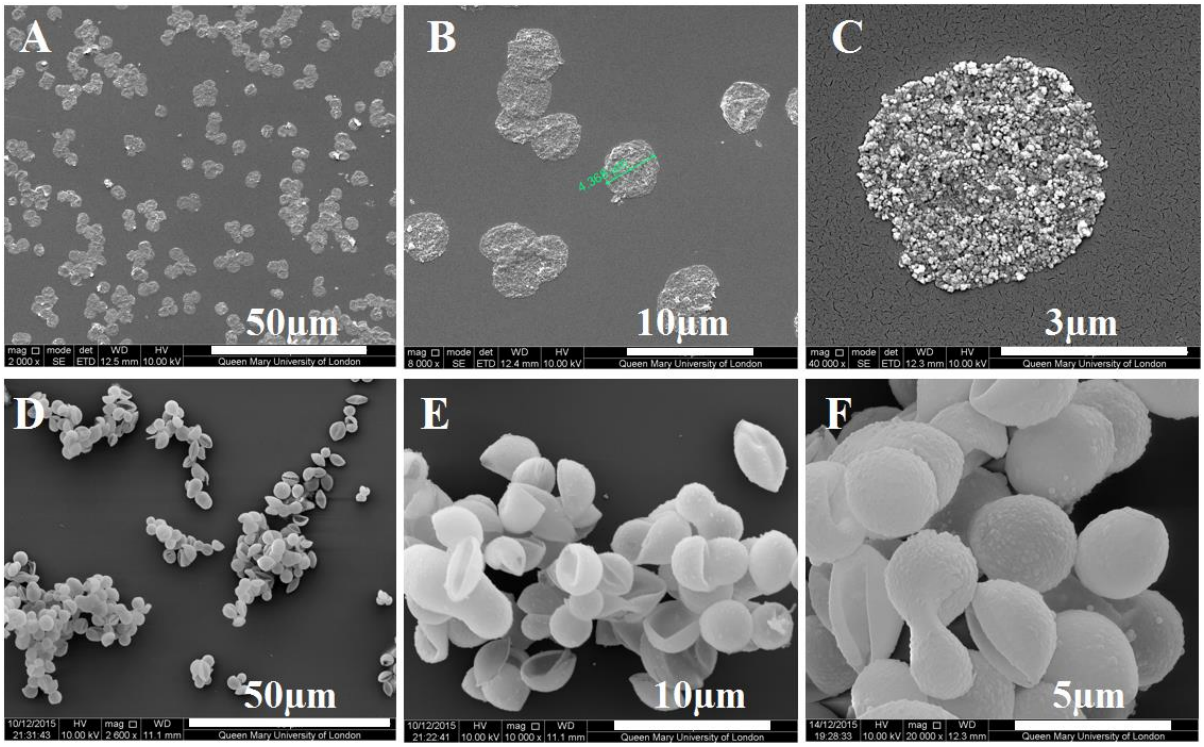

Figure 4.11 SEM images of $(PAH/PSS)_4$-Fe_3O_4 capsules before (A,-C) and after (D-F) silica coating.

$(PAH/PSS)_4$ capsules assembled with negatively charged Fe_3O_4 NPs in the middle of the multilayers were applied for silica coating. **Figure 4.11** indicated that there is no problem to *in situ* coat silica NPs on the polyelectrolyte capsules with other kinds of NPs functionalized inside them. From **Figure 4.11 C**, Fe_3O_4 NPs were obviously incorporated into the PAH/PSS multilayers driven by the electrical absorption force between PAH layers and Fe_3O_4 NPs. But such incorporation did not strength them with free-standing structures, as mentioned in Chapter 2. After introducing silica NPs *via in situ* process, all the capsules displayed spherical morphology, as indicated in **Figure 4.11 D-F**. These results further proved the significant difference between incorporation of pre-fabricated NPs and *in situ* formed NPs. No significant different in morphology between these PAH/PSS/Fe_3O_4/silica and the above PAH/PSS/silica was found.

4.4 Reinforcement Mechanism of Composite Polyelectrolyte/Silica Shells

During the reaction process, TEOS underwent hydrolysis upon contact with water, according to the net reaction of Eq. (4.1) and Eq. (4.2), *i.e.*, $Si(OC_2H_5)_4 + 2H_2O \longrightarrow SiO_2 + 4C_2H_5OH$. This forms solid SiO_2 through a series of condensation reactions catalysed by ammonia and also produces a by-product, ethanol.[50-53] In our study, the hydrolysis and nucleation process were promoted by incubating the mixture at a relatively high temperature (50 ^oC) and a further ripen process was allowed at lower temperature (25 ^oC) for a longer time. A possible incorporation and reinforcement mechanism of the composite structure is illustrated in **Figure 4.1**. The pure PSS/PAH multilayer shells were uneven and provided many numbers of nucleation sites. Based on the nucleation principle, new SiO_2 particles would preferably form at the points with low energy, such as at concave points of the shell surfaces, and the pores in

polyelectrolyte multilayers.[54] Along with the formation and growth of silica, the polyelectrolyte shell shrunk due to the consumption of water from the multilayer pores as the TEOS was hydrolysed. With prolonging the reaction time (age process), SiO_2 particles would contact and interact with each other and finally cover the whole shell, as illustrated by the TEM results, **Figure 4.7** and **Figure 4.8**. The continuous inorganic NPs would compress the capsule in some degree through the shrinkage process, and the flexible polyelectrolyte layers were restricted. All these factors would result in a decrease in capsule size and an increase in its shell thickness. The pores in capsule shells would become less in amount and smaller in size, and consequently the capsule shell permeability could be drastically reduced, which was further confirmed by CLSM results.

4.5 Reduced Permeability Induced by the *In Situ* Formed Silica NPs

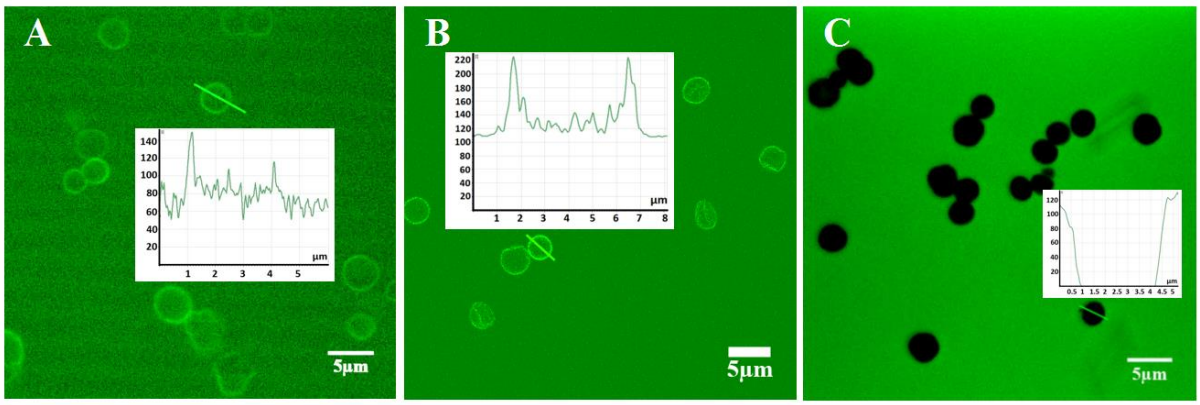

Figure 4.12 CLMS images of microcapsules dispersed in FITC solution. (A) $(PSS/PAH)_4$ after held at 50 ^oC for 30 minutes, (B) $(PSS/PAH)_3PSS$ capsules and (C) $(PSS/PAH)_4$ capsules with silica coating. The line scan insets showed relative fluorescent intensity in the corresponding capsules.

For the permeability study, capsules with PAH/PSS and PARG/DEXS functionalized by the *in situ* formed silica NPs were studied as examples. Small molecules (FITC and RhB) and big molecules (TRITC-dextran) were employed as models to characterize the shell permeability of different kinds of capsules.

It is worth mentioning that heat treatment and the surface state of capsules would affect the adsorption and transfer of dye molecule.[55,56] In fact, the permeability of polyelectrolyte capsules for various molecules decreased to some degree after heat incubation.[125] In order to eliminate the heating effect on the shell permeability for FITC molecules, the pure $(PSS/PAH)_4$ capsules were held at 50 ºC for 30 minutes then incubated in the FITC solution. **Figure 4.12 A** demonstrated that the heat treated PSS/PAH capsules were still permeable for FITC, which is consistent with the early observation that polyelectrolyte capsule was not sufficient to encapsulate small fluorescein molecules by heat treatment at 50 ºC for short time.[155] In terms of the effect of different surface charges on permeability of capsules, capsules with PSS as the top layers (negatively charged) were also studied, as FITC molecules are slightly negatively charged which could be absorbed by positively charged PAH. The result revealed that $(PSS/PAH)_3PSS$ were also permeable for FITC molecules (**Figure 4.12 B**). Hence, the PSS/PAH capsule permeability for FITC was weakly depended on their surface charge. In some case, surface wettability of capsules could influence their permeability significantly,[147,268] for example, benefitting by hydrophobic property of the capsule shells after UV irradiation, Yi *et al.*[147] successfully sealed Rh-B in $(Nafion/DAR)_4$ capsules. Here, as silica NPs are water dispersible [263] and our composite capsules were well dispersed in water, the effect of surface wettability could be neglected. The permeability of FITC for the composite PAH/PSS/silica capsules was shown in **Figure**

4.12 C. In sharp contrast to the high permeability of capsules without silica coating (**Figure 4.12 A**), the composite capsules performed an effective interception of FITC molecules (**Figure 4.12 C**). Some composite capsules aggregated together due to the interaction of silica NPs on their surface. The corresponding line scan image demonstrated an average fluorescent signal intensity of ~ 112 units outside the capsules and 0 unit inside the capsules.

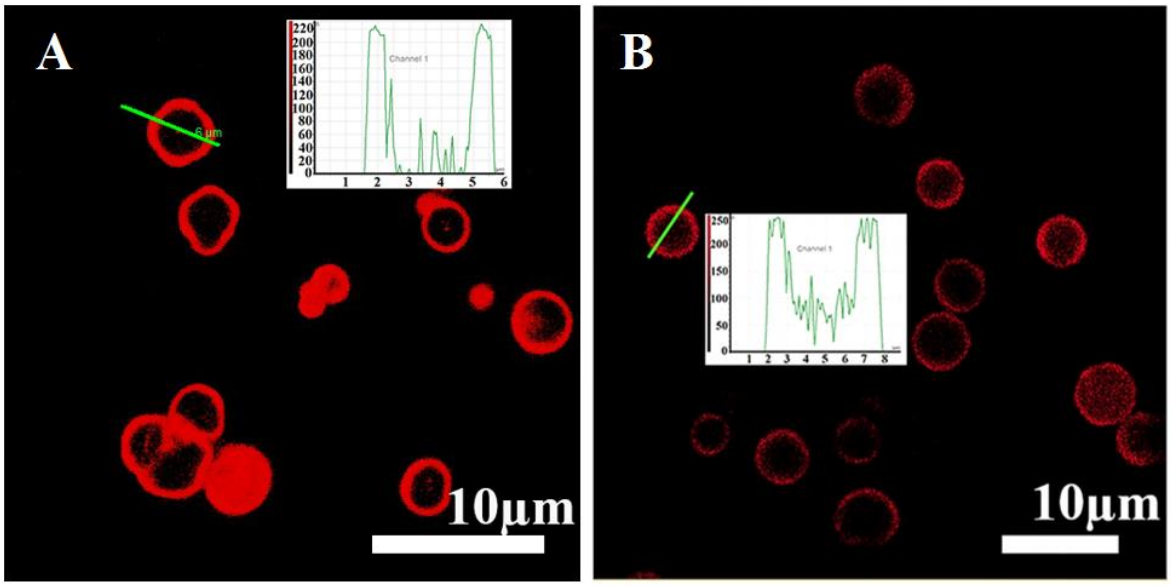

Figure 4.13 CLSM images of PAH/PSS/Silica (A) and PARG/DEXS/silica composite capsules (B) loading with TRITC-dextran. The inset line scan images showed relative fluorescent intensity in the corresponding capsules.

It is easy to encapsulate large molecules such as the TRITC-dextran (500 kDa) *via* their coprecipitation during the formation of $CaCO_3$ templates. Due to the large size of such molecules, most of them can not diffuse out of the capsules in the $CaCO_3$ dissolution process by EDTA. There is no doubt that TRITC-dextran can be sealed inside the $(PAH/PSS)_4$ and $(PARG/DEXS)_4$ capsules with an additional silica coating which drastically decreased their shell permeability. The red fluorescence (owning to the dextran labeled with the dye TRITC)

was observed with a main distribution around the inner shell of the composite capsules, **Figure 4.13**, due to the attachment of dextran to the amino-terminated inner surface of the microcapsules.[36] Actually such possible attachment could be facilitated by both hydrogen bonds and the hydrolysable covalent cross-links resulting from aldehydes and primary amines coupling.[36]

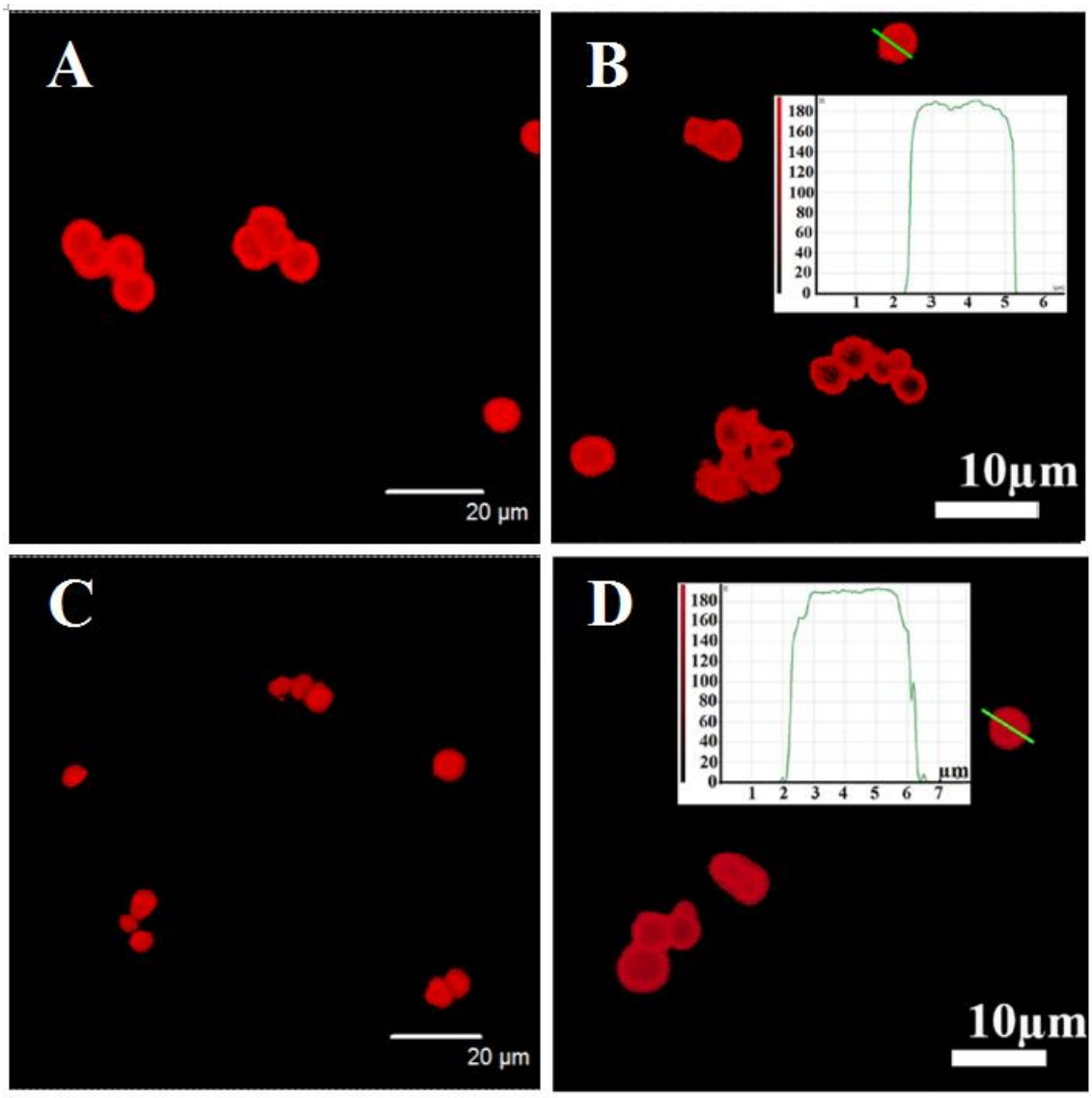

Figure 4.14 CLSM images of PAH/PSS/Silica (A, B) and PARG/DSS/Silica (C, D) composite capsules loading with Rh-B. The inset line scan images showed relative fluorescent intensity in the corresponding capsules.

In terms of whether it is possible to encapsulate small molecules, Rh-B was used as a model molecule instead of FITC due to its longer life time. It is expected that the formation and growth of silica NPs within polymer multilayers and on their internal and outside surfaces provided adequate capability to seal the shells and therefore to entrap Rh-B inside the capsule cavities. In this case, it was necessary to load them inside the capsules during silica coating process[16] rather than in the precipitation process of $CaCO_3$ cores. Because Rh-B inside $CaCO_3$ cores diffused outside during the subsequent three times washing process, showing that the obtained pink templates changed to white before assembling the polyelectrolytes layers. Also, without silica sealing, it was impossible to contain the water soluble Rh-B inside the PAH/PSS and PARD/DEXS capsules for a reasonable time. On the contrary, as the formation and growth of rigid silica inside the polyelectrolyte multilayers can block the possible diffusion or escape path for the cargos, thusly with proper control of *in situ* silica formation and incorporation process, Rh-B molecules were sealed inside these obtained composite capsules, as given in **Figure 4.14**. These two ways to encapsulate cargos showed that it is possible to load the composite capsules with a library of molecules with different molecular weights.

4.6 Enhanced Ultrasound Responsiveness of the Composite Capsules

Capsules with non-degradable PSS/PAH and degradable PARG/DEXS functionalized by the *in situ* formed silica NPs were studied as examples for ultrasound treatment.

4.6.1 PSS/PAH/Silica Composite Capsules

Remote activation of microcapsules was conducted using an ultrasonic setup operating at a frequency of 20 kHz and power output 50 W. The suspension of microcapsules was submitted to ultrasound treatment for different duration times (2, 4, and 6 s). A high ultrasonic sensitivity of the composite microcapsules was evidenced. **Figure 4.15** shows

the resulting SEM images of capsules with different shell composition stimulated for different ultrasound duration time. It is clearly seen that pure $(PSS/PAH)_4$ capsules were slightly deformed after sonication, whereas the composite capsules were broken into small fragments. Such an observation is consistent with several other reports, which showed that the ultrasound sensitivity of the PSS/PAH capsules could be remarkably increased if NPs were embedded in the polyelectrolyte network.[24,269] Most of composite capsules were broken after only 2s' sonication. From the broken fragments, it shows clearly that the shell thickness of the fragments decreased with increasing sonication time, because more silica NPs were separated from the composite shells. For 6s' ultrasonication, the fragments became much smaller with a large portion of small dots appearing. One reasonable explanation for the increased sensitivity is that the incorporation of SiO_2 NPs increased the density gradient across the water/shell interface and consequently improved the absorption of acoustic energy.[14] Another possible explanation is the modification of the shell's mechanical properties. It was known that the concentration of NPs in the capsule shell could affect the capsule stability.[23] As the concentration reached to a critical point, the nanoparticle interaction effect increased, exceeding the effect of the polyelectrolyte matrix, and played a major role in the shell mechanics.[270] In addition, embedding inorganic NPs in the microcapsule shell could increase the shell stiffness significantly.[254,271] Clearly the presence of rigid NPs within soft polymeric shells reduced the shell elasticity, which made them prone to break during ultrasonic treatment with different fracture patterns.

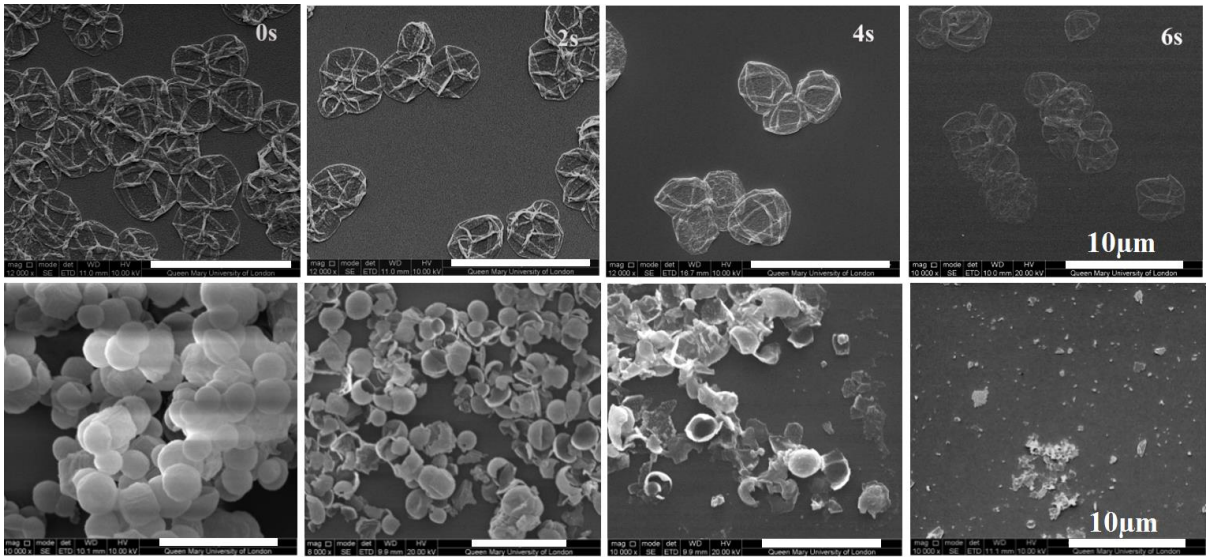

Figure 4.15 SEM images of pure $(PSS/PAH)_4$ capsules (top) and composite capsules (bottom) response to ultrasound with respect to the sonication time: 0 s; 2 s; 4 s; 6 s.

4.6.2 PARG/DEXS/Silica Composite Capsules

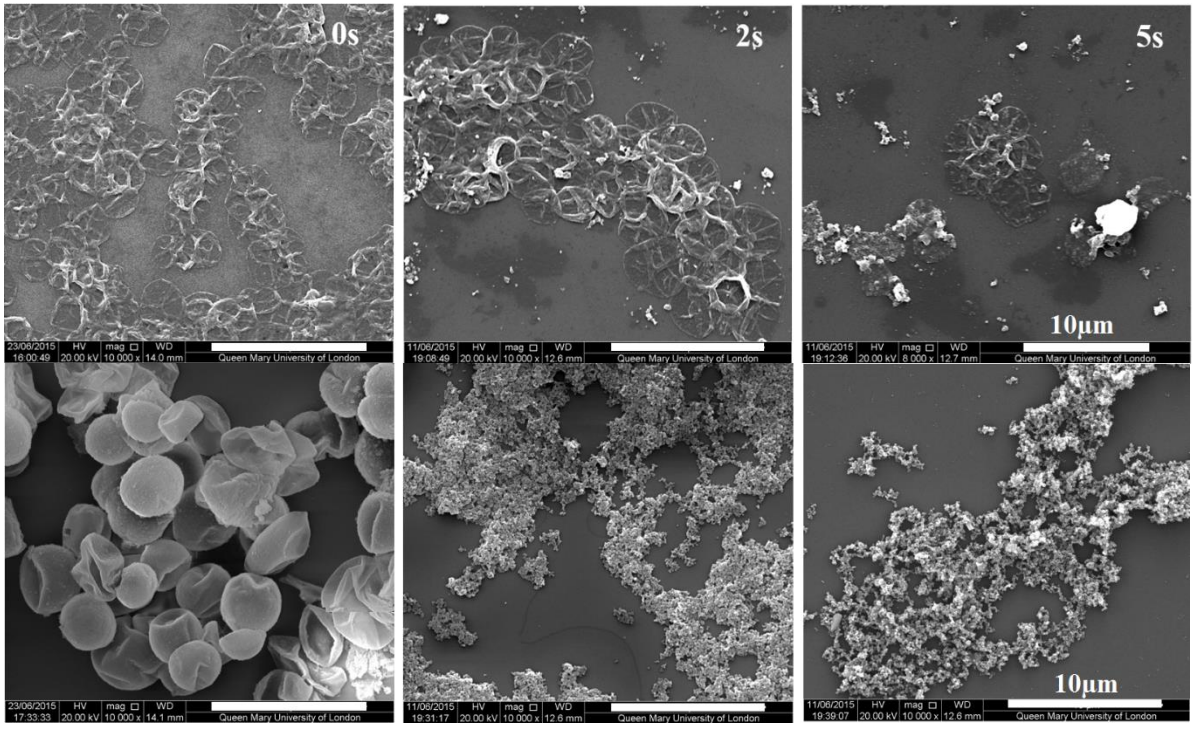

Figure 4.16 SEM images of pure $(PARG/DEXS)_4$ capsules (top) and PARG/DEXS/Silica composite capsules (bottom) response to ultrasound with respect to the sonication time: 0 s; 2 s; 5 s .

The response to ultrasonication of PARG/DEXS system was checked in the same way. Capsules were treated by ultrasound at 20 kHz with 5 W, and the corresponding SEM images were given in **Figure 4.16**. Compared with the PSS/PAH capsule system, the PARG/DEXS capsules without and with silica coating displayed a higher sensitivity. For pure PARG/DEXS capsules, some small pieces were found after only 2 s of ultrasonication and more capsules were broken when prolonging time to 6s. After silica coating, the obtained capsules were all smashed into small pieces within only 2 s of ultrasonication and no change was observed if prolong the treatment time. These results indicated that silica NPs increased their sensitivity to ultrasound treatment and that 2 s of ultrasonication was enough to break all of the PARG/DEXS/silica composite capsules.

4.7 Ultrasound Triggered Release from PSS/PAH/Silica Capsules

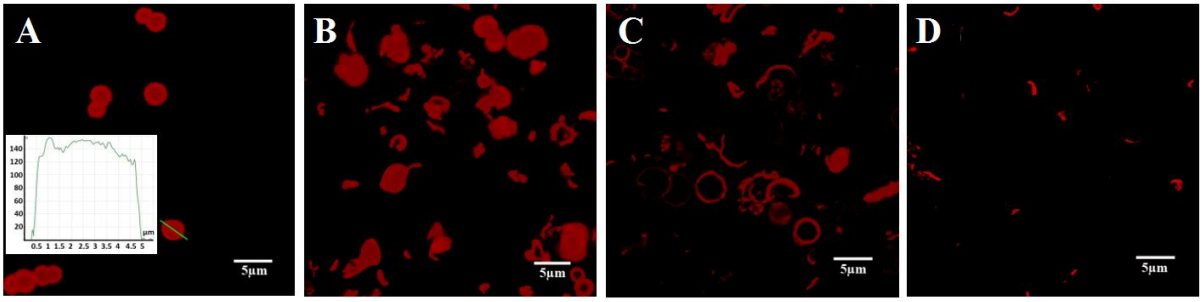

Figure 4.17 CLSM images of Rh-B containing PSS/PAH/silica microcapsules after ultrasound treatment with different time: (A) 0 s; (B) 2 s; (C) 4 s; (D) 6 s. The free Rh-B was removed by washing for several times before the measurement. Line scan inset showed relative fluorescent intensity in the corresponding capsules.

PSS/PAH/silica capsules were chosen as a model to study the Rh-B release triggered by ultrasound. The capsules loading with Rh-B after treated by ultrasound for different time were measured by CLSM, **Figure 4.17**. Obviously, ultrasonication caused a rapid

release of capsule ingredients. After 6 s of ultrasound irradiation, only very small debris with limited fluorescent signal can be observed (**Figure 4.17 D**).

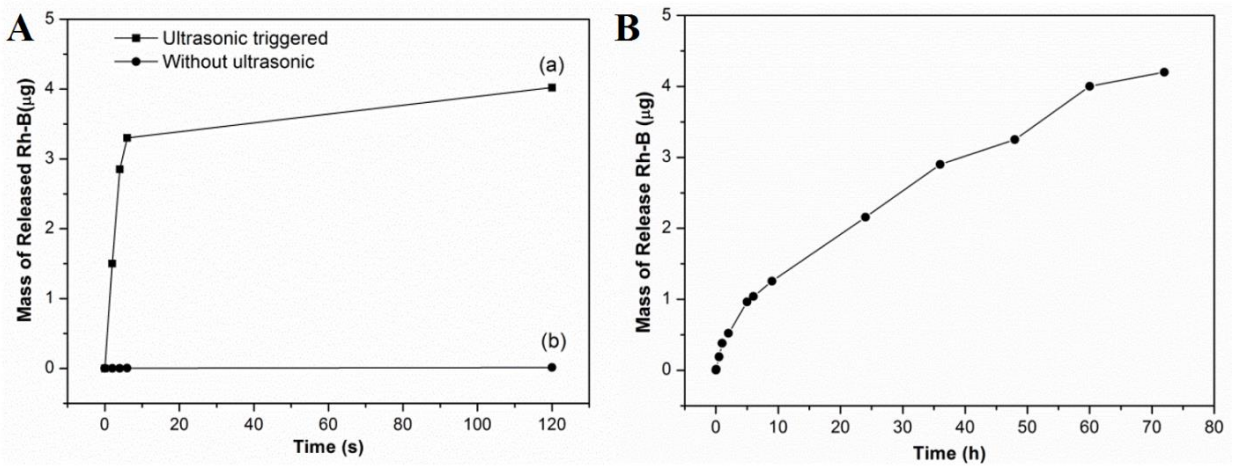

Figure 4.18 Mass of released Rh-B from composite capsules. Square: ultrasonic triggered release; Spheres: without any treatment.

Quantitative measurement of the dye release characteristics (*i.e.*, a combined effect of diffusion and ultrasound effect) was shown in **Figure 4.18.** It was estimated that the total mass of the encapsulated Rh-B was 5.0 μg inside ~6.25×10^6 capsules in this work (*i.e.*, ~ 0.8 pg per capsule). As shown in **Figure 4.18 A (a)**, the released Rh-B increased rapidly following the ultrasound triggering. ~30% of the fluorescent dyes was released in just 2s, and it increased to 66% in 6 s. The release curve became flatted after that, reaching a value of ~80% after 120 s. In contrast, without ultrasound triggering, the encapsulated Rh-B released very slowly (**Figure 4.18 A(b)**), only ~0.26% of the encapsulated dyes was detected after 120s. If prolonging the time to 1 hour, the value reached to 7.6% and 48h later, 43% of the dyes were diffused outside the capsules (**Figure 4.18 B**). Obviously, ultrasonic stimulation is an effective and efficient way to release the encapsulated compounds in PAH/PSS/SiO_2 capsules. It should be noted here that not all the encapsulated dyes were released (as detected). Besides the possible

photobleaching effect, some fluorescent dyes were adsorbed on composite capsule shells, as shown in CLSM images (**Figure 4.17 B-D**). In addition, based on the results of **Figure 4.16**, the ultrasound triggered release from PARG/DEXS/silica capsules should be faster as they were instantly broken by ultrasound.

4.8 *In Vitro* Cytotoxicity of Polyelectrolyte/Silica Composite Capsules

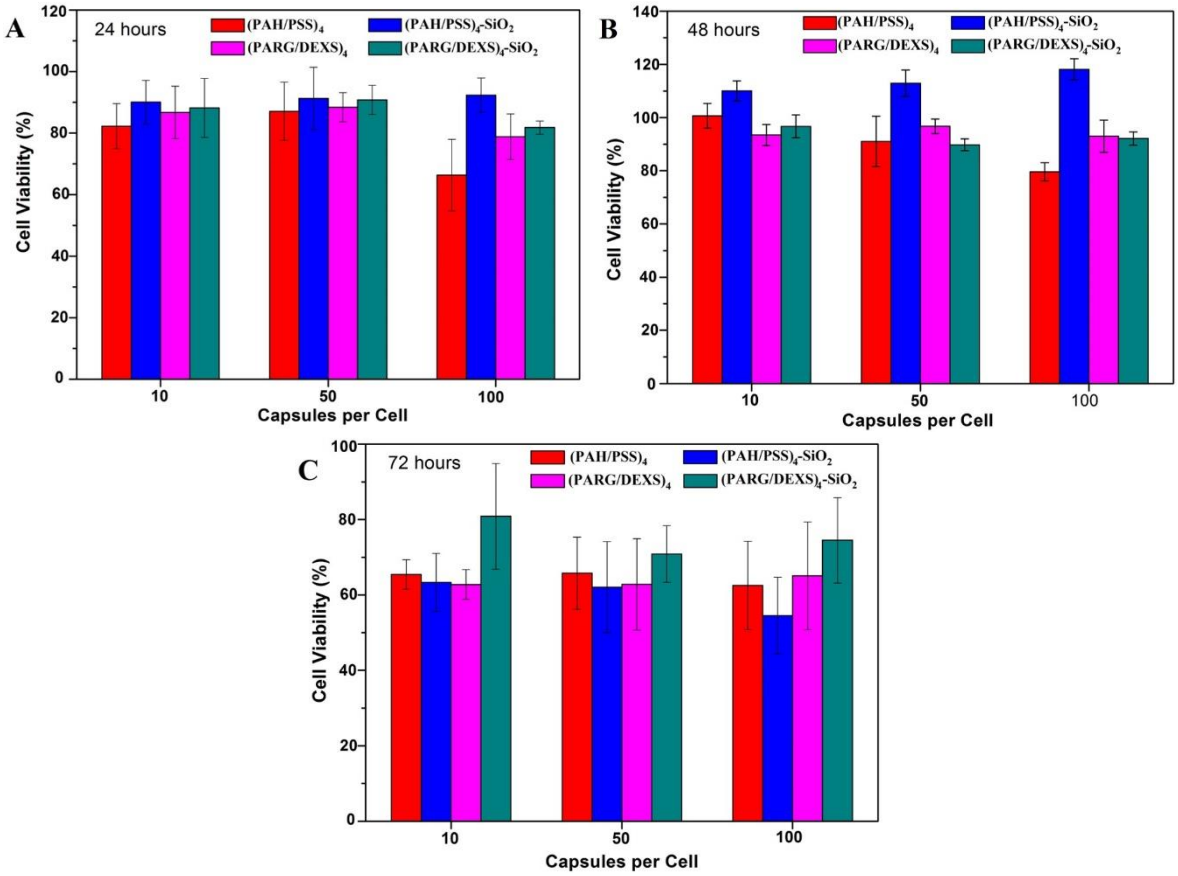

Figure 4.19 Cell viability of B50 cell line mixed with different concentration of PAH/PSS, PAH/PSS/Silica, PARG/DEXS, PARG/DEXS/silica capsules for (A) 24 h, (B) 48 h and (C) 72 h at 37 °C respectively as measured by an MTT assay compared with the control. The error bars show the standard deviations

An *in vitro* cytotoxicity study of PAH/PSS, PAH/PSS/silica, PARG/DEXS and PARG/DEXS/silica was carried out for B50 cancer cell at different concentrations of capsules/cell (10, 50, 100) for 24 h, 48 h, and 72 h as shown in **Figure 4.19**. The pre-fabricated microcapsules with various compositions were dispersed in cell culture medium and were cocultured with the B50 cells, after which the cell viability was measured by MTT colorimetric assay. The results indicated that all the investigated compositions evidently possess low cytotoxicity at concentrations equal or below 50 capsules/cell during the first 24 h as the cell viability was more than 80% (**Figure 4.19 A**). For both the normal and degradable polyelectrolyte systems, capsules with silica coating showed a higher cell viability than the corresponding polyelectrolyte capsules without silica incorporation, indicating that amorphous silica is not toxic to cells. With the concentration at 100 capsules/cell, the cell viability was about 66% only for PAH/PSS capsules, while the cell viability for other compositions were all still above 80%. Nevertheless, the concentration-dependent toxicity behavior of PAH/PSS/SiO_2 was different to that of plain PAH/PSS capsules. The cell viability of PAH/PSS/SiO_2 increased when increasing the ratio of capsules/cell, suggesting that the observed toxicity is only due to the presence of non-degradable capsules in solution, which further confirms the stability and excellent biocompatibility of capsules with silica coating in cell systems. After the next 24 h, the MTT assay revealed for all that the cell viability increased in a great amount (≥90%) except PAH/PSS capsules at high ratio (100). It is worth mentioning that PAH/PSS/SiO_2 capsules displayed the best cell viability, which means the B50 cells already get used to these capsules with silica coating and show good cell proliferation. Cell viability of biodegradable polyelectrolyte capsules with silica was not as good as that even through still remained around 100%, which might because a certain amount of nontoxic silicic acid produced by the hydrolysis of silica NPs slightly inhibited the cell proliferation process by decreasing local extracellular or intracellular pH.[108, 272] Interestingly, after 72 h incubation

the cell viability of different capsules dropped below 70% for all concentrations except that of the bio-degradable PARG/DSS/SiO_2 composite capsules (around 80% or above), revealing PARG/DSS/SiO_2 capsules were the best biocompatible. Therefore, the above data and analysis clearly point out that microcapsules composed of biodegradable polyelectrolytes and amorphous silica have no major negative effect on cell viability.

4.9 Degradation of Polyelectrolyte/Silica Composite Capsules

When the capsule shell is raptured during *in vitro* degradation studies, the fluorescent payload molecules should be released into the cytosol and thusly stain the cells. In view of the above observation subsequent *in vitro* cell degradation experiments utilised a microcapsule : cell ratio of 20 : 1. Rh-B was employed as a model small molecule cargo which was sealed inside the composite capsules with both types of polyelectrolyte building blocks. CLSM images in **Figure 4.20** revealed a gradual degradation of PARG/DEXS/SiO_2 capsules loaded with Rh-B, which confirmed that the PARG/DEXS/SiO_2 capsules are intrinsically degradable. The B50 cells were stained into red within only two hours, revealing Rh-B molecules released outside quickly from the composite capsules as a consequence of the possible intracellular degradation of silica composite shells. More capsules were degraded into very small fragments (as indicated by the arrows) and the fluorescence intensity of the cells increased gradually with prolonging the incubation time. When time reached to 72 h, no intact composite capsules can be found, but only small red dots were observed.

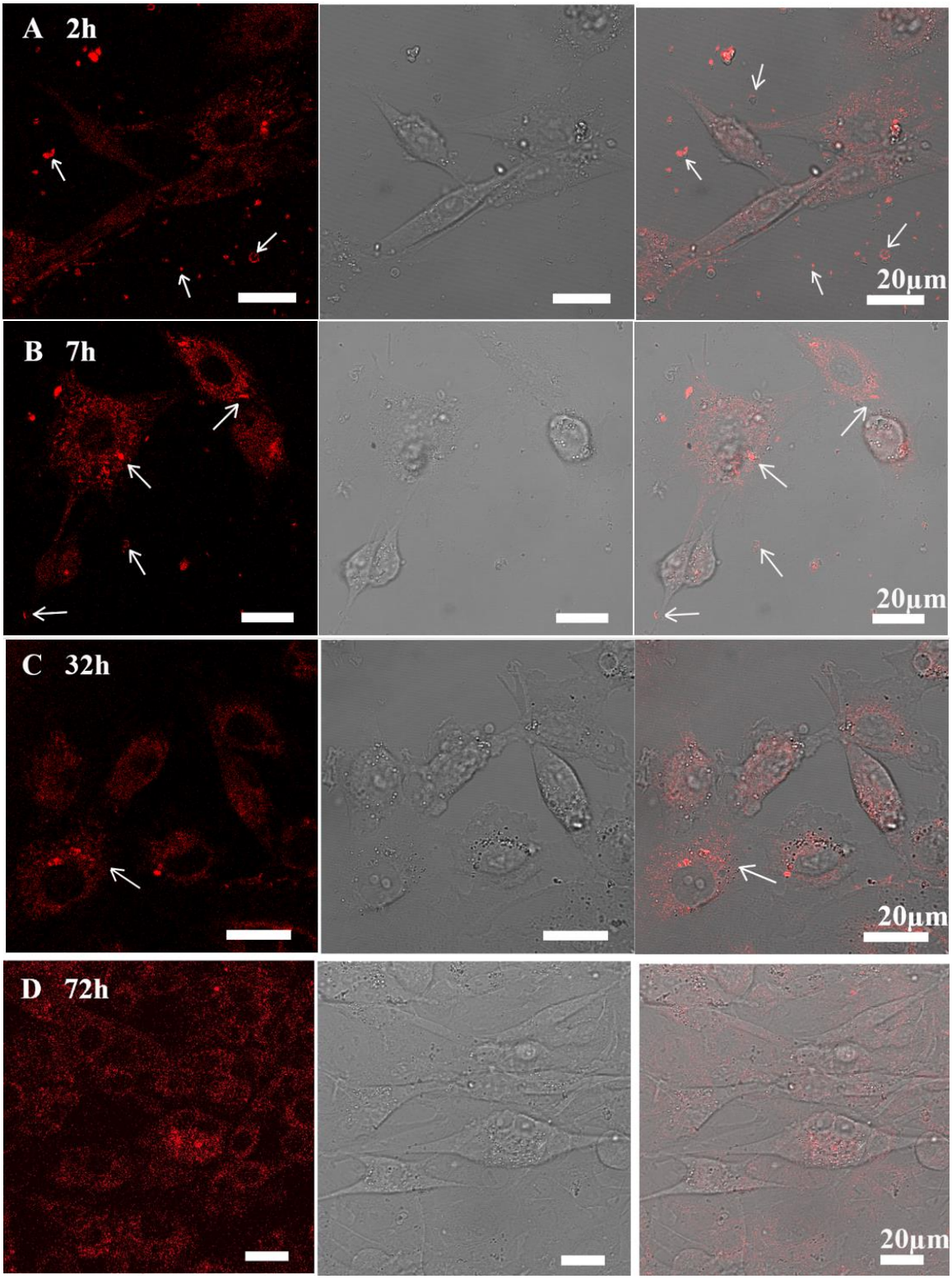

Figure 4.20 Confocal laser scanning microscopic (CLSM) images of B50 cells cocultured with the PARG/DEXS/silica composite capsules with Rh-B sealed inside their cavities for different time. (A) 2 h; (B) 7 h; (C) 32 h; (D) 72 h.

Normally, amorphous silica could be degraded by cells and finally removed from the body through liver and spleen (particle size above 10 nm)[30] into bile and feces or via renal clearance (<5:5 nm).[191,273] The degradability of silica, however, is significantly affected by their combination with different polymer.[108] Hence non-degradable polyelectrolyte/silica capsules, i.e., PAH/PSS/SiO_2, were investigated as a control comparation in this study. The corresponding CLSM data were shown in **Figure 4.21**. These images clearly point out that the PAH/PSS/SiO_2 capsules are non-degradable; *i.e.*, all the internalized capsules did not cracked into pieces over the time. In the initial 8 hours, nearly all fluorescent molecules were sealed tightly inside the capsule cavities, showing intact red fluorescent filled rings in the system. No red fluorescent Rh-B molecule were not spread along the cytosol of the cells. Such results are totally different from that of PARG/DEXS/SiO_2 capsules, which revealed that the polyelectrolyte building blocks also play a vital role on the capsule degradability. However, if we prolong the coculture time to 33 hours, few cells were slightly dyed into red (as indicated by arrows). Moreover, the number of dyed B50 cells and their fluorescence intensity increased after 72 h cultivation with PAH/PSS/SiO_2 capsules (as indicated by arrows). This might be explained by three possible reasons: (1) local crush of the silica blocks in the composite shells occurred if the capsules were subjected to intracellular pressure for long time as composite shells are more fragile than the soft PE shells;[16,108,274] (2) some minute defects appeared owing to the minor intracellular degradation of pure silica blocks on the top external surfaces of the composite shells (these parts of silica were not much entangled with soft polyelectrolytes; (3) Rh-B molecules were small enough to escape to the outside through these defect points even though the concrete-like blended parts were stable and non-degradable.

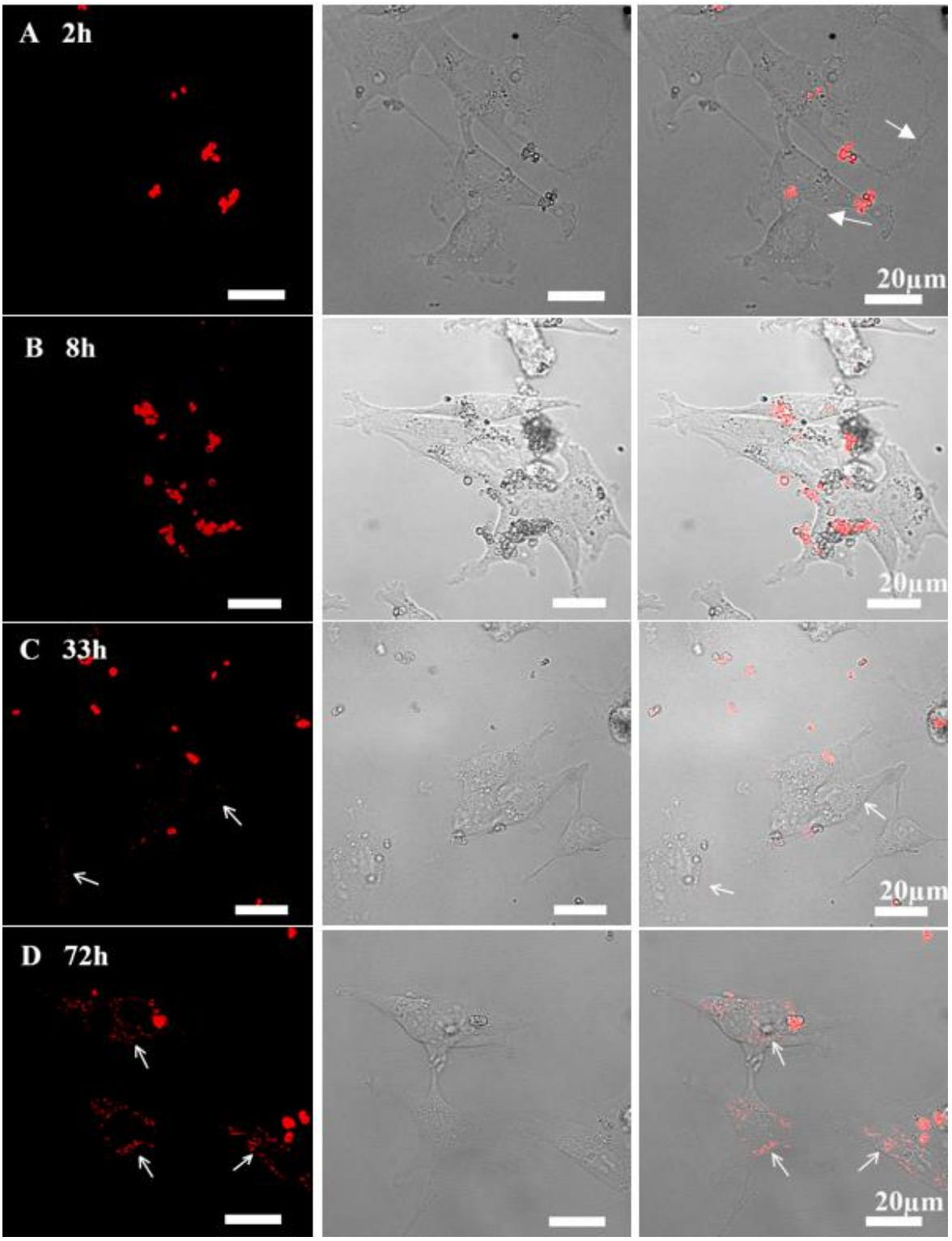

Figure 4.21 CLSM images of B50 cells cocultured with the PAH/PSS/silica composite capsules with Rh-B sealed inside their cavities for different time. (A) 2 h; (B) 8 h; (C) 33 h; (D) 72 h.

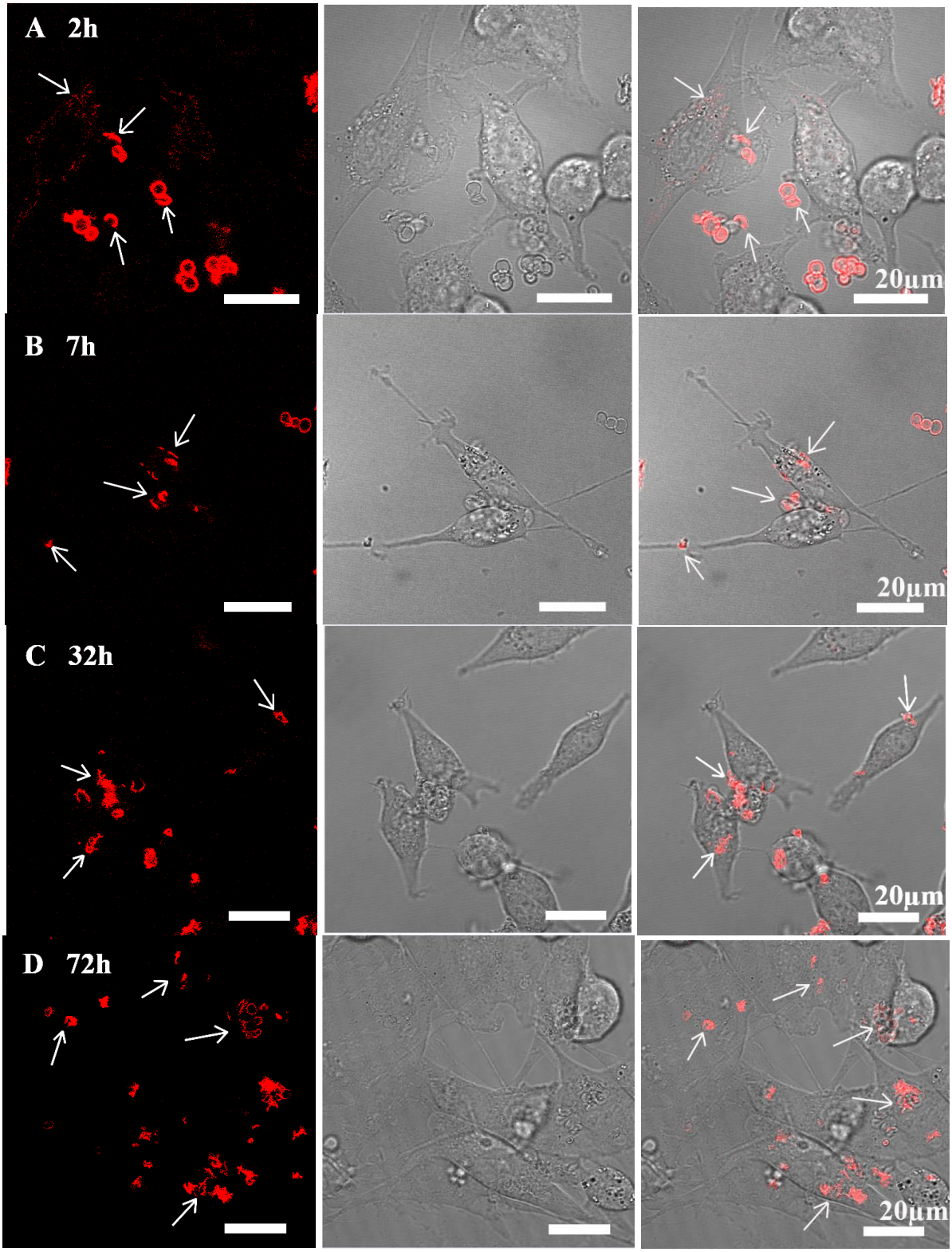

Figure 4.22 CLSM images of B50 cells cocultured with the PARG/DEXS/silica composite capsules with TRITC-dextran sealed inside their cavities for different time. (A) 2 h; (B) 7 h; (C) 32 h; (D) 72 h.

In order to illustrate this result more clearly, the degradation behaviour of PARG/DEXS/SiO_2 and the control capsules (PAH/PSS/SiO_2) encapsulated with large molecule TRITC-dextran were well studied respectively by recording the behaviour of capsules in cells. In the first two hours, most of the PARG/DEXS/SiO_2 showed complete structure with red dyes inside their cavities, and few of them were degraded into large pieces which stained some cells into weak red colour, as shown by arrows in **Figure 4.22 A**. The images acquired at later time points demonstrate a gradual intracellular degradation of PARG/DEXS/SiO_2 capsules. After 32h cultivation, **Figure 4.22 C** and **D**, all of the capsules were decomposed into red fragments (indicated by the arrows). Note that no red dots were inside the nuclei at any time point indicates that the shell fragments cannot cross the nuclear membrane.[128] However, as shown in **Figure 4.23**, after 73 h of incubation the PAH/PSS/SiO_2 microcapsules (the control) with a complete structure were still present in the cells; they clearly remained the ball-like structure filled with TRITC-dextran as indicated by the arrows. Such results clearly revealed TRITC-dextran with big molecular weight can't escapes outside form PAH/PSS/SiO_2 capsules despite some small defects might appear in their composite shells due to a possible degradation of pure silica part on the top surfaces. Therefore, the presence of four bilayers of non-degradable PEs (PAH, PSS) are enough to block the capsule degradation, in which no spontaneous release of TRITC-dextran occurs.[108,275] The presence of some kinds of polyelectrolyte layers could impede the degradation of SiO_2 which could be used as a protecting layer for some special application, as it has been reported by others.[108,275]

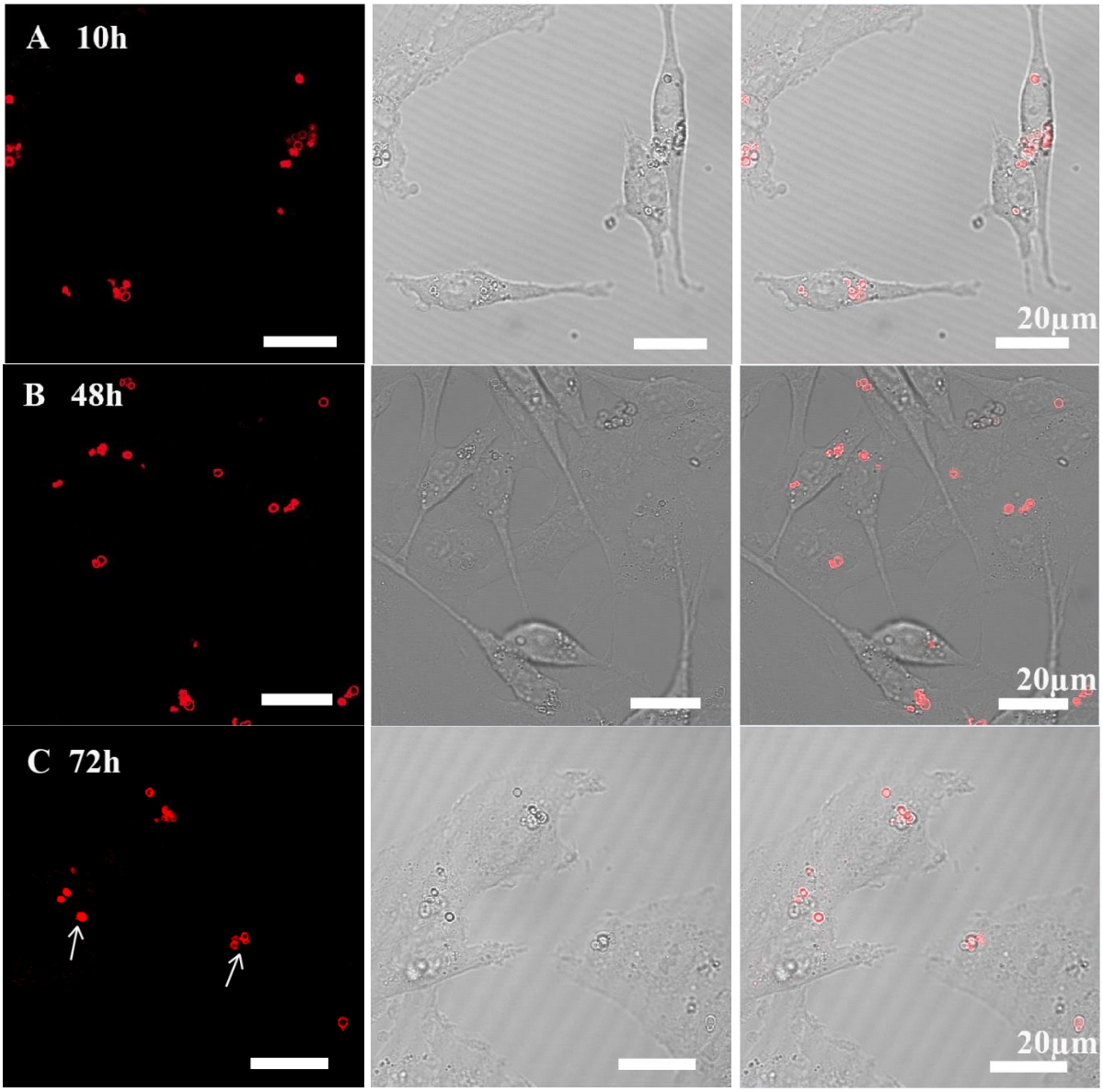

Figure 4.23 Confocal laser scanning microscopic (CLSM) images of B50 cells cocultured with the PAH/PSS/SiO_2 composite capsules with TRITC-dextran sealed inside their cavities.

We assume that the composite capsules which contains amorphous silica NPs and biodegradable PARG/DEXS polyelectrolytes spontaneously degrade in B50 cells. For the degradation mechanism, it is likely related to the combination of two effects, hydrolysis of amorphous silica and enzyme driven decomposition of PARG/DEXS polymers.[30,128,191] Recently, Andrea Ott *et al*. have produced a degradable silica capsule by depositing amorphous silica on removable templates and proved that they were degradable in cells due to the hydrolysis of such silica shells.[108] In the case of our composite capsules, they formed firstly

by concreting silica NP together with enzymatically degradable PARG/DEXS multilayers and followed by a deposition of a relatively thin pure silica layer on the outer shell surface. The degradation should start from the top surface of the composite capsules caused by the hydrolysis of silica with a by-product of free silicic acid. As we know from other work that the presence of biodegradable PARG polymer on the surface of silica shell did not block their dissolution,[108] the subsequent degradation of the concrete parts should include the enzymatic decomposition of PARG/DEXS besides the hydrolysis of silica blocks. Indeed the escape of the cargo molecules was due to the initial appearance of defects and cracks and the final complete fragmentation of the carriers. The small size of the final carrier fragments enables their easy excretion *via* renal systems.[30,191] Together with the excellent biocompatibility of SiO_2 and PARG/DEXS polyelectrolytes, the feature of their efficient drug loading, shells decomposition without any requirement of external trigger and simultaneous cargo release achieved in the PARG/DEXS/SiO_2 composite capsules make it ideal for a wide range of diagnostic and therapeutic applications with great promise for potential delivery of small molecule drugs.

4.10 Protection of $CaCO_3$ Cores by Composite PAH/PSS/Silica Shells

4.10.1 Influence of Shell Composition

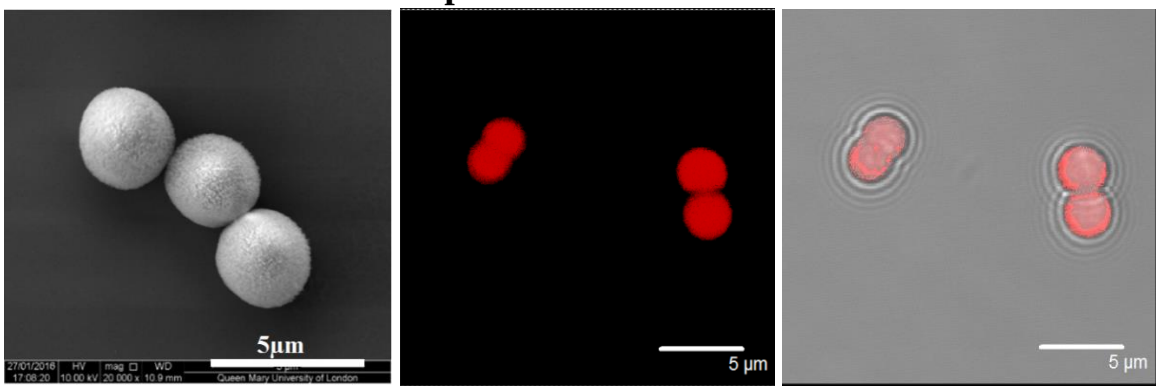

Figure 4.24 SEM and CLSM images of $CaCO_3$ cores loading with TRITC-Dextran.

As the PAH/PSS/silica composite shells were proved with a low permeability and able to encapsulate small molecules, Rh-B, the idea of applying them for core protection was motivated by this.[16] Rh-B is difficult to preload inside $CaCO_3$ cores, so TRITC-dextran was chosen as fluorescent probes. In this study, TRITC-dextran dyes were encapsulated inside $CaCO_3$ cores by co-precipitation method. SEM images in **Figure 4.24** indicated the porous structure of the formed $CaCO_3$ microparticles. Their CLSM images demonstrated that the TRITC-dextran molecules were successfully encapsulated and homogenously distributed inside the cores.

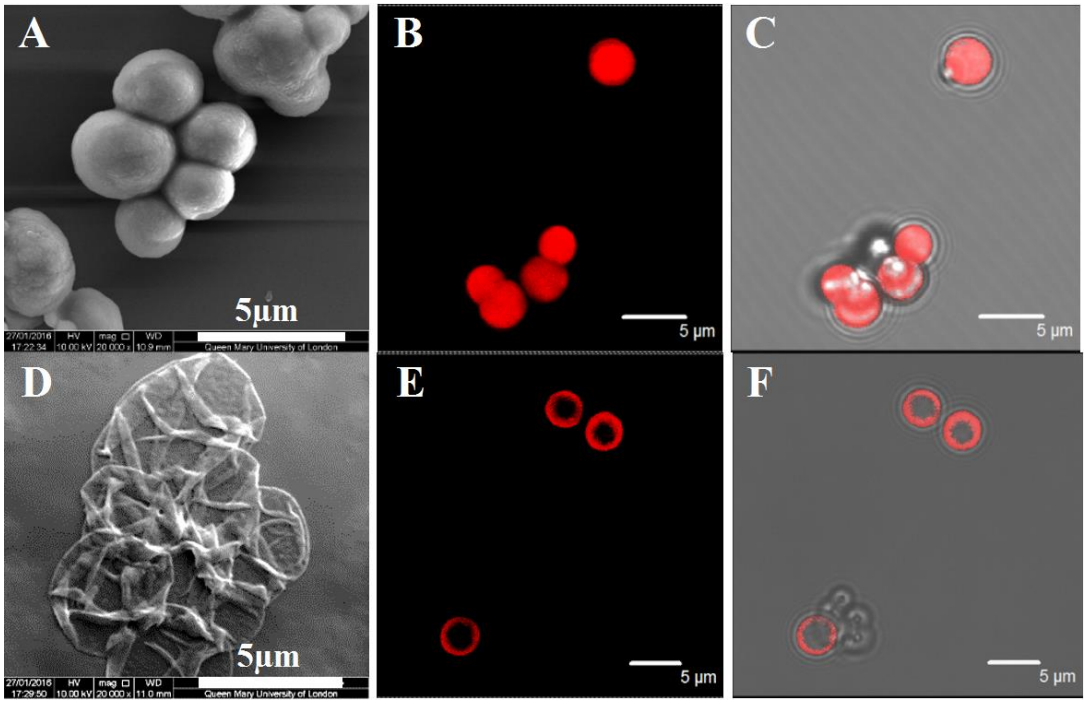

Figure 4.25 SEM (A, D) and CLSM (B, C, E, F) images of $CaCO_3$ microparticles with 8 layers without silica coating before and after EDTA treatment.

$CaCO_3$ microparticles loading with TRITC-dextran were then first coated with 4 bilayers of PAH/PSS and followed by an additional silica coating. There is no doubt that $CaCO_3$ core are facilely dissolved by EDTA treatment without silica coating, forming $(PAH/PSS)_4$ capsules, as

proved by the SEM image in **Figure 4.25 D**. SEM image in **Figure 4.25 A** revealed that with polyelectrolyte coating, surfaces of the particles became smooth. Their CLSM images confirmed that the dyes were still kept inside. However, after EDTA treatment, the collapsed structure and hollow rings proved that $CaCO_3$ core were completely removed. Notably, all the TRITC-dextran dyes preferred to locate around the inner surfaces of the PAH/PSS capsules, and such results were in good accordance with the above results in **Figure 4.13**.[123]

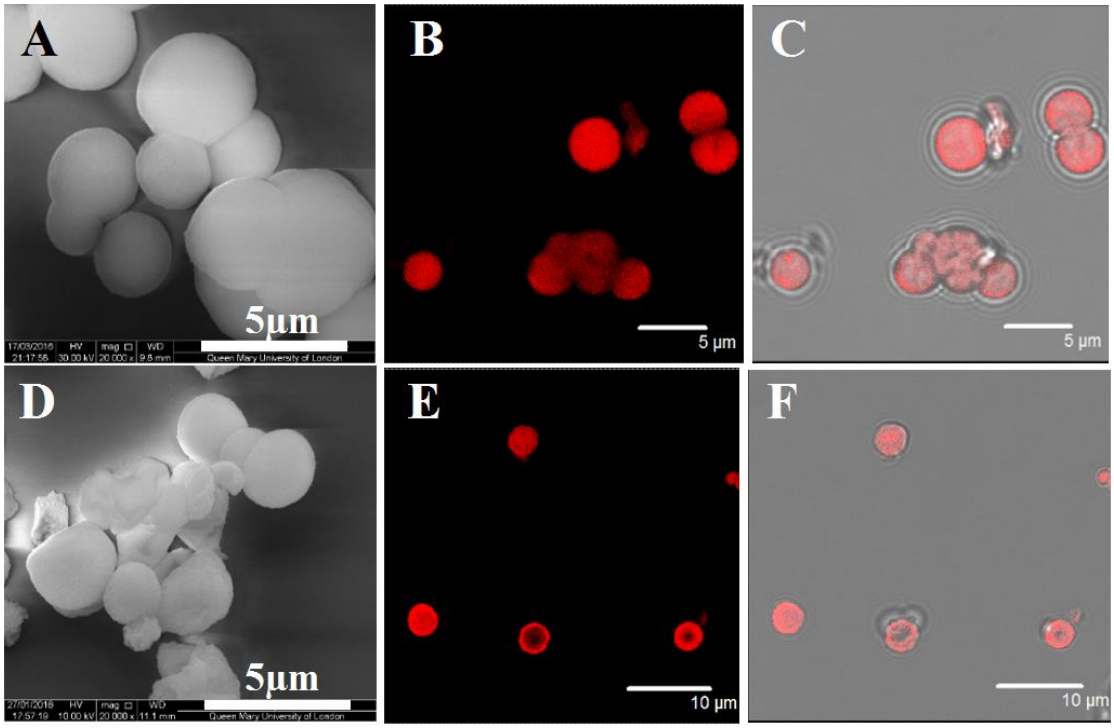

Figure 4.26 SEM (A, D) and CLSM (B, C, E, F) images of $CaCO_3$ microparticles with 8 layers with silica coating before (A-C) and after (D-F) EDTA treatment.

After coated with silica NPs, $CaCO_3$/$(PAH/PSS)_4$/silica before and after EDTA treatment were observed *via* SEM and CLSM, **Figure 4.26**. The surfaces of the particles became much smoother if compared **Figure 4.25 A** and **Figure 4.26 A**. TRITC-dextran molecules were still homogenously distributed inside the cores, **Figure 4.26 B** and **C**. However, **Figure 4.26 D** indicated that most of the cores were removed with EDTA treatment. The corresponding

CLSM images confirmed this results. In addition, the particles after EDTA treatment were further characterized by TEM and EDX spectra. Most particles in TEM image (**Figure 4.27**) were hollow. Some of them maintained solid cores, but these cores were not intact. Only small amount of Ca element was detected by EDX, **Figure 4.27**.

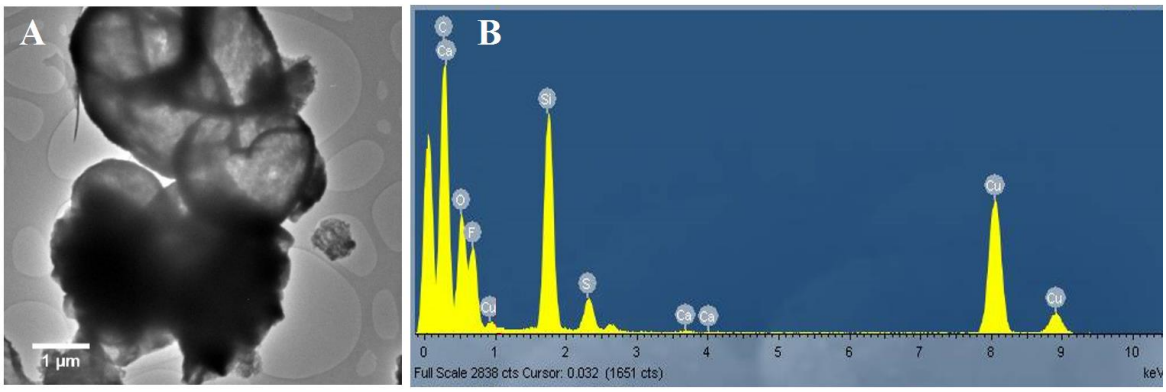

Figure 4.27 TEM images (A) and EDX spectrums (B) of $CaCO_3$/$(PAH/PSS)_4$/silica particles after EDTA treatment.

The above results illustrated that the $(PAH/PSS)_4$/silica shells were not dense enough to prevent the penetration of EDTA molecules. The poor densification of these composite shells was mainly due to that the solid $CaCO_3$ cores prevented the shrinkage degree of PAH/PSS multilayers during the silica coating process, which is totally different from the coating on hollow PAH/PSS capsules. In order to make the shell more compact, denser and thicker, introducing more polyelectrolyte layers or silica coating cycles on the surfaces of the $CaCO_3$ particles should be a promising approach. Therefore, $CaCO_3$ particles with 6 bilayers were studied. **Figure 4.28 B** indicated that the cores with 6 bilayers were removed completely by EDTA, showing a thicker folders under dry state. Results of $CaCO_3$/$(PAH/PSS)_6$ particles well coated by silica NPs (**Figure 4.28 C** and **D**) revealed a significant difference after treating by the acid. It can be seen from their SEM images that most of the particles were intact, still

possessing spherical morphology. Moreover, the CLSM images confirmed their solid structure, showing a uniform distribution of the dyes (**Figure 4.28 D**), and such result can be further proved by the EDX mapping images in **Figure 4.29**.

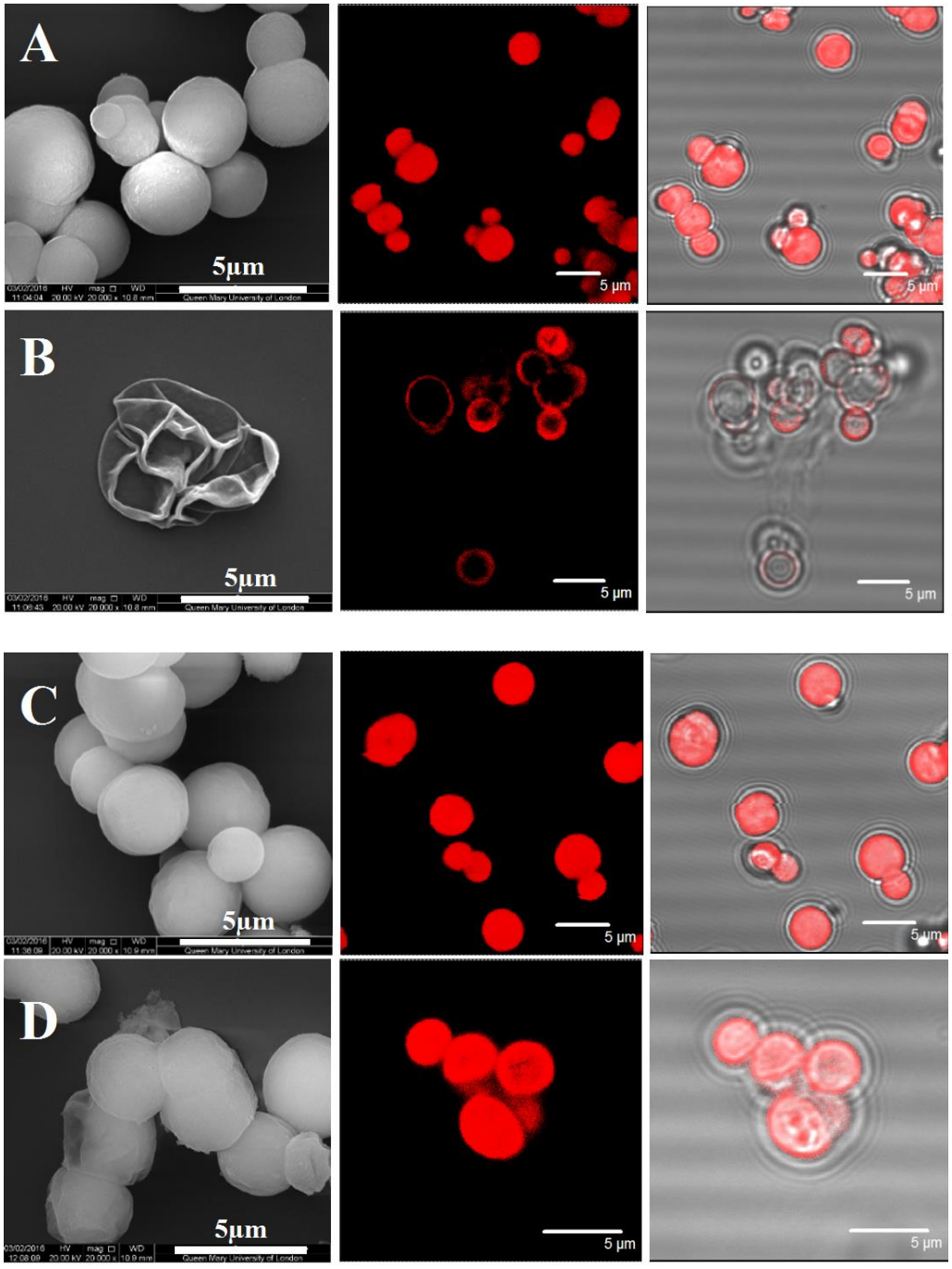

Figure 4.28 SEM and CLSM images of $CaCO_3$/$(PAH/PSS)_6$ without (A,B) and with (C,D) silica coating before (A, C) and after (B, D) EDTA treatment.

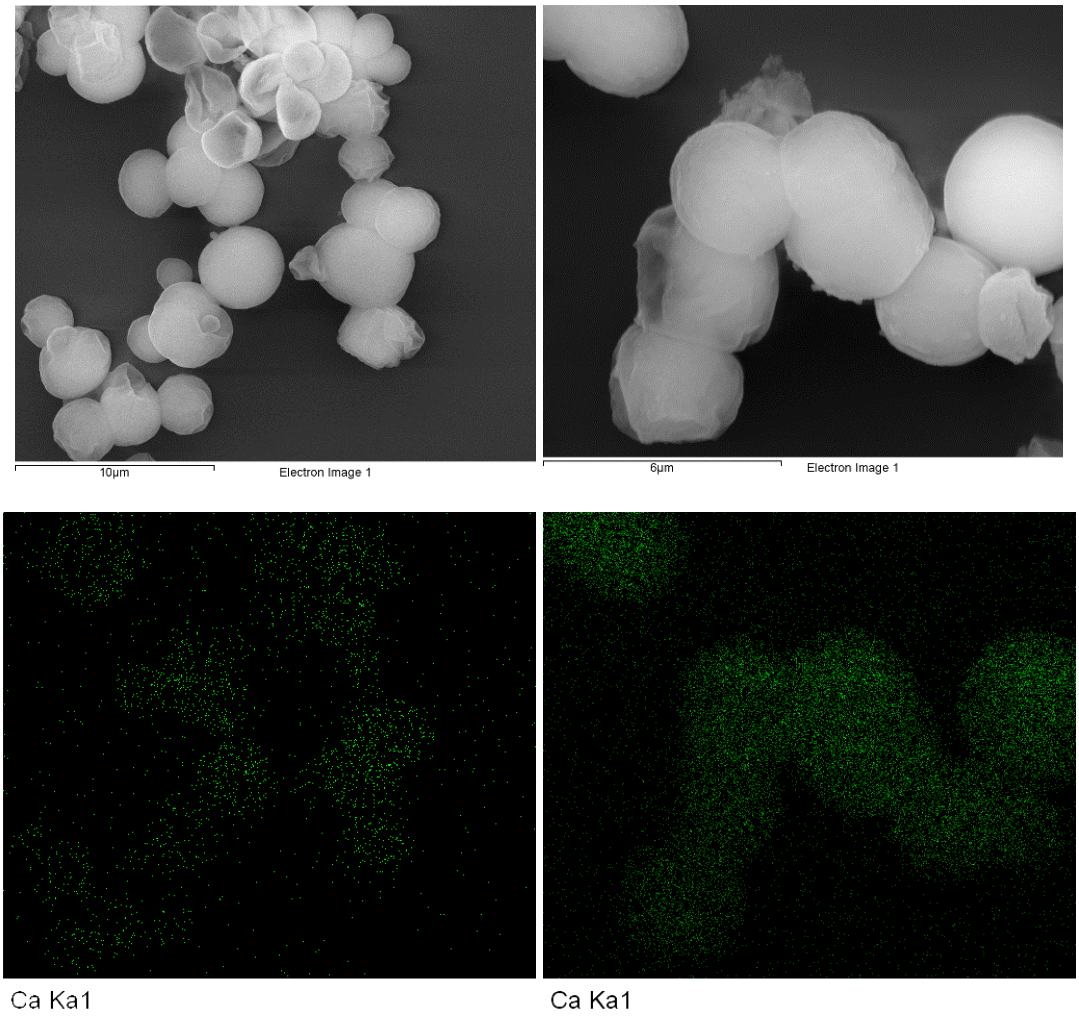

Figure 4.29 EDX element mapping of $CaCO_3$/$(PAH/PSS)_6$/SiO_2-EDTA

TEM images in **Figure 4.30** revealed that more than half of the particles were protected from dissolving by the acid, remaining their intact cores inside. EDX spectra collected from the solid point and film-like point of the particles were displayed. No Ca element was detected from the hollow point, which indicated a completely dissolving of the $CaCO_3$ core. In contrast, a huge amount of Ca was found from the solid position as indicted by the arrow, confirming the solid structure with $CaCO_3$ core inside. A reasonable explanation for the hollow particles is that

some defects or cracks existed in the composite shells that left penetration channels for EDTA molecules.

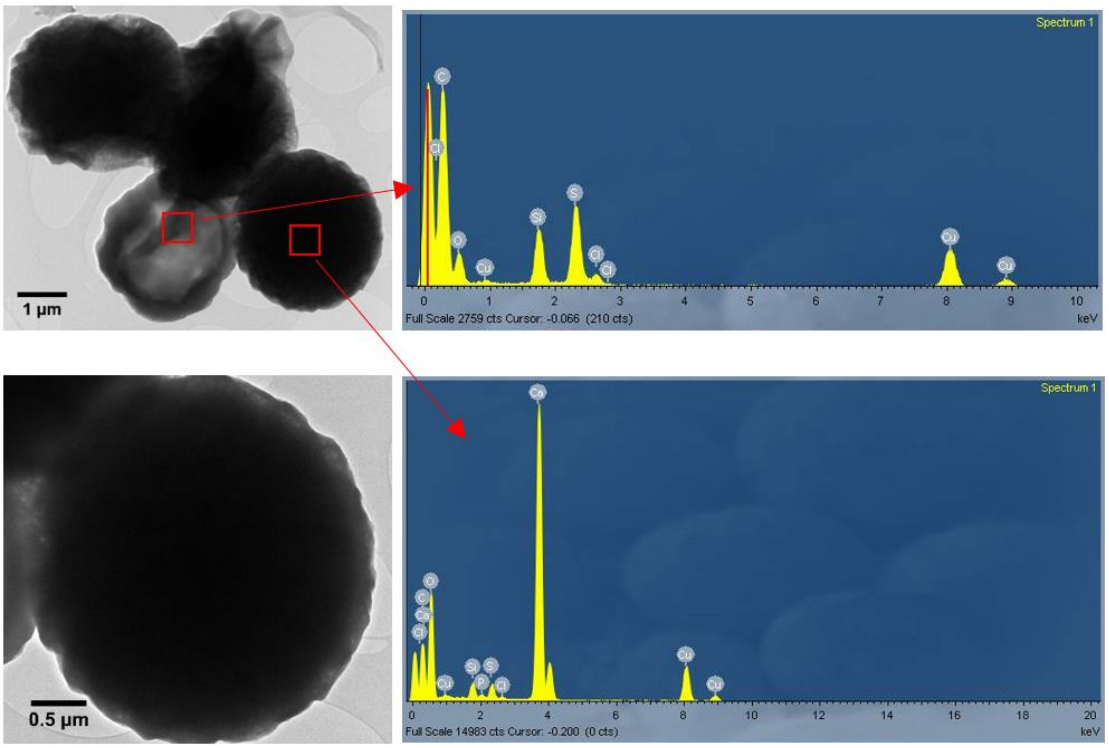

Figure 4.30 TEM images and EDX spectrums collected from different positions of $CaCO_3/(PAH/PSS)_6/SiO_2$ after EDTA treatment.

Another way to obtain the thick composite protecting shells is employing 12 layers of polyelectrolyte but 2 cycles of silica coating, *i.e.*, $CaCO_3/(PAH/PSS)_4/SiO_2/(PAH/PSS)_2/SiO_2$. Due to the one more cycle of silica coating, the formed composite shells were thicker than that with only one cycle of silica coating and showed a more protecting behaviour. The formed particles before and after acid treatment were shown in **Figure 4.31**. Nearly no difference can be seen from SEM images of the particles without and with either EDTA or HCl acid treatment. TEM images showed that $CaCO_3$ core are definitely inside, and the SEM image of one broken particles indicated the solid core wrapped under the composite shells.

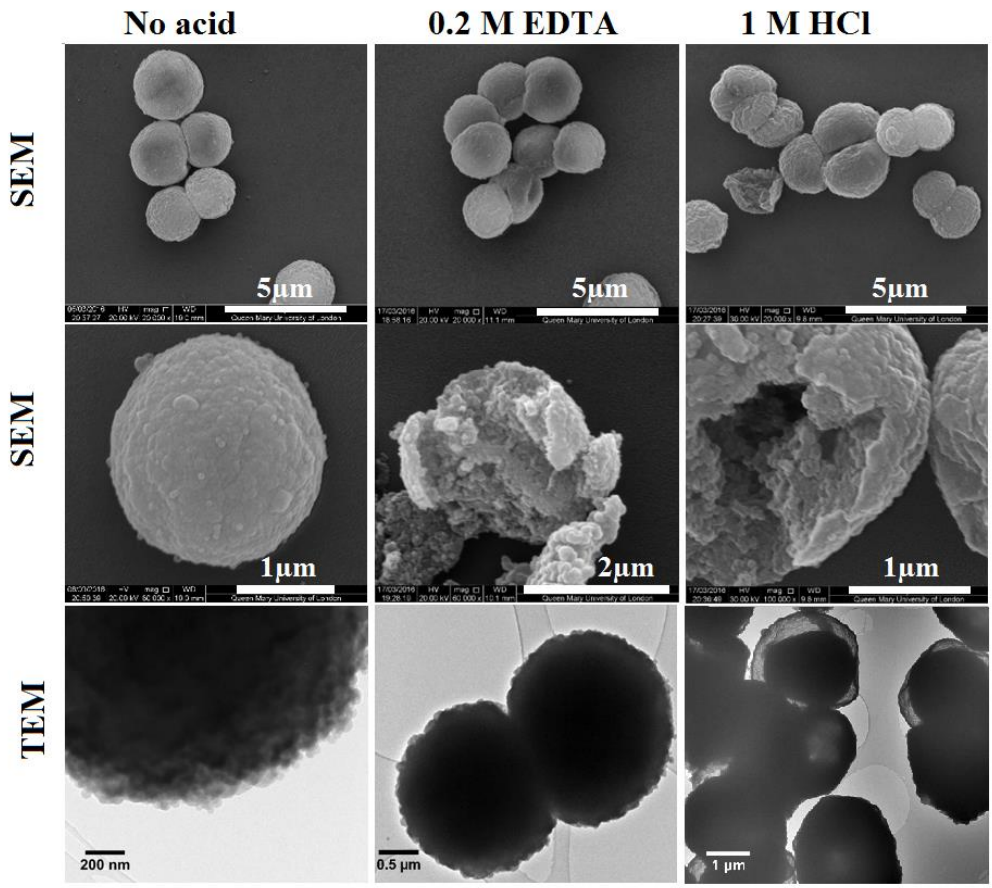

Figure 4.31 SEM images of $CaCO_3$/$(PAH/PSS)_4$/SiO_2/$(PAH/PSS)_2$/SiO_2 without (A) acid treatment and with EDTA (B) and HCl (C) treatment. TEM images of the particles after EDTA (D) and 2 minutes of 1 M HCl treatment (E).

In addition, an interesting structure was observed from the $CaCO_3$/$(PAH/PSS)_4$/SiO_2 /$(PAH/PSS)_2$/SiO_2 system after dissolving by the acid. It seems that the particles were double-shelled, as indicated by images of **Figure 4.32**. During the second cycle for PAH/PSS assembly, they may not attach on the composite shell firmly due to the high roughness of some particles and thus some gap formed after the final cycle of silica coating. But, it should be noted from the TEM image that $CaCO_3$ were intact. A possible reason is that this specific double-shelled structure prolong the diffusion time for the acid molecules and dissolved mass molecules.

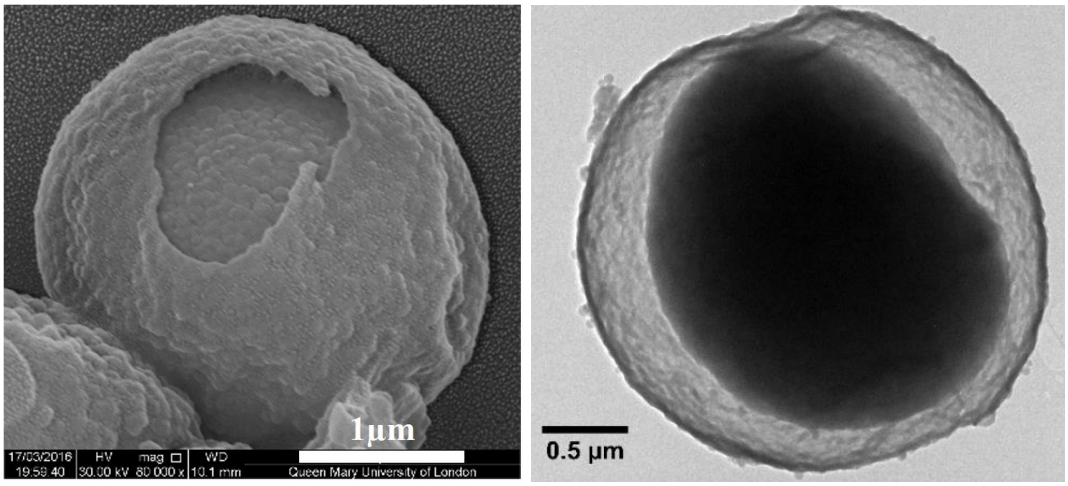

Figure 4.32 SEM and TEM images of $CaCO_3$/$(PAH/PSS)_4$/SiO_2/$(PAH/PSS)_2$/SiO_2-EDTA.

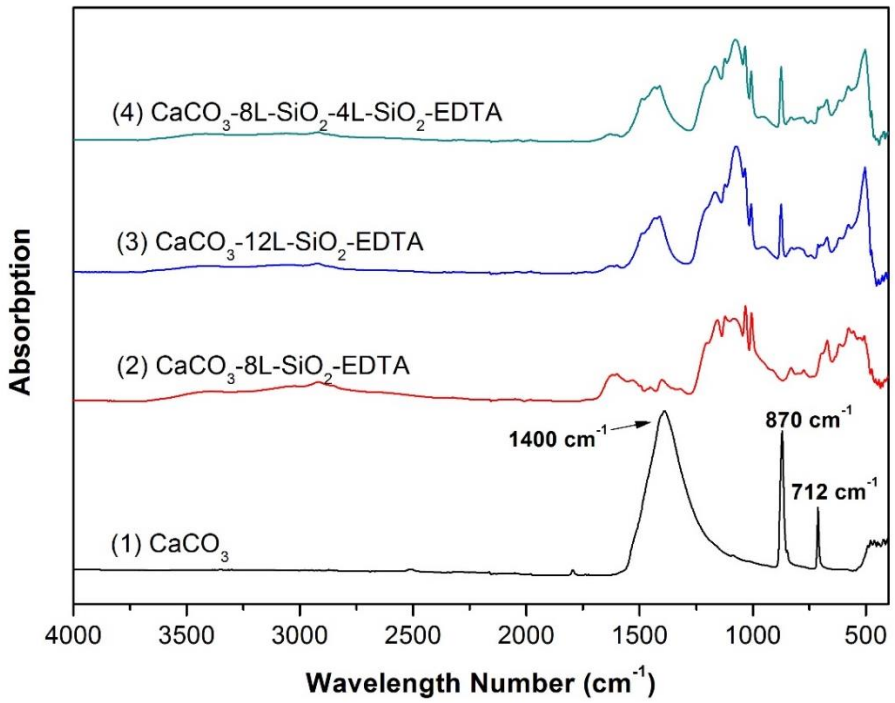

Figure 4.33 FITR spectra of particles with different composition.

Spectra of pure $CaCO_3$ and $CaCO_3$ with different coating components after EDTA treatment are shown in **Figure 4.33**. The spectrums of pure $CaCO_3$ cores mainly possessed 3 absorption peaks, ~1400, ~870 and ~712 cm^{-1}. After dissolving by EDTA acid, only a small peak at 1400 cm^{-1} was detected for $CaCO_3$/$(PAH/PSS)_4$/SiO_2 sample, however, obvious strong bands at ~1400 and ~870 cm^{-1} were observed for $CaCO_3$-

$(PAH/PSS)_6/SiO_2$ and $CaCO_3(PAH/PSS)_4/SiO_2$ /$(PAH/PSS)_2/SiO_2$ samples. The FTIR results were well in conformity with the above discussed conclusion from the SEM, CLSM and TEM data.

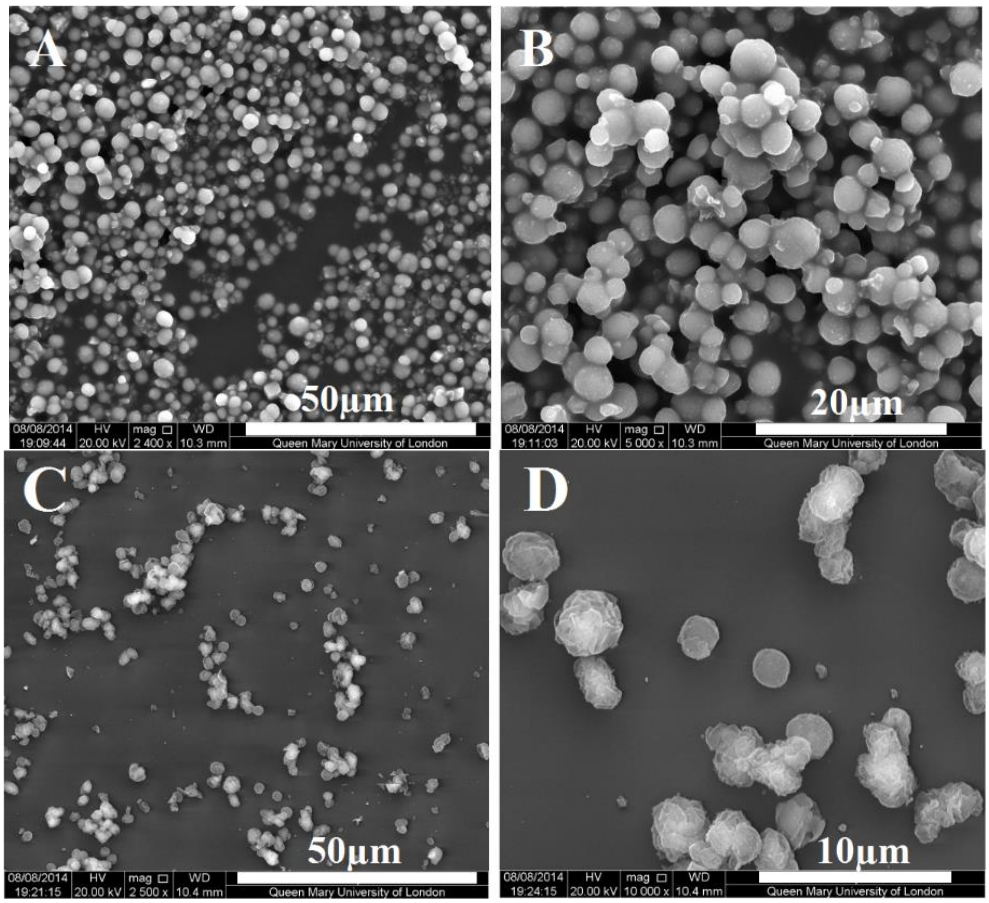

Figure 4.34 SEM images of $CaCO_3/SiO_2$ before (A, B) and after (C, D) dissolving by EDTA.

Additionally, it should be pointed out that both the soft polymer and the *in situ* formed silica NPs are all important components. The polymers play a role of glue to connect to and integrate the formed NPs. Without the polymer glue, pure silica shells can not prevent EDTA dissolving the $CaCO_3$ cores, due to the high porosity of the inorganic shells.[16] **Figure 4.34** demonstrated that with only silica coating on the surface of $CaCO_3$, most of them were removed after the EDTA treatment and only a few particles were ball-like in shape. Another key point is the amount of the polymers. As proved above, due to limited shrinkage of the shells resulted from

the robust cores, 4 bilayers is not enough to obtain the dense composite shells, but if increase the layer number to 12, a different result was obtained, *i.e.*, the formed composite thicker and denser shells proving an effectively protecting work for the cores. Therefore, the shell components are very important for their final properties.

4.10.2 Effects of Ultrasonic Treatment

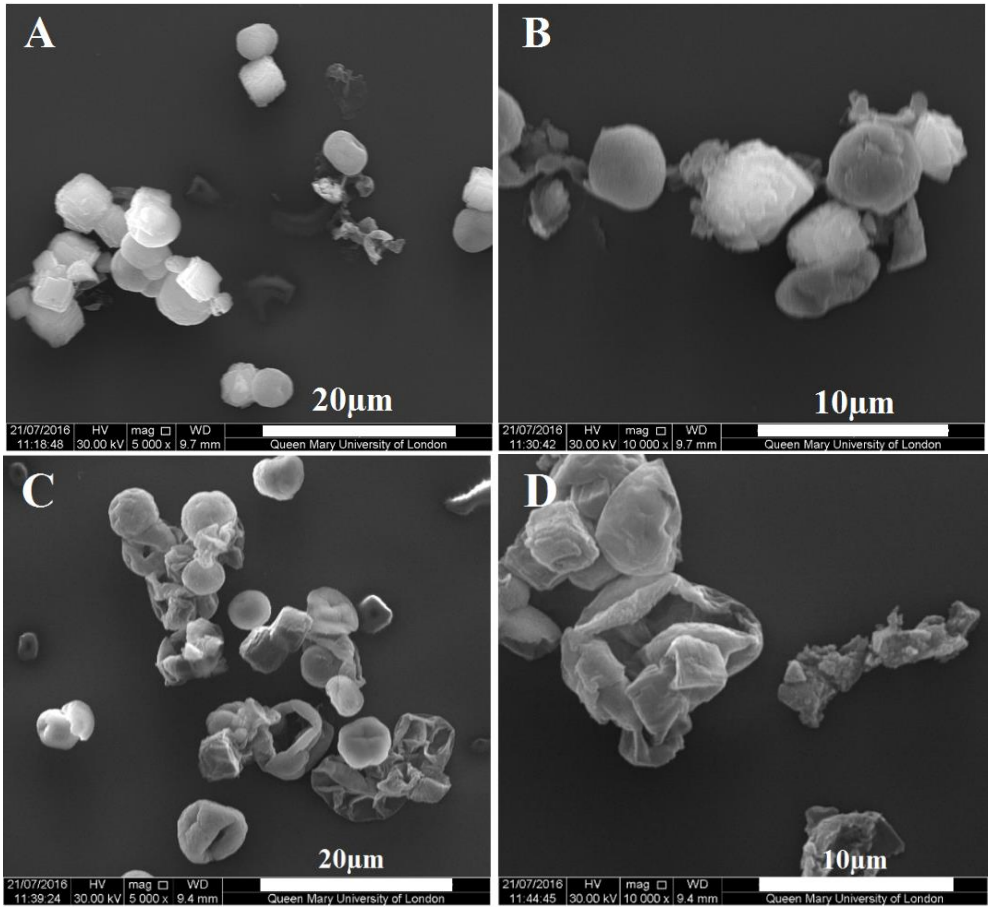

Figure 4.35 SEM images of $CaCO_3$/$(PAH/PSS)_6$/SiO_2 particles ultrasonicated for 2s before (A, B) and after (C, D) EDTA treatment.

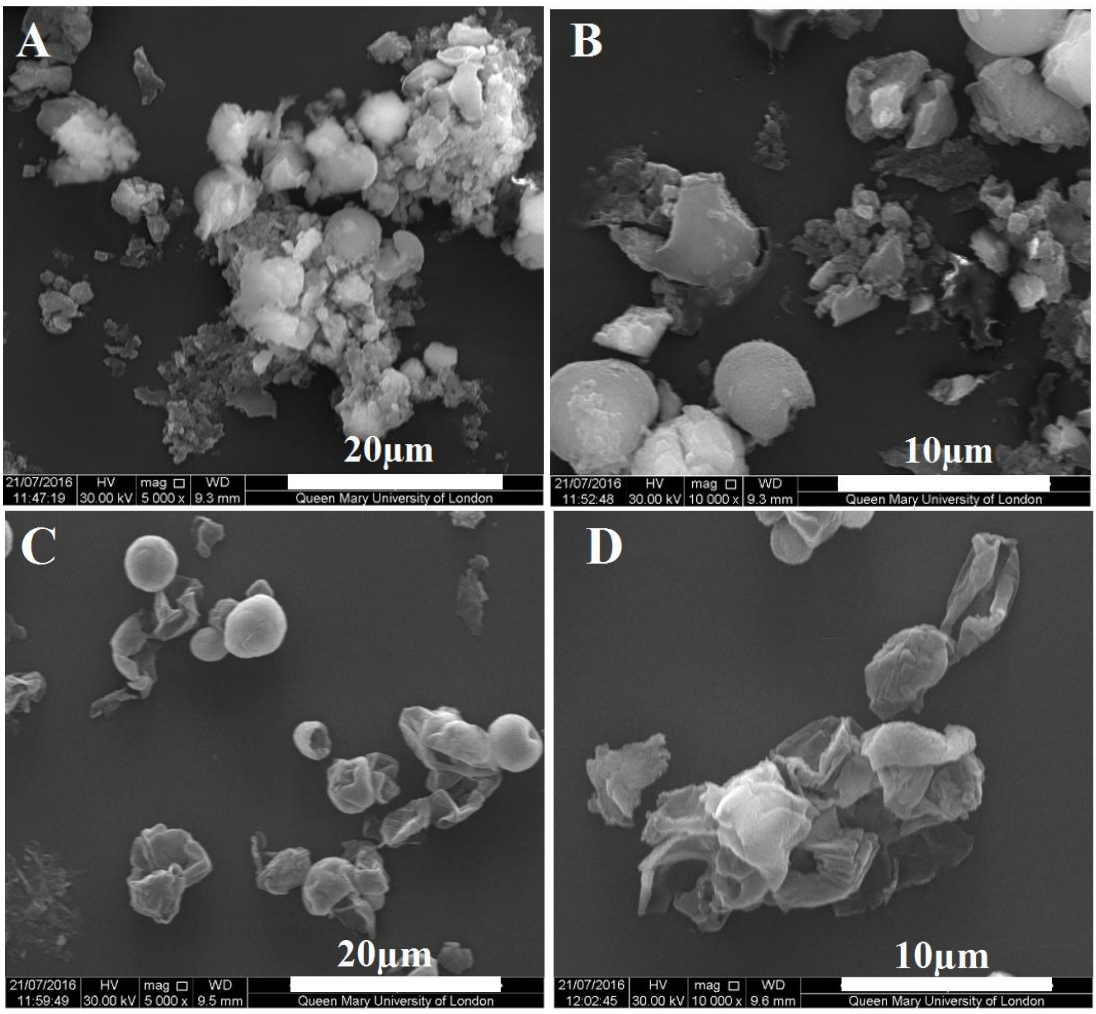

Figure 4.36 SEM images of $CaCO_3/(PAH/PSS)_6/SiO_2$ particles ultrasonicated for 6s before (A, B) and after (C, D) EDTA treatment.

Since the ultrasound sensitivity of the PAH/PSS capsules with silica coating was already proved,[16] it is expected that the integrity of $PAH/PSS/SiO_2$ composite shells covered on $CaCO_3$ particles will be lost if treat these particles with ultrasound. Here, $CaCO_3/(PAH/PSS)_6/SiO_2$ particles were chosen as an example, and similarly, the ultrasound with 20 kHz and power of 50 W was utilized to treat them. As indicated in **Figure 4.35** A and B, some debris of the composite shell were found along with spherical particles after only 2 s of ultrasonication. After treated these particles with EDTA solution, most of the $CaCO_3$ cores were dissolved completely, **Figure 4.35** C and D. If the ultrasonic time prolonged to 6 s, more

small fragments of the composite shells presented, and even some $CaCO_3$ particles were broken into a few pieces, as indicated by **Figure 4.36** A and B. After EDTA treatment, it is clearly seen that most of the particles were collapsed (no $CaCO_3$) as well as some fragments of the PAH/PSS/SiO_2 composite shells.

Obviously, the presence of rigid NPs within soft polymeric shells densified the shell and simultaneously reduced the shell elasticity, which made them able to protect most of the $CaCO_3$ cores inside and prone to be broken under ultrasonic treatment. Different from hollow PAH/PSS capsules that they could shrink as much as they can since no rigid cores were inside to inhibit the shrinkage, the polymeric shell thickness, *i.e.*, layer numbers, influenced their final permeability. The minimum 12 layers were needed to realize a promising protective behaviour. Such above results revealed that the polymeric/silica NPs composites could be potentially applied as protecting coating layer on other subjects.

4.11 Conclusions

We developed a new nanoparticle-reinforced composite shells that has low permeability, high mechanical strength and strong ultrasound sensitivity. Silica NPs were successfully introduced into LbL polyelectrolyte multilayers by *in situ* hydrolysis of TEOS. Different polyelectrolyte multilayer systems were employed in the experiment, including PAH/PSS, PDADMAC/PAZO, PARG/DEXS and PAH/PSS/Fe_3O_4. Silica NPs were successfully introduced into these LbL polyelectrolyte multilayers by *in situ* hydrolysis of TEOS. The hydrolysis consumed

water in polymer shells and formed robust SiO_2 during the precipitation process, yielding dense shells with a reduced permeability.

For PAH/PSS/SiO_2 microcapsules, the morphology and mechanical properties of these composite capsules were found to be tuneable by adjusting several parameters such as temperature, holding time, adding order and the amount of TEOS. SiO_2 NPs were shown to be distributed on the surfaces or inside polyelectrolyte shell, acting as supports for free-standing capsules in both liquid and dry environment. CLSM study confirmed that the permeability of the composite capsules was reduced significantly. As an example of study, the composite capsules were successfully used to encapsulate a small molecule cargo, Rh-B. Further exposure of these capsules to ultrasound treatment showed an irreversible shell rapture and rapid cargo release in a few seconds.

From the study of PAH/PSS/SiO_2 system, the best condition for silica coating on polyelectrolyte multilayer was found and applied to other polyelectrolyte capsules. $(PDADMAC/PAZO)_4$, $(PAH/PSS)_4$-Fe_3O_4, and $(PARG/DEXS)_4$ microcapsules were all successfully coated with silica utilizing the same procedure, and all the obtained composite capsules showed excellent morphology and structure. The results on UV sensitive $(PDADMAC/PAZO)_4$ capsules proved that silica coating showed a freezing effect which prevented them to be destroyed by 2 h of UV irradiation.

For the $(PARG/DEXS)_4$ capsule system, the study represents the first example of the intracellular delivery of various molecules using biodegradable PARG/DEXS/silica composite capsules in B50 cells. It is important because the biodegradability, low *in vitro* toxicity and especially the possibility of loading and release small molecules (≤

1000 Da) were realized in the capsules. TRITC-dextran loading and Rh-B were encapsulated as examples. PAH/PSS/silica capsules with payloads encapsulation were produced in the same way and studied as the control. The results demonstrated that the type of polyelectrolytes is a key parameter that affects the degradation behaviour of the composite capsules. The capsules with a biodegradable polyelectrolytes, *i.e.* PARG/DEXS, can be easily degraded gradually in cells and allow the cargo release, however, in contrast capsules with non-degradable polyelectrolytes, *i.e.* PAH/PSS, can't be completely decomposed even with a long incubation time (72 h) with cells. A possible degradation mechanism based on the combined effects of both hydrolytic degradation of amorphous silica and enzymatic degradation of PARG/DEXS polymers was proposed.

In addition, the feasibility of protecting $CaCO_3$ microparticles by PAH/PSS/SiO_2 composite coatings was studied. The results revealed that both the shell thickness of the polymeric part and the coating of silica NPs were important to the final properties of the formed composite shells. With the rigid $CaCO_3$ cores inside, the shell can't shrink to increase the thickness and reduce the porosity, and on the contrary, growing silica NPs and combining together with the pre-coated polymers was the only way to compact the shells. 12 layer and one cycle silica coating was a minimum requirement to prevent most of $CaCO_3$ from dissolving by EDTA. Such composite coating was also sensitive to ultrasound. Hence, ultrasound can be used to break the top shells and then dissolve the core inside to let cargos release.

In summary, such innovative composite shells are promising for many future applications. The major one is using the composite microcapsules for controlled drug delivery and release. For example, the functional biocompatible PARG/DEXS/silica

capsules are able to encapsulate small molecules and release them *via* self-degradation of the composite shells in cells which can have great potential applications in biomedicine area. Another one is employing the polyelectrolyte/SiO_2 composite films as protective coating, which could be applied under hard conditions.

5. Polyelectrolyte/TiO_2 Composite Capsules

5.1 Background

As demonstrated in Chapter 4, introducing functional inorganic components into polymeric capsule multilayers could enable to obtain smart or intelligent capsules. However, the development of such smart delivery vehicles are very complicated in practice, because usually multi-functionalities are required to satisfy real situations. Single stimulus-responsive capsules are insufficient for many practical applications, as different environmental changes may occur at the same time.[32] For instance, the patients' conditions are usually diverse and complex, thus it is necessary to regulate the drug release rate and dosage according to patients' individual differences.[32] Multifunctional materials can overcome challenges that cannot be solved by their individual components. It is much more favourable and promising that microcapsules possess multi-responsive properties simultaneously. Therefore, designing capsules with multi-functionalities that could be triggered by different stimuli (*i.e.*, enzymes, temperature, pH, ionic strength, *etc.*) is of high scientific and technical importance.[32,33]

It shall be noted, however, that polyelectrolyte/SiO_2 capsules show ultrasound responsiveness only and no other types of conventional triggers. If other stimuli sensitivity could be combined with ultrasound-responsive microcapsules, the formed double stimuli responsive capsules should find a broader range of applications. As rigid inorganic NPs could empower the formed polymeric/inorganic hybrid capsules with ultrasound sensitivity, other responsiveness intrinsically possessed by the inorganic NPs can also be customized by incorporating them in polymeric shells.[276] In many cases, capsules with light sensitivity such as ultraviolet (UV) light are desirable for controlled releases, especially in the fields of surface sciences and environmental applications, where light would be the only available stimulus to trigger the

systems.[104,137,277] The fabrication of such capsules can be generally categorized into two approaches. The first approach is to use polyelectrolytes with either photo-responsive or photo-cleavable groups as the layer material, such as azobenzene, spirobenzopyran, triphenylmethane, or cinnamonyl that can undergo reversible structural changes under UV-vis light.[137,277,278] Typical examples included LbL microcapsules containing azobenzene using poly[1-[4-(3-carboxy-4-hydroxyphenylazo)- benzenesulfonamido]-1,2-ethanediyl, sodium salt] (PAZO) and poly(diallyldimethyl ammonium) chloride (PDADMAC) as the assembling materials, and the UV responsiveness was achieved by UV induced isomerization of PAZO.[104,279] However, such an approach is constrained by the building materials and polyelectrolytes where special groups have to be used. The second approach is to assemble inorganic NPs that can absorb UV light. Due to its excellent biocompatibility, great UV-responsive performance, and good ability for immobilizing biomolecules onto their surfaces, TiO_2 NPs have been widely used.[194-196] But to date only a few reports have involved fabrication of hybrid TiO_2/polyelectrolyte capsules.[3,14,280,281]

It shall be noted that the properties of microcapsules not only depend on the shell composition, but also strongly affected by the preparation method. For example, the mechanics, shell permeability and morphology of the obtained capsules are greatly depended on the fabrication procedure, as demonstrated by the polymer-silica capsules in Chapter 4. Therefore, the procedure of introducing TiO_2 building blocks into polyelectrolyte matrixes also become of great importance. Currently the design and synthesis of hybrid TiO_2/polyelectrolyte capsules mainly *via* three different approaches based on using pre-fabricated TiO_2 NPs: (1) liquid-phase deposition method (LPD); (2) infiltration, absorption and deposition method; (3) Pickering emulsion polymerization method. H. Strohm *et al*. have introduced the TiO_2 coating to polyamide microcapsules through LPD method, yielding polymer/TiO_2 hybrid capsules.[199,

[282,283] In this paper, no further property studies of this hybrid capsules are described. By impregnating PAH/PSS capsules in the pre-fabricated TiO_2 sol, TiO_2-modifed PAH/PSS capsules have been prepared by Dmitry G. Shchukin and the co-workers.[281] They have also demonstrated that the incorporated TiO_2 components can be applied as photocatalysts to reduce metal salts from aqueous solutions.[281] Inspired by these works, T. Chen, *et al.* have investigated employing TiO_2 NPs as the Pickering stabilizer for the preparation of TiO_2-polystyrene hybrid spheres.[280] The hybrid hollow spheres with diameter of 10-50 μm have been obtained by core solvent evaporation method. Even though such techniques allow to embed TiO_2 NPs into polymer shells, but all the above-discussed polymer/TiO_2 capsules have not been proved with the potentials of loading cargos and releasing them by external stimuli triggering. Here, similar to the silica system, we also use *in situ* synthesis and assembly strategy to embed TiO_2 in LbL capsules. Since TiO_2 NPs have good UV-responsive property,[197] it is expected that the formed composite capsules would possess UV sensitivity and could be used for UV-induced release. In addition, benefiting from the existence of numerous hydrogen, van der Waals, or ionic bonds between organic and inorganic materials, the incorporation of *in situ* formed TiO_2 would empower capsules with enhanced mechanical strength, increased thermal and chemical stability, and better ultrasound sensitivity. Generally, the obtained composite microcapsules would possess both ultrasound and UV responsive functions.

5.2 Aim and Objectives

The aim here is to fabricate novel organic/inorganic hybrid capsule systems containing polyelectrolytes and *in situ* formed TiO_2 NPs, and to use them as potential microcontainers for potential triggered release by ultrasound and UV irradiation. The idea is stimulated by the advantages of natural materials that assembling different building blocks together into functional materials and that, the employment of *in situ* formed silica NPs brought certain

promising features to the polyelectrolyte capsule system, which has been demonstrated in Chapter 4. The incorporated robust inorganic NPs increase the ultrasound sensitivity. Hence, following a proper selection of the inorganic NPs, other functions besides ultrasound responsiveness could also be introduced. TiO_2 could absorb UV light and have a good photocatalyst performance. This property could be used to degrade polymeric shells and further release the payloads.

Therefore the main objectives of this chapter are:

1) To fabricate polyelectrolyte capsules $(PAH/PSS)_4$ and to functionalize them with TiO_2 NPs *via in situ* nucleation and growth of TiO_2 inside or on the polyelectrlyte shell surfaces based on hydrolysis of titanium butoxide (TIBO) .

2) To investigate the reaction parameters corresponding to *in situ* formation and assembly TiO_2 in (PAH/PSS) capsules. For example, the reaction time may influence the final morphology and properties of the formed composite PAH/PSS/TiO_2 capsules.

3) To analyse the morphology, structure and stimuli-responsive properties of the PAH/PSS/TiO_2 capsules.

4) To study the cargo substances (macro-molecules, Dextran-TRITC) encapsulation and their triggered release behaviour under UV irradiation and ultrasound treatment.

5.3 Capsules Functionalized by the *in situ* Formed TiO_2

5.3.1 Fabrication and Characterization

5.3.1.1 Fabrication Details

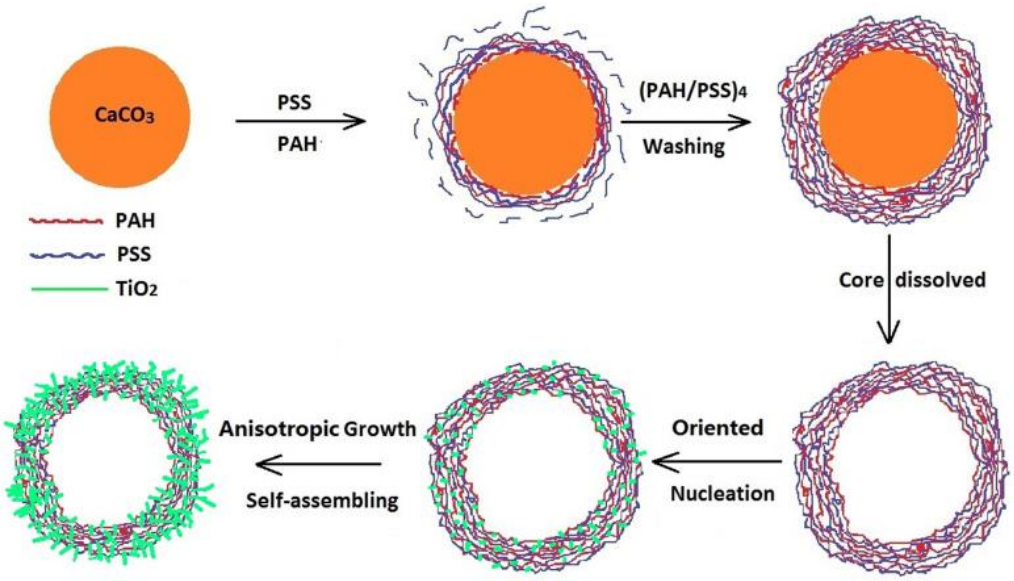

Figure 5.1 Schematic representation of the formation process of the TiO_2/polyelectrolyte composite microcapsules

As shown in **Figure 5.1**, both LbL assembly technique and TiO_2 *in situ* formation were involved in the preparation of composite polyelectrolyte/TiO_2 microcapsules. All the $(PAH/PSS)_4$ capsules were pre-fabricated *via* LbL method. Then, TiO_2 NPs were incorporated into the polymer layers through the *in situ* hydrolysis of TIBO. Ethanol (EtOH) was used as solvent to disperse the capsules. Two precursor solutions were prepared: TIBO/EtOH solution (1:15 in volume ratio) and H_2O/EtOH (1:10 in volume ratio). As the nucleation and growth rates of TiO_2 nanoparticles were strongly dependent on reaction parameters such as reaction temperature, time, concentration of solutions, *etc.*, morphology, structure and properties of the formed capsules would also influenced by these factors.[16] To better control the capsule morphologies, the influence of a few key parameters was investigated. Generally, the capsules were washed with ethanol for a few time to remove free H_2O in the system. Then they were re-dispersed in ethanol. Different amounts of the above-mentioned precursor solutions were introduced to the system and then kept under different temperature for various holding time. The detailed conditions for each sample were shown in **Table 5.1**.

Table 5.1 Detailed experimental reaction conditions of different TiO_2 coated samples.

	EtOH	Titanium/EtOH(1:15)	H_2O/EtOH(1:10)	Temperature & Time
S0	0	0	0	0
S1	5 ml	800 µl	600 µl	50°C-30 min; RT-20 h
S2	5 ml	800 µl	600 µl	50°C-30 min; RT-2 h
S3	5 ml	400 µl	400 µl	50°C-1 min; RT-20 h
S4	5 ml	400 µl	300 µl	25°C -20 h
S5	5 ml	400 µl	300 µl	25°C-10 h
S6	5 ml	200 µl	150 µl	25°C -10 h
S7	5 ml	200 µl	150 µl	25°C -20h
S8	0	1.5 ml	0	25°C -24h
S9	0	1.5 ml	0	25°C -72h

5.3.1.2 Influence of Reaction Conditions on Morphology

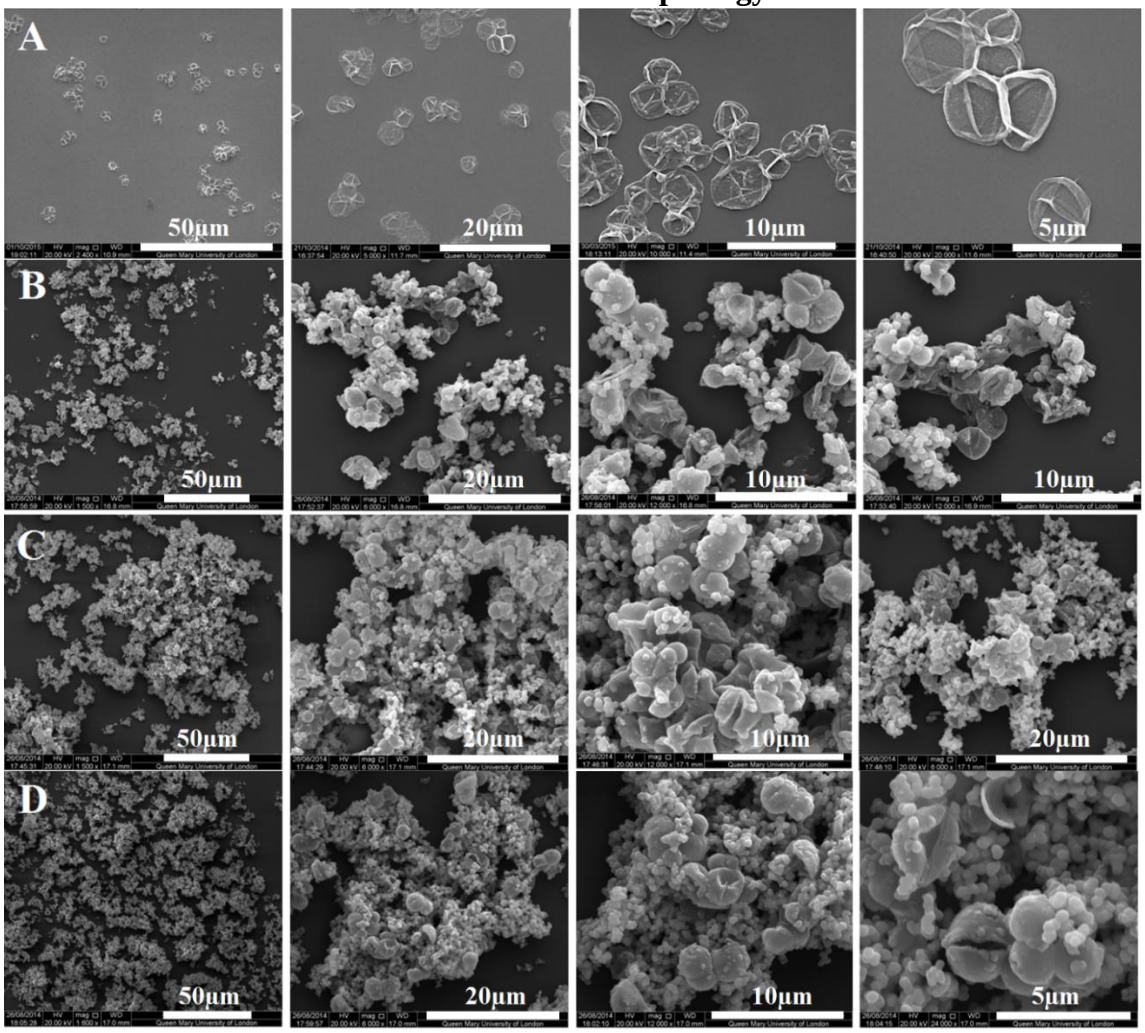

Figure 5.2 SEM images of composite samples produced under various reaction conditions. (A) S0; (B) S1; (C) S2; (D) S3.

As proved in the procedure of fabricating silica NPs in Chapter 4, heating could facilitate a higher rate of reactivity (hydrolysis, nucleation and growth), due to the increase in the mobility of reactive components, and therefore promote the possible condensation effect between the *in situ* formed NPs and the soft polymer shells.[16] For TiO_2 deposition, ethanol (EtOH) was employed as solvent, and two precursor reaction solutions were used: (1) TIBO/EtOH solution (1:15 in volume ratio); (2) H_2O/EtOH (1:10 in volume ratio). By fixing the initial treatment temperature at 50 ^oC and the amount of pure $(PAH/PSS)_4$ capsules, the effects of reaction time and amount of precursor solutions on the morphology of the obtained capsules were studied. SEM images in **Figure 5.2 B** showed that most of the modified capsules were not collapsed like the untreated pure $(PAH/PSS)_4$ capsules, indicating that TiO_2 NPs were *in situ* formed and assembled within the polymer multilayers, forming a kind of mechanically strengthened composite shells. But numerous free TiO_2 NPs were also obtained along with the composite capsules. In order to reduce the amount of free TiO_2 particles, the holding time at room temperature (25 ^oC) for aging of TiO_2 was decreased from 20 h to 2 h. Compared with S1, no significant improvement was observed for this sample (S2), **Figure 5.2 C**. Long holding time at 50 ^oC and too much amount of reaction agents would induce such phenomenon. By reducing these two factor, sample 3 was prepared, as shown in **Figure 5.2 D**. Free TiO_2 particles still existed even through reducing amount of the precursor solution and only holding them to react one minute at 50^oC. The results indicated that heating treatment to accelerate the hydrolysis of TIBO was not a good choice, because TIBO possessed an intrinsic high hydrolysis rate when reacting with H_2O. It is a big challenge to control their hydrolysis process. As indicated in **Figure 5.2**, the free TiO_2 particles displayed a relatively big sizes compared with the free silica NPs (**Figure 4.2, Chapter 4**)

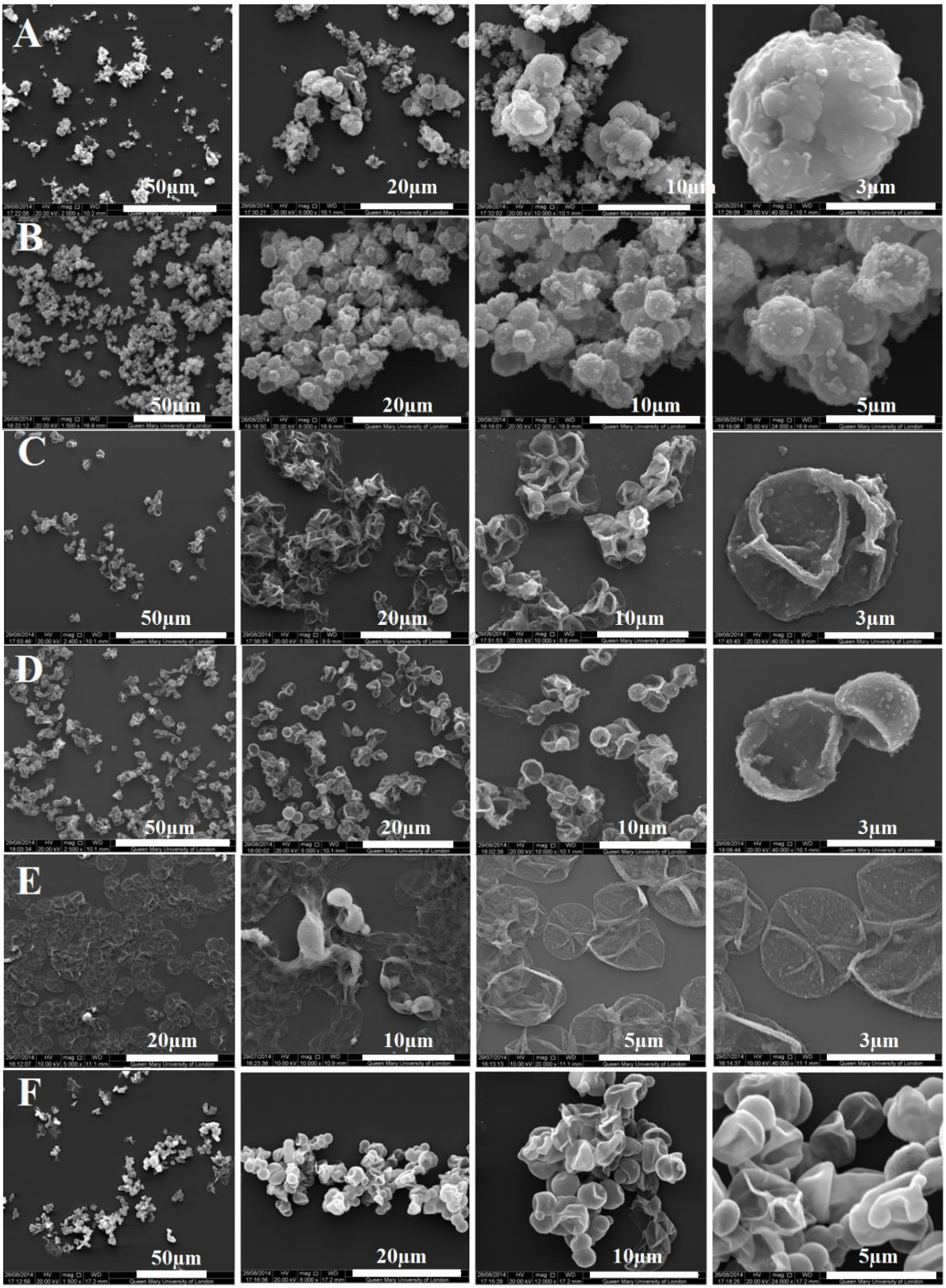

Figure 5.3 SEM images of composite samples produced under various reaction conditions. (A) S4; (B) S5; (C) S6; (D) S7; (E) S8; (F) S9.

Without heating treatment and halving the added precursor solutions compared with S1 and S2, S4 was fabricated after holding at room temperature for 20 h. SEM images were given in **Figure 5.3 A**, which revealed that the amount of free TiO_2 particles and their sizes were greatly reduced. If the reaction time was decreased to 10 h, **Figure 5.3 B (S5)**, nearly no free TiO_2 particles were obtained and all the collapsed polymer capsules were strengthen into ball-like and free-standing composite capsules. It can been obviously seen from the SEM image with a higher magnification in **Figure 5.3 B** that, TiO_2 NPs were attached on the capsule surfaces, forming a relatively high roughness. The particles on the surface with different sizes indicated that the incorporated TiO_2 NPs were not homogeneously distributed in the shells. Keeping the reaction time for 10 h, the amount of the reaction agents were halved again, we obtained S6 (**Figure 5.3 C**). The capsules with thicker folders collapsed under dry state, as they were not strong enough to support themselves. TiO_2 NPs can be found on the multilayers but no free NPs existed in the system. Such results indicated that the amount of added TIBO and H_2O was not excessed the needed amount and that, the holding time for reaction did not beyond the critical point. Hence, we increased the time to 20 h, capsules with much bulked-like structure were obtained, as indicated in **Figure 5.3 D**. However, the problem of uneven size distribution of TiO_2 NPs was still unsolved. This might induced by the poor control of the distribution of the added H_2O in the reaction system. TIBO precursor solution was firstly introduced into the capsules/ethanol mixture, and then added H_2O/EtOH solution dropwise under magnetic stirring. Because TIBO hydrolysis very fast, the added H_2O/EtOH drops didn't have enough time to be well dispersed by magnetic stirring before react with TIBO molecules. In other words, TIBO reacted with H_2O/EtOH drops quickly and consequently formed TiO_2 particles with different size distributions. In order to solve this problem, the amount of H_2O molecules and their

distribution need to be precisely controlled. Therefore, the H_2O should not be introduced as an addition agent.

Different from all the above-discussed samples, S8 and S9 were produced by only incubating $(PAH/PSS)_4$ capsules in TIBO/EtOH solution for different reaction and aging time. **Figure 5.3 E** showed that loads of TiO_2 NPs with uniform size were homogenously embedded within the polymer multilayers after incubation them in the TiO_2 precursor solution (TIBO/ethanol) for 24 h. Most of the composite capsules collapsed and possessed thicker folds when compared with pure polymeric capsules (S0, **Figure 5.2 A**), while only a few of them presented bulked structures. These capsules maintained approximately their original shape and size. No free TiO_2 NPs were found along with the composite capsules, which demonstrates that TiO_2 were formed preferably on capsule surfaces.

After prolonging the reaction time to 72h, a significant shape change was found for S9, showing that almost all the formed microcapsules were structurally reinforced into robust free-standing capsules with a confirmed ball-like morphology. No free NPs can be seen from the SEM images in **Figure 5.3 F**. If compared S9 with S0, it is clearly seen that there were significant differences in the size. Before incorporation with NPs, the flattened and collapsed pure $(PAH/PSS)_4$ capsules showed a diameter of ca. 4.38±0.33 μm, while S9 presented a reduced diameter, *i.e.*, 2.65±0.38 μm. It is plausible that the TiO_2 NPs were formed *in situ* inside polymer multilayers or on the shell surfaces, which would cross-link and compress the soft polymers, resulting in a decrease in capsule size yet with an increase in shell thickness and mechanical strength. Interestingly, S9 showed a very smooth surface (**Figure 5.3 F**), indicating that the formed TiO_2 NPs were finer grained, assembled and homogeneously distributed and integrated within the polymer multilayers or on their surfaces.

To further investigate the influence of TiO_2 incorporation on the morphology, structure and shell thickness of the capsules and to analyse the distribution, size, and morphology of the *in situ* formed TiO_2 NPs, S9 was measured by TEM, as shown in **Figure 5.4**.

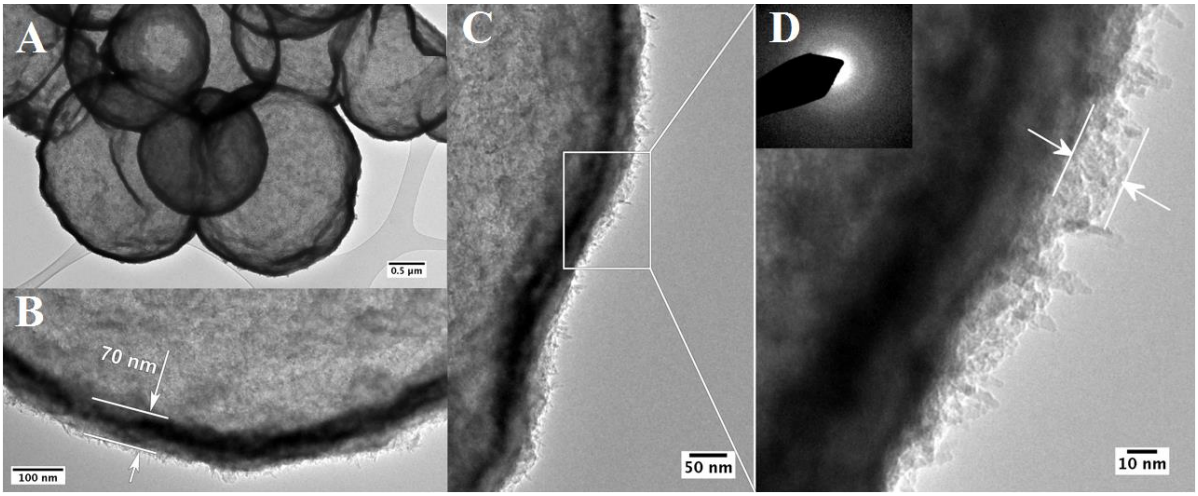

Figure 5.4 TEM images and selected area electron diffraction (SAED) patterns (inset) of PAH/PSS/TiO_2 composite capsules.

TEM images revealed that TiO_2 NPs were embedded uniformly in the polyelectrolyte shells and those as-made composite capsules showed an unbroken but hollow structure. High resolution TEM images of **Figure 5.4 C** and **D** indicated that the TiO_2 NPs were less than 5 nm in diameter and shaped in an oriented direction, *i.e.*, a needle-like morphology. To our best knowledge, such anisotropic shaped TiO_2 NPs was firstly synthesized at room temperature and synchronously incorporated into polyelectrolyte multilayers. Generally, sol-gel derived precipitates are amorphous in nature and require further annealing treatment to induce crystallization.[284] Here, these needle-like TiO_2 NPs were also of amorphous feature, as demonstrated by the electron diffraction (SAED) pattern, the inset of **Figure 5.4 D**. It is clear that the overall size of the microcapsules decreased and the wall thickness increased upon integrating with TiO_2 NPs, which is consistent with the SEM results, **Figure 5.3 F.** The shell

thickness reached to around 70 nm (**Figure 5.4 B**) which might be many times of the pure polyelectrolyte capsules (~20 nm). Another worth mentioning point is that the needle-like TiO_2 NPs were fully covered the top surface of the dense composite shell (the relative dark part) and formed around 15-25 nm pure TiO_2 layer, as marked in **Figure 5.4 D**.

In addition, to monitor every layer including PAH, PSS and *in situ* formed TiO_2 was successfully assembled onto the templates, typical zata potential of capsules with different layer number was measure, as shown in **Figure 5.5 A.** The capsules terminated with PSS showed a negative charge of -25.8 mV, while increased to -13.7 mV after TiO_2 coating, revealing that TiO_2 NPs partially neutralized these capsules' negative charge. In terms of the elementary composition of the formed composite capsules, S9 was measured by EDX for analysis of the elements, **Figure 5.5 B**.

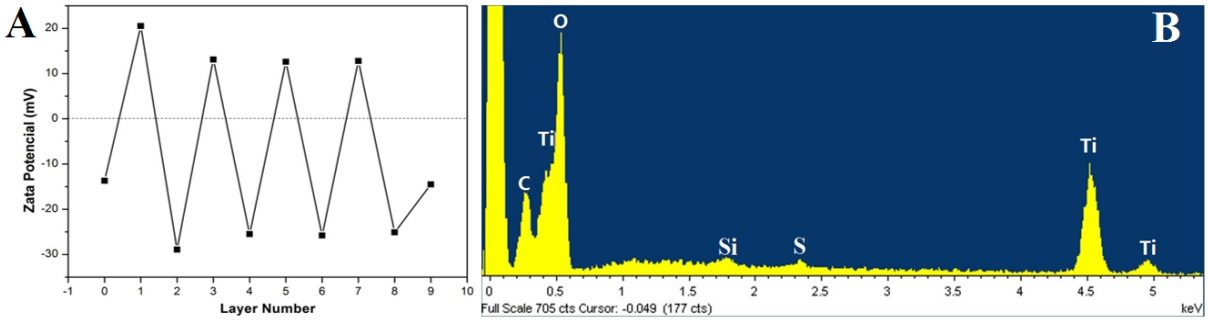

Figure 5.5 A, Zeta potential *vs.* layer number for the LBL self-assembly of PSS, PAH and titania coating. The layer numbers 1, 3, 5 and 7 correspond to PAH assembly and 2, 4, 6 and 8 correspond to PSS assembly. Layer number 9 corresponds to titania coating. Layer number 0 corresponds to $CaCO_3$ cores. **B,** EDX spectrum of the composite capsules.

EDX spectrum of the composite capsules indicated the presence of large amounts of C, O, and Ti and a tiny amount of S (**Figure 5.5 B**). The results prove that the capsule wall was built up

by the polymer layer and inorganic TiO_2. No traces of calcium were seen in the spectrum, revealing that $CaCO_3$ templates were completely removed by EDTA.[16] The small peaks of Si should originate from the glass slide for preparation of SEM sample because no Si source was used for capsule preparation. The data of SEM, TEM, zeta potentials and EDX demonstrated that incubation of polymer capsules in TIBO/EtOH solution without adding additional H_2O is a promising approach to growing TiO_2 NPs directly in polymer multilayers and that, the obtained composite capsules displayed good morphology and structures.

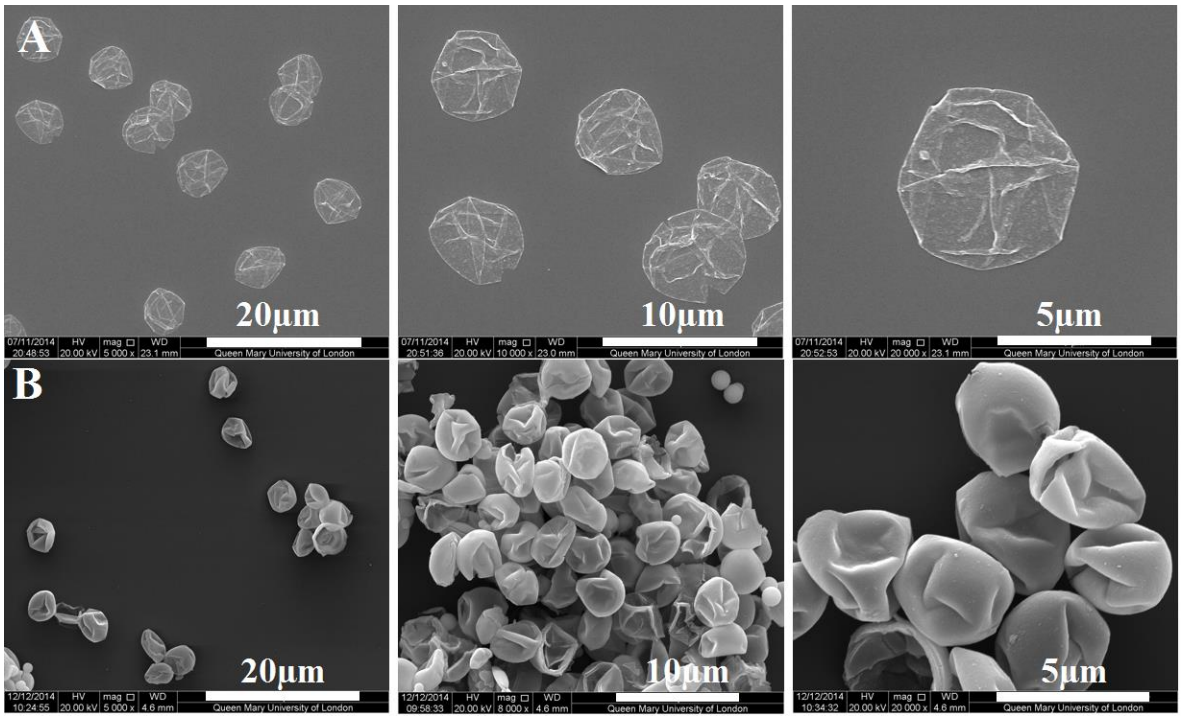

Figure 5.6 SEM images of $(PAH/PSS)_4$ capsules before (A) and after (B) *in situ* TiO_2 coating for 72 hours. $(PAH/PSS)_4$ capsules were prepared by LbL method using SiO_2 microparticles (5.53µm) as sacrificial templates. TiO_2 coating was produced in the exact same procedure.

Furthermore, $(PAH/PSS)_4$ capsules with bigger size (5.96 µm) were produced and used for TiO_2 functionalization employing the same reaction condition with that of S9. Capsules before and after 72 hours incubation in TIBO/ethanol solution were examined by SEM technique,

Figure 5.6. The SEM results were highly consistent with the capsules with smaller size (S9) as shown in **Figure 5.3 F,** containing features of free-standing spherical morphology and quite smooth surface (**Figure 5.6**). Before TiO_2 coating, the size of the capsules was 5.96 ±0.465 μm, while after TiO_2 coating, it reduced to 4.07±0.345 μm, showing a decrease around 31%. Such result confirmed the repeatability of the procedure of *in situ* TiO_2 incorporation into polymer capsules with different sizes.

5.4 TiO_2-Deposition and Strengthen Mechanism

The above SEM, TEM and EDX results of **S9** confirmed that the obtained hybrid microcapsules were mainly composed of inorganic TiO_2 NPs and organic polyelectrolytes. We know that LbL microcapsules can be easily included of prefabricated NPs in a middle layer assisted by weak driven force such as electrical absorption [18,254] but here we show that TiO_2 NPs can directly form and grow within and onto the polymer multilayers, which dramatically reinforced their final mechanical strength. In addition, these TiO_2 NPs were uniform in size and needle-like in shape. As a matter of fact, the nucleation and growth anisotropy of crystal is attributed to various factors such as solution composition, surfactants and deposition surface conditions. The existence of foreign particles or substrates in the precursor solution may well promote the heterogeneous nucleation on their surfaces. Previously De Guire *et al.* demonstrated that it was possible to have substrate-related oriented growth of anatase TiO_2 toward the hydrophilic substrate surface.[285] So for the production and deposition of these needle-like TiO_2 NPs, it is believed that a deposition took place through heterogeneous nucleation and columnar growth inside or on the soft polyelectrolyte multilayers, rather than through the conventional aggregation of colloidal particles into spherical TiO_2.[123]

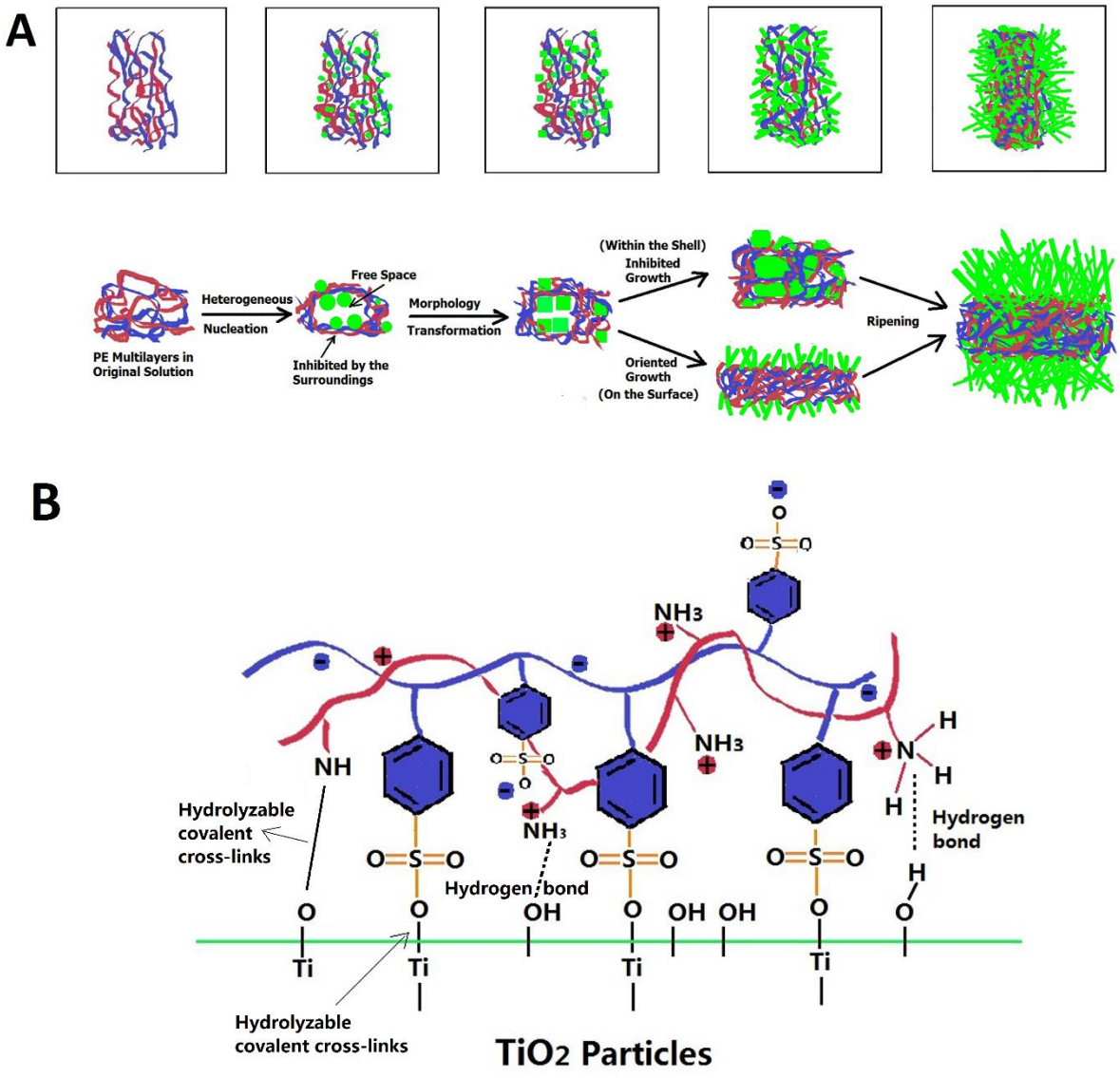

Figure 5.7 (A) Sketch of the morphology evolution and growth of TiO_2 NPs; (B) Polyelectrolyte structures and the potential interactions with TiO_2 NPs.

A possible nucleation, growth and morphology evolution process of TiO_2 NPs is proposed in **Figure 5.7 A**. Despite washing PAH/PSS capsules twice with ethanol before their incubation in TIBO/ethanol solution, a small amount of water was still reserved within the polyelectrolyte multilayers as both PSS and PAH are hydrophilic polyelectrolytes. Consequently, TIBO may immediately react with these H_2O molecules which results in the formation of abundant spherical TiO_2 crystal nuclei within the flexible polyelectrolyte layers as well as their surfaces

through heterogeneous nucleation (**Figure 5.7 A**). It should be pointed out that the soft PAH/PSS multilayers are entangled which provide many voids such as the concave points on the shell surfaces and the pores inside the polyelectrolyte multilayers.[16] Based on the crystal nucleation and growth principle, a TiO_2 nucleus would initially form at these positions with low energy, for example, the concave points and pores inside the shells.[16,286] Shin *et al.* suggested in their work that the TiO_2 coating formation was based on the agglomeration of the NPs primarily formed by homogeneous nucleation in solution with the aid of a large amount of H_2O.[287] However, in our system, homogeneous precipitation of free TiO_2 and their further agglomeration in liquid would not occur due to the minute quantities of H_2O.[288]

The slow reaction and precipitation rate result in that the TiO_2 inside the multilayers were tightly integrated with soft polyelectrolytes and that the formation of the external layer composed of the needle-like TiO_2 NPs, which were confirmed by the SEM and TEM data.[288] As shown schematically in **Figure 5.7 A**, the preliminarily formed spherical nucleus will transform into cubic particles, as supported by the thermodynamic theory.[289] Further anisotropic growth of TiO_2 would continue by the selective adsorption of coordinating species on the TiO_2 planes, presenting a growth preference in one direction and a growth inhibition in other directions. Practically, inside the polyelectrolyte multilayers, the TiO_2 particle growth direction and their final morphology will be restricted by their surrounding polyelectrolyte building blocks, **Figure 5.7 A**. Once they grow big enough to occupy the individual free spaces provided by their locations, they will begin to connect with the soft polyelectrolyte building blocks and other adjacent TiO_2 NPs produced inside the layers, then they will compact together and finally form a concrete-like structure. In this process, the polyelectrolyte building blocks act as the scaffold while the *in situ* formed NPs act as the filling materials. Hence, the final shape of the TiO_2 NPs should be dependent on the free space they obtained from their locations,

which would also be affected by the growth of the adjacent TiO_2 as well as their squeezing action and the consequent transformation of the soft polyelectrolyte layers.[123] Such a morphology evolution mechanism is remarkably different from that of the in situ formation of NPs on the surfaces of hard porous templates.[290] However, as for the TiO_2 nucleus initially formed on the shell surfaces, with the benefit of more free space, they will act as the tiny crystal seeds, which could sprout individual needlelike TiO_2 particles, as indicated in **Figure 5.7 A**. By prolonging the reaction time, most of the H_2O was consumed, thusly the hydrolysis rate of the Ti precursor reduced greatly. This will promote an oriented particle growth on the surface of the TiO_2 grains by the slow diffusion of Ti cations through the network of TiO_2 grain boundaries.[291] Limited by the total amount of H_2O, no free TiO_2 NPs were found in the system, but the needle-like TiO_2 NPs with an open end were fully covered on the composite shell surfaces, as shown in **Figure 5.3 F** and **Figure 5.4**.

In terms of reinforcement effects, with the benefit from a large amount of sulfonate groups and amino groups on polyelectrolyte chains, PAH/PSS building blocks act as enhancers and cross linkers to connect the adjacent TiO_2 nanoparticles into a stable shell (*i.e.*, through the formation of hydrogen bonds, covalent bonds, *etc.*), and protect them against movement, see **Fiure 5.7 B**.[36,194,292-294] The attractive potential between the sulfonated monolayers and TiO_2 NPs by van der Waals forces, which could be predicted using the Derjaguin, Landau, Verwey, and Overbeek (DLVO) theory, also promoted this interaction process.[287,288] As a consequence, the formed NPs were firmly mixed and combined together with polyelectrolytes with the assistance of these potential interactions. Once the capsule pores and surfaces were completely covered by the oriented TiO_2 NPs, further nucleation and growth would continue to occur on the formed composite shell surfaces if both H_2O and TIBO still exist. And the formation and growth mechanism is similar to that occurring inside the polyelectrolyte shells, because the formed

composite shells also showed a surface with nanoscale roughness available for further material deposition. Indeed, the TEM data in **Figure 5.4** generally uphold this standpoint, with the formation of a 15-25 nm top layer composed of pure TiO_2 (**Figure 5.4 D**). In addition, the demonstration of enhanced shell density of the composite capsules which was associated with their decreased size and increased shell thickness compared to pure polyelectrolyte capsules is another important observation of this study. Although hydrophobic polyelectrolyte capsules will swell slightly if dispersed in ethanol, the introduction of TiO_2 NPs into polyelectrolyte multilayers would make them twist and curl up together due to the consumption of the residue water from the multilayer pores as the TIBO was hydrolyzed, resulting in a significant shrinkage of the capsules. Upon prolonging the reaction time, TiO_2 particles would contact and interact with each other with the assistance of PSS and finally cover the whole shell, as illustrated by the TEM results. The continuous inorganic TiO_2 NPs would compress the capsule with a further consequent shrinkage, and thusly the flexible polyelectrolyte layers were restricted. Therefore, the pores in capsule shells would decrease in number and become smaller in size, and consequently the capsule shell permeability should be reduced in some degree.[123]

5.5 Ultrasound and UV Effects on PAH/PSS/TiO_2 Capsules

The S9 sample was the most promising sample and thus it was chosen for further studies. TiO_2 has been widely used as a UV-absorbing agent for environmental applications and here they were expected to be used as UV light absorber so as to increase the permeability of the composite capsules.[291,292] Firstly, the UV absorbance spectra of the composite capsules were measured by means of UV-vis spectrometer, as given in **Figure 5.8.** The polyelectrolyte/TiO_2 composite capsules showed two absorbance peaks with a wide tailing area up to 700 nm whereas no obvious absorbance peak was found for PAH/PSS capsules without TiO_2 incorporation. Further upheld by UV absorbance data of TiO_2/PSS observed by Wang *et al.*,

we can conclude that the peaks at 228 nm and 282 nm are mainly attributed to the incorporated TiO_2 NPs.[165] Thus, the formed composite capsules were imparted with a strong UV absorbance property. Subsequently, the effect of UV irradiation on the morphology of these capsules was examined by means of SEM.

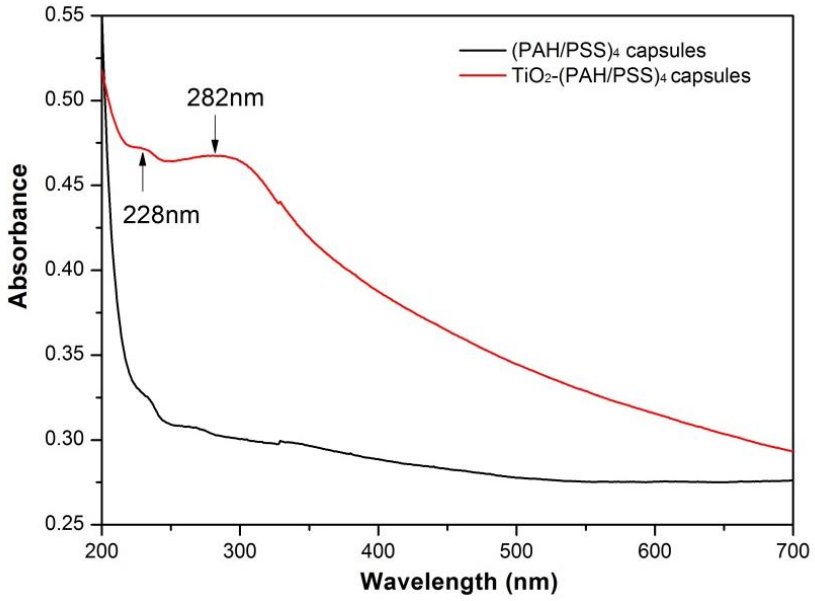

Figure 5.8 UV-vis spectra of the PAH/PSS/TiO_2 composite capsules.

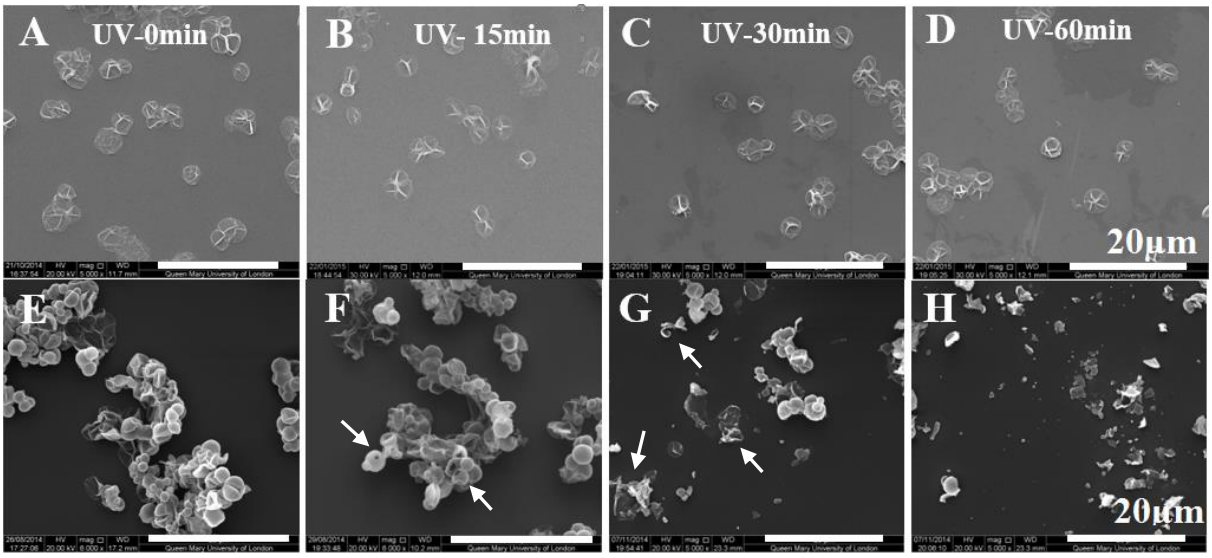

Figure 5.9 SEM images of capsules irradiated with UV light for different times: (A, B, C, D) (PAH/PSS)4 capsules treated for 0 min, 15 min, 30 min and 60 min respectively; (E, F, G, H) PAH/PSS)$_4$/TiO_2 composite capsules treated for 0 min,15 min, 30 min and 60 min respectively. The arrows represent broken capsules.

Figure 5.9 shows SEM images of the capsules with and without TiO_2 NPs after exposure to UV light (320-400 nm, ~110 mW cm^{-2}) for different duration times (*i.e.*, 0 min, 15 min, 30 min and 60 min). It is clearly seen that the capsules without TiO_2 were unaffected by UV irradiation, as evident from the little morphology changes before and after UV treatment. However, a significant difference was found for the PAH/PSS/TiO_2 composite capsules. For those, capsules had spherical shapes prior to the UV irradiation, and more than half of them were decomposed after UV irradiation for 30 minutes and nearly all of them were broken into small fragments when the time reached to 60 minutes (**Figure 5.9 H**). Comparing the different reactions between these two kinds of capsules responding to UV irradiation, it can be safely concluded that the incorporation of TiO_2 made polyelectrolyte capsules with photocatalytic activeness. Upon UV radiation, electron-hole pairs in TiO_2 were generated and the holes residing in the valence band of TiO_2 performed high oxidative activity.[295] It is believed that the deconstruction of composite capsules can be caused by two reasons. One is that the polyelectrolytes might be partly decomposed by the photocatalytic effect of TiO_2 in the composite layer. The other is the large amount of electron-hole pairs in TiO_2 stimulated by UV light may transfer to the polyelectrolytes, which prompts the disconnection of polyelectrolytes and inorganic NPs. For example, the bonding forces like hydrogen bonds and van der Waals forces between TiO_2 and polyelectrolytes would decrease. Promisingly, such a capsule system could find applications in the fields of cosmetics and agriculture, where naturally-present UV light can trigger the release of encapsulated materials.

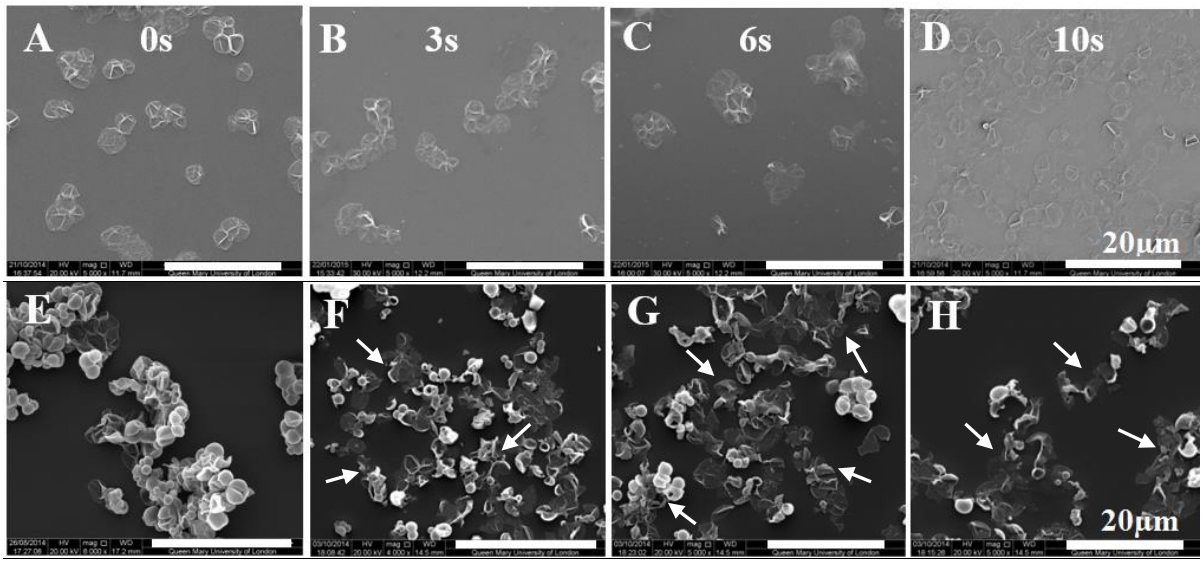

Figure 5.10 SEM images of capsules treated by ultrasound for different times: (A, B, C, D) $(PAH/PSS)_4$ capsules treated for 0s, 3s, 6s and 10s respectively; (E, F, G, H) $(PAH/PSS)_4/TiO_2$ composite capsules treated for 0s, 3s, 6s and 10s respectively. The arrows show broken capsules.

Previously we have demonstrated that the ultrasound sensitivity of the PSS/PAH capsules can be remarkably increased if rigid SiO_2 NPs were embedded in the polyelectrolyte network.[16] In this study we again prove that the composite capsules with *in situ* formed TiO_2 NPs also show strong ultrasound sensitivity.[123] The suspensions of microcapsules without and with TiO_2 composition were treated by means of ultrasound sonication for different duration times (3, 6, and 10 s). The resulting SEM data are shown in **Figure 5.10**. Pure $(PAH/PSS)_4$ capsules were not affected if the sonication time was less than 6 seconds (**Figure 5.10 B and C**) and only slight deformations were observed after 10 seconds of sonication (**Figure 5.10 D**). However for the TiO_2/polyelectrolyte composite capsules, obvious breakage was observed at t = 3 s, and complete destruction was achieved at t = 10 s. The increased ultrasonic sensitivity of the TiO_2/polyelectrolyte microcapsules is clear. Similar with the silica modified polymeric capsules, the strong response to ultrasound of the TiO_2 modified capsules was attributed to the increased density gradient across the water/shell interface, the enhanced of the shell stiffness,

and the decreased shell elasticity, all of which would improve the absorption of acoustic energy, leading to the increased ultrasound responsiveness.[16,253,270]

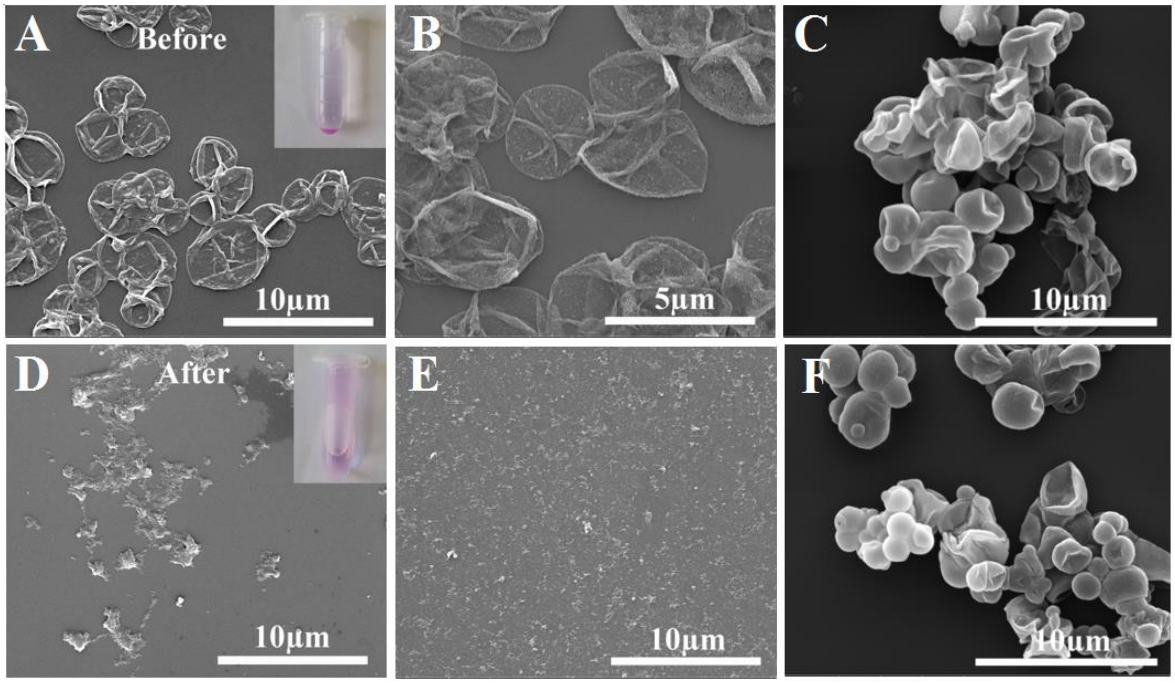

Figure 5.11 SEM images of capsules before and after NaOH (pH=13) treatment. (A, B) $(PAH/PSS)_4$ microcapsules, before and after soaking in NaOH for 2 minutes; (C, D) $(PAH/PSS)_4/TiO_2$ capsules with *in situ* titania coating for 24 hours, before and after soaking in NaOH solution for 10 minutes respectively; (E, F) $(PAH/PSS)_4/TiO_2$ capsules with *in situ* coating for 72 hours, before and after soaking for 10 minutes respectively. The insets are images of pure $(PAH/PSS)_4$ labelled with TRITC dyes centrifuged at 8000 r min^{-1} for 2 minutes before and after NaOH (pH=13) treatment for 2 minutes.

Despite of the two types of stimuli response, $PAH/PSS/TiO_2$ hybrid capsules also displayed a different response to the pH of the environment compared to the pure PAH/PSS capsules. We know from other work that LbL microcapsules composed of weak polyelectrolytes are generally sensitive to the pH of the environment.[32,165,295] For the PSS/PAH capsule system, when the pH of the environment becomes higher than the pKa of polybases, *i.e.* PAH, the

polyelectrolytes become uncharged thus resulting in the disassembly of the capsules. However, as shown in **Figure 5.11**, the strengthened hybrid capsules (S9) kept their initial shape after treated by strong alkali solution (NaOH, pH =13) for 10 minutes, whereas the pure PAH/PSS capsules were totally destroyed into floccules after only 2 minutes of treatment, consistent with the pH-responsive study of PSS/PAH capsules by De´jugnat *et al.*.[295] Interestingly, hybrid capsules obtained after 24 hours *in situ* TiO_2 incorporation (S8) were similarly dissolved into small floccules after 10 minutes of soaking in the NaOH solution. This might be due to the small amount of TiO_2 deposited on polyelectrolyte multilayers, which was not continuously covered the shell and was not strong enough to rigidly support the shell in harsh acidic or alkaline environments, leading to their separation of the polyelectrolyte building blocks. Experiment data showed that the capability of pH resistance of the composite capsule increased with the increase of TiO_2 concentration, indicating a promising potential of applying their tunability by either ultrasound or UV stimulus in harsh conditions.[123]

5.6 Encapsulation and Release Study

To study the feasibility of loading cargos in polyelectrolyte/TiO_2 capsules, TRITC-dextran (500kDa) was used as an example cargo due to its mature application in LbL capsule systems. Their encapsulation was carried out through a co-precipitation process. The corresponding CLSM images of capsules loaded with TRITC-Dextran are given in **Figure 5.12.** Before dissolving the $CaCO_3$ cores by EDTA, the bright red balls and strong fluorescent signals (**Figure 5.12 A** and the inset) were observed. **Figure 5.12 B** revealed most of the TRITC-dextran molecules were still entrapped inside the cavities that after removing the cores despite of a slight loss during the process of core dissolving. The inset shows an average fluorescent signal intensity of 86 units inside the capsule. It is worth mentioning that the permeability of PAH/PSS capsules would increase if they were transferred into ethanol, which means the

cargos inside their cavities would leak out.[270] But TRITC-dextran is not soluble in ethanol, hence most still stays inside the cavities during the formation process of TiO_2. After the *in situ* synthesis and incorporation of TiO_2, the freshly synthesized composite capsules with TRITC-dextran loading contained ~140 units of fluorescent intensity, as shown in **Figure 5.12 C**. A possible reason for the increased fluorescent intensity is the increased concentration of TRITC-dextran due to the decrease in capsule size. The composite capsules were also measured after 50 days' storage in the dark. Some TRITC-Dextran molecules leaked out and an average fluorescent signal intensity of ~ 80 units was kept inside.

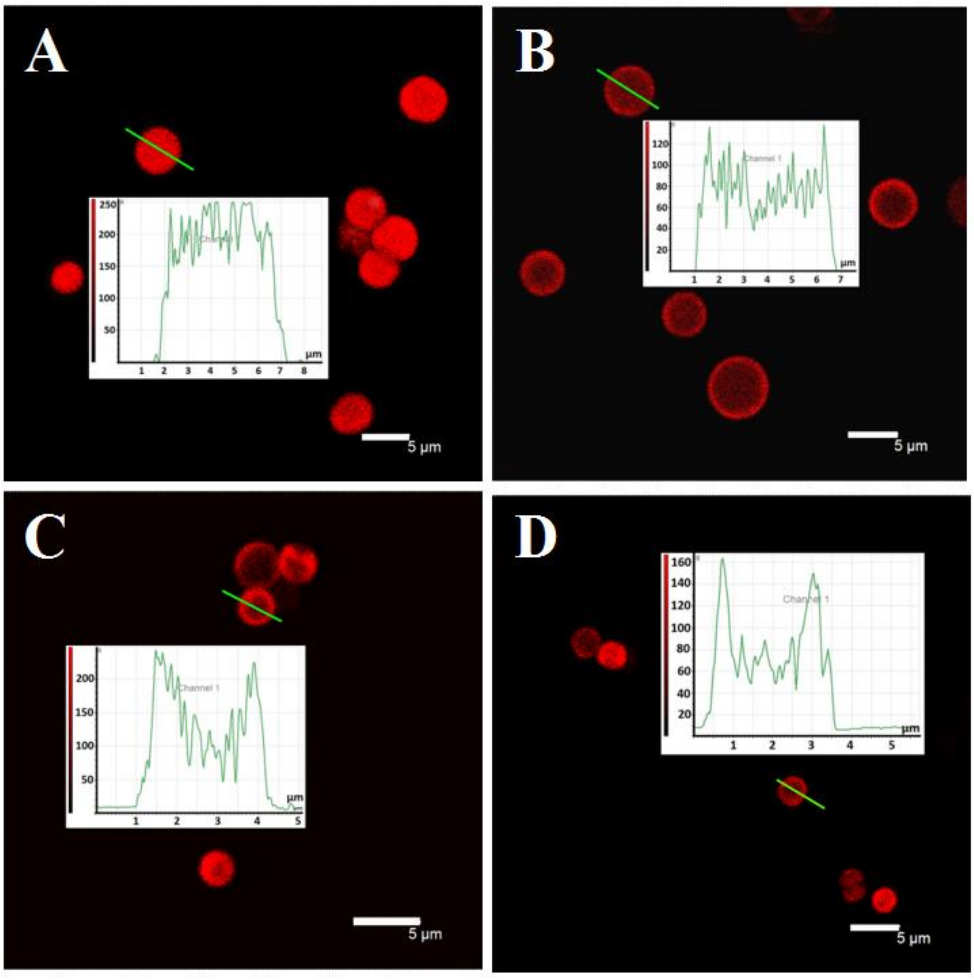

Figure 5.12 CLSM images of capsules loaded with TRITC-Dextran. (A) $(PAH/PSS)_4$ before removing the $CaCO_3$ cores; (B) $(PAH/PSS)_4$ after removing the cores; (C) $(PAH/PSS)_4/TiO_2$ capsules; and (D) $(PAH/PSS)_4/TiO_2$ capsules after being kept for 50 days in the dark.

As already been demonstrated above, the incorporated TiO_2 NPs in the capsule shells enabled them be responsive to UV light and ultrasound, which could offer a promising strategy for the controlled release of the encapsulated substances, especially for the applications where the abundant UV light (*e.g.*, sunlight) or ultrasonic could be used. To determine the possibility, UV and ultrasound stimulated dextran release was studied. The initial amount of encapsulated TRITC dextran in PAH/PSS capsule cavities was calculated as 4.47 mg in total with an encapsulation efficiency of ~56%. The TRITC-Dextran containing PAH/PSS capsule suspension was divided into two parts: one was for the release study of pure polyelectrolyte capsules and the other was coated with TiO_2 NPs for their further release study of TiO_2/polyelectrolyte composite capsules. Then the polyelectrolyte and TiO_2/polyelectrolyte capsule suspensions were diluted into 30 mL, respectively, both of which referred to the working samples. Then 0.5 mL of the working sample was collected after UV or ultrasound treatment at every sampling time point. Indeed, if there was no TRITC-Dextran loss from the pure polyelectrolyte capsules, each portion used for TRITC-Dextran quantification should contain 37.250 μg of dextran in the capsules. For composite capsules, it is worth mentioning that a small amount of TRITC-Dextran would diffuse out of the capsules during the TiO_2 coating process even though dextran is not soluble in ethanol, with an estimated loss of ~5 %. So each portion of composite capsules used for TRITC-Dextran quantification contains 35.387 μg of dextran. In order to facilitate the comparison between pure and composite capsules, the release amount (M_R) was plot as a percentage of the initial encapsulation amount (M_I), as shown in **Figure 5.13.**

TRITC-dextran molecules were not tightly sealed in these capsule cavities, so partial release induced by diffusion through the porous multilayer shells was inevitable. A slow release rate of TRITC-Dextran was observed for all non-irradiated samples. Notably, compared to pure

polyelectrolyte capsules, the incorporation of TiO_2 reduced the leaking amount which is more likely due to the reduction of shell permeability and the increase of shell thickness.[123] As for the UV-irradiated samples, the release from pure polyelectrolyte capsules was nearly identical with the non-irradiated samples because they were not responsive to UV light, showing a released amount about 4.6% after 2 hours of UV irradiation. In contrast, the UV accelerated the dextran release from TiO_2/polyelectrolyte capsules rapidly, reaching a plateau after ~100 minutes irradiation. It is clearly seen that only 27.3% of the initial dextran was released outside even though nearly all composite capsules were broken when treatment time reached to 60 minutes (**Figure 5.9 H**). Such a small percentage was caused by both the photobleaching effect due to long-time UV irradiation, and the attachment of dextran to the amino-terminated inner surface of the microcapsules.[123] Actually such possible attachment could be facilitated by both hydrogen bonds and the hydrolyzable covalent cross-links resulting from aldehydes and primary amines coupling.[289]

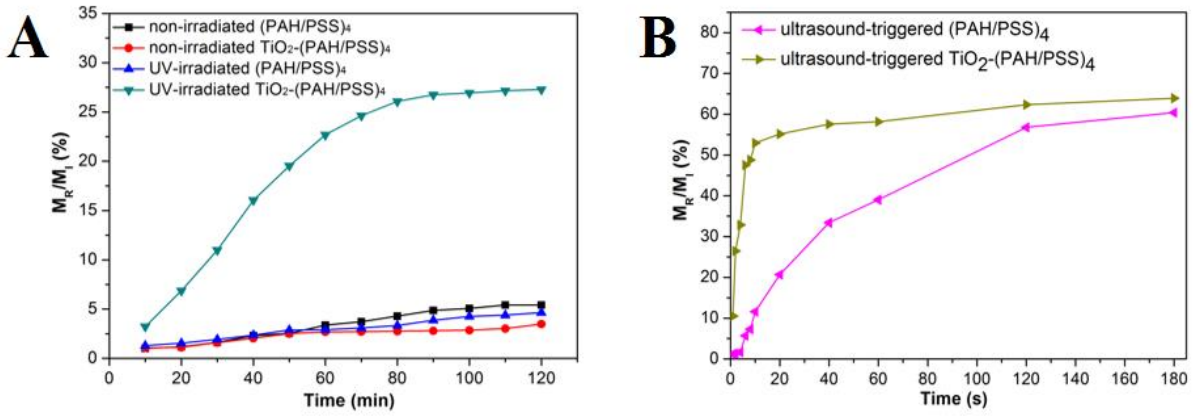

Figure 5.13 Trigger-induced TRITC-Dextran release as a function of irradiation time.

Compared to UV-irradiated samples, the released TRITC-Dextran amount of both the ultrasound-treated samples increased quickly during the duration time. But the capsules with TiO_2 coating displayed a much faster release rate when compared to the polyelectrolyte

capsules (more than 10 folds within the first 10 seconds) as a result of their higher sensitivity to ultrasound. Around 26% of the fluorescent dextran was released in just 2 seconds, and it increased to 48% in 6 seconds. The release curve became flatted after 10 seconds when reaching a value of ~53%. However, for the pure polyelectrolyte capsules, the encapsulated TRTTC-Dextran was released slowly in the initial 10 seconds. Only ~1% was detected after 2 seconds, and 6% in 6 seconds. After reaching 11% at t= 10s, the release rate increased because the polyelectrolyte capsules start to be broken by the ultrasonic processing, as proved by the SEM data (**Figure 5.14**). Total release amounts of ~60% were observed for both capsules after 180 seconds of sonication due to the full breakage of both capsules (**Figure 5.13 B**). All the $(PAH/PSS)_4$ capsules were broken into small pieces when the sonication time reach to 120 seconds, while all the composite capsules can be destroyed in 60 seconds. But particularly worth mentioning is that the composite capsules showed an efficient release within a short duration of applied ultrasound, which might be desirable for certain medical applications (minimizing the damage to healthy tissues).

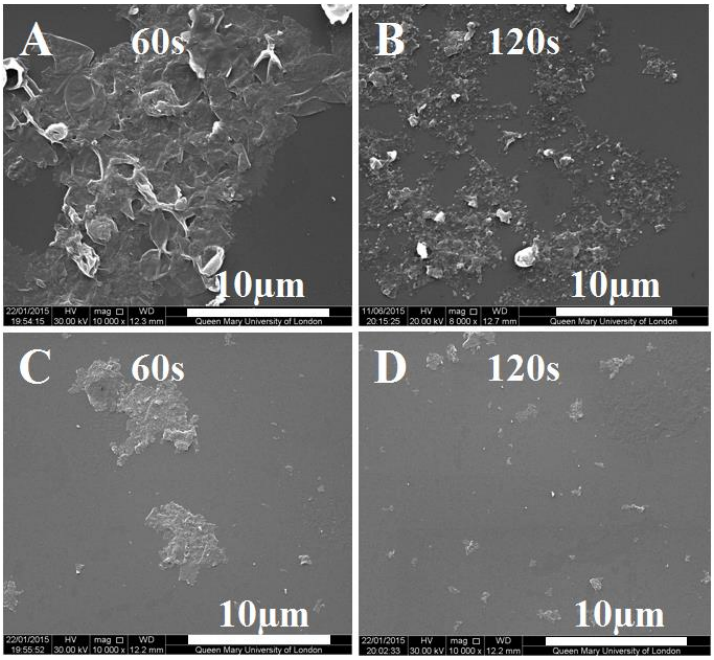

Figure 5.14 SEM images of different capsules treated by ultrasound for different longer time: (A, B) $(PAH/PSS)_4$ capsules; (C, D) $(PAH/PSS)_4/TiO_2$ composite capsules.

5.7 Cell Viability Study

Toxicity is one critical issue while fabrication of drug carriers. To study the compatibility of PAH/PSS/TiO_2 composite capsules, B50 cells were used as a model cancer cell line and capsules of S9 were applied for this study. The MTT data demonstrated the composite capsules with modification of TiO_2 NPs were well tolerated by B50 cells at a capsule : cell ratio of 10 : 1 and no obvious signs of toxicity were displayed (**Figure 5.15).** If we raise the capsule : cell ratio to 50:1, the PAH/PSS capsules showed a significant toxicity to cells especially in the first 24 hours, however the PAH/PSS/TiO_2 capsules performed a much better cell viability than the polyelectrolyte capsules. Such results revealed that TiO_2 NPs are not toxic and show good biocompatibility.[123]

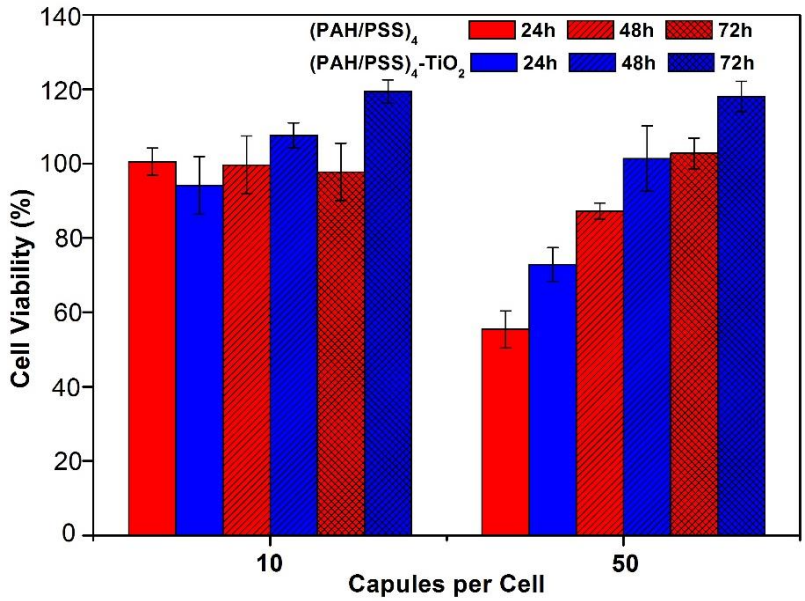

Figure 5.15 Cell viability of B50 cell line mixed with different concentration of PAH/PSS, PAH/PSS/TiO_2 capsules for 24 h, 48 h and 72 h at 37 °C respectively as measured by an MTT assay compared with the control. The error bars show the standard deviations.

5.8 Conclusion

In summary, we proposed and validated a novel approach for fabricating multi-functional organic/inorganic composite capsules *via in situ* production of TiO_2 NPs in polyelectrolyte shells. The influences of different reaction parameters including reaction temperature, holding time and amount of chemical agents on the morphology, mechanics, and structures of composite capsules were studied. Through carefully tuning and controlling these parameters, needle-like TiO_2 NPs were synthesised and assembled into prefabricated PAH/PSS microcapsules through the *in situ* hydrolysis of TIBO, which made the obtained microcapsules become of enhanced mechanical strength and demonstrate UV and ultrasound responsiveness as well as good biocompatibility. The formation of needle-like nanoparticles was through a deposition mechanism *via* a heterogeneous nucleation approach rather than forming agglomeration from a bulk solution. Similar to the result of polyelectrolyte/silica composite capsules, the *in situ* formed TiO_2 NPs filled gaps inside the polymer multilayers during the hydrolysis and precipitation process, which might yield denser shells with reduced permeability. The formed PAH/PSS/TiO_2 capsules showed a free-standing structure with smaller size, smoother surface and larger shell thickness. Besides the needle-like TiO_2 also acted as UV absorbing agent and ultrasound sensitivity enhancer, yielding the composite capsules with multifunction. The exposure of the formed TiO_2/polyelectrolyte capsules to either UV or ultrasound triggering showed an irreversible shell rapture and efficient cargo release. Such multifunctional capsules are promising for various future applications including drug delivery systems, cosmetic products and environment engineering. The capability of pH resistance of the composite capsule were also demonstrated in this study, indicating a promising potential of applying them in harsh conditions.

6. Polyelectrolyte/CDs Composite Capsules

6.1 Background

Capsules used as drug carriers for biomedicine application are often required to be traceable.[201] Usually, in order to make the polyelectrolyte capsules detectable, they were labelled with fluorescent agents which endow them with optical properties for easy tracing by detecting their fluorescence signal. The most widely used fluorescent agents for labelling polyelectrolyte capsules are organic dyes, which are particularly advantageous in biological research because of their low toxicity and high sensitivity.[204,205] But their intrinsic photoquenching feature limits their applications for long-term tracing.[206] To overcome this disadvantage, semiconducting quantum dots (QDs) is developed as another attractive fluorescent imaging agent, which possess better stability, intensive fluorescence and excellent resistance to photobleaching allowing them suitable for long-term measurements.[206] However, semiconducting QDs have certain problems associated with the inherent heavy metal toxicity, high cost and bad biocompatibility, limiting their practical medicine application.[187] In contrast, recently explored fluorescent CDs with tunable emission show excellent superiority in biochemical applications over semiconductor QDs and conventional organic dyes due to their excellent biocompatibility, low photobleaching, chemical stability, and facile production with low cost.[210] There have been many successful reports on the synthesis of CDs [35, 211,212] and applied them as bioimaging agents and sensors, but nearly no report is about their usage in drug carrier system. Because they can't be directly used as drug carriers due to their solid structures. Recently, hollow CDs with cavity size about 2 nm has been synthesized for both bioimaging and drug delivery.[296] The results demonstrated that CDs have great potential for application in drug delivery. However, the small size of such hollow CDs limited their loading capacity for DOX and their circulation time in human body.[296] On the contrary, despite the lack of

optical traceability, polyelectrolyte capsules could be easily achieved high loading capacity and long circulation time, because they can be facilely fabricated with tuneable size, morphology, composition, *etc*.. These features motivates us with an exciting idea to achieve high loading capacity, long circulation time and traceability into one entity, which is to incorporate CDs into shells of polyelectrolyte capsules. The obtained composite polyelectrolyte/CDs capsules are expected to be a kind of hollow particles with suitable size, large capacity and long-term fluorescence, which cannot only be used as optical imaging agent, but also as a drug carrier for high therapeutic efficacy.

Incorporation luminescent CDs with size less than 10 nm into polyelectrolyte capsules is extraordinary difficult, because the present technologies to fabricate robust and dense membranes incorporated with ordinary NPs is still not mature, no exception for CDs. Russell's group designed a series of crosslinking routes to prepare stable membranes of semiconducting QDs at fluid interfaces. However, despite this progress, it is still a great challenge to simultaneously realize the interfacial synthesis of NPs and their assembly into robust and stable 2D membranes at the liquid-liquid interface.[297] The popular two-step approach to assemble pre-fabricated NPs such as ZnO into polyelectrolyte multilayers assisted by electrostatic attraction is not promising for CDs incorporation.[3,13,14,18,298] Similar with silica and TiO_2 works, CDs could be synthesized *in situ* within polyelectrolyte capsules and integrated together with the soft polyelectrolytes. As inspired by recent numerous reports of conversion of a variety of aromatic hydrocarbon to light emitting carbon dots (CDs) under relatively mild conditions of hydrothermal carbonisation (HTC), polyelectrolyte capsules can be incubated with proper carbon source and heated at a relatively high temperature to realize carbonisation. Dextran can be employed as the carbon source, because it was found that dextran molecules are efficiently absorbed to polyelectrolyte multilayers. In addition, it shall be noted that heat treatment was

reported in 2007 as an effective and simple method to reduce permeability of polyelectrolyte multilayer capsules.[155] Hence, besides the fluorescent property, the obtained composite capsules are also expected to possess low permeability.

6.2 Aim and Objectives

The aim of this chapter is to fabricate fluorescent capsules with low permeability and possible ultrasound sensitivity. A facile interfacial synthesis and assembly method assisted by heat treatment is used for incorporation of CDs into polyelectrolyte. In this method, the polyelectrolyte multilayers play a role of a scaffold for nucleation and growth of the CDs, and simultaneously the formed CDs adhere the soft polymer together with the CDs, which could offer a much strong interactions among CDs and provide novel properties for the resultant composite capsules. The obtained composite capsules are expected to exhibit bright emissions and are particularly promising for bio-imaging and biosensors. As employed high temperature in the fabrication process, the composite capsules are also expected to be able to entrap small molecules. The CDs embedding within the polyelectrolyte shells will enhance their sensitivity to ultrasound treatment.

Therefore the main objectives of this chapter are:

1) To fabricate polyelectrolyte capsules $(PAH/PSS)_4$, $(PAH/DEXS)_4$ and $(PARG/DEXS)_4$ and to functionalize them with CDs *via in situ* nucleation and growth of CDs inside or on the polyelectrolyte shell surfaces based on hydrothermal decomposition of carbon source, *i.e.*, dextran and pre-confined DEXS within the multilayers.

2) To investigate the mechanism corresponding to *in situ* formation and assembly fluorescent CDs in polyelectrolyte capsules.

3) To analyse the morphology, structure, fluorescent property, biocompatibility and stimuli-responsive properties of the formed fluorescent capsules.

4) To study the cargo substances (Rh-B) encapsulation in PAH/PSS/CDs and their triggered release behaviour under ultrasound treatment.

6.3 Fabrication of Fluorescent Composite Capsules

6.3.1 Fabrication of Fluorescent CDs

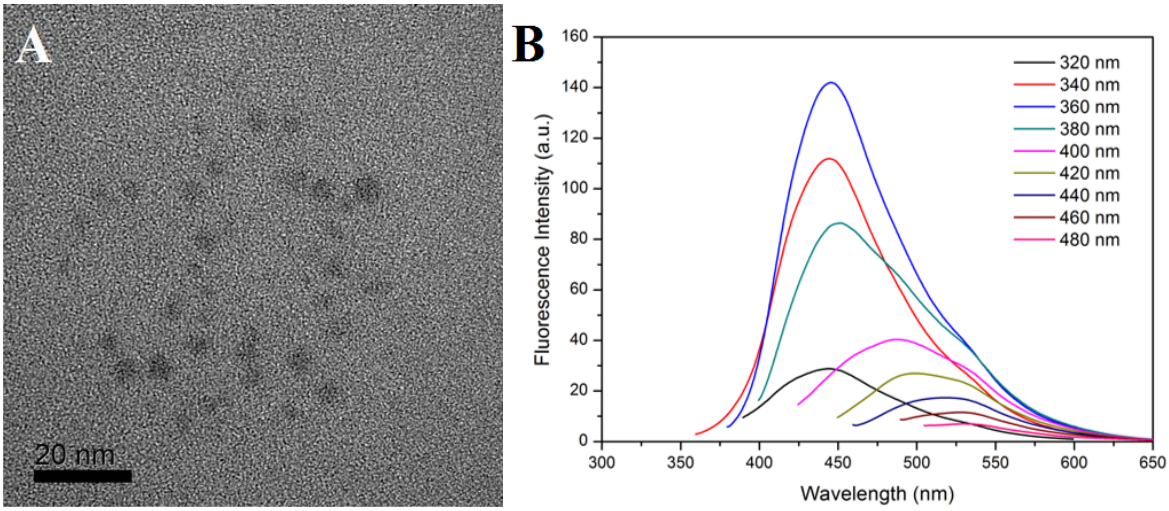

Figure 6.1 TEM image (A) and FL spectra (B) of pure CDs from dextran at different excitation wavelength.

As dextran molecules are found to be easily absorbed into polyelectrolyte shell, they can be used as the raw material for CDs synthesis. Before synthesis of fluorescent composite capsules, the feasibility of fabricating fluorescent CDs from dextran was first studied. 2mg/mL dextran in water was heated at 160 ^{o}C for 20 h, and then the brown liquid was obtained and measured by TEM and fluorescence spectrameter. The sole dots referred to CDs with ~ 5 nm in size can be clearly seen from the TEM image, **Figure 6.1 A**. To explore the optical properties of the CDs, a detailed photoluminescence (PL) study was carried out under different excitation wavelengths (λ_{ex}). As shown in **Figure 6.1 B,** these CDs exhibited an excitation-dependent

emission position phenomenon. When the λ_{ex} increases from 320 nm to 480 nm, the emission peaks shift to longer wavelength and the PL intensity decreases gradually. The maximum PL emission locates at 440 nm obtained with λ_{ex} = 360 nm. The TEM and PL spectra were in good accordance to glucose-based CDs which were fabricated at 200 °C for 6h.[35] Furthermore, UV-vis Absorption measurements (Figure 6.2) show spectra of CDs also similar to those previously reported for CQDs/CDs.[35] Such results proved that monodispersed CDs with strong fluorescence were successfully synthesized by the gentle hydrothermal reaction of dextran.

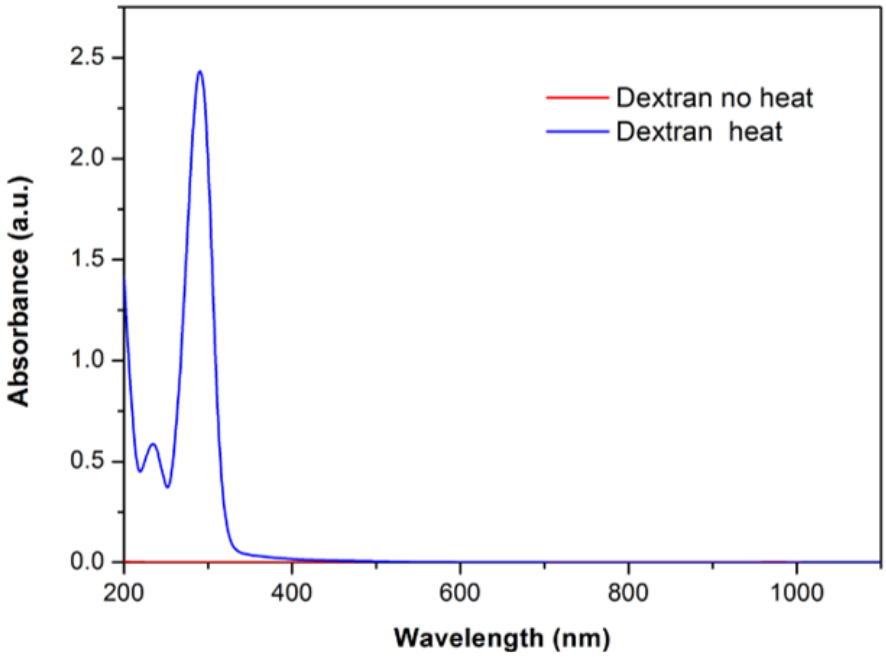

Figure 6.2 UV-vis absorption spectra of 2 mg/mL dextran before and after hydrothermal treatment.

6.3.2 Fabrication of Fluorescent PAH/PSS/CDs Capsules

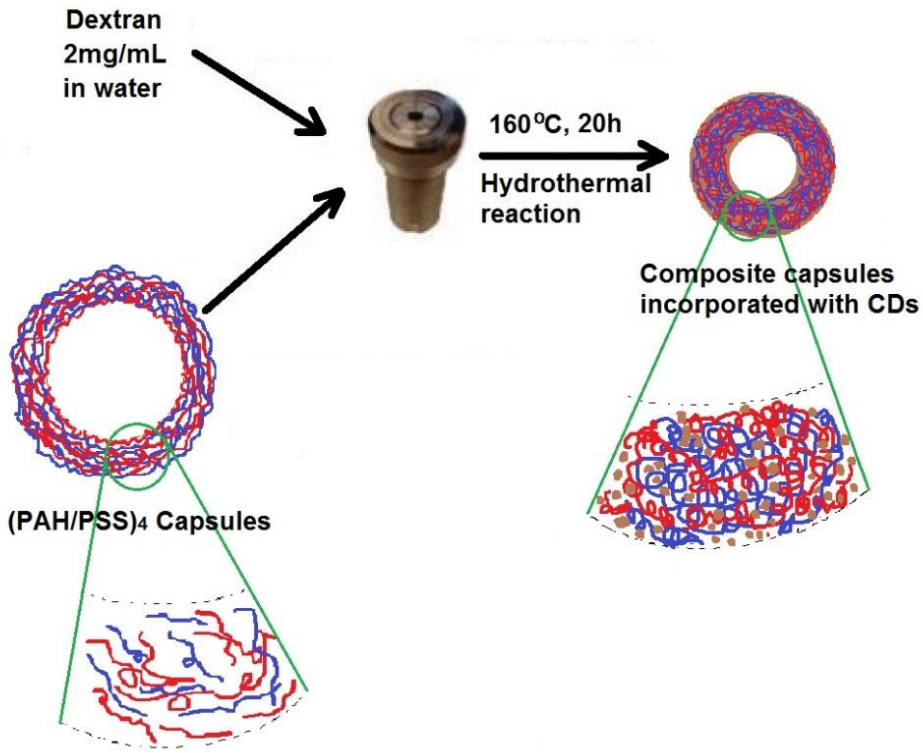

Figure 6.3 Schematic diagrams of composite capsules fabrication, PSS (red lines), PAH (blue lines) and CDs (brown dots).

Based on the above results, the synthesis and assembly of fluorescent CDs polyelectrolyte capsules are expected to be produced by one-step hydrothermal reaction method using dextran as a carbon source, as indicated in (**Figure 6.3**). Initially, $(PAH/PSS)_4$ capsules were obtained by LbL assembly technique and then, they are autoclaved with the presence of 2mg/mL dextran/H_2O solution and heated at the same condition (160 ^oC, 20 h). Subsequently, the CDs gradually should *in situ* form at the solid-liquid interfaces (capsules-water), which were naturally and homogeneously embedded in the PAH/PSS multilayers. The resultant PAH/PSS/CDs composite capsules were easily separated and purified from the solution by centrifuging and washing with DI-water. Notably, the images in **Figure 6.4 A** showed that the white capsules change into slightly brown ones after the hydrothermal reaction with dextran, indicating that the newly formed carbon particles were successfully embedded in their shells.

The FTIR spectra indicated the characteristic O-H and C=O stretching peaks of the pure CDs (**Figure 6.4 B**), which further confirmed the formation of CDs from autoclaved dextran/H_2O solution. In terms of capsules, no significant difference can be found for the capsules before and after CDs incorporation. This might because PAH/PSS capsules contain the bonds of CDs so as that they overlap together.

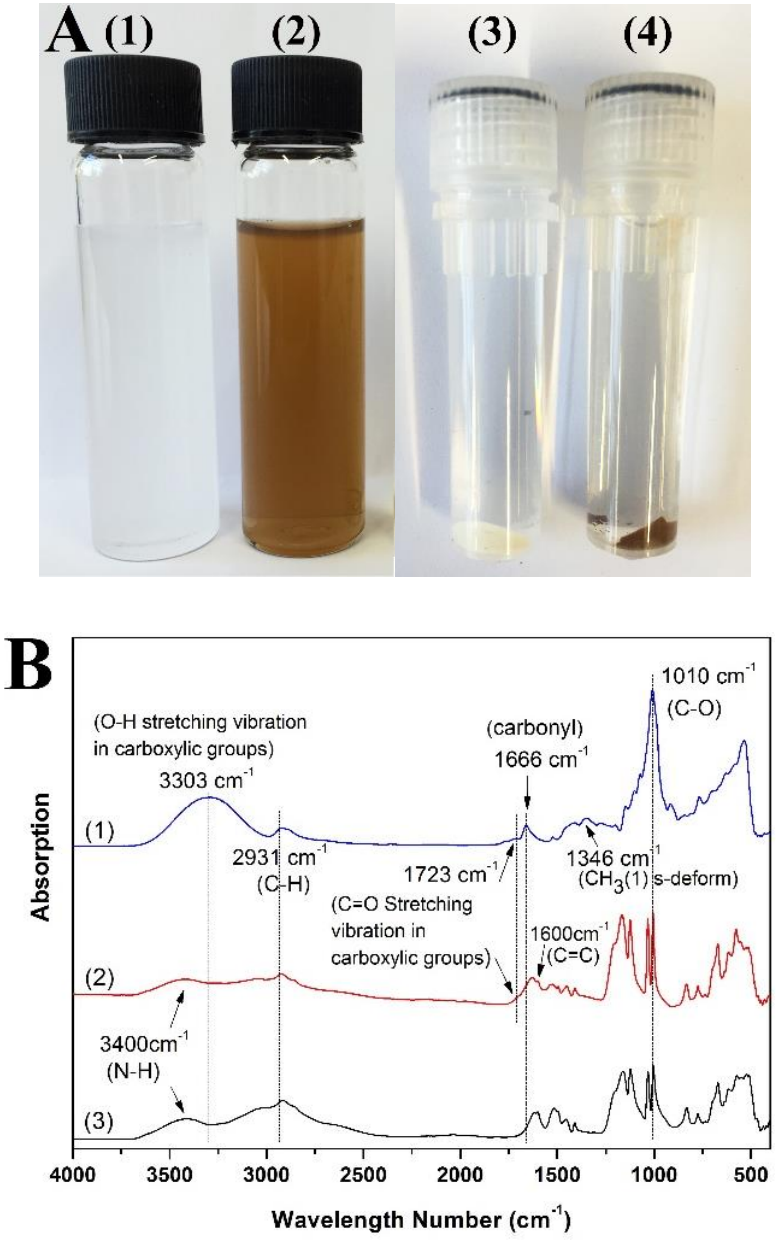

Figure 6.4 (A) Images of capsule suspensions and precipitation (1, 3) before and (2, 4) after incorporation with CDs; (B) FTIR spectra of (1) pure CDs, (2) PSS/PAH/CDs capsules and (3) $(PAH/PSS)_4$ capsules.

The weigh percentage of CDs inside the polymeric shells was briefly determined by TGA analysis which was carried out under nitrogen gas. The formation and incorporation of CDs into PAH/PSS capsules were confirmed, as shown in **Figure 6.5**. After the temperature reaching to 1000 ºC, only around 2.89% of the initial weight for pure PAH/PSS capsules was left, while around 9.61% of that for PAH/PSS/CDs composite capsules retained. The difference reveals that ~7% C NPs were embedded in the polyelectrolyte matrixes.

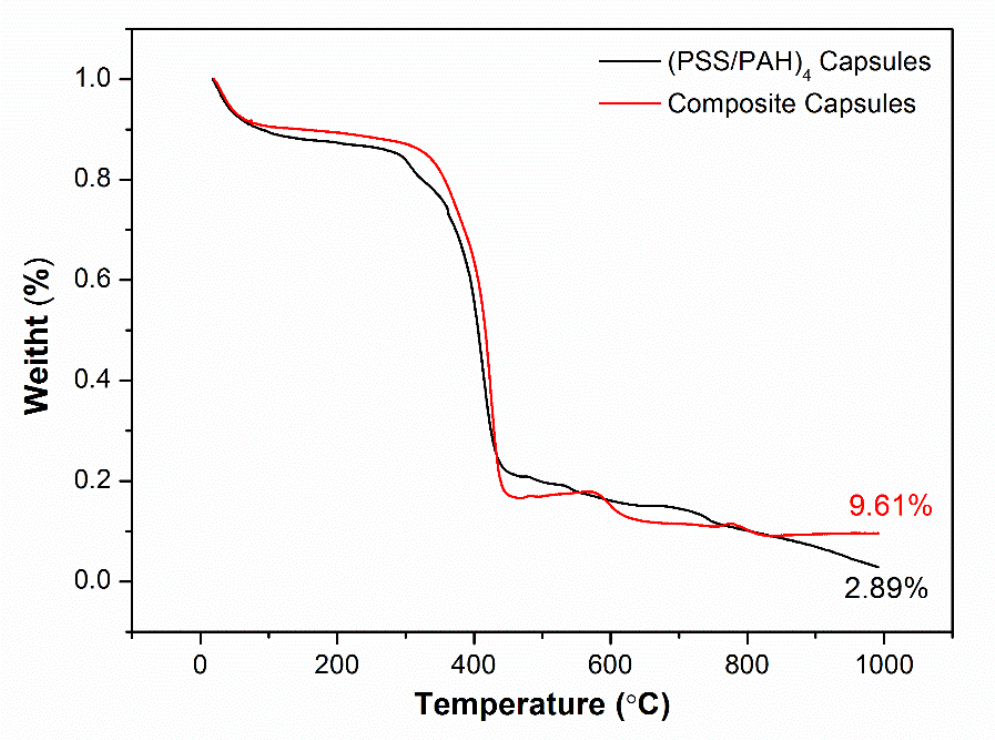

Figure 6.5 TGA profiles of pure polyelectrolyte and carbon composite microcapsules.

To study the morphology and structure changes of capsules before and after modified by CDs and to validate the formation of CDs in the polyelectrolyte matrix, scanning electron microscopy (SEM) and transmission electron microscopy (TEM) were applied to characterize these microcapsules. It is obvious that unlike the original $(PAH/PSS)_4$ capsules which are flat, collapsed and foldable (**Figure 6.6 A-B**), the PAH/PSS/CDs capsules show a bowl-like shape, decreased size, increased shell thickness and enhanced free-standing mechanics (**Figure 6.6 C-**

D) after being incorporated with CDs. The capsule size decreased from 4.5 ± 0.37 μm to 1.56 ± 0.4 μm via statistically determination.

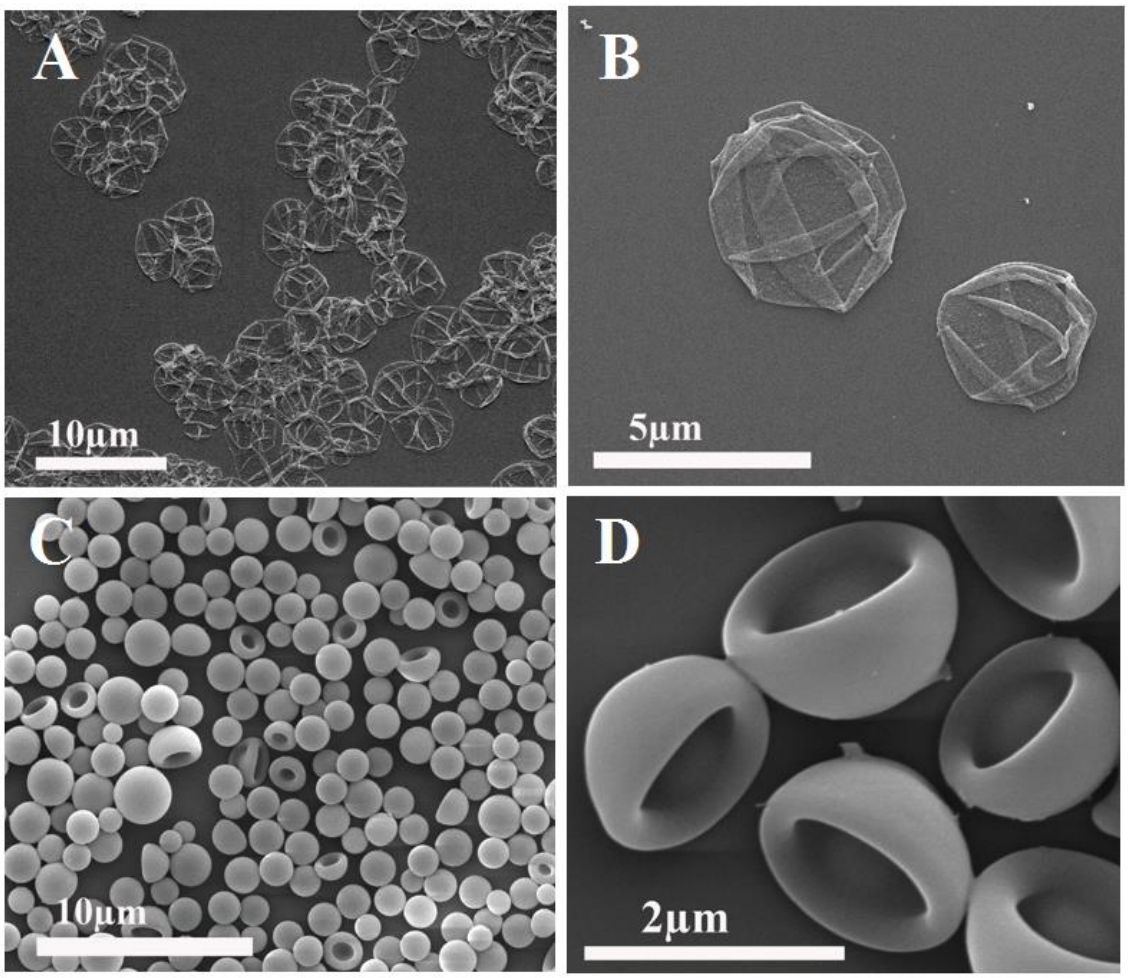

Figure 6.6 SEM images of capsules before (A, B) and after (C, D) CDs incorporation.

The TEM images in **Figure 6.7**, demonstrated the composite capsules kept the hollow structure. In terms of shell thickness, it is usually less than 20 nm for PAH/PSS capsules with 8 layers [92] illustrated by their very thin and transparent films in **Figure 6.7 A,** whereas the shell thickness of PAH/PSS/CDs capsules increased to ~178.4 nm (**Figure 6.7 C**). High magnification TEM image (**Figure 6.7 D and E**) indicated that the surface of PAH/PSS/CDs capsule was slight rough, with load of small dots on the surface.

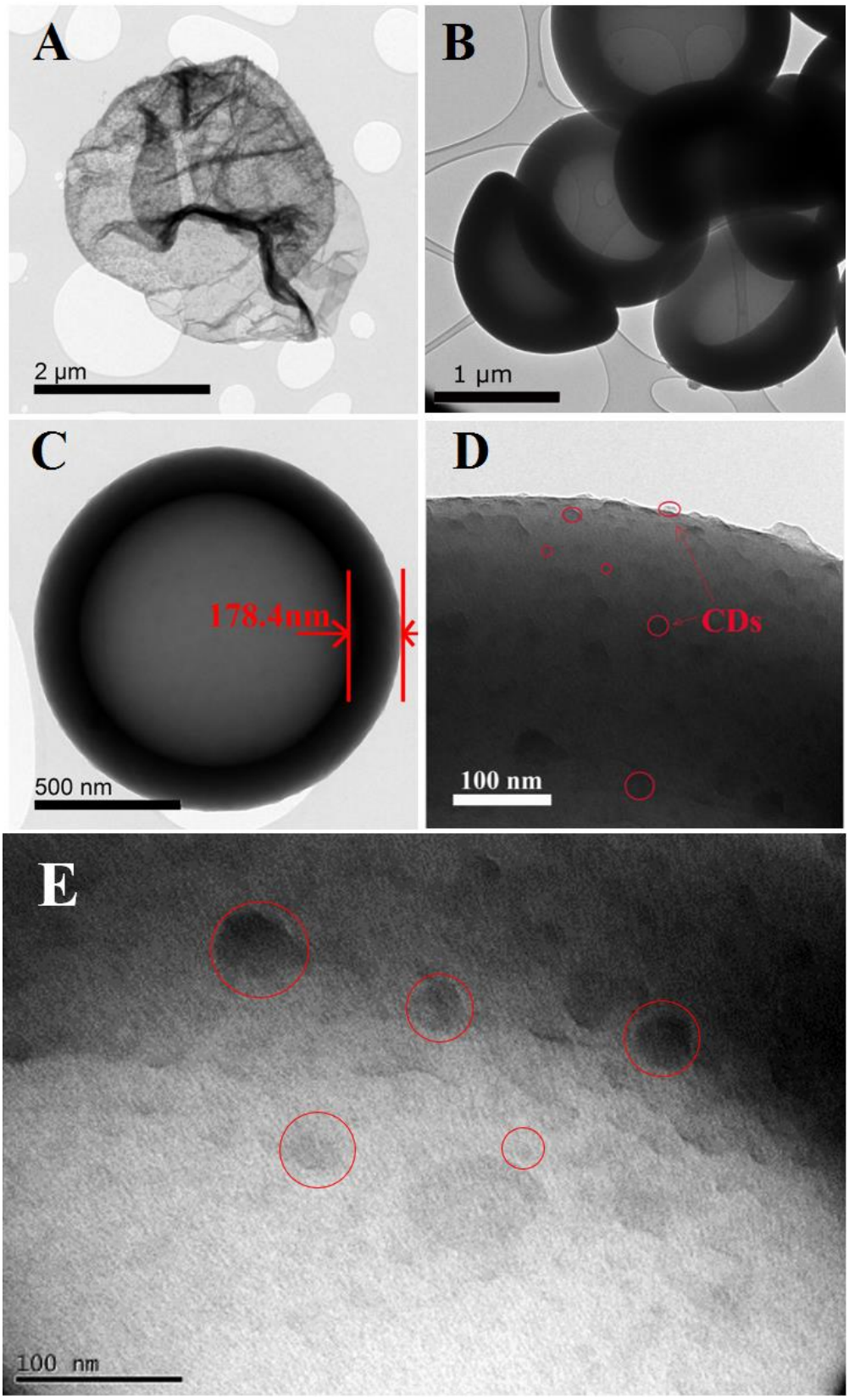

Figure 6.7 TEM images of capsules before (A) and after (B-D) incorporation with CDs.

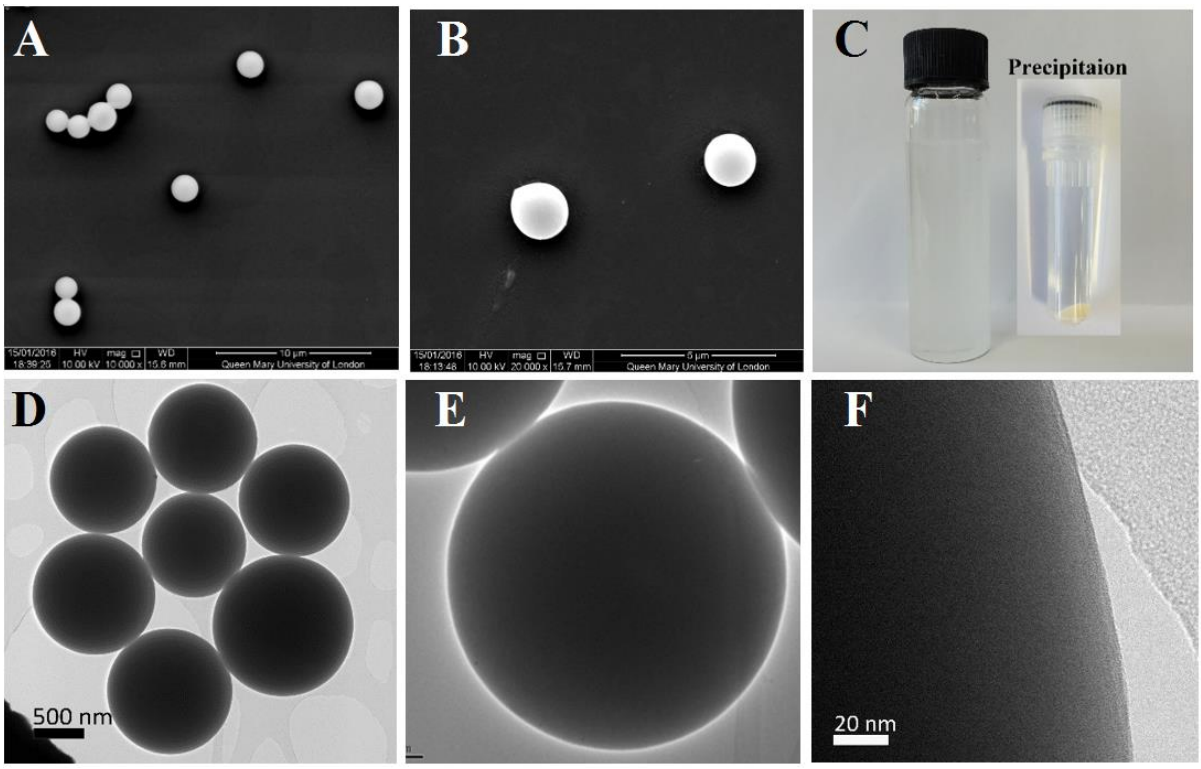

Figure 6.8 SEM (A, B), optical photos (C) and TEM (D-F) images of capsules after heated in H_2O.

In order to confirm formed CDs is from the carbonization of dextran and to illustrate the influence of heating on PAH/PSS multilayers, one controlled experiment was carried out, *i.e.*, autoclaving $(PAH/PSS)_4$ capsules at the same condition but without dextran. The obtained sample was studied by SEM and TEM. It was found that the $(PAH/PSS)_4$ capsules shrink into solid spheres under heating. As show in **Figure 6.8**, they were proved to be filled balls with very smooth surfaces and the precipitation kept their white colour. It is the influence of hydrophobic forces that greatly surpasses the electrostatic forces, so that the shells prefer to rearrange their structure and shrink to decrease the surface area exposed to the solvent and finally appear as filled balls.[155,299] Such result is in good accordance to previous reports. Compared with the coarse surface of composite PAH/PSS/CDs capsule (**Figure 6.8 D)**, no dots can be found on the smooth surfaces of the filled spheres, as shown in **Figure 6.8 C**. Therefore,

the visible small dots on PAH/PSS/CDs capsule surfaces belong to the slightly aggregated CDs formed from carbonization of dextran.

In addition, compared with capsules heated in pure H_2O, the capsules with CDs incorporation retain their hollow structure despite of a significant shrinkage (decrease in size). A reasonable explanation is that the *in situ* formed CDs buried within the soft polyelectrolyte multilayers (especially the positions with low energy, *e.g.*, pores, concave surfaces, *etc*.) greatly prevent the shrinkage of polyelectrolyte caused by heat treatment.[123] Besides, the formed CDs are negatively charged (-11.1 mV, **Figure 6.9**), which potentially increase the electrostatic repulsion between the negatively charged layers and reduce the shrink effect caused by hydrophobic forces. Hence the interaction and combination of these two factors are responsible for their hollow structure.

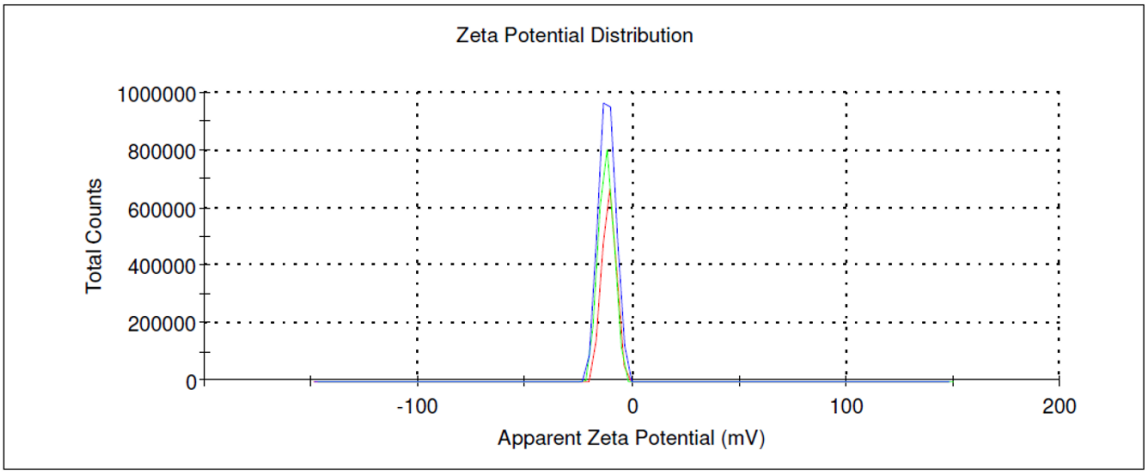

Figure 6.9 Zeta potential of pure CDs.

To explore the optical properties of the PAH/PSS/CDs capsules, a detailed photoluminescence (PL) study was carried out, as shown in **Figure 6.10 A**. The capsules with CDs incorporation showed broad emission peaks without the excitation-dependent emission (**Figure 6.10 A**). It shall be noted that PL property of PAH/PSS capsules heated in H_2O were also measured, but

no PL emission peaks were found for them. This result support the hypothesis that the fluorescence of PAH/PSS/CDs capsules arises only due to the *in situ* formation and assembly of CDs into PAH/PSS matrixes by hydrous pyrolysis of dextran, rather than heating induced change of the PAH/PSS multilayers. In addition, in order to further confirm the fluorescent property, the PAH/PSS/CDs composite capsules under wet state were characterized by CLSM. The bright red and green circles in **Figure 6.10 B** verified the fluorescent property of the PAH/PSS/CDs capsules. The fluorescence was originated from the embedded CDs.

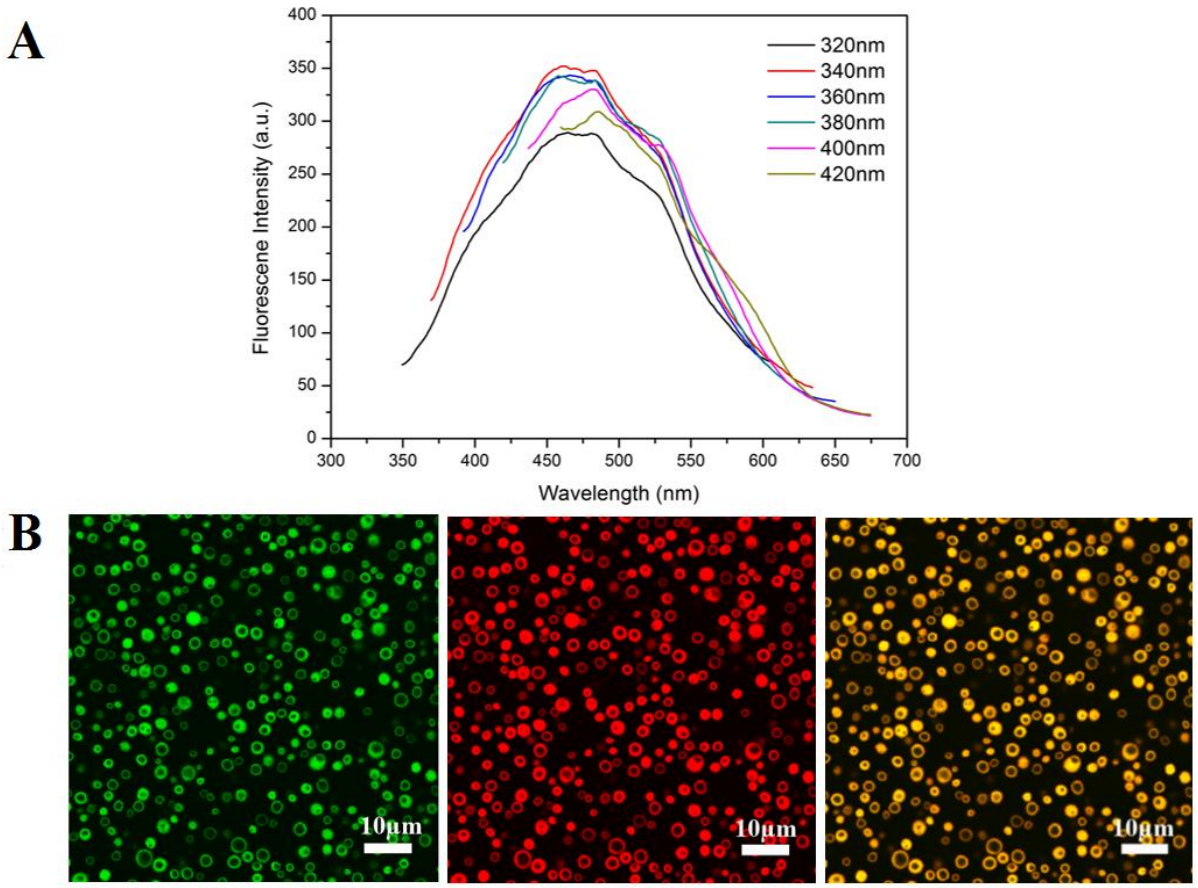

Figure 6.10 Characterization of fluorescent properties. (A) Fluorescence spectrums of aqueous dispersion PAH/PSS/CDs composite capsules; (B) CLSM images of PAH/PSS/CDs composite capsules.

Usually, the excitation-dependent PL properties of CDs reflect a distribution of the different surface energy traps and different size of the CDs.[187] An interesting phenomenon found here

is that, different from the PL behaviour of CDs in water, PL emission of the CDs incorporated into the microcapsule did not show excitation-dependent emission (**Figure 6.10 A**). This may be an indication that wavelength dependent emission is environment-related effect. Such hypothesis was further proved in our experiment. Inspired by the observation of disassembly of PAH/PSS capsules in strong alkaline environment,[101] the PAH/PSS/CDs were incubated in NaOH solution (pH=13) for 24 h and then were measured by fluorescence spectrometer and SEM. It was expected that the composite capsules could be slightly dissolved and free some embedded CDs in the solvent.

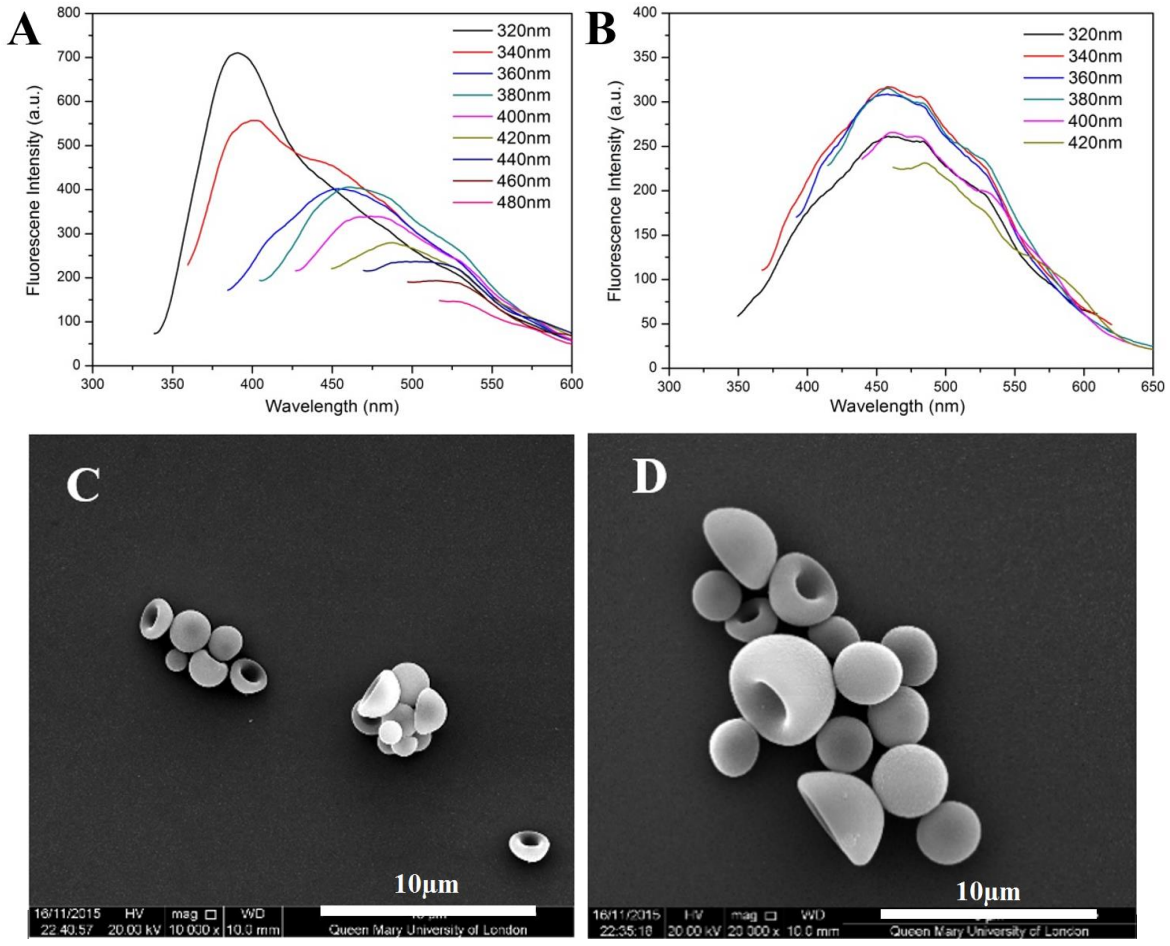

Figure 6.11 Fluorescence spectra of PAH/PSS/CDs composite capsule after dissolving by NaOH solution (pH=13) for 24 h without (A) and with (B) further wash. SEM images (C, D) of PAH/PSS/CDs capsules treatment by NaOH solution for 24 h after wash (different magnification).

As indicated in **Figure 6.11**, before wash with DI-H_2O to remove the disassembled free CDs, the mixture presented an excitation-dependent PL properties. However, if the mixture were washed 3 times with DI-H_2O, the excitation-dependent phenomenon disappeared, and a similar PL spectra were obtained. Such results proved that wavelength dependent emission of CDs is environment-related effect.[101] In this case, the CDs confined within the shells of capsules showed no emission position shift under laser irradiation at different wavelength. Another interesting phenomenon is that PAH/PSS/CDs composite capsules showed high chemical stability. They did not disassembled by soaking in NaOH (pH=13) even holding for 24 h, which was different from pure PAH/PSS capsules, showing disassembly after only a few seconds of alkaline treatment.[101]

The luminescent phenomena were also found for 2D PAH/PSS/CDs membrane assembled on glass substrate by the same one-step method applied for capsules, as shown in **Figure 6.12**. Therefore the procedure described here is not only limited to 3D structures, but can also be explored as a general strategy for the accomplishment of luminescent 2D nanocomposite membrane.

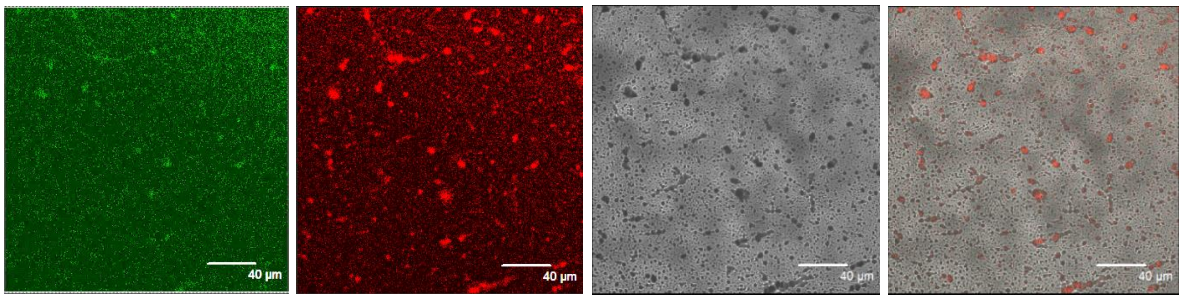

Figure 6.12 CLSM images of flat LbL $(PAH/PSS)_{10}$ films with *in situ* formed CDs inside.

6.3.3 Fluorescent PAH/DEXS/CDs Spheres-No Added Dextran

Based on the above results, it is reasonable to suppose that polyelectrolyte capsules, with one component that can be carbonized under hydrothermal condition, are able to be facilely empowered with fluorescence without introducing other carbon sources. Dextran sulphate sodium salt (DEXS) is one negatively charged biocompatible polyelectrolyte, which often used as the building blocks for polyelectrolyte LbL capsules. In this thesis, $(PAH/DEXS)_4$ and $(PARG/DEXS)_4$ capsules were prepared for further carbon functionalization. Similarly, the possibility to carbonize DEXS into fluorescent CDs was checked first. **Figure 6.13** showed the FL spectra of the CDs formed from 2mg/mL DEXS/H_2O solution. Obviously, similar with the CDs fabricated from dextran (**Figure 6.1 B)**, the sample obtained from DEXS also exhibited a fluorescent property (**Figure 6.13**). An excitation-dependent emission position phenomenon was proved by their FL spectra, displaying the emission peaks shifting to longer wavelength and the PL intensity decreasing gradually when the λ_{ex} increases from 320 nm to 500 nm.

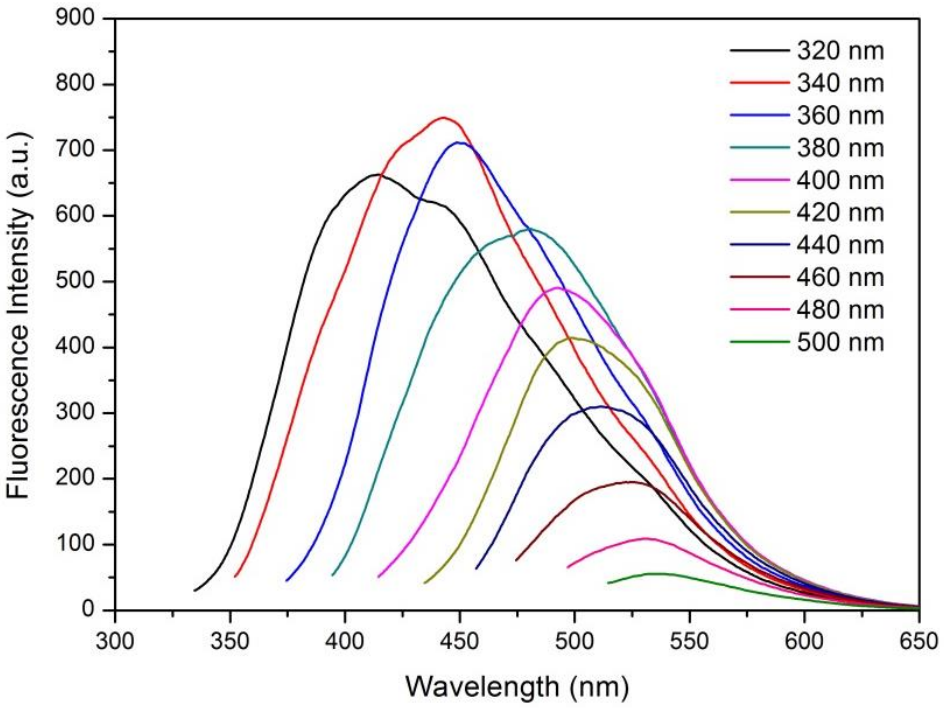

Figure 6.13 FL spectrums of 2 mg/mL Dextran sulphate sodium salt (DEXS) in water at 160 ^oC for 20 h.

The FL data above demonstrated that DEXS molecules were able to be carbonized when heated at 160 ^{o}C. Herein, it is expected that heating PAH/DEXS capsules in DI-water can also bring a significant change in their optical behaviour. The treated PAH/DEXS capsules were characterized by CLSM (**Figure 6.14**). Bright green and red particles were clearly seen in these CLSM images, which confirmed the above assumption, *i.e.*, hydrothermal treatment of the PAH/DEXS capsules without adding dextran in the system can also endow them with fluorescence. This results indicated that the pre-confined DEXS molecules in the shells were converted to fluorescent dots. However, it seems that capsules after carbonisation lost their hollow structure as no rings can be found in the CLSM images. To further analyse the morphology and structure change of the capsules before and after carbonization, the capsules were studied by SEM and TEM techniques, as given in **Figure 6.14** and **Figure 6.16**.

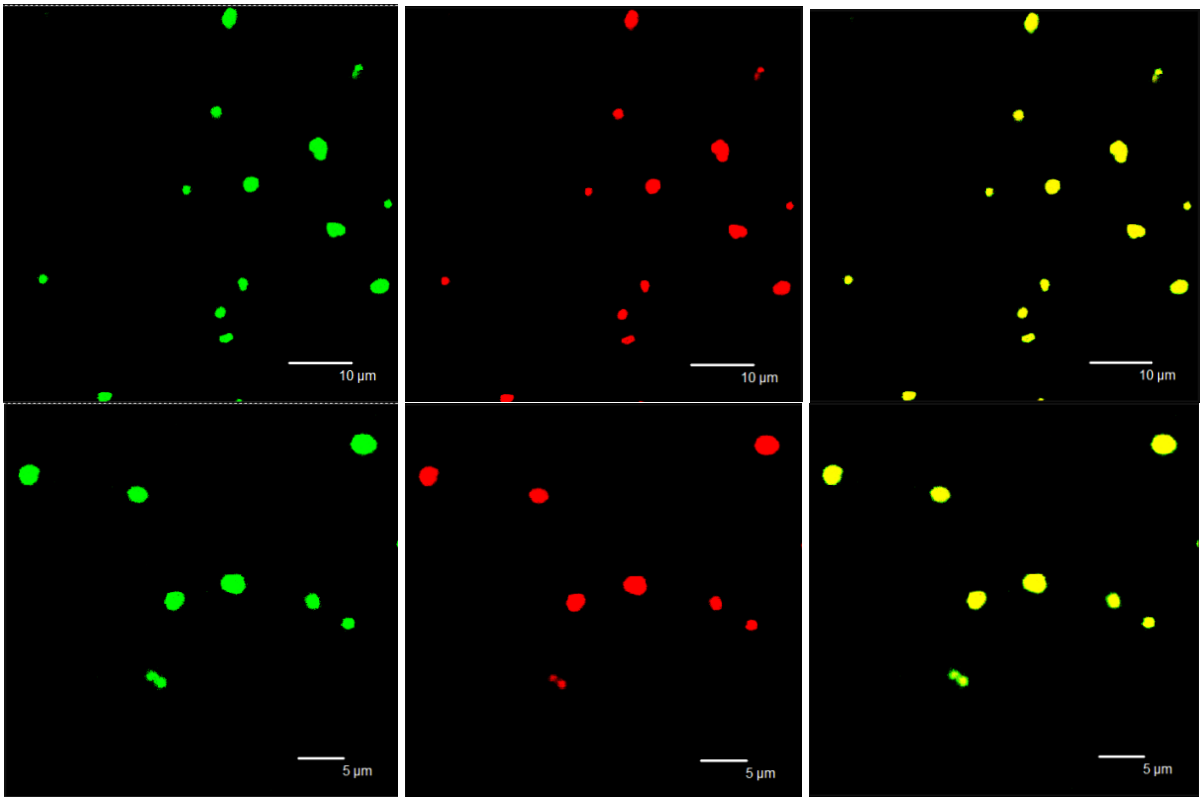

Figure 6.14 CLSM images of $(PAH/DXES)_4$ capsules after carbonization in DI-water (different magnification).

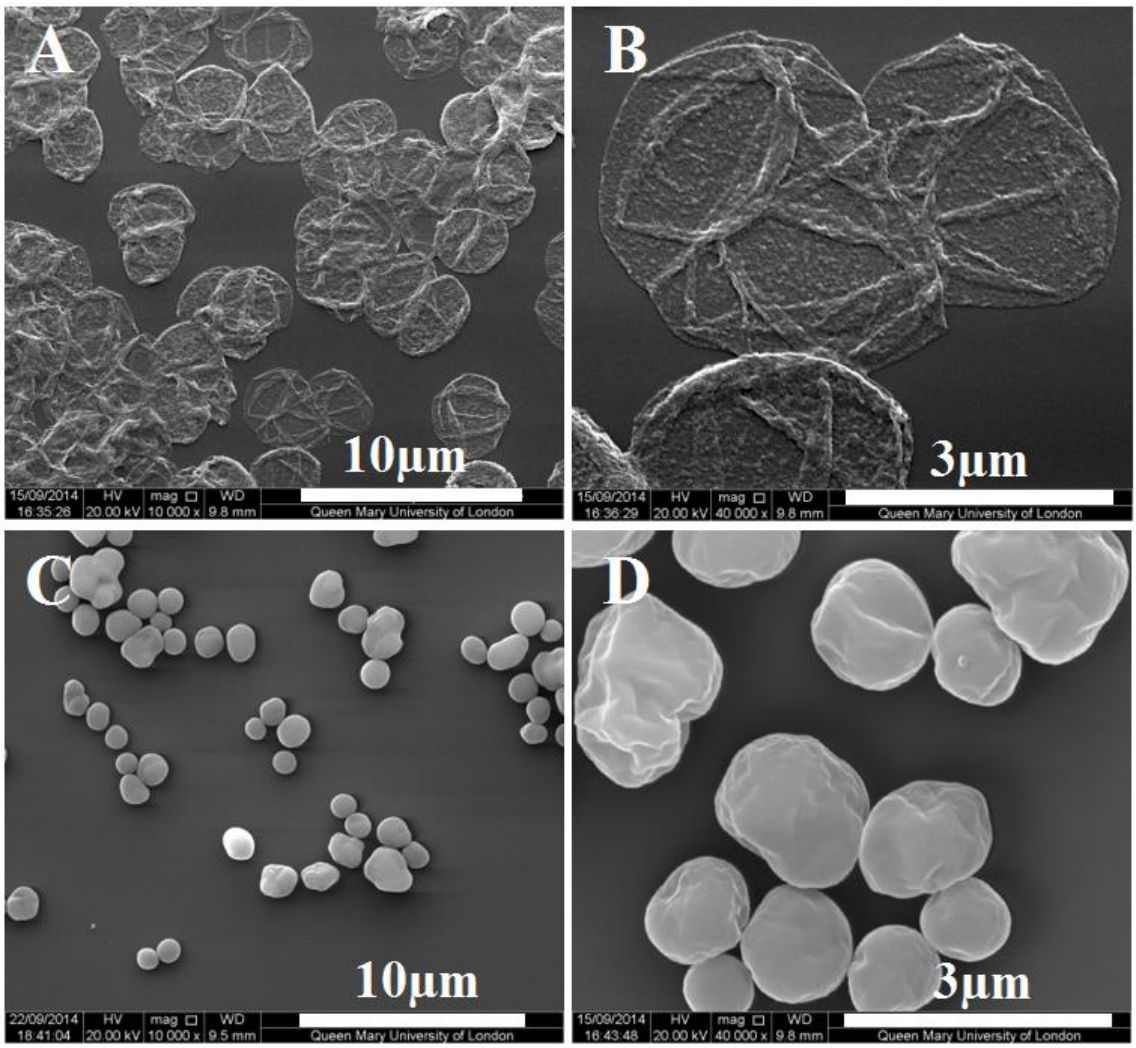

Figure 6.15 SEM images of $(PAH/DEXS)_4$ capsules before (A, B) and after (C, D) carbonization in DI-water.

The SEM images in **Figure 6.15** indicated a drastic difference in their morphology. Before hydrothermal treatment at 160 ^{o}C, the $(PAH/DEXS)_4$ capsules showed a similar morphology with $(PAH/PSS)_4$ capsules, presenting a collapsed and flatted film-like morphology. After the treatment, these capsule changed into robust 3D spheres with some notable pits on their surfaces. The size greatly decreased as heating caused shrinkage of the soft polyelectrolyte shells. TEM images of the hydrothermal treated $(PAH/DEXS)_4$ capsules revealed that these particles are solid in structure, which further confirmed the above CLSM results. As discussed

in the above PAH/PSS/CDs system, for polyelectrolyte capsules, the influence of hydrophobic forces greatly surpasses the electrostatic forces so that their shells would rearrange their structure under heating and shrink to decrease the surface area exposed to the solvent and finally appear as filled balls.[155,299] Here, in this system, even though the DEXS components entangled with PAH were carbonized into CDs and buried within the shells, it's not enough to prevent them shrinking into solid balls. Because the amount of CDs was limited to the pre-assembled amount of DEXS in the multilayers. Besides, the location of the formed CDs were also pre-determined and they could not move freely to block the pores. In addition, compared with the $(PAH/PSS)_4$ capsules that were hydrothermally treated in pure H_2O, these particles did not possess standard spherical shapes. This might due to the carbonization effect of the layer component (DEXS), which inhibited homogeneous shrinkage of the multilayers. Some sags and crests formed, as proved by the SEM images. Therefore, after hydrothermal treatment, the capsules were shrink into solid particles with fluorescent CDs buried inside.

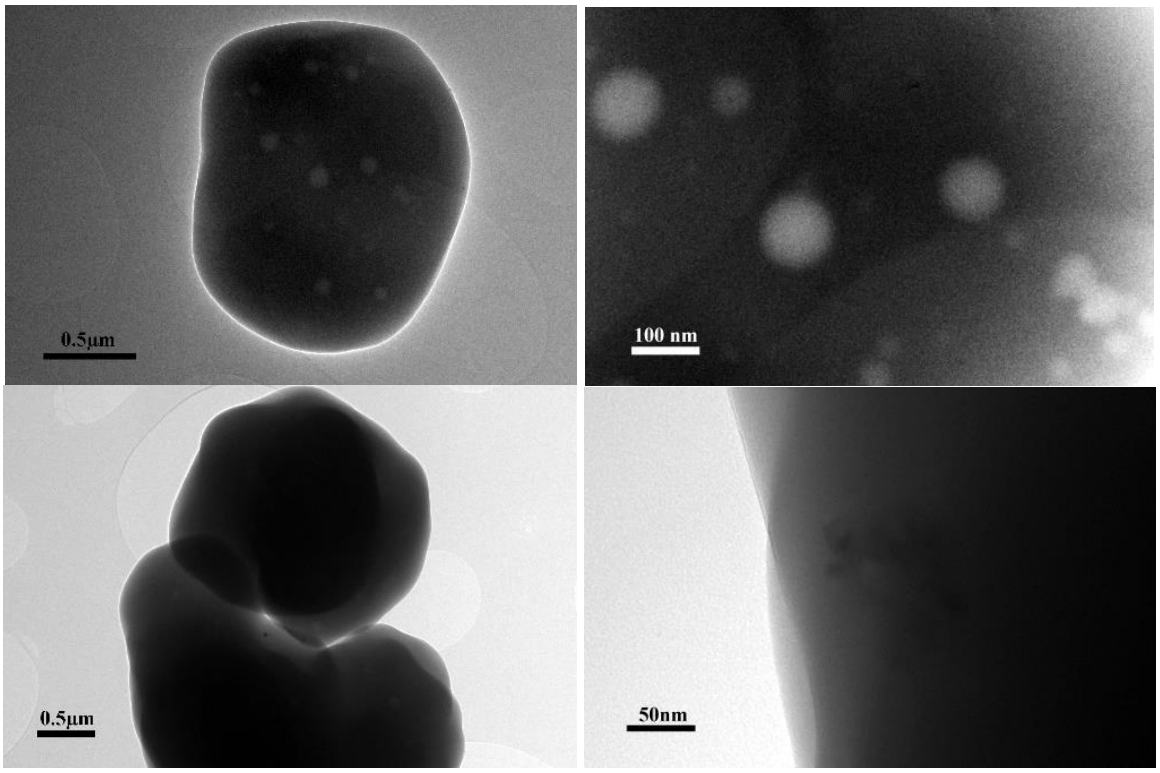

Figure 6.16 TEM images of $(PAH/DEXS)_4$ capsules after carbonization in DI-water.

The study in this part reveals that carbonization of polyelectrolyte shell components can bring fluorescence but is difficult to maintain the hollow structure of capsule. But this method could be potentially used for 2D films.

6.3.4 PARG/DEXS/CDs Capsules-Add Dextran

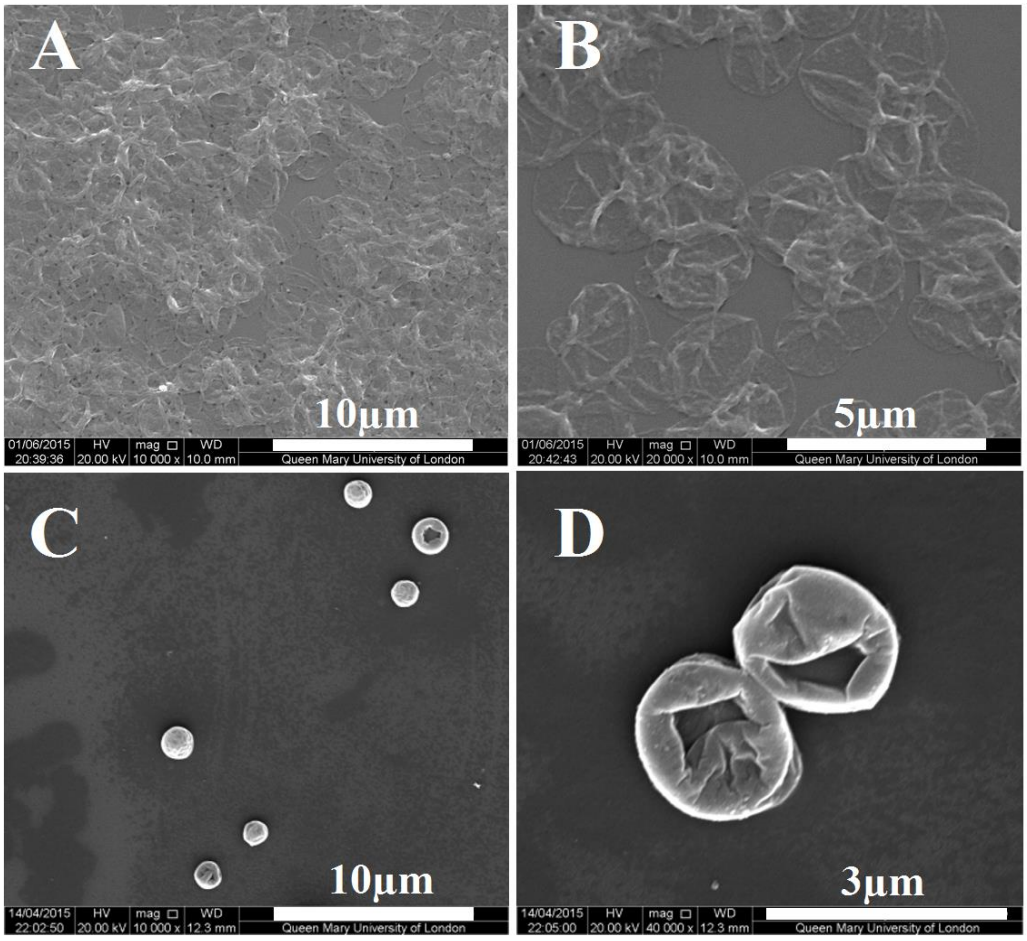

Figure 6.17 Pure $(PARG/DEXS)_4$ capsules and after heated at 160 for 20 h with 2 mg/mL dextran.

Based on the above results and explanations, in order to remain the hollow structure, the free dextran molecules need to be introduced into the capsule systems. Hence, for functionalization of biodegradable $(PARG/DEXS)_4$ capsules with fluorescent CDs, dextran was added into the reaction system. Similar with the PAH/PSS/CDs system, $(PARG/DEXS)_4$ capsules were also incubated in 2 mg/mL dextran/H_2O solution and then hydrothermal treated at 160 ^oC for 20 h.

Their morphology and fluorescent property were investigated by SEM and CLSM measurements, as shown in **Figure 6.17** and **Figure 6.18**.

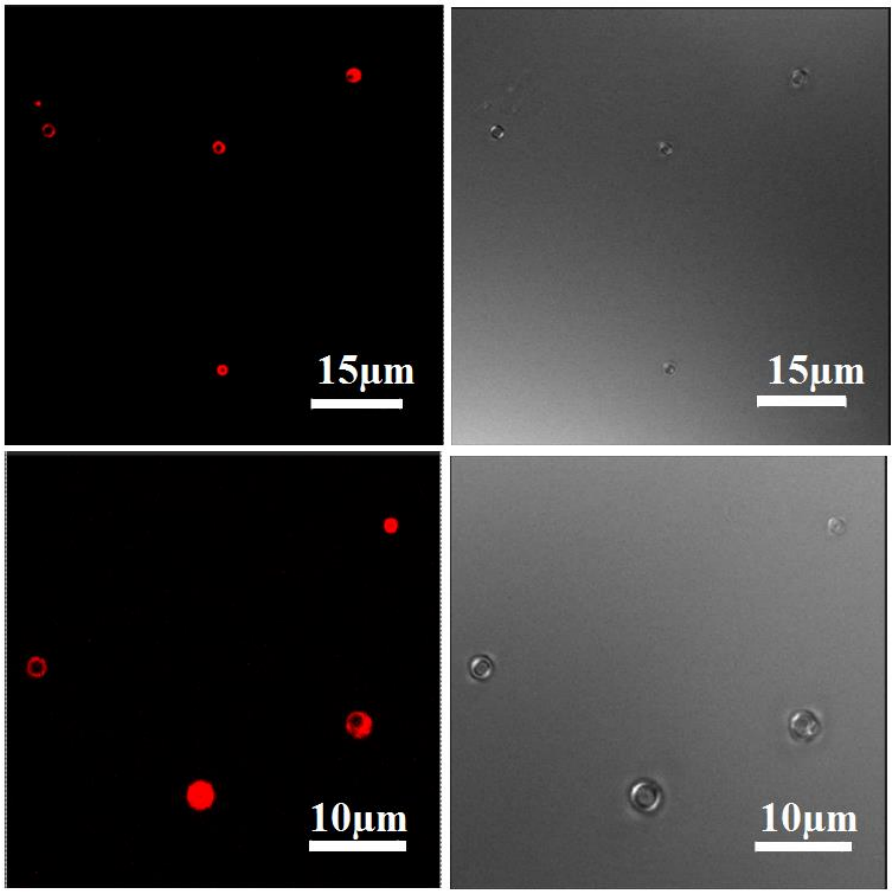

Figure 6.18 CLSM images $(PARG/DEXS)_4$ capsules after heated at 160 ºC for 20 h with 2mg/mL dextran. (Measured by CLSM after two months)

SEM images in **Figure 6.17** showed the morphology change before and after the hydrothermal treatment. After carbonization, these capsules were strengthened with a higher mechanics, thicker shell and reduced size. Interestingly, it seem that their morphology combined the features of PAH/PSS/CDs and PAH/DEXS-CDs systems, slightly bowl-like and with pits on their surfaces. The hollow structure and fluorescent property were demonstrated by the CLSM data. Red rings were obviously shown in **Figure 6.18**.

The fluorescence of hydrothermal treated PARG/DXES capsules came from two parts: (1) carbonization of DEXS within the shell; (2) carbonization of free dextran molecules in the solution. These two effects led to the final morphology, structure and optical features of the composite capsules. After the investigation on morphology and fluorescent properties of the above-discussed carbonized capsules, other features including photostability, permeability, ultrasound responsiveness, cell viability and biodegradable behaviours of two obtained composite capsules were studied in detail: (1) PAH/PSS/CDs; (2) PARG/DEXS/CDs.

6.4 Photostability of Fluorescent PAH/PSS/CDs

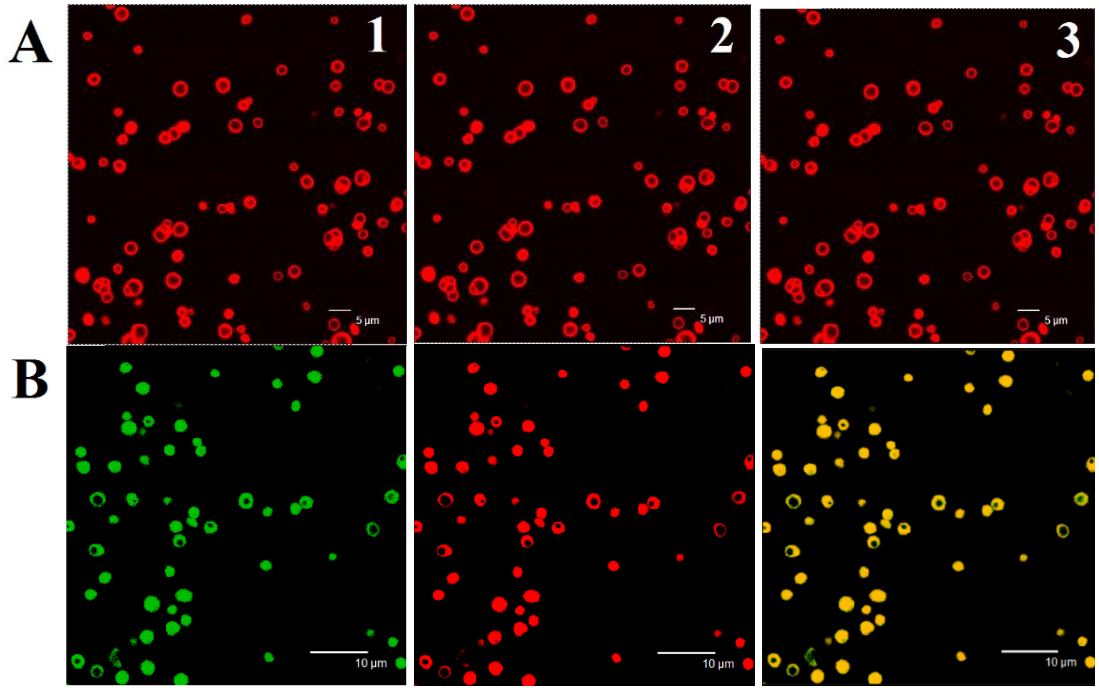

Figure 6.19 CLSM images of PAH/PSS/CDs composite capsules. (A) Irradiated with laser (561nm) for different time: (1) 0 min; (2) 15 mins; (3) 30 mins. (B) Images obtained after 8 months' storage in fridge at 5 ^{o}C.

The photostability of PAH/PSS/CDs composite capsules were checked by CLSM technique. **Figure 6.19 A** revealed that the PAH/PSS/CDs capsules did not show fluorescent signal change

after a continuous irradiation with the excitation laser at 561 nm for 30 minutes, which indicates that the PAH/PSS/CDs have excellent stability against light illumination. The capsules were also measured after 8 months storage in fridge (5 ^{o}C) (**Figure 6.19 B**), showing that they still possessed good fluorescent signal and no significant morphology change was found. Such results proved that the PAH/PSS/CDs capsules were very stable, which could be potentially used for long-term imaging application.

6.5 Carbonization Permeability Change and Encapsulation of Small Molecules

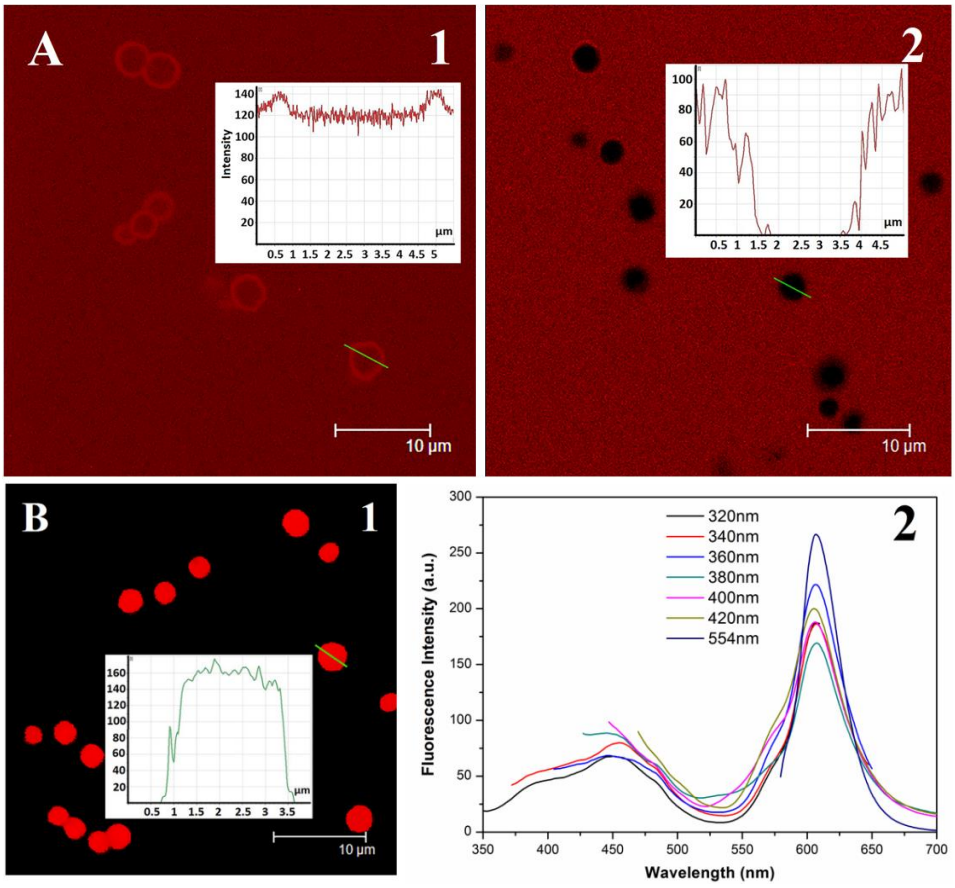

Figure 6.20 Characterization of reduced permeability. (A) CLSM images of pure PAH/PSS capsules (1) and PAH/PSS/CDs composite capsules (2) dispersed in Rh-B/H_2O solution (300 μg/mL). (B) CLSM images (1) and fluorescence spectra (2) of composite capsules with Rh-B encapsulated. The line scan inserts shows relative fluorescent intensity in capsules.

A key question for these novel PAH/PSS/CDs capsules is whether they are able to sequester materials without allowing them to leak out. To investigate PAH/PSS/CDs capsule's ability to encapsulate small molecular, stable sequestration and encapsulation of Rh-B (Mw=489), CLSM and Fluorescence spectrometer were employed here. **Figure 6.20 A** shows the CLSM images of $(PAH/PSS)_4$ capsules immersed in Rh-B/H_2O solution before and after CDs incorporation. The polyelectrolyte capsules without any treatment were completely permeable to Rh-B molecules, which was further proved by the inset in **Figure 6.20 A1** showing the fluorescence intensities outside and inside the capsules were similar. However an effective interception of Rh-B by the PAH/PSS/CDs capsules shells was found in **Figure 6.20 A2**, with a fluorescence intensity of zero inside capsules due to reduced permeability. Such phenomenon can be interpreted as a result of several factors. The first one attributes to the heat treatment.[155,178] When dispersed in DI-water, they can only prevent macro-molecules (~70 kDa) from penetrating but definitely can't block small ions and molecules with a molecule weight less than 1000 Da.[155] But *via* hydrothermal reaction, a drastically shrinkage of the polyelectrolyte multilayers occurred because of heating,[155] with a result of that, the whole capsule size was reduced and shell thickness was increased, as detected by SEM and TEM in **Figure 6.6** and **Figure 6.7** respectively. Another contribution is the incorporation of the *in situ* formed CDs which could block pores and reduce permeability of the shell consequently.

The reduced permeability of composite capsules was further verified by their encapsulation of Rh-B, as shown in **Figure 6.20 B1**. The capsules with Rh-B dyes inside were shown in the CLSM image, in which the line scan inset indicates an average fluorescent signal intensity of ~ 150 units inside capsules and 0 unit outside capsules. In addition, compared with the PL spectrums of PAH/PSS/CDs capsules in **Figure 6.10**, PAH/PSS/CDs capsules loading with Rh-B exhibited new emission peaks around 620 nm (**Figure 6.20 B2**) which were

corresponding to Rh-B, meaning Rh-B molecules were successfully sealed in the capsule cavities.

6.6 Ultrasound Induced Rupture and Cargo Release

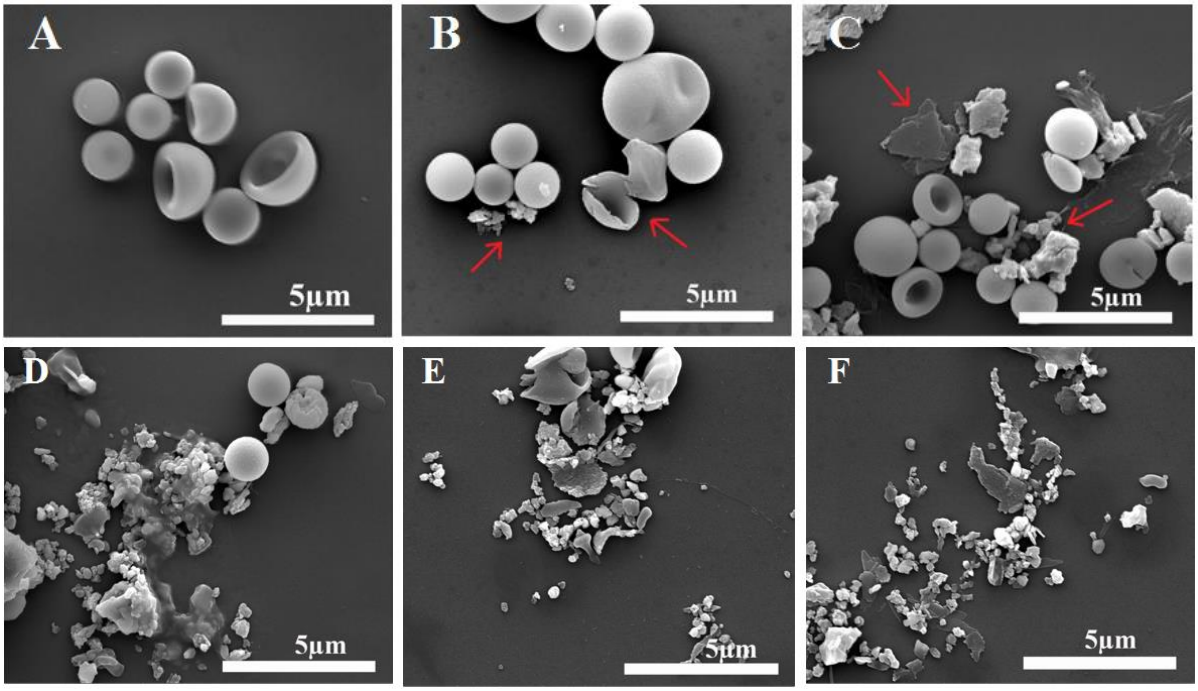

Figure 6.21 Characterization of ultrasound sensitivity. SEM images of PAH/PSS/CDs capsules treated with ultrasound for different duration time (A) 0 s; (B) 2 s; (C) 10 s; (D) 20 s; (E) 60 s; (F) 120 s.

Controlled release of the encapsulated drugs from the carriers at the predetermined areas is a major challenge for any drug delivery system. As we proved in Chapter 4 and Chapter 5, ultrasound is an effective stimuli for the composite polyelectrolyte/inorganic NPs capsules. Because in comparison with nanoparticle-free polyelectrolyte capsules, embedding of these kind of inorganic NPs in the polyelectrolyte shells proved a pronounced stiffness increase and therefore, increased the density gradient across the water/shell interface and consequently improved the absorption of acoustic energy.[14,23] As in this case, the CDs were buried in the PAH/PSS multilayers, which are expected to empower the formed composite capsules with higher sensitive to ultrasound. To investigate whether the PAH/PSS/CDs capsules could be deconstructed by ultrasound, we performed the experiment of remote activation of

PAH/PSS/CDs capsules by using the ultrasonic setup GEX 750 (Sonics & Materials, Inc., USA), operating at a frequency of 20 kHz and power output 50 W with an amplitude at 30%. The suspension of polyelectrolyte/CDs capsules was submitted to ultrasound during various time intervals (2, 10, 20, 60 and 120 s) and analysed. Ultrasonic effects on these microcapsules were evidenced. **Figure 6.21** displays the SEM investigation data of PAH/PSS/CDs capsules response to ultrasound in dependence on the sonication time. It can be seen from these images that the capsules showed intact ball-like morphology before the ultrasound treatment (t=0 s). Some fragments and break capsules appeared after only 2 s of ultrasonication, as indicated by the arrows in **Figure 6.21 A2**. More PAH/PSS/CDs composite capsules were broken into pieces when prolonging the treatment time. It can be seen that very few capsules were kept intact when time reaches to 20 s. The image in **Figure 6.21 A6** indicates that 120 s of sonication lead to complete destruction of the capsules and only debris of the broken capsules were visible.

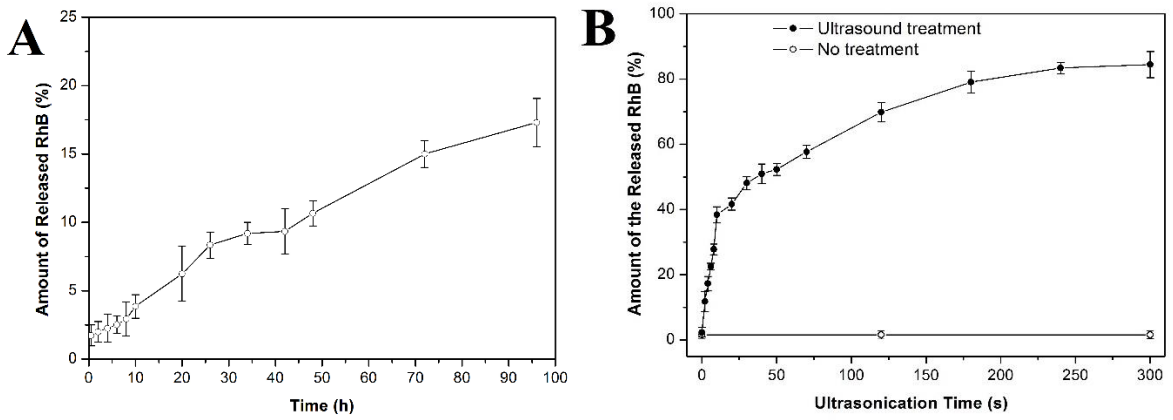

Figure 6.22 Amount of released Rh-B from the composite capsules. (A) long-time release without triggering; (B) triggered release corresponding to the ultrasound treatment time.

As proved above, ultrasound can break these PAH/PSS/CDs capsules, so it can be applied for triggered release. Hence, the released Rh-B from the sealed PAH/PSS/CDs capsules as response to sonication time was then investigated. In fact, the release could be caused either by diffusion or by ultrasound effect. In order to make sure that the release from the capsules was

mainly due to the ultrasound effects, the release behaviour of capsules (kept in dark) without any treatment was first recorded as the control group, **Figure 6.22 A**. It revealed that the PAH/PSS/CDs capsules perform an excellent package for sealing small molecules, showing a good stability against the diffusion effect. After 12 h, less than 4% of Rh-B was detected. When prolonging time to 3 days, only ~15% of Rh-B was released outside. Therefore, it could be assumed that here the influence of diffusion on Rh-B release from capsules within 300 s was negligible, and the data of ultrasound-triggered Rh-B release could be reliable in this duration.

Generally, for ultrasound triggered release, the detected Rh-B tended to increase rapidly in the first 1 minute with the increase of sonication time, as shown in **Figure 6.22 B**. The released Rh-B was found to be around 17% in only 6s of sonication, and it then increased to ~ 40% in 20 s. When ultrasound treatment was extended to 60 s, more than 50% of Rh-B was released from the capsules. The release curve became flatted after this time point, indicating a relative slow release rate. A value of 70% of the initial Rh-B was detected in the supernatant. Finally, it was demonstrated of an ultrasound-triggered release efficiency of ~80% at t= 4 min. No significant increase was found if further increased the treatment time. It should be noted here that not all the encapsulated Rh-B was released (as detected) even after 5 minutes of sonication, which was caused synthetically by the adsorption of Rh-B inside or on capsule shells, and the possible photobleaching effect. Based on these results, it is notable that ultrasonic stimulation is an effective and efficient way to release the encapsulated compounds in PAH/PSS/CDs capsules.

6.7 Laser Induced Selective Break

Single wall carbon nanotubes were reported to be embedded in polyelectrolyte capsules, and the formed polyelectrolyte/carbon nanotube composite capsules showed selective open by

irradiation with laser operating at 473 nm.[214] Inspired by this observation, whether laser can be also used as tool to open the PAH/PSS/CDs composite capsules was checked in this study. UV-vis absorption results of CDs in water displayed in Figure **6.1 B** demonstrated their strong absorbance in range of 200-400 nm. However, the UV-NIR spectrum of PAH/PSS/CDs capsules in water exhibits a broad absorption band, as shown in **Figure 6.23 A**. Moreover, it is found that CDs performed an up-conversion behaviour (**Figure 6.23 B**), *i.e.*, emission peaks located around 460 nm were obtained by laser irradiation at wavelength from 680-800 nm. This feature of CDs might promote the effect induced by NIR laser irradiation on PAH/PSS/CDs composite capsules. But it shall be mentioned that the up-conversion phenomenon is a controversial discovery even though a huge amount of researchers reported this phenomenon and described the mechanisms in past few years. Because Xiaoming Wang *et al.* demonstrated in 2014 that the so-called up-conversion fluorescence originates from the normal fluorescence which excited by the leaking component from the second diffraction in the monochromator of the fluorescence spectrophotometer.[300] To clearly understand this phenomenon, more deep research on the up-conversion fluorescence should be carried out by people worked in this area in the future.

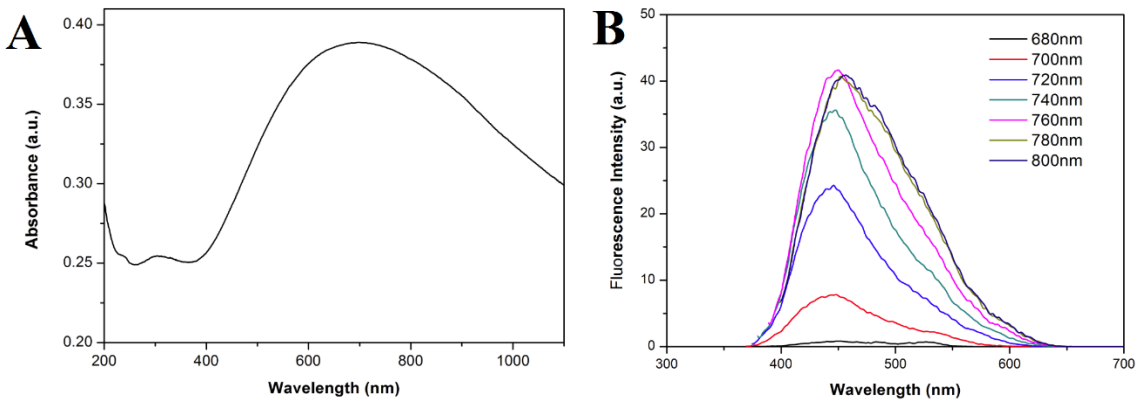

Figure 6.23 (A) Absorption spectrum of PAH/PSS/CDs composite capsules in water; (B) Up-conversion PL spectra of CDs in water.

The above UV-NIR absorption spectrum indicated that laser with wavelength from 400-1000 nm can be employed. Here, NIR laser at 840 nm was chosen to be used to open PAH/PSS/CDs capsules. SEM and TEM images of PAH/PSS/CDs composite capsules after remote addressing by NIR laser irradiation for different duration are shown in **Figure 6.24**. The PAH/PSS/CDs capsules showed pits on their surfaces after 10 s of irradiation, **Figure 6.24 A** and **D**. Holes appeared on the capsules when prolonging the irradiation time to 30 s (**Figure 6.24 B** and **E**). With longer treatment time, the size of the holes increased to around 600 nm, as indicated in **Figure 6.24 C** and **F**. Such results proved our hypothesis, indicating that the CDs functionalized polyelectrolyte capsules can be selectively opened by NIR laser which is not harmful for human body.

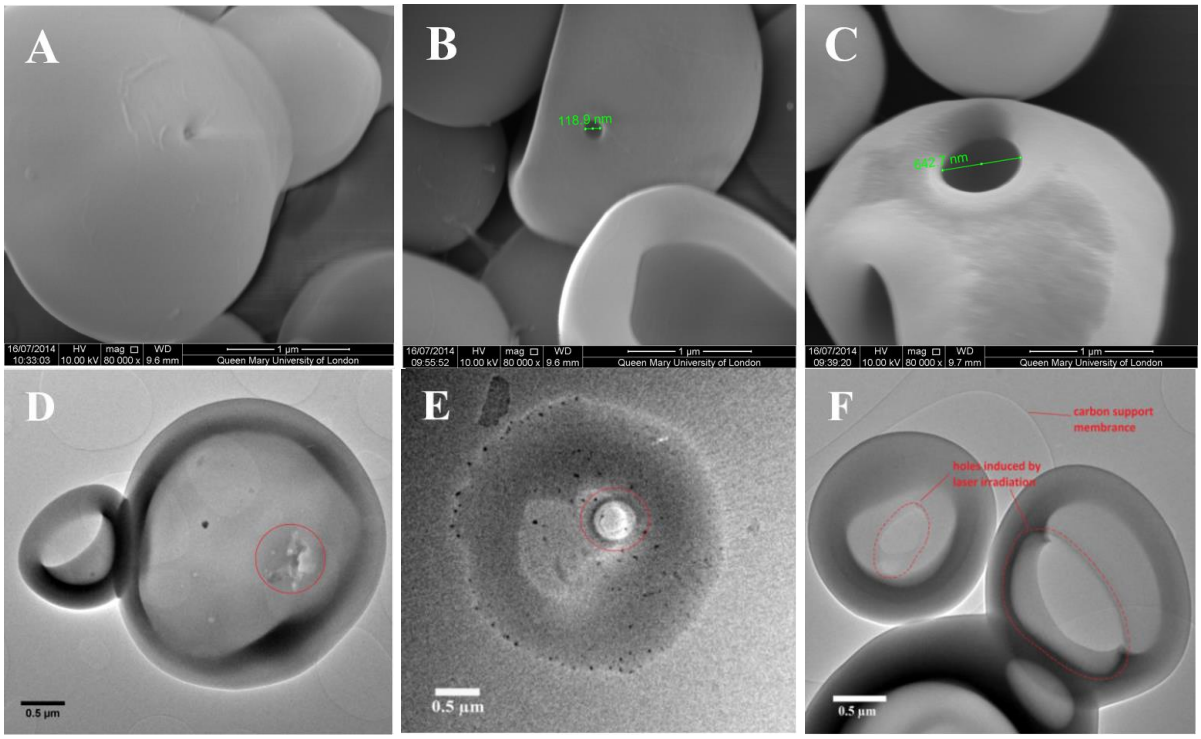

Figure 6.24 SEM and TEM images of PAH/PSS/CDs capsules treated by IR laser (840nm) for different time: (A, D) 10 s; (B, E) 40 s; (C, F) 120 s.

Similarly, PAH/PSS/CDs films deposited on glass substrates were also treated by NIR laser. SEM images of the films before and after laser irradiation at 840 nm for 60 s were given in **Figure 6.25**. Before laser irradiation, no big cracks or holes were found on the films, **Figure 6.25 A** and **B**. If the laser was on and then move the objective position, it was observed that the films were burned along the movement of the laser, showing straight lines with width around 550 nm (**Figure 6.25 C**). However, if without movement, single hole with similar diameter size (~550 nm) was obtained after 60 s of irradiation, as shown in **Figure 6.25 D**. These results were consistent with that of laser-treated PAH/PSS/CDs capsules. Hence, NIR laser can be used as a potential external trigger to open the CDs functionalized capsules.

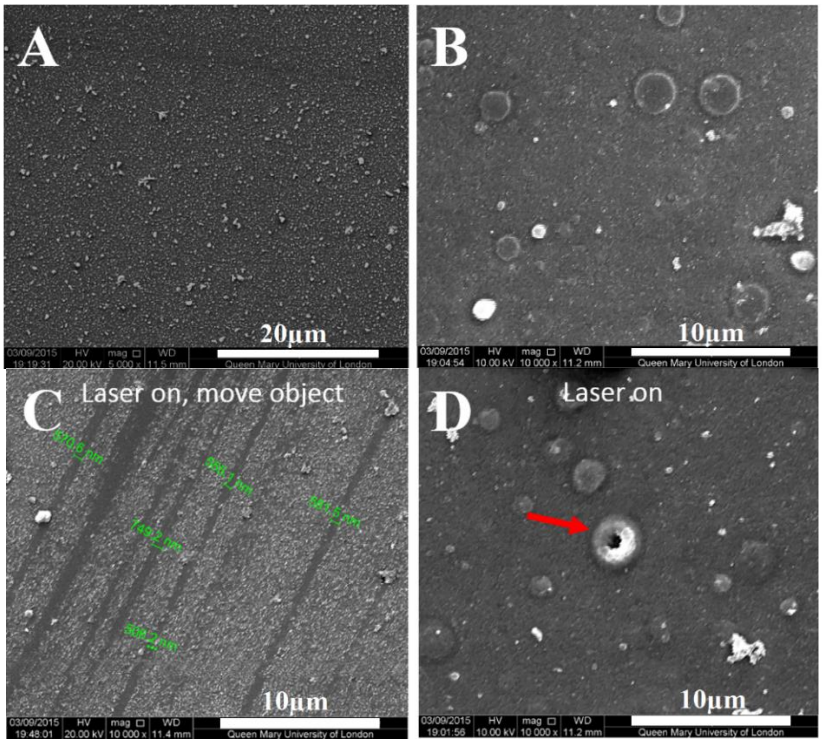

Figure 6.25 SEM images of $(PAH/PSS)_8$/CDs films before (A, B) and after (C, D) treated by laser (840 nm) for 60 s.

6.8 Cell Viability and Biodegradability of CDs and Composite Capsules

6.8.1 Cell Viability and Cellular Uptake of Fluorescent CDs

To assess the cell viability and cellular uptake of luminescent CDs, B50 cells were used as model cancer cells. B50 cells were incubated with CDs with different concentrations and studied by MTT assays. The cell viability data were presented in **Figure 6.26 A**. Briefly, no significant cell toxicity was indicated. It is clear that the cell viability was depended on the concentration of CDs, showing that CDs with a concentration lower than 200 µg/mL was not toxic to B50 cells, but the cytotoxicity increased as increasing the concentration of CDs to 400 µg/mL. Prolonging the coculture time also had some influence on cell viability, indicating a slightly decrease. Based on the *in vitro* cytotoxicity data, CDs with a concentration of 20 µg/mL was chosen to study their cellular uptake behaviour. After 4h of incubation with B50 cells, they were visualized by CLSM under the irradiation of laser with a wavelength at 561 nm. As shown in **Figures 6.26 B**, the intracellular red fluorescence in B50 cells was proved, which means that CDs were uptake by B50 cells effectively within 4 hours. This result demonstrates the cellular imaging function of the CDs.

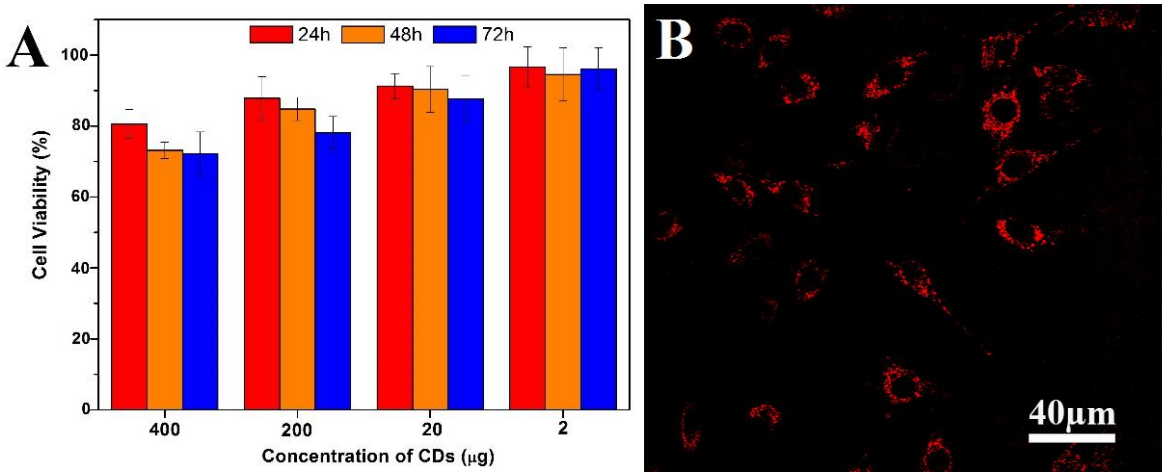

Figure 6.26 (A) Cell viability of B50 cell line mixed with different concentration of CDs for 24 h, 48 h and 72 h at 37°C respectively as measured by an MTT assay compared with the control. The error bars show the standard deviations. (B) CLSM images of B50 cells after incubation with 20 µg/mL for 4 h.

6.8.2 Cell viability and cellular uptake of composite capsules

Following proof-of-concept of good cell viability and cell imaging potential of the fluorescent CDs, investigation of cytotoxicity and cellular internalization of PAH/PSS/CDs and PARG/DEXS/CDs capsules were also carried out in B50 cancer cells using the MTT cell viability assays. The *in vitro* cytotoxicity of the PAH/PSS/CDs and PARG/DEXS/CDs capsules with various cell-to-capsule ratios were examined and shown in **Figure 6.27 A and B,** respectively. No significant changes in cell viability were observed for all treatments with PAH/PSS/CDs capsules indicating negligible cytotoxicity of the PAH/PSS/CDs capsules. **Figure 6.27 A** proved the cell-to-capsule ratio also slightly vary the toxic effect on B50 cells, showing litter higher toxicity at lower ratio (1:20). But the cell viability are all above 80% for all the treatment ratios used in the experiment even after incubation for 72 h. Such data demonstrated an excellent biocompatibility of PAH/PSS/CDs capsules and their negligible cytotoxicity. In terms of PARG/DEXS/CDs capsules, they even presented better cell viability data, **Figure 6.27 B**. This might because of the outstanding biocompatibility of PARG and DEXS polyelectrolytes.

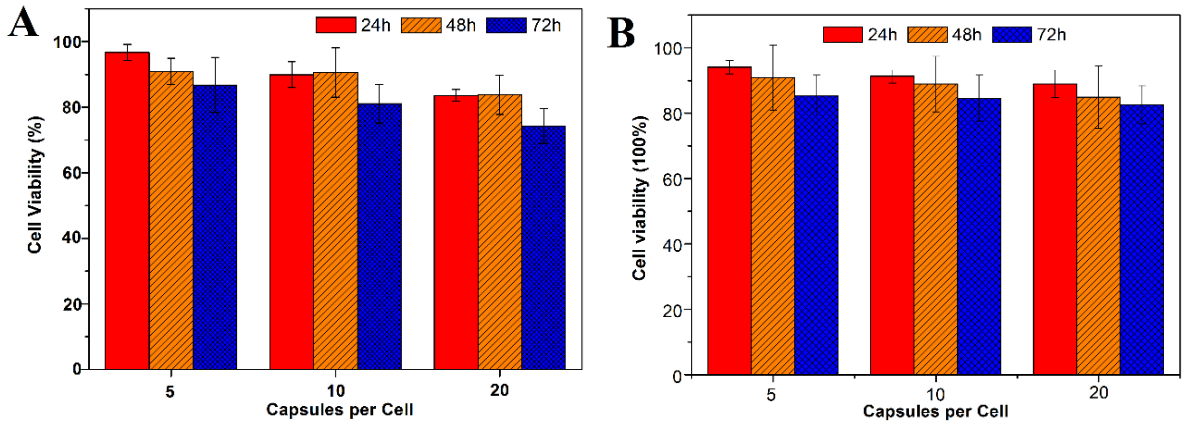

Figure 6.27 Cell viability of B50 cell line mixed with different concentration of PAH/PSS/CDs (A) and PARG/DEXS/CDs capsule (B) for 24 h, 48h and 72 h at 37°C respectively as measured by an MTT assay compared with the control. The error bars show the standard deviations.

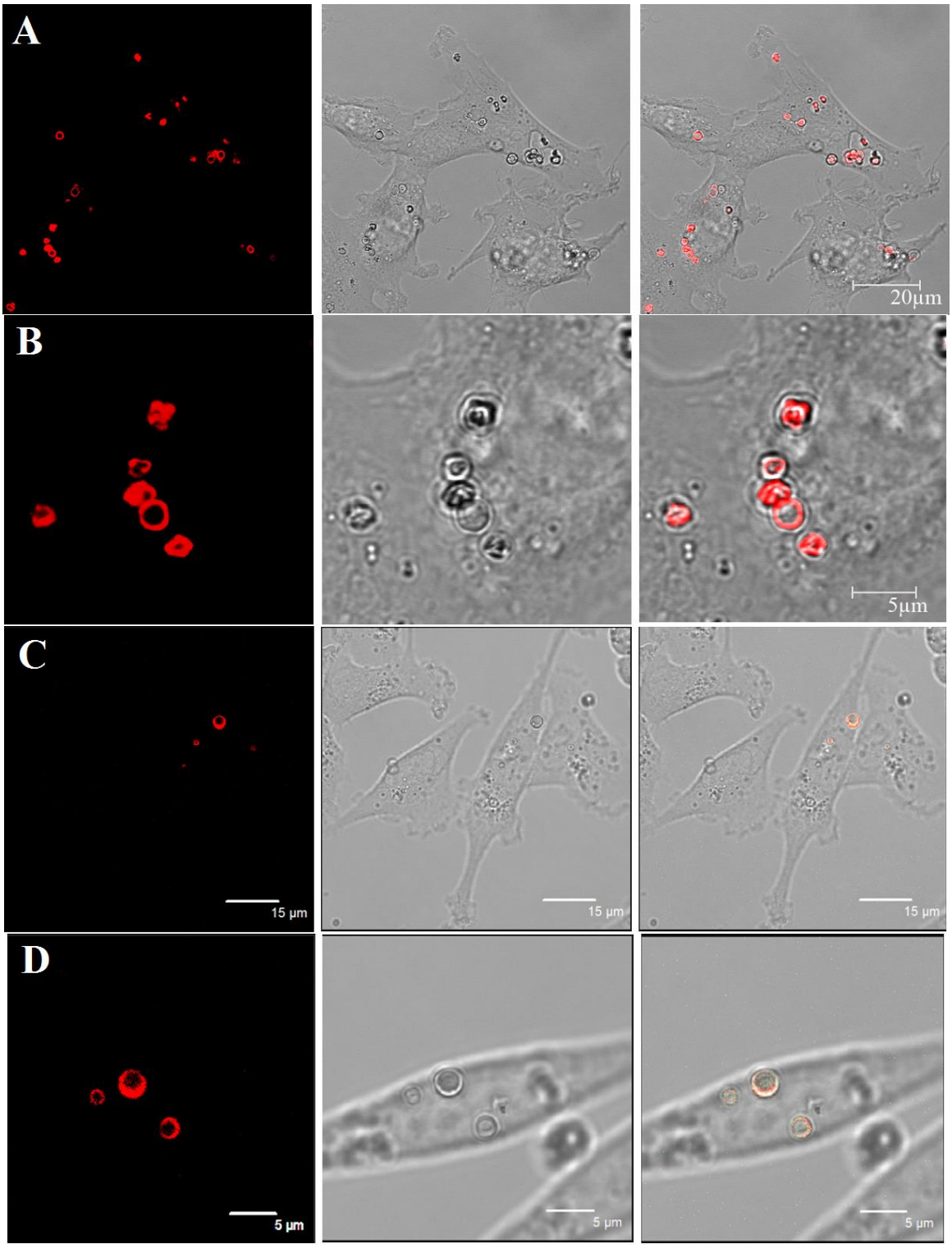

Figure 6.28 CLSM image of PAH/PSS/CDs (A, B) and PAH/DEXS/CDs capsules (C, D) incubated with B50 cells for 6 h and 3 h, respectively.

To assess the cellular uptake of luminescent composite capsules, B50 cells incubated with PAH/PSS/CDs capsules (cell-to-capsule ratio is 1:20) for 6 h were measured by CLSM under the irradiation of laser with a wavelength at 561 nm. As shown in **Figures 6.28 A and B**, the capsules were indeed internalized by B50 as evidenced by the fact that the capsules are localized within the same confocal plane as the enclosure of the cell membrane. It is worth mentioned that in contrast to many soft LbL polyelectrolyte capsules, those internalized PAH/PSS/CDs capsules remained their spherical morphology, showing only slight deformation in CLSM with higher magnification (**Figure 6.28 B**). This is probably arising from their thicker and denser shells (~180 nm), leading to an increased mechanical strength. Similarly, as indicated in **Figure 6.28 C and D**, PARG/DEXS/CDs capsules were also uptake by B50 cells after 3 h of incubation, and they still kept their intact structure.

6.8.3 Biodegradability of the Composite Capsules

It was known that PAH/PSS capsules are not degradable in cells. Here, we checked whether there was some change about the degradability of PAH/PSS capsules after modified with fluorescent CDs. CLSM images of PAH/PSS/CDs incubation with B50 cells for different times were obtained for analysis of their degradable behaviours. **Figure 6.29** indicated that similar with pure PAH/PSS capsules, these composite capsules were not degradable in B50 cells. No obvious change in morphology and structure of the PAH/PSS/CDs capsules when prolonging the incubation time was observed from the CLSM results. Even after 72 h of incubation, these capsules were still stable, maintaining their fluorescent property and intact shapes.

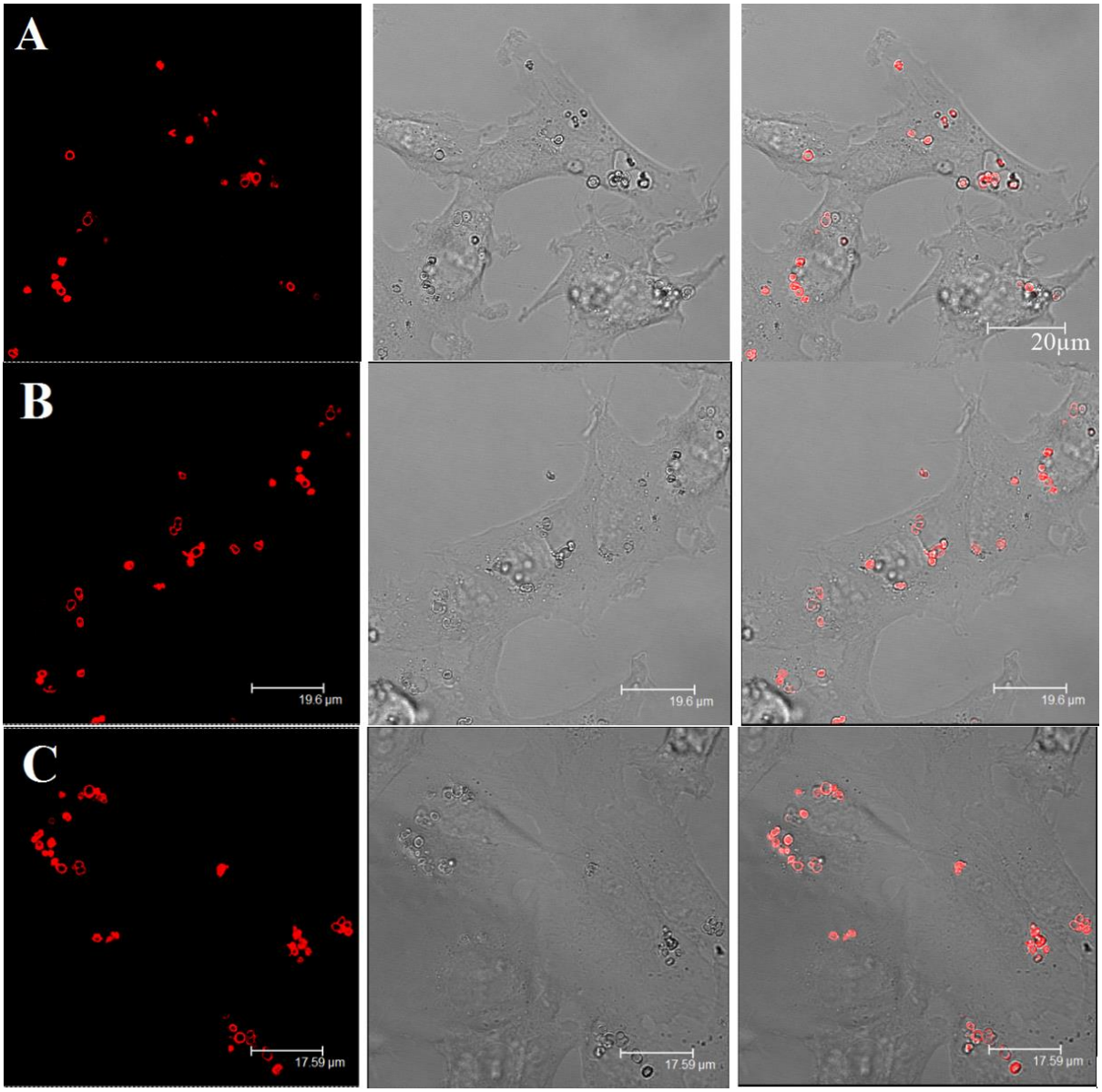

Figure 6.29 CLSM images of PAH/PSS/CDs capsules incubated with B50 Cells for (A) 6 h, (B) 34 h and (C) 72 h.

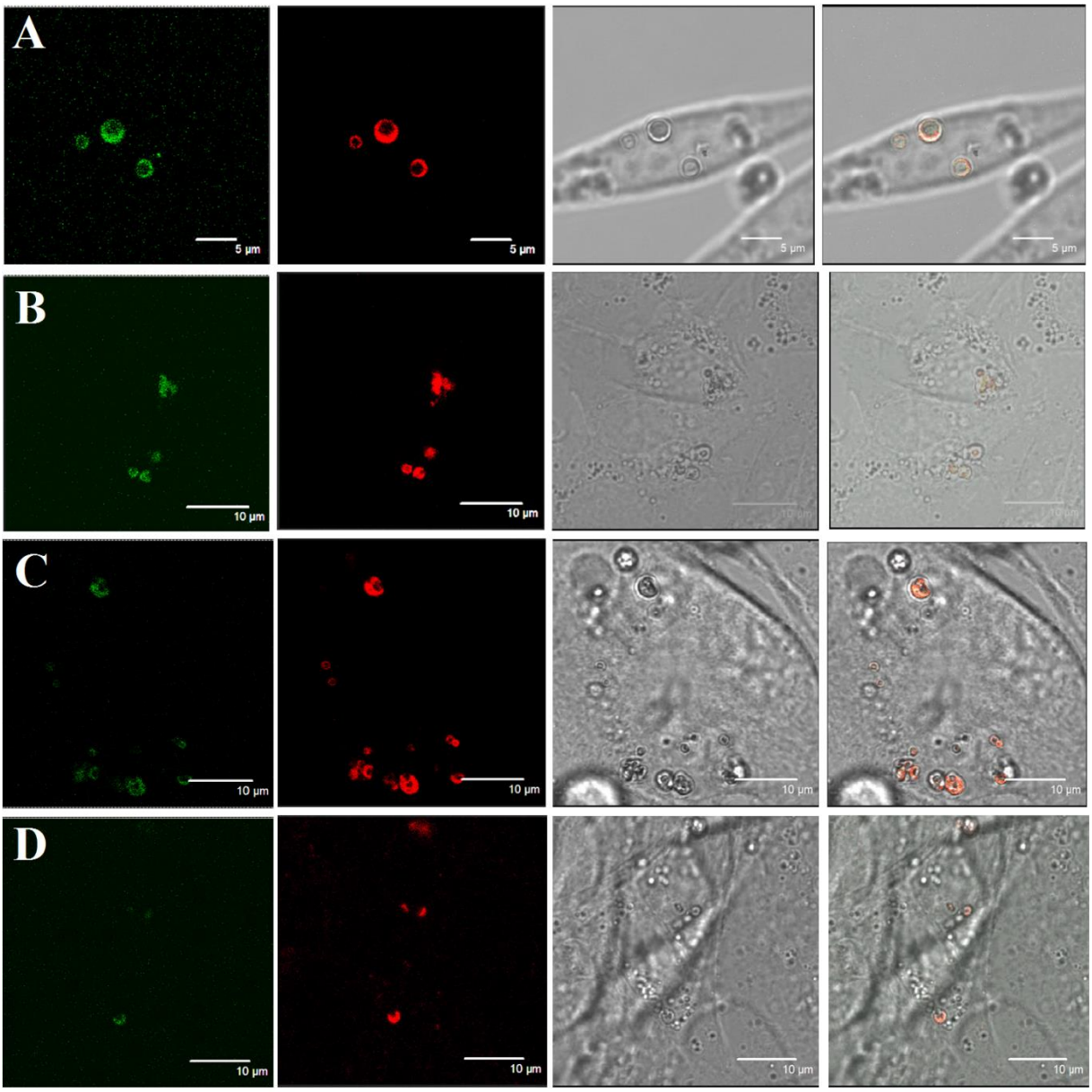

Figure 6.30 CLSM images of PARG/DEXS/CDs capsules incubated with B50 Cells for (A) 3 h, (B) 23 h, (C) 52 h and (D) 73 h.

In terms of PARG/DEXS capsule system, PARG is famous for its biocompatible and biodegradable features. Hence, the composite capsules composed of PARG and fluorescent CDs should still be degradable in cells. To make it clear, PARG/DEXS/CDs capsules were incubated with B 50 cells and visualized by CLSM at different time points, as shown in **Figure 6.30**. In the first 3 h, PARG/DEXS/CDs capsules in B50 cells presented intact spherical

structure, indicating that they were not degraded. When time reached to 23 h, some capsules with blurry spherical shapes were found and importantly some pieces appeared, as indicated by the arrow in **Figure 6.30 B**. After 52 h of incubation, it was clearly to seen more pieces in the CLSM images (**Figure 6.30 C**) and nearly no intact and complete composite capsules can be found. When increased the incubation time to 73 h, **Figure 6.30 D** indicated that all capsules were broken into pieces due to the degradation effect of the B50 cells. Therefore, we can conclude that the PARG/DEXS/CDs composite capsules were degradable in B50 cells. If they were loaded cargos, they could be simultaneously released outside into cells due to the degradation of the composite shells. But notably it took longer time than that of pure PARG/DEXS microcapsule.[128] This might because that the HTR treatment affected the structure and properties of PARG, and that the incorporation of CDs by carbonisation of DEXS and dextran increased the shell thickness, density and mechanics.

6.9 Conclusion

In summary, the fluorescent CDs and polyelectrolyte/CDs composite capsules were fabricated and studied in this chapter. A one-step hydrothermal strategy was employed for the synthesis and assembly of luminescent CDs in polyelectrolyte multilayers. To the best of our knowledge, this work is the first example on the polysaccharide-based synthesis of CDs and embedding them in polyelectrolyte shells. Similar with pure CDs, the fluorescent feature of the composite capsules were verified by the fluorescent spectra and CLSM data. Their stability in fluorescence and morphology was also proved in this chapter. PAH/PSS/CDs were proved to be able to encapsulate small molecules (Rh-B) and be broken by ultrasound treatment within a few minutes. Hence, ultrasound were used as a stimuli to trigger the capsules and their release behaviours were monitored. The long-time release profile proved that the PAH/PSS/CDs capsules sealed Rh-B effectively, showing that only 15% of Rh-B was released outside after 3

days. Besides ultrasound treatment, NIR laser could also be employed as one potential tool to selectively open the CDs functionalized capsules. As proved by the MTT assays, the as-prepared pure CDs, PAH/PSS/CDs and PARG/DEXS/CDs capsules exhibited excellent cyto-compatibility. CLSM data demonstrated that the PAH/PSS/CDs capsules were not degradable in B50 cells while the PARG/DEXS/CDs capsules can be degraded efficiently. Compared with conventional dye-based capsules, the CDs-based capsules provide an attractive alternative drug carriers for long-term tracking and drug delivery. In fact, this technique could be potentially extended to synthesize libraries of various types of NPs to functionalize polymeric capsules and membranes.

7. Conclusions and Future works

7.1 General Conclusions

By using the template-assisted LbL technique, various kinds of polyelectrolyte-based microcapsules have been synthesized and investigated in past few decades.[12] There is a vast number of LbL polymeric capsules with various sizes, densities, stimuli-responsiveness *etc.*, which provided their potential application in drug delivery system. In order to reduce the side effects, realize targeted delivery or release substance controllably, the polymeric capsules are usually be tailored and modified by functional inorganic NPs, forming organic/inorganic composite capsules with more new high functions. LbL assembly of pre-fabricated NPs into polyelectrolyte multilayers is a more developed method to incorporate NPs but shows a few limitations, including insufficient encapsulation of small molecules, poor chemical stability, poor distribution of NPs, *etc.*. *In situ* synthesis and assembly is an alternative method, showing promising potential in reducing permeability, increasing mechanic strength and more available stimuli-responsiveness. This work was intended to make a step further on the way to using *in situ* formed inorganic NPs to modify LbL polyelectrolyte microcapsules, and investigate the new functions of the formed polyelectrolyte/inorganic NPs composite capsules. Three different types of inorganic NPs, *i.e.*, silica, TiO_2 and CDs, were *in situ* formed and incorporated into polyelectrolyte microcapsule systems.

Polyelectrolyte microcapsule with different components were all fabricated *via* LbL method and then functionalized by NPs, *i.e. in situ* formed silica from hydrolysis of TEOS, TiO_2 from hydrolysis form TIBO and CDs from the hydrothermal carbonisation of dextran. The changes of morphology, structure, shell stability and permeability before and after incorporation with the NPs were characterized and studied. Their potential applications for encapsulation of small

molecules and triggered release by ultrasound treatment or UV irradiation were also investigated. Cell viability and/or degradation behaviour of the three types of composite capsules were observed by employing B50 cell lines.

In general, the sol-gel synthesis of silica spheres is based on Stöber process: silane precursor is added to the water/ethanol mixture containing ammonia hydroxide as a catalyst.[31] Mesoporous silica nano/micro-particles were intensively studied in the past years by employing hard or soft templates. But introduce silica NPs into polyelectrolyte capsule systems was rarely reported. In Chapter 4, the synthesis and deposition of silica NPs into polyelectrolyte microcapsules were carried out by sol-gel method, employing TEOS as silane precursor. The reaction conditions need to be well controlled and investigated. Experiment results demonstrated that temperature, reaction time, amount of TEOS and ammonia hydroxide showed significant influence on the final morphology and properties of the formed polyelectrolyte/silica composite capsules. The composite capsules formed under the most suitable conditions showed a completely and uniformly covered silica and low permeability. The successful encapsulation of Rh-B proved the proposed idea: *in situ* formed inorganic NPs can effectively reduce the pore size, densify the shell and thusly reduce the shell permeability. $CaCO_3$ templates wrapped by composite PAH/PSS/silica layers were more stable under acid treatment, showing that half of them was not dissolved, which further confirmed the low porosity of composite shells. Ultrasonic irradiation, as a very promising candidate for release cargos from capsules, was employed to treat the silica functionalized capsules. All the composite capsules were found to be broken into pieces in only a few seconds of ultrasonication. Another interesting phenomenon found in this study is that biodegradable PARG/DEXS capsules with silica coating can also be easily degraded gradually in B50 cells and allow the cargo release, but same experiments carried out for PAH/PSS/silica capsules indicated only

small defects formed due to the degradation of silica fractions. Hence, a possible degradation mechanism was proposed as the combined effects of both hydrolytic degradation of amorphous silica and enzymatic degradation of PARG/DSS polymers. Results achieved in this study are very interesting and promising for medical applications, if compared the short-time breakage performance to the reported earlier use of high-power ultrasound for a few minutes to break capsules,[16,24] and if compared the superior ability to seal small molecules inside the cavities to the previous reported polyelectrolyte/inorganic NPs capsules.[231]

Compared with functionalize capsules with TiO_2, films with TiO_2 incorporation were investigated more in the past few decades. Limited by the quite high hydrolysis rate of titania precursor, TiO_2 were usually prefabricated as sols or colloids and then introduced into polymeric films.[28,288] Until now, only a few reports are related to TiO_2-polymer capsules and are mainly based on pre-fabricated TiO_2 NPs. In Chapter 5, bifunctional polylectrolyte/TiO_2 composite capsules were prepared *via in situ* hydrolysis of TIBO within and on the surfaces of the polyelectrolyte shells. The amount of H_2O in the reaction system must be well controlled to avoid the formation of excess TiO_2. Needle-like TiO_2 NPs were synthesised and assembled into prefabricated PAH/PSS microcapsules, which made the obtained microcapsules become of enhanced mechanical strength, UV and ultrasound responsiveness as well as good biocompatibility. Similar with silica coated capsule systems, the incorporated TiO_2 also performed as an ultrasound sensitivity enhancer to make the composite capsule responsive to ultrasound treatment. In addition, the exposure of the formed TiO_2/polyelectrolyte capsules to either UV or ultrasound triggering showed an irreversible shell rapture and efficient cargo release. Until now, no successful and promising method of one-step incorporation of TiO_2 into polyelectrolyte capsules were reported, however, there are publications where silica and TiO_2

NPs were synthesized together at O/W interfaces as shell fractions to perform as UV protective coating.[301]

Polyelectrolyte microcapsules possess large cavity volume that is beneficial for drug delivery but besides their intrinsic high permeability, the poor optical traceability is also a limitation for their application. Poor traceability is usually addressed by incorporating fluorophores. As discussed, compared with fluorescent dyes and semiconducting QDs, CDs are more promising but until now only one publication is related to incorporation of pre-fabricated CDs into polyelectrolyte microcapsules. In fact, no publication of introduce CDs using *in situ* synthesis and assembly method. In Chapter 6, fluorescent CDs were first introduced to PAH/PSS and PARG/DEXS multilayers by one-step hydrothermal reaction method. The formed PAH/PSS/CDs and PARG/DEXS/CDs composites were demonstrated with strong fluorescence, good chemical stability, and excellent photo-stability. Compared with the ever reported collapsed polyelectrolyte/CDs capsules with weak fluorescent signal in 2007,[213] our polyelectrolyte/CDs capsules showed free-standing mechanics, and their the morphology and hollow structure were clearly proved by the CLSM and TEM images. Moreover, the possibility of *in situ* encapsulation of small molecules, Rh-B, and effectively release of them was all demonstrated. We also found that the incorporated CDs promoted the absorption of Vis-NIR light in PAH/PSS/CDs capsules. If exposed one capsule with NIR laser irradiation for more than 30s, a single hole on the shell was obtained, demonstrating the laser-induced selective break performance. These results introduce new promising type of fluorescent composite capsules with low permeability and sensitivity to ultrasound and NIR laser. The method of introduce fluorescent CDs provide the evidence of conversion dextran into CDs within the polyelectrolyte multilayers. In fact, various kinds of carbon source that have reported previously for producing CDs can be used, for example, glucose, chitin, chitosan, *etc*..

Apart from the fabrication process of polyelectrolyte capsules, promisingly, these techniques developed in this thesis for *in situ* incorporation of three types of NPs could be potentially extended to synthesize libraries of various types of NPs to functionalize polymeric capsules, polymeric membranes, and even microparticles or inorganic hollow particles. For polymer capsule systems, the employed inorganic NPs could offer a series of attractive functionalities, especially the strengthened ultrasound sensitivity. NPs with other intrinsic features are also expected to enable more functions to their incorporated capsules. In this thesis, we proved that TiO_2 NPs can empower the formed composite capsules with UV responsiveness, and CDs can endow their fluorescent property to the polyelectrolyte/CDs capsules. In my opinion, it is *in situ* encapsulation of small molecules assisted by the shell densification *via* silica and CDs incorporation, break the composite shells by ultrasonic irradiation or photodynamic techniques as well as the fluorescence introduced by CDs that are most useful for drug delivery system. The predicted applications of the composite polyelectrolyte/NPs capsules could potentially be found usage in various fields, including environmental science, agricultural, cosmetic and biomedical areas. This thesis was intended to make a step further on the way to make contributions to existing knowledge of inorganic NPs functionalized microcapsules. Major findings of this thesis are provided as below:

(1) Silica NPs were facially deposited within/on polyelectrolyte multilayers, showing reduced size, increased shell thickness, decreased permeability and enhanced ultrasound sensitivity. Biodegradable PARG/DEXS capsules coated with silica were still able to be degraded by B50 cells, while non-degradable PAH/PSS capsules coated with silica can't be completely degraded but the encapsulated small molecules, Rh-B, were able to diffuse outside from the defect points due to the partly degradation of silica NPs. The composite polyelectrolyte/silica shells can also be used to protect $CaCO_3$ cores.

(2) PAH/PSS/TiO_2 capsules were instantly destroyed by ultrasound treatment (20 KHz, 50W) and gradually ruptured by ~366 nm UV light.

(3) PAH/PSS/CDs composite capsules were fluorescent with excellent chemi-/photo- stability. Rh-B were *in situ* entrapped in their cavities and efficiently released outside with the ultrasound treatment for a few minutes. NIR laser was one potential trigger to selectively break the PAH/PSS/CDs capsules.

7.2 Future Work

This thesis has initiated different types of functional polyelectrolyte/inorganic NPs composite capsule systems and these composite capsules have already been demonstrated with promising properties such as low permeability, ultrasound, UV and NIR laser sensitivity, and strong fluorescence. However, there are still some challenges left that need to be overcame for further improvement. In addition, hurdles still remain in applying these experimental works into practical applications.

(1) Chemical stability of the composite capsules. $(PAH/PSS)_4$ capsules lose their pH-responsiveness after modified with all the three types of *in situ* formed NPs. This means that the formed composite capsules demonstrate excellent chemical stability, *i.e.*, they could sustain harsh acidic or alkaline environment. In order to better understand the interaction between the *in situ* formed inorganic NPs and the soft polyelectrolytes, the mechanism of this interesting behaviour should be carefully investigated.

(2) Permeability change of PDADMAC/PAZO/silica composite capsules upon UV irradiation. The permeability change of $(PDADMAC/PAZO)_4$ capsules after silica coating need to be

examined. Previous publications revealed that pure $(PDADMAC/PAZO)_4$ capsules can be ruptured by UV irradiation. The UV effects on $(PDADMAC/PAZO)_4$/silica composite capsules should be explored, since UV irradiation might change the permeability of the composite capsule but the incorporated silica might protect them without rupture.

(3) MHz ultrasound triggered release from the composite capsules. The composite capsules are all proved to be able to open by ultrasound treatment, however, the ultrasound employed in this thesis is quite strong. The effects of mild MHz ultrasound on these composite capsules should also be investigated in the future.

(4) Effects and mechanism of NIR laser irradiation on PAH/PSS/CDs composite multilayers. PAH/PSS/CDs composite multilayers are demonstrated with a potential to be selectively break by NIR laser irradiation. But this phenomenon need to be further confirmed by additional experiments, and the mechanism of such phenomenon has to be explored.

(5) Fluorescent microspheres. $(PAH/DEXS)_4$ capsules were changed into fluorescent microspheres after heating in DI-water, as demonstrated in Chapter 6. Such microspheres can be used for various areas, such as blood flow determination (flow tracing, flow visualization, and fluid mechanics studies, *etc.*), biological imaging and monitoring, and testing filtration media and systems. The size of the formed microspheres should depend on the initial size of the employed capsules. Experiments should carried out to find this relationship, into order to synthesis of fluorescent spheres with different sizes.

Obviously, if these issues could be fully studied in the future, it should be one great step for the development and improvement of functional polymeric/inorganic composite materials that

can be used for as biomedicine, environment, cosmetics and food industry. The results that already obtained in this thesis reveal that the *in situ* synthesis of inorganic NPs into polymeric matrix is a promising approach to fabricate inorganic/organic composite materials. Polymeric capsules were used as model examples, such method could be extended to other material systems to realize multi-functionalization, for instance, inorganic or organic particles, films, *etc.*. Various polymers and inorganic NPs with different specific functions are able to be designed integrated in one entity, possessing promising multi-functions.

8. Bibliography

1. X. Huang, M. A. El-Sayed. *J. Adv. Res.,* **2010,** *1*, 13-28.
2. T. Wada, K. Inui, T. Uragami. *J. Appl. Polym. Sci.,* **2006,** *101,* 2051-2056.
3. A. M. Pavlov, S. A. Gabriel, G. B. Sukhorukov, D. J. Gould. *Nanoscale,* **2015,** *7,* 9686-9693.
4. J. J. Richardson, M. Björnmalm, F. Caruso. *Sci.,* **2015**, *348,* 411-422.
5. R. K. Iler. Multilayers of colloidal particles. *J. Colloid Interface Sci.,* **1966,** *21*, 569-594.
6. G. Decher, J. D. Hong, J. Schmitt. *Thin Solid Films,* **1992,** *210-211,* 831-835; G. Decher. *Sci.,* **1997,** *277,* 1232-1237.
7. G. B. Sukhorukov, E. Donath, S. Davis, H. Lichtenfeld, F. Caruso, V. I. Popov, H. Möhwald. *Polym. Adv. Technol.,* **1998,** *9,* 759-767; E. Donath, G. B. Sukhorukov, F. Caruso, S. A. Davis, H. Möhwald. *Angew. Chem. Int. Ed.,* **1998,** *37,* 2201-2205.
8. D. G. Shchukin, G. B. Sukhorukov, H. Möhwald. *Angew. Chem. Int. Ed.,* **2003,** *42,* 4472-4475.
9. K. Kohler, G. B. Sukhorukov. *Adv. Funct. Mater.,* **2007,** *17,* 2053-2061.
10. T. Mauser, C. Déjugnat, G. B. Sukhorukov. *J. Phys. Chem. B,* **2006,** *110,* 20246-20253.
11. V. V. Lulevich, O. I. Vinogradova. *Langmuir,* **2004,** *20*, 2874-2878.
12. H. Saito, N. Kato. *Jap. J. Appl. Phys.,* **2016,** *55,* 03DF06 (1-4).
13. A. M. Pavlov, B. G. D. Geest, B. Louage, L. Lybaert, S. De Koker, Z. Koudelka, A. Sapelkin, G. B. Sukhorukov. *Adv. Mater.,* **2013,** *25*, 6945-6950.
14. T. A. Kolesnikova, D. A. Gorin, P. Fernandes, S. Kessel, G. B. Khomutov, A. Fery, D. G. Shchukin, H. Möhwald. *Adv. Funct. Mater.,* **2010,** *20,* 1189-1195.

15. O. Kreft, M. Prevot, H. Mohwald, G. B. Sukhorukov. *Angew. Chem. Int. Ed.,* **2007,** *46,* 5605-5608.

16. H. Gao, D. Wen, G. B. Sukhorukov. *J. Mater. Chem. B,* **2015,** *3,* 1888-1897.

17. K. Katagiri, M. Nakamura, K. Koumoto. *ACS Appl. Mater. Interfaces,* **2010,** *2,* 768-773.

18. Alexandra S. Angelatos, B. Radt, Frank Caruso *J. Phys. Chem. B,* **2005,** *109,* 3071-3076.

19. D. G. shchukin, I. L. Radtchenko, G. B. Sukhorukov. *J. Phys. Chem. B,* **2003**, *107,* 952-957.

20. T. A. Kolesnikova, G. G. Akchurin, S. A. Ortnov, G. B. Khomutov, G. G. Akchurin, O. G. Naumova, G. B. Sukhorukov, D. A. Gorin. *Laser Phys. Lett.,* **2012,** *9,* 643-648.

21. A. G. Skirtach, A. M. Javier, O. Kreft, K. Kohler, A. P. Alberola, H. Mohwald, W. J. Parak, G. B. Sukhorukov. *Angew. Chem. Int. Ed.,* **2006,** *45,* 4612-7.

22. A. Marzo, S. A. Seah, B. W. Drinkwater, D. R. Sahoo, B. Long, S. Subramanian. *Nat. Commun.,* **2015,** *6,* 1-7.

23. D. G. Shchukin, D. A. Gorin, H. Möhwald. *Langmuir,* **2006,** *22,* 7400-7404.

24. A. G. Skirtach, B. G. D. Geest, A. Mamedov, A. A. Antipov, N. A. Kotov, G. B. Sukhorukov. *J. Mater. Chem.,* **2007,** *17,* 1050-1054.

25. S. H. Wu, Y. Hung, C. Y. Mou. *Chem. Commun.,* **2011,** *47,* 9972-85.

26. Y. Hu , J. Ge, Y. Sun , T. Zhang , Y. Yin. *Nano Lett.,* **2007,** *7,* 1832-1836.

27. K. Jiang, S. Sun, L. Zhang, Y. Lu, A. Wu, C. Cai, H. Lin. *Angew. Chem. Int. Ed.,* **2015,** *54,* 5360-5363.

28. S. Akhavan, A. Yeltik, H. V. Demir. *ACS Appl. Mater. Interfaces,* **2014,** *6,* 9023-9028.

29. S. C. Zhang, C. Z. Yin, C. Zhang, G. Lin, Q. Li. *J. Am. Chem. Soc.,* **2013,** *135,* 5709-5716.

30. D. Cassano, D. R. Martir, G. Signore, V. Piazza, V. Voliani. *Chem. Commun.,* **2015,** *51*, 9939-9941.

31. Z. Bao, M. R Weatherspoon, S. Shian, Y. Cai, P. D. Graham, S. M. Allan, G. Ahmad, M. B. Dickerson, B. C. Church, Z. Kang, H. W. Abernathy Iii, C. J. Summers, M. Liu, K. H. Sandhage. *Nat.,* **2007,** *446*, 172-175.

32. J. Wei, X. J. Ju, X. Y. Zou, R. Xie, W. Wang, Y. M. Liu, L. Y. Chu. *Adv. Func. Mater.,* **2014,** *24*, 3312-3323.

33. Y. C. Yeh, R. Tang, R. Mout, Y. Jeong, V. M. Rotello. *Angew. Chem. Int. Ed.,* **2014,** *53*, 5137-5141.

34. W. J. Tseng, C.-C. Cheng, J. H. Hsieh, J. Ballato. *J. Am. Ceram. Soc.,* **2014,** *97*, 407-412.

35. J. Briscoe, A. Marinovic, M. Sevilla, S. Dunn, M. Titirici. *Angew. Chem. Int. Ed.,* **2015,** *54*, 4463-4468.

36. D. Usov, G. B. Sukhorukov. *Langmuir,* **2010,** *26*, 12575-12584.

37. A. Dobrynin, M. Rubinstein. *Prog.Polym. Sci.,* **2005,** *30*, 1049-1118.

38. D. Zhou, H. Xiao, F. Meng, S. Zhou, J. Guo, X. Li, X. Jing, Y. Huang. *Bioconjugate Chem.,* **2012,** *23*, 2335-2343.

39. A. P. Johnston, L. Lee, Y. Wang, F. Caruso. *Small,* **2009,** *5*, 1418-1421.

40. J. M. Y. Carrillo, A. V. Dobrynin. *Macromolecules,* **2011,** *44*, 5798-5816.

41. B. G. D. Geest, S. D. Koker, G. B. Sukhorukov, O. Kreft, W. J. Parak, A. G. Skirtach, J. Demeester, S. C. D. Smedt, W. E. Hennink. *Soft Matter,* **2009,** *5*, 282-291.

42. Nithya Joseph, P. Ahmadiannamini, Richard Hoogenboom, Ivo. F. J. Vankelecom. *Polym. Chem.,* **2014,** *5*, 1817-1831.

43. L. Seon, P. Lavalle, P. Schaaf, F. Boulmedais. *Langmuir,* **2015,** *31*, 12856-12872.

44. A. M. Pavlov. Multilayer Microcapsules for Delivery, Control and Triggered Release of Bioactive Compounds. *PhD Thesis,* **2012,** 19-99.

45. J. Skolnich, M. Fixman. *Macromolecules,* **1977,** *10*, 944-948.

46. J. L. Barrat, J. F. Joanny. *Europhys. Lett.* **1993,** *24*, 333-338.

47. Y. Luo, Q. Wang. *Inter. J. Biological Macromolecules,* **2014,** *64*, 353-367.

48. Y. Jia, J. Fei, Y. Cui, Y. Yang, L. Gao, J. Li. *Chem. Commun.,* **2011,** *47*, 1175-1177.

49. W. Tong, C. Gao. *J. Mater. Chem.,* **2008,** *18*, 3799-3812.

50. Alexander N. Zelikin, J. F. Quinn, and Frank Caruso. *Biomacromolecules,* **2006,** *7*, 27-30.

51. Seong Jin Park, K. Yamaguchi, and Jong-In Hong, *Bull. Korean Chem. Soc.,* **2008,** *29*, 205-207.

52. S. K. Gubbala. *Int. J. Pharm. Bio. Sci.,* **2012,** *2*, 399-407.

53. J. Borges, J. F. Mano. *Chem. Rev.,* **2014,** *114*, 8883-8942.

54. M. Nishio. *Physi. Chem. Chem. Phys.,* **2011,** *13*, 13873-13900.

55. E. Kharlampieva, V. Kozlovskaya, S. A. Sukhishvili. *Adv. Mater.,* **2009,** *21*, 3053-3065.

56. C. S. Picone, R. L. Cunha. *Carbohydrate Polym.,* **2013,** *94*, 695-703.

57. C. Li, S. Hein, K. Wang. *ISRN Biomaterials,* **2013,** *2013*, 1-6.

58. F. N. Crespilho, V. Zucolotto, O. N. Oliveira, F. C. *Nart. Int. J. Electrochem. Sci.,* **2006,** *1*, 194-214.

59. A. S. Sergeeva, E. K. Volkova, D. N. Bratashov, M. I. Shishkin, V. S. Atkin, A. V. Markin, A. A. Skaptsov, D. V. Volodkin, D. A. Gorin. *Thin Solid Films,* **2015,** *583*, 60-69.

60. P. K. Deshmukh, K. P. Ramani, S. S. Singh, A. R. Tekade, V. K. Chatap, G. B. Patil, S. B. Bari. *J. Control. Release,* **2013,** *166*, 294-306.

61. W. Cui, J. Li, G. Decher, *Adv. Mater.*, **2016**, *28*, 1302-1311

62. M. M. D. Villiers, D. P. Otto, S. J. Strydom, Y. M. Lvov. *Adv. Drug Deliv. Rev.,* **2011,** *63*, 701-715.

63. K. Ariga, Q. Ji, J. P. Hill, Y. Bando, M. Aono. *NPG Asia Mater.,* **2012,** *4*, 1-11.

64. I. F. Patel, M. V. Kiryukhin, N. L. Yakovlev, H. S. Gupta, G. B. Sukhorukov. *J. Mater. Chem. B,* **2015,** *3*, 4821-4830.

65. R, V. Klitzing. *Physi. Chem. Chem. Phys.,* **2006,** *8*, 5012-5033.

66. B. Schoeler, G. Kumaraswamy, F. Caruso. *Macromolecules,* **2002,** *3*, 889-897.

67. B. Schoeler , S. Sharpe, T. A. Hatton, F. Caruso. *Langmuir,* **2004,** *20*, 2730-2738.

68. B. S. Kim, S. W. Park, P. T. Hammond. *ACS Nano,* **2008,** *2*, 386-392.

69. F. Huo, H. Xu, L. Zhang, Y. Fu, Z. Wang, X. Zhang. *Chem. Commun.,* **2003,** 7, 874-875.

70. F. X. Xiao, M. Pagliaro, Y. J. Xu, B. Liu. *Chem. Soc. Rev.,* **2016,** *45*, 3088-3121.

71. N. A. Kotov. *Nanostruct. Mater.,* **1999,** *12*, 789-796.

72. J. Zhao, F. Pan, P. Li, C. Zhao, Z. Jiang, P. Zhang, X. Cao, *ACS Appl. Mater. Interfaces,* **2013,** *5*, 13275-13283.

73. Y. Shimazaki , M. Mitsuishi, S. Ito, M. Yamamoto. *Langmuir,* **1997,** *13*, 1385-1387.

74. P. A. Chiarelli, M. S. Johal, J. L. Casson, J. B. Roberts, J. M. Robinson, H. L. Wang. *Adv. Mater.,* **2001,** *13*, 1167-1171.

75. G. K. Such , J. F. Quinn, A. Quinn , E.Tjipto, F. Caruso. *J. Am. Chem. Soc.,* **2006,** *128,* 9318-9319.

76. G. K. Such, E. Tjipto, A. Postma, A. P. R. Johnston, F. Caruso. *Nano Lett.,* **2007,** *7*, 1706-1710.

77. P. Bieker, M. Schönhoff. *Macromolecules,* **2010,** *43*, 5052-5059.

78. D. Yoo, S. S. Shiratori, M. F. Rubner. *Macromolecules,* **1998,** *31*, 4309-4318.

79. S. S. Shiratori, M. F. Rubner. *Macromolecules*, **2000,** *33*, 4213-4219.

80. K. Itano, J. Choi, M. F. Rubner. *Macromolecules,* **2005,** *38*, 3450-3460.

81. K, Büscher, K. Graf, H. Ahrens, C. A. Helm. *Langmuir,* **2002,** *18*, 3585-3591.

82. C. Porcel, P. L., V. Ball, G. Decher, B.Senger, J. C. Voegel, P. Schaaf. *Langmuir,* **2006,** *22*, 4376-4383.

83. H. L. Tan, M. J. Mcmurdo, G. Pan, P. G. V. Patten. *Langmuir,* **2003,** *19*, 9311-9314.

84. C. R. Correia, R. L. Reis, J. F. Mano. *Biomacromolecules,* **2013,** *14*, 743-751.

85. Stephan T. Dubas , J. B. Schlenoff. *Langmuir*, **2001,** *17*, 7725-7727.

86. Stephan T. Dubas, J. B. Schlenoff. *Macromolecules,* **2001,** *34*, 3736-3740.

87. Z. Feldoto, I. Varga, E. Blomberg. *Langmuir,* **2010,** *26*, 17048-17057.

88. J. Heuvingh, M. Zappa, A. Fery. *Langmuir,* **2005,** *21*, 3165-3171.

89. E. Poptoshev, B. Schoeler, and F. Caruso, *Langmuir,* **2004,** *20*, 829-834.

90. S. D. Koker, B. G. D. Geest, S. K. Singh, R. D. Rycke, T. Naessens, Y. V. Kooyk, J. Demeester, S. C. D. Smedt, J. Grooten. *Angew. Chem. Int. Ed.,* **2009,** *48*, 8485-8489.

91. M. Matsusaki, H. Ajiro, T. Kida, T. Serizawa, M. Akashi. *Adv. Mater.,* **2012,** *24*, 454-74.

92. A. A. Antipov, G. B. Sukhorukov. *Adv. Colloid Interface Sci.,* **2004,** *111*, 49-61.

93. P. R. Gil, L. L. Mercato, P. P. Pino, A. Muñoz Javier, W. J. Parak. *Nano Today,* **2008,** *3*, 12-21.

94. C. S. Peyratout, L. Dahne. *Angew. Chem. Int. Ed.,* **2004,** *43*, 3762-3783.

95. M. T. Garcia, I. Gracia, G. Duque, A. Lucas, J. F. Rodriguez. *Waste Manag.,* **2009,** *29*, 1814-1818.

96. H. A. Gad, M. A El-Nabarawi, S. S. Abd El-Hady. *AAPS Pharm. Sci. Tech.,* **2008,** *9*, 878-884.

97. C. Gao, S. Moya, H.Lichtenfeld, A. Casoli, H. Fiedler, E. donath, H. Möhwald. *Macromol. Mater. Eng.,* **2001,** *286,* 355-361.

98. C. Gao, E. Donath, H. Möhwald, J. Shen. *Angew. Chem. Int. Ed.,* **2002,** *41,* 3789-3793.

99. C. Gao,S. Moya, E. Donath, H. Möhwald. *Macromol. Chem. Phys.,* **2002**, *203,* 953-960.

100. C. Gao, S. Leporatti, S. Moya, E.Donath, H. Möhwald. *Langmuir,* **2001,** *17,* 3491-3495.

101. G. B. Sukhorukov, A. A. Antipov, A. Voigt, E. Donath, H. Möhwald. *Macromol. Rapid Commun.,* **2001,** *22,* 44-46.

102. O. Shchepelina, M. O. Lisunova, I. Drachuk, V. V. Tsukruk. *Chem. Mater.,* **2012,** *24,* 1245-1254.

103. D. Volodkin. *Adv. Colloid Iinterface Sci.,* **2014,** *207,* 306-324.

104. Q. Yi, G. B. Sukhorukov. *Soft Matter,* **2014,** *10,* 1384-1391.

105. Q. Wei, H. Ai, Z. Gu. *Colloids Surf. B Biointerfaces,* **2011,** *85,* 63-72.

106. A. Yu, Y. Wang, E. Barlow, F. Caruso. *Adv. Mater.,* **2005,** *17,* 1737-1741.

107. Q. Yi, G. B. Sukhorukov. *Part. Part. Syst. Charact.,* **2013,** *30,* 989-995.

108. A. Ott. Y. Xiang, R. Hartmann, R. Joanna, A. Schütz, M. Ochs, W. J. Parak. *Chem. Mater.* **2015,** *27,* 1929-1942.

109. O. S. Sakr, G. Borchard. *Biomacromolecules,* **2013,** *14,* 2117-2135.

110. S. Demir, S. B. Gök, M. V. Kahraman. *Starch/Stärke,* **2012,** *64,* 3-9.

111. M. Kakran, M. Muratani, W. J. Tng, H. Liang, D. B. Trushina, G. B. Sukhorukov, H. H. Ng, M. N. Antipina. *J. Mater. Chem. B,* **2015,** *3,* 5842-5848.

112. H. Zhou, J. Wei, Q. Dai, L. Wang, J. Luo, T. Cheang, S. Wang. *Int. J. Nanomedicine,* **2015,** *10,* 4255-4266.

113. B. Neu, A. Voigt, R. Mitlohner, S. Leporatti, C. Y. Gao, E. Donath, H. Kiesewetter, H. Mohwald, H. J. Meiselman, H. Baumler. *J. Microencapsulation,* **2001,** *18,* 385-95.

114. R. Georgieva, S. Moya, M. Hin, R. Mitlöhner, E. Donath, H. Kiesewetter, H. Möhwald, H. Bäumler. *Biomacromolecules,* **2002,** *3,* 517-524.

115. H. Daiguji, S. Takada, J. J. M. Cornejo, F. Takemura. *J. Phys. Chem. B,* **2009,** *113*, 15002-15009.

116. L. Chen, H. Z. An, P. S. Doyle. *Langmuir,* **2015,** *31*, 9228-35.

117. T. Hikima, Y. Nonomura. *J. Oleo Sci.*, **2011,** *60*, 351-354.

118. S. M. Marinakos, J. P. Novak, L. C. Brousseau, A. B. House, E.M. Edeki, J. C. Feldhaus, D. L. Feldheim. *J. Am. Chem. Soc.,* **1999,** *121*, 8518-8522.

119. C. Zhu, S. Guo, Y. Zhai, S. Dong. *Langmuir,* **2010,** *26*, 7614-7618.

120. S. Zuin, P. Scanferla, A. Brunelli, A. Marcomini, J. E. Wong, W. Wennekes, I. Genné. *Ind. Eng. Chem. Res.,* **2013,** *52*, 13979-13990.

121. L. Li, S. Puhl, L. Meinel, O. Germershaus. *Biomaterials,* **2014,** *35*, 7929-7939.

122. O. Shchepelina, I. Drachuk, M. K. Gupta, J. Lin, V. V. Tsukruk. *Adv. Mater.,* **2011,** *23*, 4655-4660.

123. H. Gao, D. Wen, N. V. Tarakina, J. Liang, A. Bushby, G. B. Sukhorukov. *Nanoscale,* **2016**, *8*, 5170-5180.

124. R. Luo, S. S. Venkatraman, B. Neu. *Biomacromolecules,* **2013,** *14*, 2262-2271.

125. S. Leporatti, C. Gao, A. Voigt, E. Donath, H. Möhwald. *Eur. Phys. J. E,* **2001,** *5*, 13-20.

126. C. Gao, E. Donath, S. Moya, V. Dudnik, H. Möhwald. *Eur. Phys. J. E,* **2001,** *5*, 21-27.

127. K. Yoshida, T. Ono, Y. Kashiwagi, S. Takahashi, K. Sato, J. Anzai. *Polymers*, **2015,** *7*, 1269-1278.

128. B. G. Geest, R. E. Vandenbroucke, A. M. Guenther, G. B. Sukhorukov, W. E. Hennink, N. N. Sanders, J. Demeester, S. C. Smedt. *Adv. Mater.,* **2006,** *18,* 1005-1009.

129. L. Brunsveld, B. J. B. Folmer, E. W. Meijer, R. P. Sijbesma. *Chem. Rev.,* **2001,** *101*, 4071-4097.

130. W. C. Mak, K. Y. Cheung, D. Trau. *Chem. Mater.,* **2008,** *20*, 5475-5484.

131. A. G. Skirtach, A. M. Yashchenok, H. Möhwald. *Chem. Commun.,* **2011,** *47*, 12736-12746.

132. Z. She, M. N. Antipina, J. Li, G. B. Sukhorukov. *Biomacromolecules,* **2010,** *11*, 1241-1247.

133. D. V. Volodkin, A. I. Petrov, M. Prevot, G. B. Sukhorukov. *Langmuir,* **2004,** *20*, 3398-3406.

134. A. I. Petrov, D. V. Volodkin, G. B. Sukhorukov. *Biotechnol. Prog.,* **2005,** *21*, 918-925.

135. C. Lu, H. Möhwald, A. Fery. *J. Phys. Chem. B,* **2007,** *111*, 10082-10087.

136. B. Jianhao, B. Sebastian, T. S. Yein, T. Dieter. *ACS Appl. Mater. Interfaces,* **2011,** *3*, 1665-1674.

137. W. Xu, I. Choi, F. A. Plamper, C. V. Synatschke, A. H. E. Müller, V. V. Tsukruk. *ACS Nano,* **2013,** *7*, 598-613.

138. C. Gao, S. Leporatti, S. Moya, E. donath, H. Möhwald. *Chem. Eur. J.,* **2003,** *9*, 915-920.

139. T. Mauser, C. Déjugnat, G. B. Sukhorukov. *Macromol. Rapid Commun.,* **2004,** *25*, 1781-1785.

140. R. Georgieva, R. Dimova, G. B. Sukhorukov, G. Ibarz, H. Möhwald. *J. Mater. Chem.,* **2005,** *15*, 4301-4310.

141. M. Medebach, T. Palberg. *Colloids Surf. A,* **2003,** *222*, 175-183.

142. Q. Zhao, B. Li. Nanomedicine, **2008,** *4*, 302-310.

143. Q. Wang. *J. Phys. Chem. B,* **2006,** *110*, 5825-5828.

144. Yuri Lvov, A. A. Antipov, Arif Mamedov, Helmuth Mo Gleb B. Sukhorukov. *Nano Lett.,* **2001,** *1,* 125-128.

145. M. Bédard, A. G. Skirtach, G. B. Sukhorukov. *Macromol. Rapid Commun.,* **2007,** *28*, 1517-1521.

146. Q. Yi, G. B. Sukhorukov. *Adv. Colloid Interface Sci.,* **2014,** *207*, 280-289.

147. Q. Yi, G. B. Sukhorukov. *ACS Appl. Mater. Interfaces,* **2013,** *5*, 6723-31.

148. H. Y. Koo, H. J. Lee, J. K. Kim, W. S. Choi. *J. Mater. Chem.,* **2010,** *20*, 3932.

149. X. Gong, C. Gao. *Phys. Chem. Chem. Phys.,* **2009,** *11*, 11577-86.

150. K. Zhang, W. Wu, K. Guo, J. Chen, P. Zhang. *Langmuir,* **2010,** *26*, 7971-80.

151. L. Shao, J. L. Lutkenhaus. *Soft Matter,* **2010,** *6*, 3363-3369.

152. G. Ibarz, L. Dähne, E. Donath, H. Möhwald. *Adv. Mater.,* **2001,** *13*, 1324-1327.

153. K. Kohler, D. G. Shchukin, H. Möhwald, G. B. Sukhorukov. *J. Phys. Chem. B*, **2005,** *109*, 18250-18259.

154. K. Kohler, H. Möhwald, G. B. Sukhorukov. *J. Phys. Chem. B,* **2006,** *110*, 24002-24010.

155. S. Juul, F. Iacovelli, M. Falconi, S. L. Kragh, B. Christensen, R. Frøhlich, O. Franch,E. L. Kristoffersen, M. Stougaard, K. W. Leong, Y. P. Ho, E. S. Sørensen, V. Birkedal, A. Desideri, B. R. Knudsen. *ACS Nano*, **2013**, *7*, 9734-9734.

156. H. Langhals. *Angew.Chem. Int. Ed.,* **2004,** *43*, 5291-5292.

157. A. I. Petrov , A. A. Antipov, G. B. Sukhorukov. *Macromolecules,* **2003,** *36*, 10079-10086.

158. R. A. McAloney, M. Sinyor, V. Dudnik, M. C. Goh. *Langmuir,* **2001,** *17*, 6655-6663.

159. A. A. Antipov, G. B. Sukhorukov, H. Möhwald. *Langmuir*, **2003,** *19*, 2444-2448.

160. I. Reytblat, K. K.Adamsky, J. H. Chill, H. E. Gottlieb, A. Gedanken, G. Goobes. *Phys. Chem. Chem. Phys.,* **2015,** *17*., 2235-2240.

161. T. Kidchob, S. Kimura, Y. Imanishi. Preparation, *J. Control. Release*, **1996,** *40*, 285-291.

162. A. C. Mendes, E. T. Baran, P. Lisboa, R. L. Reis, H. S. Azevedo. *Biomacromolecules,* **2012,** *13*, 4039-4048.

163. A. Szarpak, D. Cui, F. Dubreuil, B. G. De Geest, L. J. D.Cock, C. Picart, R. Auzély-Velty. *Biomacromolecules,* **2010,** *11*, 713-720.

164. S. E. Kudaibergenov. *Express Polym. Lett.,* **2008,** *2*, 101-110.

165. Z. Wang, T. Sasaki, M. Muramatsu, Y. Ebina, T. Tanaka, L. Wang, M. Watanabe. *Chem. Mater.*, **2003,** *15*, 807-812.

166. Y. Liu, A. Wang, R. Claus. *J. Phys. Chem. B,* **1997,** *101*, 1385-1388.

167. N. Ferreyra, L. Coche-Guérente, J. Fatisson, M. L. Teijelo, P. Labbé. *Chem. Commun.,* **2003,** *16*, 2056-2057.

168. B. S. Kim, K. D. Suh. *Macromol. Res.,* **2008,** *16*, 76-80

169. N. A. Kotov; I. Dékány, J. H. Fendler. *J. Phys. Chem. B,* **1995,** *99*, 13065-13069.

170. N. Gaponik, I. L. Radtchenko, M. R. Gerstenberger, Y.A. Fedutik, G. B. Sukhorukov, A. L. Rogach. *Nano Lett.,* **2003,** *3*, 369-372.

171. L. P. Balogh, S. M. Redmond, P. Balogh, H. Tang, D. C. Martin, S. C. Rand. *Macromol. Biosci.,* **2007,** *7*, 1032-1046.

172. S. R. Puniredd, C. M. Yin, Y. S. Hooi, P. S. Lee, M. P. Srinivasan. *J. Colloid. Interface. Sci.*, **2009,** *332*, 505-510.

173. N. Malikova, I. P. Santos., M. Schierhorn, N. A. Kotov, L.M. Liz-Marzán. *Langmuir*, **2002,** *18*, 3694-3697.

174. A. M. Yashchenok, D. A. Gorin, M. Badylevich, A. A. Serdobintsev, M. Bedard, Y. G. Fedorenko, G. B. Khomutov, D. O. Grigoriev, H. Möhwald. *Phys. Chem. Chem. Phys.*, **2010,** *12*, 10469-10475.

175. J. Caruso, F. Caruso. *Chem. Mater.*, **2005,** *17*, 4547-4553.

176. F.Caruso, A. S. Susha, M. Giersig, H. Möhwald. *Adv. Mater.*, **1999,** *11*, 950-952.

177. T. P. Mokone, R. P. V. Hille, A. E. Lewis. *J. Colloid. Interface Sci.*, **2010,** *351*, 10-18.

178. A. A. Antipov, G. B. Sukhorukov, E. Donath, H. Möhwald, *J. Phys. Chem. B*, **2001,** *105*, 2281-2284.

179. S. Anandhakumar, S. P. Vijayalakshmi, G. Jagadeesh, A. M. Raichur. *ACS Appl. Mater. Interfaces*, **2011,** *3*, 3419-3424.

180. M. A. El-Sayed. *Acc. Chem. Res.*, **2001,** *34*, 257-264.

181. S. Link, M. A. El-Sayed. *J. Phys. Chem. B*, **1999,** *103*, 8410-8426.

182. H. C. Huang, S. Barua, G. Sharma, S. K. Dey, K. Rege. *J. Control. Release*, **2011,** *155*, 344-357.

183. S. Anandhakumar, A. M. Raichur. *Colloids Surf. B*, **2011,** *84*, 379-383.

184. D. G. Shchukin, I. L. Radtchenko, G. B. Sukhorukov. *Chemphyschem*, **2003,** *4*, 1101-1103.

185. A. O. Govorov, W. Zhang, T. Skeini, H. Richardson, J. Lee, N. A. Kotov. *Nanoscale Res. Lett.*, **2006,** *1*, 84-90.

186. A. G. Skirtach, A. A. Antipov, D. G. Shchukin, G.B. Sukhorukov. *Langmuir*, **2004,** *20*, 6988-6992.

187. H. Wang, J. Shen, Y. Li, Z. Wei, G. Cao, Z. Gai, K. Hong, P. Banerjee, S. Zhou. *Biomater. Sci.*, **2014,** *2*, 915-923.

188. Q. A. Pankhurst, J. Connolly, S. K. Jones, J. Dobson. *J. Phys. D: Appl. Phys.*, **2003,** *36*, 167-181.

189. C. Alexiou, W. Arnold, R. J. Klein, F. G. Parak, P. Hulin, C. Bergemann, W. Erhardt, S. Wagenpfeil, A. S. Lübbe. *Cancer Res.*, **2000,** *60*, 6641-6649.

190. Chiappini, C. D. Rosa, E. Martinez, J. O. Liu, X. Steele, J. Stevens, M. M. Tasciotti, E., *Nat. Mater.*, **2015,** *14*, 532-539.

191. J. H. Park, L. Gu, G. von Maltzahn, E. Ruoslahti, S. N. Bhatia, M. J. Sailor. *Nat. Mater.*, **2009,** *8*, 331-336.

192. J. F. Popplewell , S. J. King, J. P. Day, P. Ackrill, L.K. Fifield, R.G. Cresswell, M. L. di Tada, Kexin Liu. *J. Inorg. Biochem.*, **1998,** *69*, 177-180.

193. K. Zhang, Q. Wang, H. Meng, M. Wang, W. Wu, J. Chen. *Particuology*, **2014,** *14*, 12-18.

194. L. Ye, R. Pelton, M. A. Brook. *Langmuir*, **2007,** *23*, 5630-5637.

195. Y, Hu, J. Ge, Y, Sun,T,Zhang, Y, Yin. *Nano Lett.*, **2007,** *7*, 3203-3207.

196. V. Klimkevicius, T. Graule, R. Makuska. *Langmuir*, **2015,** *31*, 2074-2083.

197. J. Yuan, S. Zhou, L.Wu, B. You. *J. Phys. Chem. B*, **2006,** *110*, 388-394.

198. J. H. Kim, S. Shiratori. *Jap. J. Appl. Phys.*, **2005,** *44*, 7588-7592.

199. H. Strohm, M. Sgraja, J. Bertling, P. Löbmann, *J. Mater. Sci.*, **2003,** *38*, 1605-1609.

200. J. Marques, L. F. Oliveira, R. T. Pinto, P. J. G. Coutinho, P. Parpot, J. R. Góis, J. F. J. Coelho, F. D. Magalhães, C. J. Tavares. *Int. J. Photoenergy*, **2013,** *2013*, 1-9.

201. D. Shi. *Adv. Funct. Mater.*, **2009,** *19*, 3356-3373.

202. G. B. Sukhorukov, A. L. Rogach, M. Garstka, S. Springer, W. J. Parak, A. Munoz-Javier, O. Kreft, A. G. Skirtach, A. S. Susha, Y. Ramaye, R. Palankar. M. Winterhalter. *Small*, **2007,** *3*, 944-955.

203. M. A. Stuart, W. T. Huck, J. Genzer, M. Muller, C. Ober, M. Stamm, G. B. Sukhorukov, I. Szleifer, V. V. Tsukruk, M. Urban, F. Winnik, S. Zauscher, I. Luzinov, S. Minko. *Nat. Mater.*, **2010,** *9*, 101-113.

204. L. Yuan, W. Lin, Y. Yang, H. Chen. *J. Am. Chem. Soc.*, **2012,** *134*, 1200-1211.

205. D. B. Mitzi. *Chem. Mater.*, **2001,** *13*, 3283-3298.

206. M. Adamczak, H. J. Hoel, G. Gaudernack, J. Barbasz, K. Szczepanowicz, P. Warszynski. *ColloidS Surf. B,* **2012,** *90,* 211-216.

207. D. Wang, A. L. Rogach, F. Caruso. *Nano Lett.*, **2002,** *2*, 857-861.

208. B. A. Kairdolf, A. M. Smith, T. H. Stokes, M. D. Wang, A.N. Young, S. Nie. Annu. *Rev. Anal. Chem*., 2013, 12, *6*, 143-162.

209. S. Bera, S. K. Maity, D. Haldar. *CrystEngComm,* **2014,** *16,* 4834-4841.

210. M. M. Titirici, R. J. White, N. Brun, V. L. Budarin, D. S. Su, F. Monte, J. H. Clark, M. J. MacLachlan. *Chem. Soc. Rev.*, **2015,** *44*, 250-290.

211. S. Y. Lim, W. Shen, Z. Gao. *Chem. Soc. Rev.*, **2015,** *44*, 362-381.

212. G. Chen, S. Wu, L. Hui, Y. Zhao, J. Ye, Z. Tan, W. Zeng, Z. Tao, L. Yang, Y. Zhu. *Sci. Rep.,* **2016,** *6,* 19028.

213. X. Yang, L. Peng, J. Zong, Y. Zhu. *Particuology*, **2013,** *11*, 334-339.

214. A. M. Yashchenok, D. N. Bratashov, D. A. Gorin, M. V. Lomova, A. M. Pavlov, A. V. Sapelkin, B. S. Shim, G. B. Khomutov, N. A. Kotov, G. B. Sukhorukov, H. Möhwald, A. G. Skirtach. *Adv. Funct. Mater.*, **2010,** *20*, 3136-3142.

215. J. Shi, Y. Jiang, X. Wang, H. Wu, D. Yang, F. Pan, Y. Su, Z. Jiang. *Chem. Soc. Rev.*, **2014,** *43*, 5192-5210.

216. D. Wang, F. Caruso. *Chem. Mater.,* **2002,** *14,* 1909-1913.

217. J. W. Morse , R. S. Arvidson, A. Lüttge. *Chem. Rev.,* **2007,** *107*, 342-381.

218. F. Dubreuil, D. G. Shchukin, G. B. Sukhorukov, A. Fery. *Macromol. Rapid Commun.*, **2004,** *25*, 1078-1081.

219. W. Wang, L. Liu, X. J. Ju, D. Zerrouki, R. Xie, L. Yang, L. Y. Chu. *Chemphyschem,* **2009,** *10*, 2405-2409; S. H. Hu, C. H. T., C. F. Liao, D. M. Liu, S. Y. Chen. *Langmuir,* **2008,** *24*, 11811-11818; M. Delcea, H. Mohwald, A. G. Skirtach. *Adv. Drug Deliv. Rev.,* **2011,** *63,* 730-747.

220. Z. Lu, M. D. Prouty, Z. Guo, V. O. Golub, C. S. S. R. Kumar, Y. M. Lvov. *Langmuir*, **2005,** *21*, 2042-2050.

221. M. Babincová, P. Cicmanec, V. Altanerová, C. Altaner, P. Babinec. *Bioelectrochemistry*, **2002,** *55*, 17-19.

222. P. A. L. Fernandes, M. Delcea, A. G. Skirtach, H. Möhwald, A. Fery. *Soft Matter*, **2010,** *6*, 1879-1883.

223. C. J. Simon, D. E. Dupuy, W. W. Mayo-Smith. *Radiographics*, **2005,** *25*, 69-84; A. R. Smolock, M. M. Cristescu, T. A. Potretzke, T. J. Ziemlewicz, M. G. Lubner, J. L. Hinshaw, C. L. Brace, F. T. Lee. *J. Vasc. Interv. Radiol.*, **2016,** *27*, 244-249.

224. T. Liu, Y. Pang, M. Zhu, S. Kobayashi. *Nanoscale*, **2014,** *6*, 2447-2454.

225. S. Banik, S. Bandyopadhyay, S. Ganguly. *Bioresour. Technol.*, **2003,** *87*, 155-159.

226. A. Hoz, A. Diaz-Ortiz, A. Moreno. *Chem. Soc. Rev.*, **2005,** *34*, 164-178.

227. D. A. Gorin, D. G. Shchukin, A. I. Mikhailov, K. Kohler, S. A. Sergeev, S. A. Portnov, I. V. Taranov, V. V. Kislov, G. B. Sukhorukov. *Tech. Phys. Lett.*, **2006,** *32*, 70-72.

228. Y. V. Gulyaev, V. A. Cherepenin, V. A. Vdovin, I. V. Taranov, G. B. Sukhorukov, D. A. Gorin, G. B. Khomutov. *J. Commun. Technol. Electron.*, **2015,** *60*, 1286-1290.

229. M. Jazirehpour, S. A. S. Ebrahimi. *J. Alloys Compd.*, **2015,** *638*, 188-196; J. J. Xu, J. W. Liu, R. C. Che, C. Y. Liang, M. S. Cao, Y. Li, Z. Liu. *Nanoscale*, **2014,** *6*, 5782-5790.

230. Y. Jing, Y. Zhu, X. Yang, J. Shen, C. Li. *Langmuir*, **2011,** *27*, 1175-1180.

231. H. Ke, J. Wang, Z. Dai, Y. Jin, E. Qu, Z. Xing, C. Guo, J. Liu, X. Yue. *J. Mater. Chem.*, **2011,** *21*, 5561-5564.

232. T. Yu, Z. Wang, T. J. Mason. *Ultrason. Sonochem.*, **2004,** *11*, 95-103.

233. Ghaleb A. Husseini, W. G. Pitt. *Adv. Drug Deliv. Rev.*, **2008,** *60*, 1137-1152.

234. V. F. Korolovych, O. A. Grishina, O. A. Inozemtseva, A. V. Selifonov, D. N. Bratashov, S. G. Suchkov, L. A. Bulavin, O. E. Glukhova, G. B. Sukhorukov, D. A. Gorin. *Phys. Chem. Chem. Phys.,* **2016,** *18,* 2389-2397.

235. Y. Ji, Y. Zhou , C. Ma, Y. Feng, Y. Hao, Y. Rui, W. Wu, X. Gui, V. N. Le, Y. Han, Y. Wang, B. Xing, L. Liu, W. Cao. *Plant Physiol. Biochem.*, 2016, In press.

236. B. G. De Geest, A. G. Skirtach, T. R. M. De Beer, G. B. Sukhorukov, L. Bracke, W. R. G. Baeyens, J. Demeester, S. C. De Smedt. *Macromol. Rapid Commun.,* **2007,** *28,* 88-95.

237. D. A. Gorin, S. A. Portnov, O. A. Inozemtseva, Z. Luklinska, A. M. Yashchenok, A. M. Pavlov, A. G. Skirtach, H. Möhwald, G. B. Sukhorukov. *Phys. Chem. Chem. Phys.,* **2008,** *10,* 6899-6905.

238. Y. Wu, J. Frueh, T. Si, H. Möhwald, Q. He. *Phys. Chem. Chem. Phys.,* **2015,** *17,* 3281-3286.

239. A. N. Shipway, M. Lahav, R. Gabai, I. Willner. *Langmuir,* **2000,** *16,* 8789-8795.

240. C. Déjugnat , G. B. Sukhorukov. *Langmuir,* **2004,** *20,* 7265-7269.

241. S. Link, M. A. El-Sayed. *J. Phys. Chem. B,* **1999,** *103,* 4212-4217.

242. A. G. Skirtach , C. Dejugnat, D. Braun, A. S. Susha , A. L. Rogach, W. J. Parak, H. Möhwald, G. B. Sukhorukov. *Nano Lett.,* **2005,** *5,* 1371-1377.

243. W. Miao, G. Shim, S. Lee, Y. K. Oh. *Biomaterials,* **2014,** *35,* 4058-4065.

244. Y. Hashida, H. Tanaka, S. Zhou, S. Kawakami, F. Yamashita, T. Murakami, T. Umeyama, H. Imahori, M. Hashida. *J. Control. Release,* **2014,** *173,* 59-66; J. W. Kim, E. V. Shashkov, E. I. Galanzha, N. Kotagiri, V. P. Zharov. *Lasers Surg. Med.,* **2007,** *39,* 622-634.

245. A. G. Skirtach, P. Karageorgiev, B. G. De Geest, N. Pazos-Perez, D. Braun, G. B. Sukhorukov. *Adv. Mater.,* **2008,** *20,* 506-510.

246. Y. Wang, A. Hu. *J. Mater.Chem. C,* **2014,** *2*, 6921-6939.

247. Q. Yi. UV-triggered Encapsulation and Release by Multilayer Microcapsules. *PhD Thesis*, 2013.

248. Double layer. https://en.wikipedia.org/wiki/Double_layer_(surface_science).

249. http://hydrology1.nmsu.edu/Teaching_Material/SOIL698/Student_Reports/Automatic _Soil/html/project620theory.html.

250. S. She, Q. Li, B. Shan, W. Tong, C. Gao. *Adv. Mater.,* **2013,** *25*, 5814-8; K. Chen, S. Zhou. *RSC Adv.*, **2015,** *5*, 13850-13856.

251. C. Jiang, V. V. Tsukruk. *Adv. Mater.,* **2006,** *18*, 829-840.

252. E. Donath, G. B. Sukhorukov, F. Caruso, S. A. Davis, H. Möhwald. *Angew. Chemi. Int. Ed.*, **1998,** *37*, 2202-2205.

253. S. Thirumalai, M. Mobed-Miremadi, M. Sridhar-Keralapura *Conf. Proc. IEEE Eng. Med. Biol. Soc.*, 2011, *2011*,7207-7210

254. A. M. Pavlov, V. Saez, A. Cobley, J. Graves, G. B. Sukhorukov, T. J. Mason. *Soft Matter,* **2011,** *7*, 4341-4347.

255. E. Blomberg, E. Poptoshev, P. M. Claesson, F. Caruso. *Langmuir,* **2004,** *20*, 5432-5438.

256. W. F. Dong, J. K. Ferri, A. Thorsteinn, S. Monika, G. B. Sukhorukov, H. Möhwald. *Chem. Mater.*, **2005,** *17*, 2603-2611.

257. J. O. Eloy, M. C. Souza, R. Petrilli, J. P. Barcellos, R. J. Lee, J. M. Marchetti. *Colloids Surf. B,* **2014,** *123*, 345-63.

258. A. Kidane, P. P. Bhatt. *Curr. Opin. Chem. Biol.,* **2005,** *9*, 347-351.

259. Z. G. Chen. *Trends Mol. Med.,* **2010,** *16*, 594-602.

260. W. Song, H. Qiang, H. Möhwald, Y. Yang, J. Li. *J. Control. Release,* **2009,** *139*, 160-166.

261. Kim, C. S. M., R. Zhao, Y. Yeh, Y. C. Tang, R. Jeong, Y. Duncan, B. Hardy, J. A. Rotello, V. M., *Bioconjugate Chem.* **2015,** *26* (5), 950-954.

262. K. J. Whittlesey, L. D. Shea. *Exp. Neurol.,* **2004,** *190*, 1-16.

263. B. Sun, S. A. Mutch, R. M. Lorenz, D. T. Chiu. *Langmuir,* **2005,** *21*, 10763-10769.

264. P. Erni, G. Dardelle, M. Sillick, K. Wong, P. Beaussoubre, W. Fieber. *Angew. Chemi. Int. Ed.,* **2013,** *52*, 10334-10338.

265. S. Fouilloux, O. Tache, O. Spalla, A. Thill. *Langmuir,* **2011,** *27*, 12304-12311.

266. T. Yokoi, J. Wakabayashi, Y. Otsuka, W. Fan, M. Iwama, R. Watanabe, K. Aramaki, A. Shimojima, T. Tatsumi, T. Okubo. *Chem. Mater.*, **2009,** *21*, 3719-3729.

267. Z. Czigany, L. Hultman. *Ultramicroscopy,* **2010,** *110*, 815-819.

268. W. C. Mak, J. Bai, X. Y. Chang, D. Trau *Langmuir,* **2009,** *25*, 769-775.

269. M. N. Antipina, G. B. Sukhorukov. *Adv. Drug Deliv. Rev.,* **2011,** *63*, 716-29.

270. M. F. Bédard, A. Munoz-Javier, R. Mueller, P. Pino, A. Fery, W. J. Parak, A. G. Skirtach, G. B. Sukhorukov. *Soft matter,* **2009,** *5*, 148-155.

271. X. Liang, B. Xu, S. Kuang, X. Wang. *Adv. Mater.,* **2008,** *20*, 3739-3744.

272. S. Sripanyakorn, R. Jugdaohsingh, W. Dissayabutr, S. H. C. Anderson, P. H. Thompson, J. J. Powell. *Br. J. Nutr.* **2009,** *102*, 825-834.

273. H. S. Choi, W. Liu, P. Misra, E. Tanaka, J. P. Zimmer, B. I. Ipe, M. G. Bawendi, J. V. Frangioni. *Nat. Biotech.,* **2007,** *25*, 1165-1170.

274. R. Gomez-Martinez, A. M. Hernández-Pinto, M. Duch, P. Vazquez, K. Zinoviev, E. J. Rosa, J. Esteve, T. Suarez, J. A. Plaza. *Nat. Biotech.,* **2013,** *8*, 517-521.

275. L. You, T. Wang, J. Ge. *Chemistry,* **2013,** *19*, 2142-2149.

276. R. R. Costa, E. Castro, F. J. Arias, J. C. Rodriguez-Cabello, J. F. Mano. *Biomacromolecules,* **2013,** *14*, 2403-2410.

277. K. Katagiri, A. Matsuda, F. Caruso. *Macromolecules,* **2006**, *39*, 8067-8074.

278. M. Motornov, Y. Roiter, I. Tokarev, S. Minko. *Prog. Polym. Sci.,* **2010,** *35*, 174-211.

279. Q. Yi, G. B. Sukhorukov. *ACS Nano,* **2013,** *7*, 8693-8705.

280. T. Chen, P. J. Colver, S. A. F. Bon. *Adv. Mater.,* **2007,** *19*, 2286-2289.

281. D. G. Shchukin, E. Ustinovich, D. V. Sviridov, Y. M. Lvov, G. B. Sukhorukov. *Photochem. Photobiol. Sci.,* **2003,** *2*, 975-977.

282. H. Kishimoto, K.Takahama, N. Hashimoto, Y.Aoi, S. Deki. *J. Mater. Chem.,* **1998,** *8*, 2019-2024.

283. M. Sgraja, J.Blömer, J. Bertling, P. J. Jansens. *Chem. Eng. Technol.,* **2010,** *33*, 2029-2036.

284. A. P. R. Johnston, A. N. Zelikin, F. Caruso. *Adv. Mater.,* **2007,** *19*, 3727-3730.

285. H. Pizem, C. N. Sukenik. *Chem. Mater.,* **2002,** *12*, 2476-2485.

286. X. Wang, W. Zhou, J. Cao, W. Liu, S. Zhu. *J. Colloid Interface Sci.,* **2012,** *372*, 24-31.

287. H. Shin, M. Agarwal, M. R. D. Guire, A. H. Heuer. *Acta Mater.,* **1998,** *46*, 801-815.

288. H. Strohm, P. Löbmann. *Chem. Mater.,* **2005,** *17*, 6772-6780.

289. Y. Sun, Y. Xia. *Sci.,* **2002,** *298*, 2176-2179.

290. S. Chang, Z. A. Combs, M. K. Gupta, R. Davis, V. V. Tsukruk, *ACS Appl. Mater. Interfaces,* **2010,** *2*, 3333-3339.

291. D. Guan, Y. Wang. *Nanoscale,* **2012,** *4*, 2968-2977.

292. J. J. De Yoreo, P. G. Vekilov. *Rev. Mineral. Geochem.,* **2003,** *3*, 57-89.

293. S. Spange, A. Grund. *Adv. Mater.,* **2009,** *21*, 2111-2116.

294. T. Levy, C. Déjugant, G. B. Sukhorukov. *Adv. Funct. Mater.,* **2008,** *18*, 1586-1594.

295. K. Katagiri, K. Koumoto, Shogo Iseya, Mototsugu Sakai, Atsunori Matsuda, and Frank Caruso. *Chem. Mater.* **2009,** *21*, 195-197.

296. Q. Wang, X. Huang, Y. Long, X. Wang, H. Zhang, R. Zhu, L. Liang, P. Teng, H. Zheng. *Carbon,* **2013,** *59*, 192-199.

297. S. Yang, C. Zhou, J. Liu, M. Yu, J. Zheng. *Adv. Mater.*, **2012,** *24*, 3218-3222.

298. H. Skaff, Y. Lin, R. Tangirala, K. Breitenkamp, A. Böker, T. P. Russell, T. Emrick. *Adv. Mater.*, **2005,** *17*, 2082-2086.

299. K. Kohler, D. G. Shchukin, G. B. Sukhorukov, H. Mohwald. *Macromolecules,* **2004,** *37*, 9546-9550.

300. X. Wen, P. Yu, Y. R. Toh, X. Ma, J. Tang. *Chem. Commun.*, **2014,** *50*, 4703-4706.

301. Y. Zhang, Y. Wu, M. Chen, L. Wu. *Colloids Surf. A,* **2010,** *353*, 216-225.

9. Publications

1. Hui Gao, Dongsheng Wen, Gleb B. Sukhorukov*, Composite silica nanoparticle/polyelectrolyte microcapsules with reduced permeability and enhanced ultrasound sensitivity, *Journal of Materials Chemistry B*, **2015**, 3, 1888-1897.
2. Hui Gao, Dongsheng Wen, Nadezda V. Tarakina, Jierong Liang, Andy J. Bushby, Gleb B. Sukhorukov*, Bifunctional ultraviolet/ultrasound responsive composite TiO_2/polyelectrolyte microcapsules, *Nanoscale*, **2016**, 8, 5170-5180.
3. Hui Gao, Olga A. Goriacheva, Nadezda V. Tarakina, Gleb B. Sukhorukov*, Intracellularly biodegradable polyelectrolyte/silica composite microcapsules as carrier for small molecule, *ACS Applied Materials & Interfaces*, **2016**, 8, 9651-9661.
4. Alexander Timin, Hui Gao, Denis Voronin, Dmitry Gorin, Gleb Sukhorukov*, Inorganic/Organic multilayer capsule composition for improved functionality and external triggering, *Advanced Materials Interfaces*, **2016**, 1600338 (1-22).
5. Hui Gao, Andrei V. Sapelkin, Magdalena Titirici, Gleb B. Sukhorukov*, *In situ* synthesis of fluorescent carbon Dots/polyelectrolyte nanocomposite microcapsules with reduced permeability and ultrasound sensitivity, *ACS Nano*, **2016**, 10, 9608-9615.
6. Hui Gao, Gleb B. Sukhorukov*, Composite polyelectrolyte/silica shells for protection of porous $CaCO_3$ particles, *Physical Chemistry Chemical Physics,* In preparation.